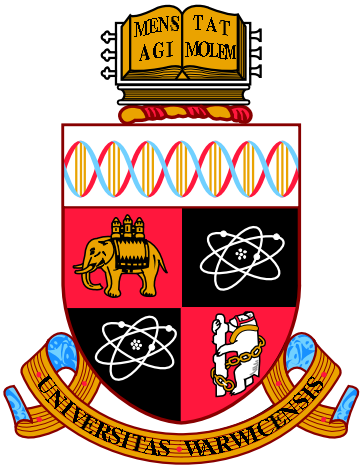

The dynamics of thermostatically controlled loads for power system frequency control

by

Ellen Elizabeth Webborn

Thesis

Submitted to the University of Warwick

for the degree of

Doctor of Philosophy in

Mathematics and Complexity Science

Centre for Complexity Science

July 2018

Contents

List of Tables

List of Figures

Acknowledgments

This thesis would not have been possible without the guidance, support and inspiration of my supervisors, Robert MacKay and Mike Waterson. You have taught me a great deal and pushed me to become a better mathematician and researcher. I am very proud of what we have achieved and I'm extremely grateful for your supervision over the last 5 years. I'd like to thank Lisa Flatley, for all of your encouragement and assistance with my research, particularly in the early days when I was searching for research direction. I'm also grateful to the IMAGES research group for support and stimulating discussions.

To all the people whom I had the pleasure of working with at National Grid, thank you for helping me to take the leap into the world of engineering, and for teaching me about the energy industry. I'm particularly grateful to Vandad Hamidi for supporting me from the start and championing my career at the company. To Matt Roberts, Roy Cheung and Will Ramsay for your great work with the Frequency Engine and continued support, which made a huge difference to my simulations, thank you very much. To Ben Marshall for your generosity of spirit and expertise, Beth Warnock for your continued encouragement and publication support, and to everyone in the System Performance team, many thanks.

I have had the privilege of being part of a doctoral training centre full of interesting, friendly and supportive people. I'd like to thank the many staff and students with whom I discussed my work and who helped to challenged my thinking. I've had great office mates over the years, Pantelis, Sergio, Chris, Fede, Bernd, Joe, Iliana, Sami, Ayman and Roger - thank you for the laughs, the encouragement, and the maths

chats. Additional thanks go to the Smoothie Club for brightening my Thursdays with intriguing concoctions, long may it continue.

Although there are too many people to mention by name, and many things I'll remember, I'll take this opportunity to thank a few people who stand out at this point in time. Thank you Joe for your wit, genuine compliments, and occasional tough love. Iliana your cakes are amazing and I've been touched by your generosity of baking spirit. Thank you Ayman for your help with Inkscape, and to you and Michael for letting me use your computer when I was in need of computing power. Tom and Davide, thank you for being inspirational researchers and friends. Mike, you always livened up lunchtime discussions with your weird and wonderful debates. Roger, thank you for your help with simulations and tikz, and for being a wonderful dance partner. Dancing has been a real source of joy and stress relief, and I'm also grateful to Josh, Kevin and Nick for being amazing and making me a better dancer during my time in Complexity. My housemates have always been there for me in times of celebration and sadness alike. Jamie, Georgia, my Irish boys Barry, Andy and Conley, also Sophie and Craig, Cyril, Te-Anne and Steph, it's been a pleasure. Thank you Dario, for standing by me through thick and thin, always there with hearty food for late night chats and musical times. Thank you Rachel, who was there with me when it all began and returned in time to cheer me over the PhD finish line with tea and friendship.

Finally, I am infinitely grateful to my family, without whom I would not be the person I am nor have achieved what I have. Thank you Mum, Dad, and Annie.

Declarations

This Thesis is submitted to the University of Warwick in support of my application for the degree of Doctor of Philosophy. I have read and understood the rules on cheating, plagiarism and appropriate referencing as outlined in my handbook and I declare that the work contained in this assignment is my own. No substantial part of the work submitted here has also been submitted by me in other assessments for this or previous degree courses, and I acknowledge that if this has been done an appropriate reduction in the mark I might otherwise have received will be made.

Work contributing to this thesis has appeared in the peer-reviewed publication:

Ellen Webborn & Robert S. MacKay. A stability analysis of thermostatically-controlled loads for power system frequency control. *Complexity*, (2017).

Abstract

Major changes are under way in our power grids. Until very recently, a few hundred, very large, dependable fossil-fuelled power stations were supplying power to consumers whose only role was to use energy whenever they wanted. Today we have wind farms, solar farms, solar panels on millions of roofs, smart metering. Electric vehicles are on the rise and storage technologies are developing rapidly. Achieving a low-carbon, affordable, and secure electricity system, the so-called 'energy trilemma,' presents many challenges and opportunities. As energy becomes more dependent on volatile resources such as the wind and sun, flexibility will become increasingly important for maintaining system security at palatable costs. One new source of flexibility could come from domestic appliances. Thermostatically-controlled loads (TCLs), such as fridges, freezers, air-conditioners and hot-water tanks are effectively energy stores that can be adapted to meet the needs of the grid with negligible impact on consumers. By allowing their operating set points to vary (a little) according to the electricity frequency, they could provide a valuable resource to the grid. However, a thorough understanding of their potential to exhibit synchronisation will be needed to understand and mitigate against the potential risks of a decentralised response provider.

In this thesis I outline the operation of the electricity grid in Great Britain and describe the existing research into using TCLs for demand-side response. I present a new continuum model for a population of deterministic frequency-sensitive TCLs that is sufficiently tractable to allow for our stability analysis. I also solve for the long-term behaviour of a fully synchronised group of TCLs and analyse its stability to splitting into two groups, and hypothesise about the stability of N groups. Using system data from National Grid, the operation of the GB electricity system is simulated over ten-day periods with, and without, a population of fridges providing frequency response to determine their impact. I find that synchronisation issues should always be expected when the fridge population is identical, but with even very low levels of parameter diversity, such issues are eradicated in our simulations. Given the inherent diversity in a population of TCLs, this research shows that decentralised, deterministic control schemes are a viable option for using TCLs for frequency response, and that such a scheme could provide a valuable resource.

Abbreviations

AC	alternating current
DC	direct current
DSR	demand-side response
FES	Future Energy Scenarios
FLC	fuzzy logic controller
GB	Great Britain
GW	gigawatt = 10^9 (one billion) watts of electrical power
iff	if and only if
kW	kilowatt = 1000 watts of electrical power
LHS	left-hand side
MVA	megavolt-ampere = 10^6 (one million) volt-amperes of apparent power
MW	megawatt = 10^6 (one million) watts of electrical power
Ofgem	Office of Gas and Electricity Markets
PEV	plug-in electric vehicle
PHS	pumped hydroelectric storage
RHS	right-hand side
RoCoF	rate of change of frequency
SO	System Operator
TCL	thermostatically-controlled load
wrt	with respect to

Notation

Symbol	Description	Units	Appears
$\bullet$	denotes on or off depending on the context	-	(3.28)
c	inverse nominal angular momentum	Hz $(\text{MWs})^{-1}$	(3.12)
c_{OFF}	$\dot{f}$ when single group is switched off	Hz s^{-1}	(3.42)
c_{ON}	$-\dot{f}$ when single group is switched on	Hz s^{-1}	(3.42)
$D(t)$	total measured demand	MW	(4.1)
$\text{Dem}_{resp}\big(f(t),t\big)$	automatic demand response	MW	(4.3)
$\text{Dem}_{\omega 0}(t)$	demand at nominal frequency	MW	(4.2)
$E_k(t)$	total stored kinetic energy	MVAs	(4.4)
$f(t)$	grid frequency minus nominal frequency	Hz	(3.4a)
f_-	minimum frequency in single group periodic solution	Hz	(3.55a)
f_+	maximum frequency in single group periodic solution	Hz	(3.55b)
f_n^{OFF}	grid frequency at time t_n^{OFF}	Hz	(3.41a)
f_n^{ON}	grid frequency at time t_n^{ON}	Hz	(3.41a)
G_A, G_B	group A, group B	-	(3.80)
$\text{Imb}_{tot}(t)$	total imbalance	MW	(4.5)
$\text{Imb}_{under}(t)$	underlying imbalance	MW	(4.5)
k	dimensionless constant	-	(3.34)
k_0	normalisation constant	s^{-1}	(3.23)
l_{OFF}	off cycle duration of single group periodic solution	s	(3.55b)

l_{ON}	on cycle duration of single group periodic solution	s	(3.55a)
L	single group periodic solution cycle duration	s	Figure 3.21
N	number of synchronised groups	-	Table 3.2
P_c	maximum TCL population power consumption	MW	(3.12)
$S_{\text{A}}, S_{\text{B}}$	on/off state of group A, group B	-	Figure 3.12
t	time	s	(3.3)
t_n^{OFF}	time of n^{th} switch off of single group	s	(3.41a)
t_n^{ON}	time of n^{th} switch on of single group	s	(3.41a)
$T(t)$	temperature	°C	(3.3)
T_-^0	nominal lower temperature set point	°C	(3.4a)
$T_-\big(f(t)\big)$	lower temperature set point	°C	(3.4a)
T_+^0	nominal upper temperature set point	°C	(3.4b)
$T_+\big(f(t)\big)$	upper temperature set point	°C	(3.4b)
T_{OFF}	asymptotic heating temperature (room temperature)	°C	(3.3)
T_{ON}	asymptotic cooling temperature	°C	(3.3)
$T_\Gamma(t)$	temperature of the single group periodic solution	°C	Figure 3.21
$u(\theta,t)\mathrm{d}\theta$	fraction of TCLs between θ and $\theta+\mathrm{d}\theta$	-	(3.18)
$v(\theta,t)$	velocity of TCL in θ-space	s^{-1}	(3.19)
$w(\theta,t)$	perturbation function	s^{-1}	(3.29)
w_{OFF}	histogram bin width for switched off TCLs	-	(4.10)
w_{ON}	histogram bin width for switched on TCLs	-	(4.10)
$X \in \{A, ..., L\}$	switch event	-	Figure 3.12
XY	switch event progression X then Y	-	(3.89)
Z	combination of parameters	Hz s^{-1}	(3.40)

Z_0	Z with parameters from Table 3.1	Hz s^{-1}	(3.40)
α	Heating/cooling coefficient	s^{-1}	(3.3)
β	set point sensitivity to frequency (when $\beta_- = \beta_+$)	°C Hz^{-1}	(3.60)
β_-	lower temperature set point sensitivity to frequency	°C Hz^{-1}	(3.4a)
β_+	upper temperature set point sensitivity to frequency	°C Hz^{-1}	(3.4b)
γ	damping factor divided by angular momentum	s^{-1}	(3.12)
δt	generator response time lag	s	(4.7)
Δt	time step size	s	(4.7)
ΔP	surplus power generation for the TCLs	MW	(3.12)
Δ_t, Δ'_t	switch on time differences between groups A and B	°C	Figure 3.21
Δ_T, Δ'_T	temperature difference between groups A and B at group B switch on events	°C	Figure 3.21
Δu	normalised wave peak amplitude	-	Table 4.1
$\epsilon_1, ..., \epsilon_5$	time differences in single group linearisation	s	Figure 3.21
$\eta(\theta, t)$	perturbation function	s^{-1}	(3.27)
$\theta(t)$	measure of TCL phase	-	(3.17)
θ_n	nth normalised phase difference of two groups	-	(3.81b)
λ	eigenvalue	-	(3.34)
λ_1	eigenvalue	-	(3.112)
λ_2	eigenvalue	-	(3.134)
μ	combination of parameters	$(\text{Hz s})^{-1}$	(3.33c)
ν_0	combination of parameters	Hz^{-1}	(3.33a)
ν_1	combination of parameters	Hz^{-1}	(3.33b)
ξ	combination of parameters	°C s^{-1}	(3.103)
ξ_1	combination of parameters	°C s^{-1}	(3.114)
ξ_2	combination of parameters	°C s^{-1}	(3.118)
ξ_3	combination of parameters	°C s^{-1}	(3.122)

ξ_4	combination of parameters	$^\circ$C s^{-1}	(3.126)
$\rho(t)$	proportion of TCLs switched on	-	(3.12)
ρ_0	expected proportion of frequency insensitive TCLs switched on	-	(3.8)
σ	proportion in group A in two group model	-	(3.80)
τ^0_{ON}	nominal on cycle duration	s	(3.7a)
$\tau_{\text{ON}}(f)$	frequency-dependent on cycle duration	s	(3.6a)
τ^0_{OFF}	nominal off cycle duration	s	(3.7b)
$\tau_{\text{OFF}}(f)$	frequency-dependent off cycle duration	s	(3.6b)
$\phi_{\text{OFF}}(t)$	combination of parameters	Hz^{-1}	(3.21b)
$\phi_{\text{ON}}(t)$	combination of parameters	Hz^{-1}	(3.21a)

"I'm absolutely not anti-renewables. I love renewables. But I'm also pro-arithmetic."

David MacKay, *TEDxWarwick, 2012*

1 Introduction

Britain, like many countries around the world, is in midst of what could be called an 'energy revolution' [1]. In the past year alone there have been headlines such as "GB energy supply enjoys coal-free day for 'first time since the industrial revolution' " [2], "This summer was greenest ever for energy, says National Grid" [3], "Britain opens first subsidy-free solar power farm" [4], and "Jaguar Land Rover to build electric and hybrid new vehicles only from 2020" [5], to name but a few. The public is becoming increasingly aware of, and increasingly involved with, the major changes sweeping the electricity industry.

Historically electricity was supplied by a (relatively small) number of large (gigawatt (GW)-scale), predictable power plants that met the electricity needs of all consumers on the network. Energy flowed from suppliers, through the transmission and distribution systems, into homes and businesses where it was consumed. To control the power system meant controlling the power plants, and controlling and maintaining the power grid components and infrastructure. The 21st century has seen a dramatic shift away from this model to a network with thousands of uncontrolled micro-scale solar panels, hundreds of highly variable large-scale wind and solar farms (often at the extremities of the transmission network), and contributions to system balancing from large businesses such as supermarkets. Figure 1.1 shows the fuel input for

electricity generation in the UK between 1920-2016 based on government electricity statistics [6]. Over the last hundred years electricity demand has risen dramatically, and has only recently declined somewhat since its peak in 2005. We can see the rise and fall of coal and oil as our primary electricity sources. Nuclear and natural gas are the largest sources of fuel for electricity today, and other fuels such as wind and solar have been steadily rising since 1990. Figure 1.2 shows the rapid expansion of solar photovoltaics (PV) over the last eight years to almost 13GW (gigawatt) in October 2017. Wind power has seen similar trends, with current estimates for installed onshore and offshore capacity at 11.0GW and 5.3GW respectively[1] [7]. Such widespread changes offer the chance for a future less dependent on fossil fuels [8], but bring with them many challenges to the secure and affordable operation of the electricity grid that are yet to be fully addressed [1, 9].

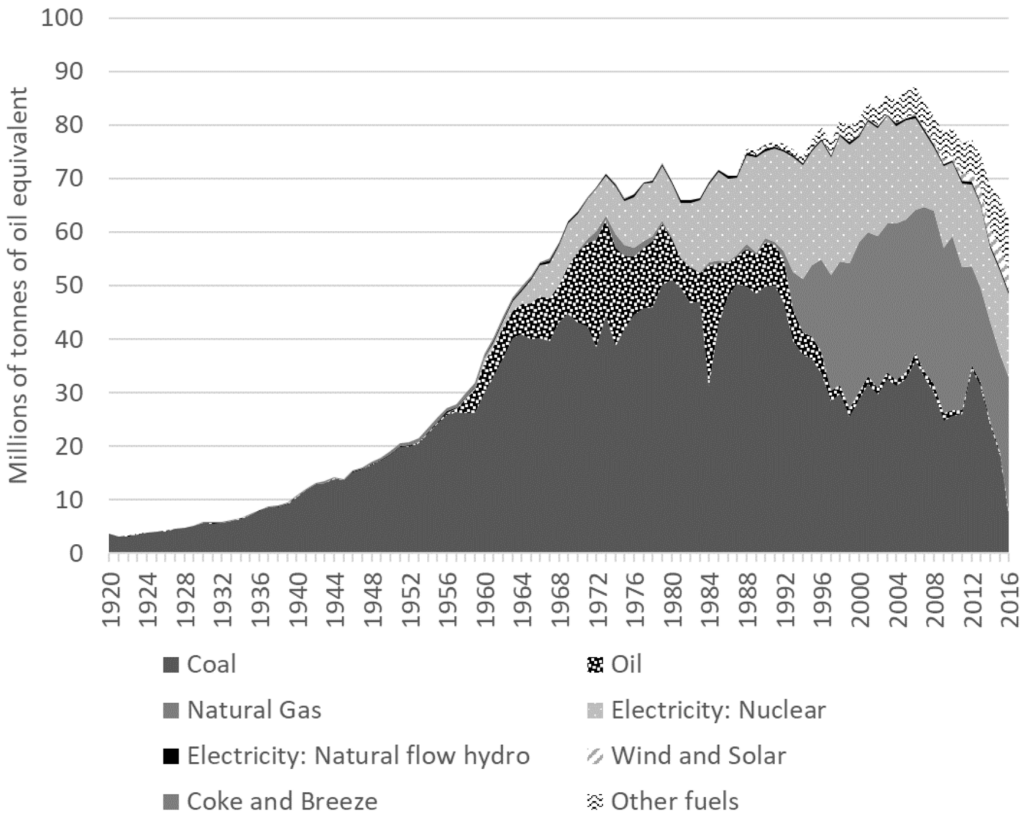

Figure 1.1: Fuel input for electricity generation in millions of tonnes of oil equivalent in the UK between 1920-2016 based on the data in [6].

Our increasing dependence on volatile and less predictable resources such as the

[1]These figures exclude projects smaller than 100kW (kilowatt).

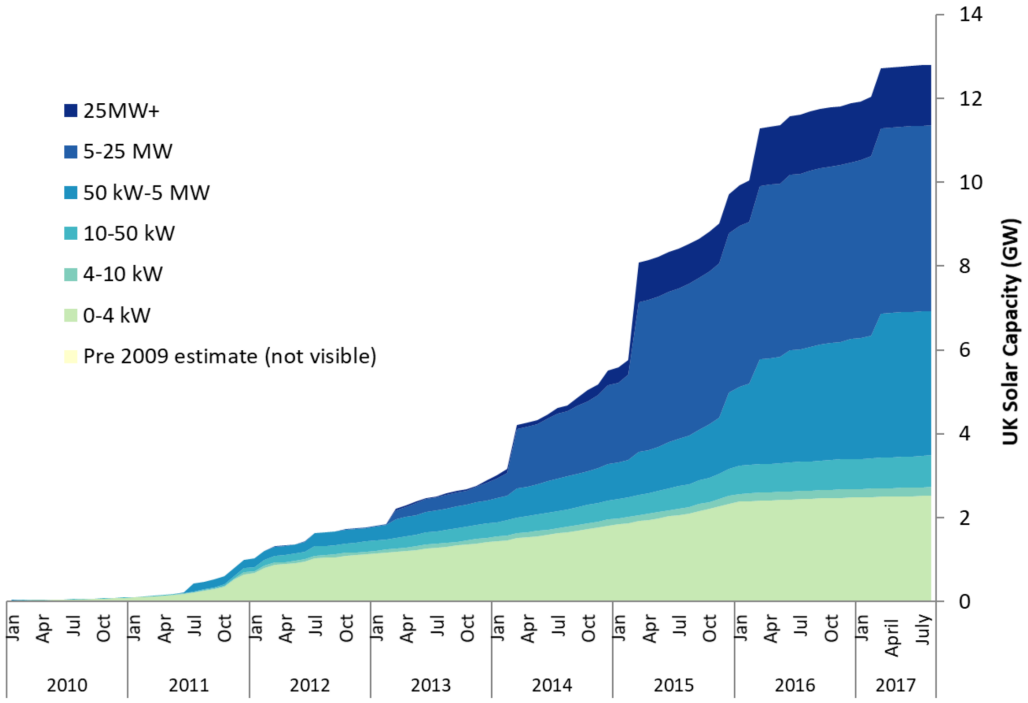

Figure 1.2: Estimated solar photovoltaics deployment, from [10].

wind and sun exposes the system to power fluctuations that need to be carefully managed. The power system's ability to respond to such changes is critical for preventing blackouts and protecting network components. Generators or consumers that can act in a flexible manner will become more valuable as the costs of meeting these operational challenges increase. Examples of current providers of flexibility include gas power plants, pumped hydroelectric storage, smaller-scale storage such as batteries, and businesses contracted to temporarily switch off freezers or air conditioning when called upon. Inflexibility is found in nuclear power stations, solar PV, wind farms (due to the high cost of requesting flexibility at present), and domestic consumers (currently). Rising flexibility requirements will most likely increase energy costs for consumers [11]. In the recent review of the evidence on the costs and impacts of intermittent electricity generation technologies by the UK Energy Research Centre, it is found that "costs are very sensitive to the flexibility of the system to which variable renewable generation is added, with estimates of costs often being dramatically lower for flexible systems". In order to become more flexible, systems will need to adapt by making "changes to both the technical and economic characteristics of electricity generating plant, potential contributions from flexible demand, storage and increased interconnection capacity, as well as changes to system

operation, regulatory frameworks and the design of electricity markets" [11].

The focus of our work is on a particular type of flexible demand. Thermostatically-controlled loads (TCLs) such as fridges, freezers, air conditioners and hot water tanks can effectively be used as energy stores on the grid. They spend periods of time switched on, and periods of time switched off in order to keep food, rooms or water near the right temperature. The precise time when they switch on or off is of no concern to the user, and so their power consumption can be delayed or advanced on the order of several minutes if needed, with no detriment to their operation. To delay consumption is similar to an energy store supplying power to the grid which will be replaced a little later, and to advance consumption is similar to filling/charging a store. By allowing the TCL operating set points to vary a small amount according to the needs of the electricity grid, a population of TCLs can act as a flexible demand resource, similar to energy storage. The rate of change of the grid frequency (RoCoF), detectable anywhere on the network, is an approximate measure of the imbalance between supply and demand. Therefore it would only require a small addition to an appliance to detect the frequency and compute the temperature set points accordingly in order for it to become a flexible resource.

There are a number of challenges with regard to making frequency-sensitive TCLs a reality on the GB grid. For example, there would need to be financial or legal incentives for companies to install the appropriate controllers in existing or new TCLs. Would individual consumers be paid for participating in such a scheme, or would it become a standard component of all new fridge-freezers, for example? If the System Operator were to pay TCLs for providing a balancing service, it would need to know how the population would respond to frequency deviations and be confident that the service could be relied upon. Who would pay if the service did not meet expectations? Beyond the economic and policy considerations, of most interest to us is the control mechanism within each TCL. Many options have been proposed in the literature, but no choice has yet emerged as the optimal solution.

What any robust solution must overcome is the risk of temperature cycle synchronisation. At present, the demand from TCLs is approximately constant throughout the day. TCLs switch on and off completely independently of one another, and so their total load is predictable and easy to supply. However, if many TCLs begin responding to a signal (the frequency) according to the same control rules, their temperature cycles may become correlated. While this may be useful in the short term as the population responds together to the frequency, over time these correlations can amplify, to the extent that large portions of the population begin switching

on and off at the same time. Understanding the propensity of TCL populations to synchronise will be key for avoiding such problems.

The first half of this thesis describes a new continuum model for a population of frequency-sensitive TCLs and presents analyses of the dynamics of a continuum of TCLs, and also of one and two synchronised groups. We consider a simple, decentralised, deterministic control scheme for a homogeneous population of TCLs. Eigenvalue analysis of our model shows that the nominal frequency equilibrium is stable, at least to small perturbations. We also solve for the periodic solution of a fully synchronised group of TCLs. This leads us to study the behaviour of two synchronised groups, which is much more complicated due to the potential for the order of switching (on or off) to change. We analyse the stability of two groups very close to the single group solution, and find the region in parameter space in which the groups will synchronise, and the region in which the groups will separate and remain distinct. This allows us to hypothesize about the long-term behaviour of N groups of identical TCLs.

The second half of our work offers a number of simulations which expand on the mathematics and provide new insights into how TCLs would perform on the real GB system under our decentralised, deterministic control scheme. We are able to simulate a large population of TCLs acting on the GB grid using real system data from National Grid from 2015-2016. The data includes system demand, stored kinetic energy, frequency, and frequency response from other providers. To the best of our knowledge, this is the first time TCLs have been simulated with this amount of system data for such long time periods (ten days). In particular, an algorithm from National Grid has allowed us to determine how the other response providers on the system would have acted had the TCLs been frequency-sensitive, and to calculate the resulting reduction (or increase) in response that they were required to provide. We test our theory that with sufficient parameter diversity, a heterogeneous population will avoid the synchronisation issues that befall homogeneous populations. We discover that even a very small amount of diversity will eradicate these problems. Since diversity exists in any real system, we conclude that the minimal levels required fall within what could be reasonably expected in a population, and so our control scheme is a viable option to implement in a TCL population. Thus potentially unpopular controls with stochasticity can be avoided, as well as infrastructure-intensive centralised control schemes that pose potential security risks.

Our novel contributions to the literature can be summarised as follows. 1) The de-

velopment of a new continuum model describing a population of frequency-sensitive TCLs on the electricity grid. 2) Stability analysis of the nominal frequency equilibrium in the model. 3) Stability analysis of a fully synchronised group of TCLs to splitting in two and a hypothesis regarding the dynamics of N groups. 4) Demonstration that very small amounts of diversity can prevent synchronisation issues in a heterogeneous population, and estimates for the GB system of the potential reduction in frequency response from other providers.

We assume that the reader has a mathematical background rather than expertise in power grids and the energy industry, and tailor the background and explanations accordingly. In Chapter 2 we describe the structure and operation of the GB electricity grid, introducing power systems concepts that are important for our work such as power system stability and balancing services (Section 2.1.2). We also expand on the topics of renewable energy (2.2), smart grids and demand-side response (2.3). Section 2.4 explains how TCLs can be used for frequency response, describes the existing literature, and discusses the topic of synchronisation. Chapter 3 contains our models and mathematical analysis of a continuum of identical TCLs and of one and two groups of identical synchronised TCLs. In Chapter 4 we explain our simulation methodologies and present the results. We conclude and propose areas for further work in Chapter 5.

"Chirping crickets, croaking frogs, flashing fireflies, gaps in the asteroid belt, generators in the power grid-[Norbert] Wiener spotted sync in all of them."

Steven Strogatz, *Sync: the emerging science of spontaneous order* [12]

2 Background

2.1 The Electricity Grid

The first electric power system began operating in 1882 supplying power (for lighting) to 59 customers in New York City [13]. Today power grids span entire continents, making electric power available to approximately 4.8 billion people [14] and transforming almost all aspects of the way we live. In this thesis, the work is applicable to AC power grids in any country, however we focus predominantly on the electricity grid and current energy policy in Great Britain (GB). We use the terms *electricity grid*, *power grid*, *grid* and *power system* interchangeably.

2.1.1 Structure

Put simply, an electricity grid connects electricity generators into a high voltage transmission network which transmits energy across long distances to distribution networks where the voltage is reduced (possibly more than once), and ultimately reaches residential and commercial consumers. The power entering the grid is known as *generation* or *supply*, and the power leaving the grid is referred to as *demand* or

load. In addition to generation and load there may also be various types of electricity storage on the network, although in all major power grids (at present), the capacity is relatively small compared to generation capacity. As of 2014 the global installed power generation capacity was approximately 6180GW [15], whereas the installed capacity of pumped hydroelectric storage (PHS), which accounts for over 99% of energy storage capacity, was approximately 127GW [16], a ratio of around 50:1. In Great Britain we have several PHS plants that typically consume electricity at night (to store energy) when demand is low and supply power to the grid during peak times of day. Other key components of an AC power system include power transformers, capacitors, transmission circuits, and control and switching systems[1]. This description would have been valid 50 years ago and is still relevant today. However, the arrival of renewable power generation, electric vehicles, smart meters and other recent innovations are dramatically altering the way power is generated and consumed. Diagram 2.1 shows a simplified representation of the electricity grid (a), and the new technologies that we are starting to see connecting to the grid (b).

Today, power is still generated predominantly by synchronous machines that convert energy sources such as fossil and nuclear fuels into mechanical energy, driving rotating turbines which in turn produce electrical energy. Alternating current is produced with a frequency equal to the angular frequency of the motor divided by 2π. In order for the grid to operate effectively, all of the generators need to be synchronised, *i.e.* they all need to be rotating at the same frequency (known as the *(electricity grid/system) frequency*) so that the phase of the current is the same at all points in the network[2]. For the purpose of our work we assume that the frequency is the same in all locations. When the power being drawn from the grid is greater than the power being supplied, the generators lose energy and slow down, and this reduces grid frequency. *Vice versa*, when demand is less than supply, the generators start to speed up and grid frequency increases. In Europe the ideal grid frequency is 50Hz, called the *nominal frequency*[3]. The components of any grid are designed to operate within a narrow range around the nominal frequency. They are vulnerable to major faults with severe repercussions for the whole system if the grid frequency deviates outside of this range (approximately 50 ± 0.5Hz).

It is the one of the roles of the System Operator (SO) to ensure that the grid frequency remains within a narrow range of the nominal frequency. Of course,

[1] For a detailed description of these components see, for example, [17].

[2] In reality the frequency typically varies a little between different locations, although larger differences are sometimes caused by 'inter-area oscillations'.

[3] In North America the nominal frequency is 60Hz.

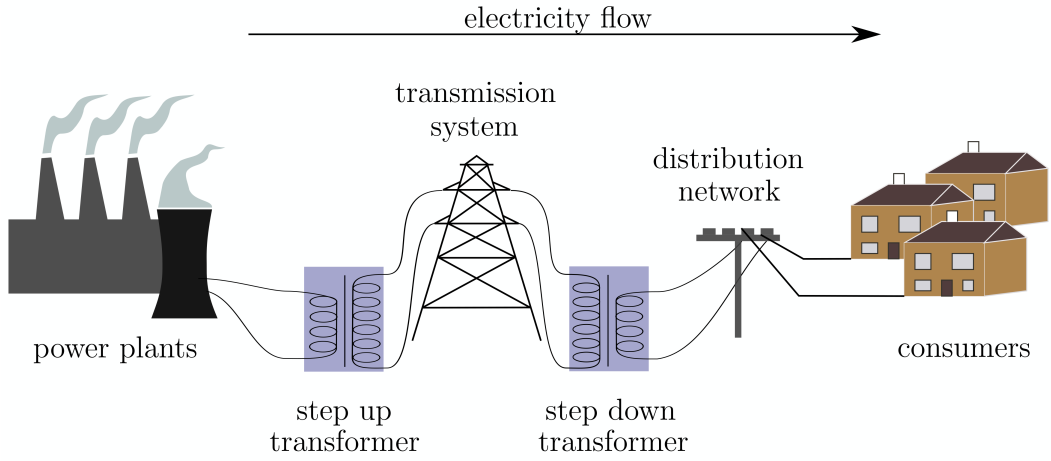

(a) Traditional Electricity Grid

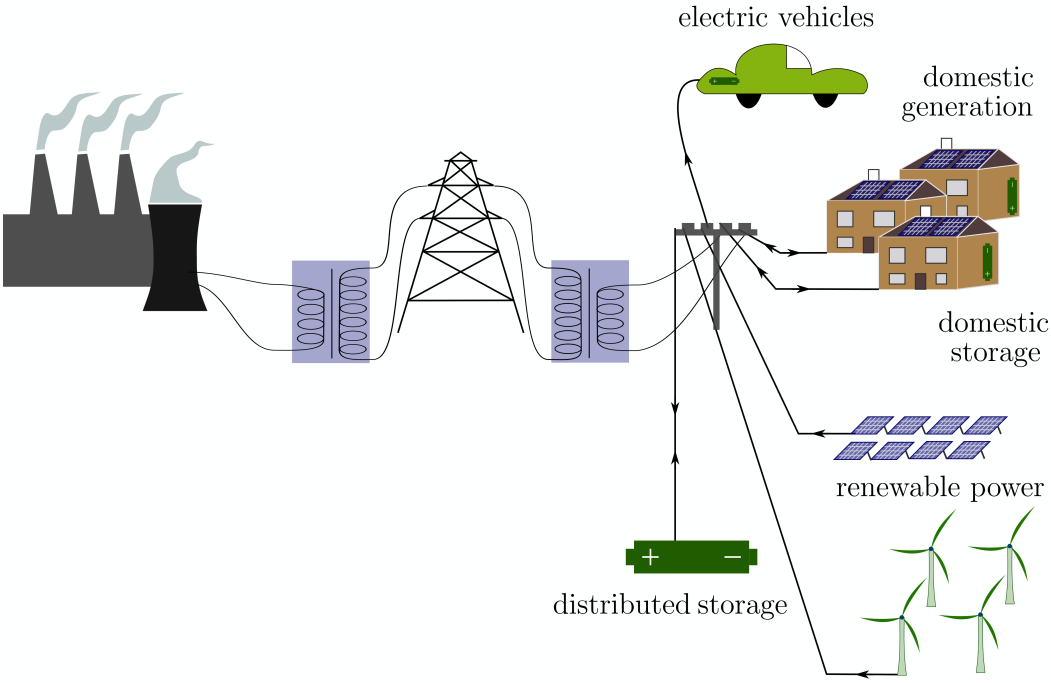

(b) 'Smart' Electricity Grid

Figure 2.1: Simplified illustration of an electricity grid. Traditionally power flowed from generators through the transmission and distribution systems to consumers (a). With the arrival of new technologies such as renewable power, smart meters and electric vehicles, electricity can also be generated, stored, and supplied into the grid from the consumer side (b).

the stable and secure operation of the electricity grid involves far more than just maintaining the frequency at its nominal value, for example, careful observance of voltage limits. Many excellent texts can be found explaining in great detail the structure and requirements of the electricity grid, such as Kundur et al. [13] and Eremia and Shahidehpour [18]. In this introduction we focus on the aspects of the electricity grid and system stability most relevant to our work.

2.1.2 Operation

Electricity Markets

Like any commodity, electricity is traded on markets. Domestic electricity consumers pay a pre-arranged tariff to companies called *suppliers*, who procure the electricity from a range of markets. Procurement time-scales range from several years down to one hour in advance of consumption. Unlike other commodities, electricity has very strict constraints on its physical flow from where it is generated to where it is consumed. In order for the electricity grid to operate, the amount of electricity being consumed (bought) must closely match the amount being generated (sold) at all times. This can be difficult to ensure, because predicting national demand ahead of time is imperfect, and generators occasionally disconnect from the system due to faults. Add in the volatility and unpredictability of renewable resources such as wind power and we have a market where few agents know precisely how much power they have to sell, and no suppliers know exactly how much to procure for their consumers. This results in small imbalances between supply and demand, causing the aforementioned physical network challenges. Electricity trading arrangements are therefore designed to incentivise accurate forecasting and to settle inaccurate payments. In this section we introduce the basics of electricity markets and the role of the System Operator (SO) in keeping the grid balanced and secure.

In GB the electricity trading arrangements are overseen by the company Elexon. Consumers are able to choose their supplier and energy can be traded between suppliers, generators (who may also be suppliers) and 'non physical traders' such as banks. Although electricity flow is continuous, for the sake of trading, time is split into half hour units called 'settlement periods' for which electricity can be traded, from several years up to one hour in advance of real time. Due to the nature of the electricity grid, although bilateral trades may exist between, for example, a generator and a supplier to a certain region, in reality it is impossible to tell where the

electricity originated from when it reaches a consumer. What is important is that the total power bought minus sold and the total power consumed minus produced, ultimately balance overall (accounting for transmission losses). The physical balancing of the system is done by the SO which in GB is National Grid, a private company regulated by the Office of Gas and Electricity Markets (Ofgem). National Grid's role as the SO is to ensure that the system operates safely and securely at all times in the most cost-effective way for consumers. This means redressing any power imbalances and preventing grid instabilities through 'imbalance settlements' and 'balancing services'. Imbalance settlements involve accepting *offers* from agents to increase their generation/reduce demand, for a price, and/or accepting *bids* from agents to pay the SO to reduce generation/increase consumption[4] so that the predicted demand matches the amount procured in the markets [19]. Alongside market balancing, the SO also ensures the physical balancing of the system by maintaining system stability, through the use of balancing services, as we explain below.

Power System Stability

Power system stability is defined by the IEEE/CIGRE Joint Task Force on Stability Terms and Definitions as "the ability of an electric power system, for a given initial operating condition, to regain a state of operating equilibrium after being subjected to a physical disturbance, with most system variables bounded so that practically the entire system remains intact" [20]. Analysis and consideration of this ability is simplified by considering the three classifications of power system stability separately: *rotor angle stability, voltage stability* and *frequency stability*. Rotor angle stability refers to "the ability of synchronous machines in a power system to remain in synchronism after being subjected to a perturbation" [20]. Voltage stability involves maintaining safe and steady voltage levels throughout the system through reactive power balancing[5]. As introduced in Section 2.1.1, frequency stability is the ability of the system to maintain the grid frequency within a small range of nominal frequency, through supply and demand balancing actions. Frequency stability is the focus of our attention for the majority of this thesis. For more information on the other types of power system stability see, for example, [13] or [20].

A vital part of power system stability (and the analysis thereof) is the concept of

[4]The exception is (currently) renewable suppliers receiving subsidies to generate power, that must be paid to reduce generation to cover the loss of earnings from feed-in tariffs.

[5]Reactive power is the "energy loaned periodically to the reactive elements in the load"[21] with frequency twice the grid frequency. For further reading on reactive power, see, for example, [13, 21, 22].

power system inertia. The inertia of a synchronous machine or spinning load is its resistance to changes in its speed of rotation. Inertial/rotational energy is stored in the rotating components of the power system and this inertia must be overcome in order to speed up or slow down the rotation. The heavier the rotating components in a generator or motor (and the greater their distance from the axis of rotation), the greater the inertia [23]. The total system inertia in a power grid equals the sum of the inertia from all synchronised components. A power system with high inertia, such as one with many synchronous generators like coal, gas and nuclear will naturally have greater frequency stability, since changes to the supply-demand balance take longer to affect the system due to the high inertia. When system inertia is low, for example in a system with many asynchronous components such as solar panels, wind turbines and DC interconnectors [6], the system is more sensitive to frequency changes, and therefore stability is lower. The anticipated reduction in system inertia over the next few decades [9] is part of the motivation behind our research into how domestic appliances can play a role in supporting system stability. Very closely-related to system inertia is the stored kinetic energy in the system. System inertia is a more commonly discussed concept in the literature, but the data we will use in Chapter 4 includes the stored kinetic energy of the system, rather than system inertia. They are related by the equation $E_k = \frac{1}{2}I\omega^2$, where I is total inertia and ω is angular velocity.

Balancing Services

Balancing services are a range of options available to the SO to mitigate against unexpected changes in supply or demand and potential faults on the transmission or distribution system. Typically the procurement of balancing services involves paying a generator or consumer to be prepared to act if a fault occurs on the system, or to act continuously to keep the system prepared for such an event. In this section we describe the current set of balancing services in Great Britain [25].

The SO is required to maintain system frequency within *statutory limits* (50±0.5Hz) and, in the absence of incidents such as generator outages or power line faults, within *operational limits* (50 ± 0.2Hz). This is achieved by employing different types of **frequency response**[7]. The most common types of frequency response service

[6] An *interconnector* is an electricity link between power grids in different countries. For example in GB there are currently four interconnectors, to France (2GW), to the Netherlands (1GW), to Northern Ireland (0.5GW) and to the Republic of Ireland (0.5GW) [24].

[7] In other countries such as the United States frequency response is known as frequency regulation.

available to the GB System Operator, National Grid, are

- *Mandatory Frequency Response:* most generators are required to provide this service in order to connect to the grid. There are three types:
  - *Primary Response:* increase power output/decrease demand within 10 seconds of a frequency incident,[8] sustained for a further 20 seconds if required
  - *Secondary Response:* increase power output/decrease demand within 30 seconds of an event and sustained for 30 minutes as required
  - *High Response:* reduce power/increase demand within 10 seconds of an event and sustain indefinitely (as required)
- *Firm Frequency Response:* procured via a tendering process, a provider must supply at least 10MW of energy as either:
  - *Dynamic Response:* continuously varying output in response to frequency deviations away from 50Hz
  - *Static Response:* delivery of a pre-determined increase/decrease in power output when the frequency hits a set level (step-function response)
- *Frequency Control by Demand Management (FCDM):* industrial/commercial consumers are paid for the interruption of their power supply for thirty minutes, typically thermal appliances such as supermarket fridge-freezers or hotel air conditioning systems
- *Enhanced Frequency Response (EFR):* a new service that requires a full response within one second of an event. The first tendering exercise was held in July 2016, when 200MW of EFR was procured from various energy storage providers.

Based on the current power system conditions such as system inertia, time of day, and the largest power generator/interconnector power supply to the system that could be lost due to a fault, National Grid procure a combination of these services from months to hours ahead of real time.

On longer time-scales (minutes to several hours) **reserve** services are used to support the system. Reserve services have a longer start-up time than frequency response

[8] A frequency incident/event is a sudden change in the power balance, such as when a line or generator experiences a fault.

services, and in some cases are initiated manually. There are three main types of reserve:

- *Fast Reserve:* response within 2 minutes of an event, increasing power/decreasing demand by a minimum of 25MW/minute and providing at least 50MW of power
  - Required to be highly reliable and paid to be constantly ready for an event
  - Typically used to take over from frequency response providers and to support 'TV pick-ups' (demand spiking due to television scheduling)
- *Short-Term Operating Reserve (STOR):* provision of at least 3MW of generation or demand reduction within 4 hours of instruction and sustained for at least 2 hours
- *BM Start-Up:* Balancing Mechanism Units (BMUs) which were not scheduled to run can be procured to be made available to National Grid for reserve.

Additional types of service include **reactive support**, current and developing **demand side response** services and **constraint management** services. More information can be found on all of the above balancing services on the National Grid website [25].

2.2 Renewable Energy

Faced with the threat of climate change, many nations have been setting targets to reduce carbon emissions. For example, the UK government has committed to reducing emissions by at least 80% of 1990 levels by 2050 [26]. To reduce our dependency on fossil fuels, we have seen a huge surge in the development of renewable energy and so-called 'smart' technologies, such as smart metering in homes, electric vehicles, and various forms of energy storage. As technologies become more cost-effective, either through technological advances, mass-production or government subsidies, they are becoming increasingly prevalent on the GB power grid. Such changes naturally bring a mixture of challenges and opportunities for system operability, which must be carefully navigated. Anticipating changes to demand and generation and the potential issues requiring mitigation is part of the role of the SO.

Each year National Grid produces its 'Future Energy Scenarios' (FES); four projec-

tions for the changes to energy supply and demand in the coming decades, based on input from stakeholders from all areas of the energy industry. The 2017 scenarios (projections to 2050) are

- Two Degrees (TD) - high economic growth and investment in green technologies and strong government policy to drive change, the only scenario in which the UK meets its carbon targets
- Consumer Power (CP) - high economic growth, lower focus on green government policies, market-led investments in smaller generation with shorter-term financial returns
- Slow Progression (SP) - low economic growth competes with desire to meet carbon targets, cost-effective long-term environmental policies
- Steady State (SS) - low economic growth, business as usual, security of supply at low cost, little investment in long-term solutions, the 'least-green' scenario.

Figure 2.2 shows the projections for the installed capacity of each class of generation for each of the four scenarios. We see a moderate-to-large increase in the installed capacity of renewables in all four scenarios. The role of interconnectors and storage also increase, as the amount of installed fossil-fuel generators reduces.

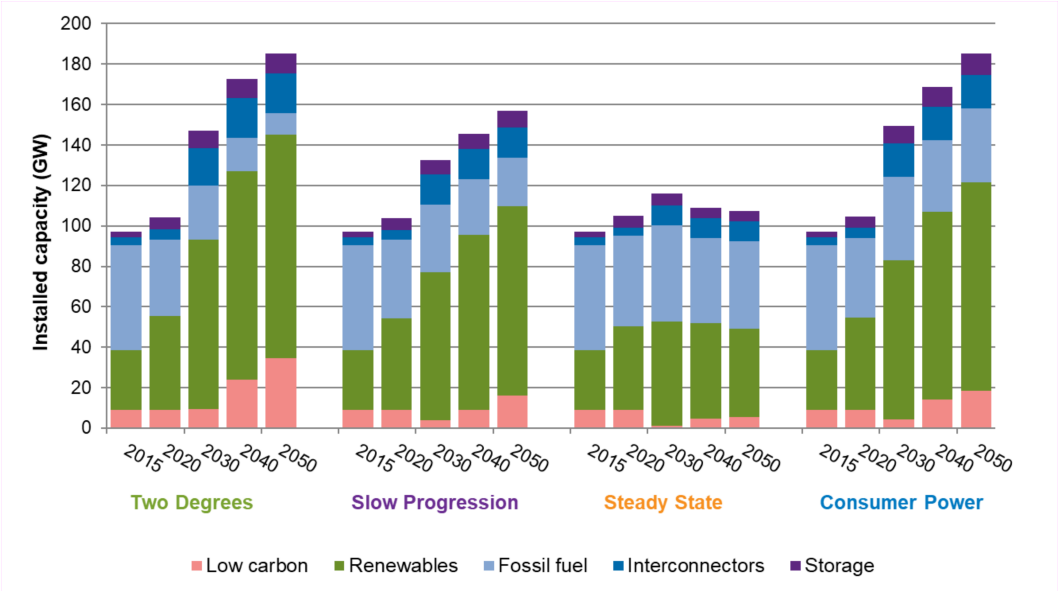

Figure 2.2: Installed generation capacity projections by type, for each energy scenario in the 2017 FES [27].

Many papers and industry reports have been written on the potential challenges for

an electricity grid that arise from increased use of renewable energy, in particular wind power and solar PV, such as [1, 9, 28–31]. The key operational challenges for a grid with a high penetration of renewables (or distributed renewables) are reduced inertia, greater RoCoF (Rate of Change of Frequency), fewer generators capable of providing frequency response, voltage fluctuation and harmonic distortion, power quality issues, and the supply volatility and unpredictability caused by the nature of the weather. The challenges most relevant to our work are the first three, which directly impact the electricity grid frequency and/or the need for greater frequency response.

As discussed above, the higher the system inertia, the slower the system will be to grid frequency fluctuations. To provide inertia to the system, a component must be synchronously connected (rather than connected with a power electronic converter). To provide a significant amount of inertia, the component needs to have large rotational inertia, such as a heavy motor or a turbine in a power plant. Solar panels have no moving parts and therefore contribute no inertia to the system. Wind turbines and interconnectors are connected via power electronic converters, and so at present they are unable to supply system inertia. With lower inertia the frequency changes more rapidly. When the RoCoF is high, the load-shedding controller will decouple its component(s) from the system to protect them. Certain renewable technologies such as solar PV are particularly sensitive to high RoCoF and in the event of a frequency incident may remove themselves very quickly from the system, exacerbating the frequency issues.

Traditionally energy was generated by a relatively small number of very large power plants, such as coal, oil and gas. In recent years energy generation has become far more distributed, meaning that we now have a large number of very small generators on the distribution network with a large spatial distribution. These generators are often invisible and beyond the control of the SO[9]. They can also dramatically alter the way power flows in the distribution network, since bi-directional flows become possible. In recent years decentralised generation has grown to comprise over a quarter of installed capacity in GB. National Grid's Future Energy Scenarios [32] anticipates that this percentage will increase to 34-40% by 2025 and to 34-50% by 2050. According to their analysis, to achieve the UK carbon targets would require the highest percentage in each of these ranges.

The analysis presented in National Grid's System Operability Framework 2015 [9]

[9]The SO does not have direct observation of these generators and their effects are seen as reducing system demand.

predicts a number of challenges for frequency control going forward. System inertia is expected to reduce over the next 20 years in all four future energy scenarios during periods of low demand and/or high renewable power generation. Primary frequency response requirements are expected to increase by 30-40% by 2020, and new response providers will be needed to meet these requirements.

2.3 Smart Grids and Demand Response

Alongside the recent advances in renewable technologies is the development of the 'smart grid' concept. According to EPRI, "The term 'Smart Grid' refers to a modernization of the electricity delivery system so it monitors, protects and automatically optimises the operation of its interconnected elements – from the central and distributed generator through the high-voltage transmission network and the distribution system, to industrial users and building automation systems, to energy storage installations and to end-use consumers and their thermostats, electric vehicles, appliances and other household devices" [33]. To some, the term 'smart grid' is something of a cliché, over-hyped and over-applied. However, it is useful to distinguish between the centrally-controlled, generator - network - consumer power flow model of the 20th century, and the vision for future electricity systems with greater complexity and control schemes. This is not to say that current (or past) power grids lacked intelligence. Indeed, complex software and automated routines are essential parts of what is an incredibly complex system, that in many cases, spans thousands of miles and/or millions of homes. Rather, by integrating new electrical and communications infrastructures that allow greater participation and support from distributed resources, such as domestic batteries or electric vehicles, the grid will become smart*er*. In the words of Borlase *et al.* "A truly modern smart grid would include sustainable concepts that leverage proven, cleaner, cost-effective technologies available today or under development" [14].

A key part of any smart grid is demand-side response (DSR)[10]. DSR refers to a change in a consumer's (or an appliance's) normal electricity demand at a certain time, in response to an incentive or control from a supplier or SO. Dehghanpour and Afsharnia [34] classify five types of demand response services:

- *Energy efficiency services* implement energy saving technologies to reduce de-

[10]The terms 'demand(-side) response' and 'demand management' are often used interchangeably in the literature, although they may distinguish between demand responding to system stability requirements and load shifting to reduce peak demand.

mand through efficiency savings

- *Price response programs* incentivise consumers or automatic controllers to schedule or interrupt demand (typically appliances such as washing machines or dishwashers) to consume power at cheaper times of day, where price may depend on prices paid by suppliers or needs of the electricity grid
- *Peak shaving programs* spread out the total load at peak times to reduce the maximum energy requirements of the system each day
- *Regulation response* employs centralised control to assist with power balancing on a highly frequent basis
- *Frequency response (spinning reserve) schemes* employ centralised or decentralised (through local measurements) control to provide demand response in real time, on very fast time-scales.

Each type of response may have an important role to play in the future of the smart grid, as flexibility becomes more important to the system. In this thesis we concern ourselves with the final type of DSR; the potential to use demand-side appliances for the provision of dynamic frequency control.

2.4 Frequency-Sensitive Thermostatically-Controlled Loads

2.4.1 Introduction

A thermostatically-controlled load (TCL) is an appliance/device whose operation is controlled by a thermostat. Examples include fridges, freezers, air conditioners, hot water tanks, heat pumps and swimming pool pumps[11]. They operate to maintain a status quo, such as keeping food, water or a building at a roughly constant temperature. Unlike other appliances such as kettles, televisions and electric lighting, users pay little or no attention to whether their TCLs are switched on or off, and have no preference, so long as the proper temperature cycling continues to maintain the room temperature, food freshness or hot water availability. This means that the exact time at which a TCL switches on or off in its cycle is relatively flexible, and it is this flexibility that renders them potential providers of DSR.

[11] Although not strictly operated by a thermostat, swimming pool pumps operate in the same manner, and so have the same DSR potential.

Although controlling a large population of small appliances brings new challenges such as control schemes and service/remuneration designs, in addition to being a potential resource that already exists, there are also benefits from using an aggregated resource compared to a single large DSR provider. For example, very fast, continuous responses are possible in ways that are not always possible with a single machine. Spatially distributed TCLs have the potential to redress local fluctuations before they create problems at the system level [35]. It can also be argued [36] that availability and reliability is improved when splitting a service between a multitude of providers, compared to a single unit which will become completely unavailable in the event of a fault or scheduled repair. It is estimated in [37] that around 40% of total demand in Europe comes from household appliances, of which fridges and freezers make up 15%, electric storage water heaters 9%, and air conditioners around 1%[12]. Therefore, although individually TCLs consume very tiny amounts of electricity (relative to say, the power generated by a gas power plant), as a large population, they have the potential to make a meaningful contribution to demand-side (and of interest to us, frequency) response.

As explained above, the electricity grid frequency is primarily affected by, and is therefore a measure of, the difference between total supply and demand on the system. Ensuring the frequency remains as close as possible to 50Hz (the nominal frequency) requires keeping supply and demand closely matched at all times. TCLs operate between two temperature set points, switching on when one is reached, and remaining on until the temperature hits the other set point. Normally these set points are fixed, unless a user interferes with operation, which is relatively rare. Figure 2.3(a) shows an example temperature trace of a cooling device such as a fridge. In this hypothetical case the fridge spends 20 minutes switched on until it reaches its lower set point when it switches off for 40 minutes.

Electricity grid frequency can be sensed anywhere in the network, and a TCL with a frequency sensor has the capability to provide sub-second response to a fluctuation [38]. We can make a TCL frequency-sensitive by allowing the set points to vary according to some function of the grid frequency. Continuing the example above, we would want the fridge to consume less power when the frequency is less than 50Hz and more power when the frequency is higher than 50Hz. Consuming less power means increasing the set points so that the fridge stays off for longer or switches off sooner in its cycle. Consuming more power requires the opposite. Figure 2.3(b)

[12] Air conditioners make up a far higher percentage of demand in summer in hot countries such as the United States, and so a large proportion of the literature is devoted to them.

gives an illustrative example of frequency-sensitive operation of a fridge. Exactly how the temperature set points depend on the frequency is an important part of any control design.

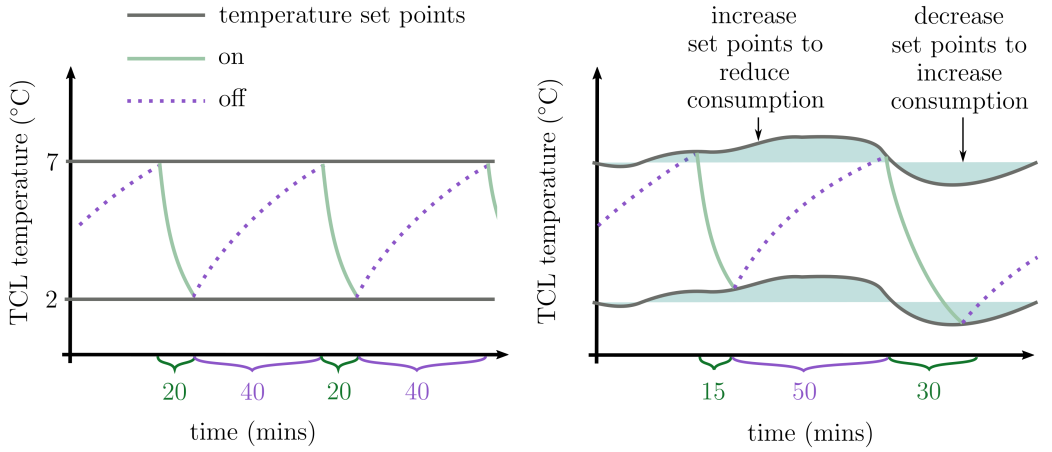

(a) Normal TCL operation

(b) Frequency-sensitive TCL operation

Figure 2.3: Illustration of how TCLs normally operate (a) and how frequency-sensitive temperature set points could increase/decrease the power consumption of a population by advancing/delaying switching of individuals.

The concept of frequency-sensitive appliances is not a new one. In fact, the technology to control a load based on some logic applied to system frequency was filed for patent in 1979 by Fred C. Schweppe at the Massachusetts Institute of Technology. He called it the *'Frequency Adaptive, Power-Energy Re-scheduler' (FAPER)*, noting that the FAPER is applicable to devices "characterized by a need for a certain amount of energy over a period of time in order to fulfil their function and an indifference as to the exact time at which the energy is furnished" [39]. More sophisticated technologies have since been developed, such as the *Grid stabilising system* by Hirst in 2010 [40] for TCL behaviour to be governed by the magnitude of grid frequency deviations. Although the technology for creating frequency-sensitive TCLs has existed for nearly 40 years, implementation remains limited to a relatively small number of trials [41–45]. There are a number of reasons for the absence of large roll-outs of highly distributed DSR schemes [46, 47]. Historically, control paradigms from both technical and economic perspectives have been established for service provision from a (relatively) few number of large power plants. Understandably, the critical nature of electricity grid operation and security deters potentially risky changes and experimentation and so a great deal of motivation is required for shifts away from traditional approaches. There is inherent complexity and potentially

reduced reliability in procuring services from thousands of very small demand-side resources, which is undoubtedly an obstacle to be overcome. Effects on consumers and their appliances will be of concern to potential participants. Finally, it will be crucial for the success of any scheme to adequately address the requirements for minimum participation numbers and to develop the right business models that ensure fair rewards and effective incentives.

Research into the possibility of using TCLs for grid balancing services began in the 1980s with key papers such as [48–52]. The changing energy landscape of the 21st century has brought a new focus to the use of TCLs for electricity grid support and a wealth of literature on the topic [34, 35, 41, 45–47, 53–78]. Work has varied in nature from mathematical frameworks to numerical simulations and real-world trials. Most of the theory can be applied to any type of TCL, and simulations have touched on many types of TCL technology. A variety of control schemes have been proposed, from centralised, direct-load control to completely distributed, autonomous load control. An important obstacle to the introduction of TCLs for frequency response, in particular, is the propensity for TCL temperature cycling to become synchronised. This can be triggered by frequency deviations that become reinforced and cause system instabilities. In the remainder of this section we introduce synchronisation phenomena in a general setting, summarise TCL synchronisation evidence and discussions in the literature, and describe the different types of control schemes that have been proposed.

2.4.2 Synchronisation

Mitchell defines a complex system as one "in which large networks of components with no central control and simple rules of operation give rise to complex collective behaviour, sophisticated information processing, and adaptation via learning or evolution" [79]. There are many different examples of complex systems and phenomena. Neurons in the brain are simple electrical pulsators that collectively receive and respond to chemical signals, from which physical actions and conscious thought emerge. In physics, complex phenomena include phase transitions, such as water freezing, ice melting, or condensation. In economic systems, bubbles in stock markets emerge from many agents buying and selling with no central director. In such systems, the individual elements are typically fairly simple, and in some cases, can be fully understood at an individual level. What makes a system more than just complicated are the interactions between components that result in emergent phenomena, which no amount of study of an individual component can predict or

explain. One such class of emergent phenomena is synchronisation.

Synchronisation Phenomena

Firefly colonies stretching miles in SouthEast Asia have been observed to flash in unison to awe-inspiring effect. Audiences in eastern-European theatres applaud and the applause becomes a beat of clapping in unison. Walkers on the Millennium Bridge in London were initially found to cause major oscillations on the bridge as their footsteps started falling in rhythm. Simple oscillators with no centralised control spontaneously synchronise their cycles to great effect [12]. In some cases the phenomenon is beautiful, mystifying to the casual observer, impressive to behold. In other cases the effects can be devastating.

Power grid stability relies on generator motors rotating in synchrony in order to prevent inter-area oscillations and large frequency perturbations [80, 81]. Modelling power grids as collections of coupled oscillators has gained recent attention in physics [82–87]. These references describe a simplified power system using the Kuramoto framework and assess the stability of the system. For example, [83] considers the impact of decentralising power on system stability and finds that self-synchronisation is still possible and that decentralised grids are "more robust to topological failures". The authors in [86] establish a synchronisation condition for a general class of coupled oscillator models and in particular apply their results to power networks. In contrast to the work that follows on synchronisation with a population of TCLs, power grids depend on synchronisation in order to operate securely. For a population of generators, synchronisation is highly *desirable*, and work such as the aforementioned references attempt to improve how quickly and robustly a network can synchronise. As explained below, the synchronisation of TCL cycles is exactly what needs to be *avoided*.

Synchronisation in TCL Populations

In 2007, Short, Infield and Freris published *Stabilization of Grid Frequency Through Dynamic Demand Control* [69]. We discuss their work in more detail below, but one area they note for further investigation is the potential for the "temperature-cycling of appliances to become synchronised (especially after a serious frequency excursion)". The fear is that if a large population of TCLs is responding to the same frequency signal, then rather than having a roughly constant total load from the

appliances, we may start to see spikes and troughs in the load as TCL population switching behaviour starts to cluster temporally. This would have a destabilising effect on the system, and lead to an overall detrimental impact on system stability. The simulations in [69] do not find evidence of synchronisation, however, we believe that this is largely due to the heterogeneity in the simulated TCL population. The population was divided into 1000 groups to be modelled separately, and each group "was randomised by altering every parameter to within ±20%". An important contribution of this thesis is to explore the effects of heterogeneity on TCL synchronisation.

A number of simulations in the literature indicate TCL synchronisation following a frequency disturbance, for example [53, 60, 61, 65, 69–71]. Of particular significance is the 2012 publication by Angeli and Kountouriotis; *A Stochastic Approach to "Dynamic-Demand" Refrigerator Control* [53]. Building on the work of Short *et al.* [69], the authors highlight the possibility for synchronisation and the resulting system instabilities through simulations. In one case the authors simulate the effects on a homogeneous fridge population of a 1.32GW power loss lasting 15 minutes before a 10 minute ramped power recovery. It should be noted that while a 1.32GW loss is possible on the GB grid, fast reserve services would begin to make up for some of the loss after around 2 minutes, rather than the 10 minutes assumed. Under the proposed control scheme in [69], the resulting deviations in system frequency and refrigerator power consumption indicate "overall unstable behaviour" and undesirable effects for the fridges and the system. The authors also offer theoretical arguments for the long-term tendency of the system towards TCL synchronisation. It is reasoned that any "small periodic ripples in power system frequency will gradually entrain oscillations of refrigerators that have similar frequencies of oscillation, thus reinforcing the frequency ripple and eventually leading to an even larger number of entrained refrigerators".

As the title suggests, *Emergent synchronisation properties of a refrigerator demand side management system* by Kremers *et al.* [61] and their subsequent book chapter [60] explore this topic in some detail. The authors use an agent-based model of frequency-sensitive refrigerators with greater detail than in the aforementioned research. For example, stochastic door opening and the impact of fridge contents on temperature are considered. They find three possible types of outcome with the same parameters due to the stochastic nature of their model, as shown in Figure 2.4.

The authors argue that the "main reason for the emergence of oscillation is the rebound effect" [60] which comes from the responding refrigerators switching back on

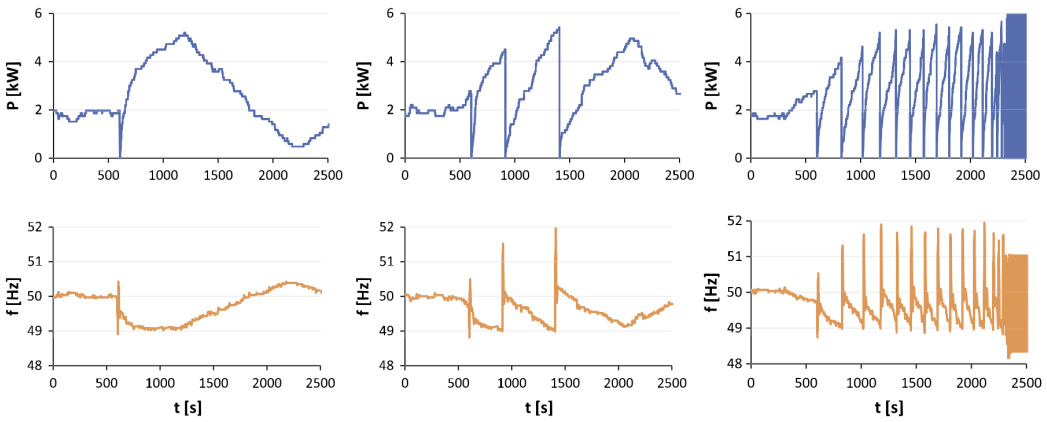

(a) Stable (b) Partial (c) Oscillating

Figure 2.4: Taken from [61]: "Examples of different regimes of the refrigerator system. On top, the total load curve of the refrigerators and below the corresponding grid frequency. The simulations were performed with the same parameters. Due to the non-deterministic nature of the model and for the given parameterisation, each of the three regimes can appear".

after having switched off to support a large frequency deviation. Although synchronisation is observed in the heterogeneous population (unlike in [69] where it is only hypothesized), the control scheme used in [60, 61] is significantly different. Rather than allow the temperature set points to vary continuously in time with the grid frequency, the refrigerators are switched off at a specific frequency point, and switched back on following a significant frequency drop at another. The benefits of the first control scheme are that the appliances best-positioned in their cycle respond fastest to the needs of the grid[13]. In the event of a frequency incident (a sudden significant drop in frequency caused by, say, an unexpected loss of a large generator), all appliances switch off at exactly the same time, and will reconnect at exactly the same time. We believe that this is a significant contributor to synchronisation observed in the simulations, and accordingly choose our analysis of frequency-sensitive temperature set points as the means to implement demand-side response. Some of the key aims of our research are to determine whether a homogeneous population of TCLs will always be at risk of synchronisation, and to what extent (if any) introducing heterogeneity can mitigate this risk.

[13]The coolest refrigerators switch off soonest and the warmest switch on soonest.

2.4.3 Control Strategies

In recent years a number of different types of control strategy for TCLs to provide frequency response have been proposed, many of which are discussed and compared in [34, 46, 74]. There are two main classes into which these types of TCL control schemes can be divided: *centralised* and *decentralised* control (with a spectrum in between). Their key features and comparative advantages and disadvantages [34] are summarised in Table 2.1.

Table 2.1: Comparison of centralised and decentralised TCL control strategies. Informed by, for example, [34, 88].

	Centralised Control	**Decentralised Control**
Key Features	• TCLs instructed by a central controller • 2-way communication in all TCLs	• Autonomous local control • Control scheme established once, may be updated periodically
Advantages	• Highly controllable • Reasonably predictable	• No communications infrastructure required • No security risks • Very fast response possible
Disadvantages	• Establishing and maintaining a secure communications network are very expensive • Response time limited by communication speed • Vast amounts of data to manage • Data and appliance control security risks • Negative public perceptions of external control of home appliances	• Response is less predictable than with centralised control • Synchronisation and instability effects possible and not yet fully understood • Errors and noise in local frequency measurements more likely

Early work on the behaviour of aggregated TCLs began in the 1980s with centralised control. Of early mathematical note, in 1985 Malhamé and Chong developed a mathematical framework for a homogeneous population of houses with thermostat-controlled heating, with a view to help reduce peak load. They derived a Fokker-Planck equation model for such a population in a stochastic envi-

ronment that was extended to a heterogeneous population through perturbation analysis [50]. A criticism of models such as [49–52] is that their complexity and lack of general closed-form solution renders them unsuitable "to be effectively used by well-understood feedback control design methods" [67]. It is noted [67] that these difficulties appear to be the reason why so many of these models are open-loop control (for example [49–52, 70]). In reality the power system feels the direct impact of TCL response and so closed-loop control models are preferable. When a centralised controller issues instructions to TCLs, these instructions do not have to be influenced by the resulting TCL behaviour, and so typically the control is open loop. Conversely, the decentralised control approaches of interest to us are closed-loop control; the system is affected by the TCL response behaviour which in turn impacts the control scheme in each TCL. Decentralised control strategies are discussed in greater detail below.

An exception to open-loop control is the work by Callaway in [57] which, developing the framework in [50], proposes manipulation of the temperature set points by a broadcast signal from a feedback controller. The approach is applied specifically to air conditioners to support wind smoothing[14]. Closed-loop dynamics are also captured in the aggregate TCL response models proposed in [68, 75] for heterogeneous populations of air conditioners.

It is widely accepted that if millions of TCLs could be used for frequency response they could potentially provide a valuable resource for the system. However, if each device needed constant communication with a central controller, sending data about its temperature and switching history and receiving operation instructions, the economics and security risks would severely outweigh the benefits of the service. Public perception of the service is also vital for the implementation of any control scheme that involves appliances in people's homes. For these reasons we choose to focus on decentralised control for our research. A better understanding, however, of the potential undesirable side-effects of decentralised control is required before any control strategy could be put in place.

[14]Wind smoothing is the varying of supply or demand to smooth out the natural fluctuations in wind power generation caused by continually varying windspeeds. It is important for improving the stability and secure operation of electricity grids in the presence of large amounts of wind generation.

Deterministic temperature set point control

The simplest form of decentralised TCL control is to change the TCL temperature set points according to some deterministic function of system frequency. The advantages are that simple rules require little processing and the TCLs in the best position to respond to frequency deviations respond first, allowing those that are least ready to wait a little longer before altering their preferred behaviour. In 2007, Short, Infield and Freris published *Stabilization of Grid Frequency Through Dynamic Demand Control* [69] which inspired and influenced a significant body of work in this area. The authors simulate the operation of 1320MW of non-identical fridge-freezers responding to large deviations in grid frequency and fluctuations in wind power. They propose a control scheme whereby the TCL temperature set points are linearly dependent on the grid frequency. Figure 2.5 (reproduced from [69]) shows the difference between the normal operation of a fridge and the devised linear frequency-sensitive control scheme proposed. When the frequency is higher than 50Hz the temperature set points decrease, allowing the fridges to switch on sooner or stay on longer, thereby advancing power consumption to meet the generation surplus causing the frequency rise, and *vice versa* when the frequency drops below 50Hz. Short *et al.* conclude that the use of many TCLs in this way "has the potential to provide significant added frequency stability to power networks, both at times of sudden increase in demand (or loss of generation) and during times of fluctuating wind power" and "may result in considerable cost savings" [69]. It is perhaps unsurprising, then, that this initial study of TCLs for frequency smoothing led to a surge of interest from the research community.

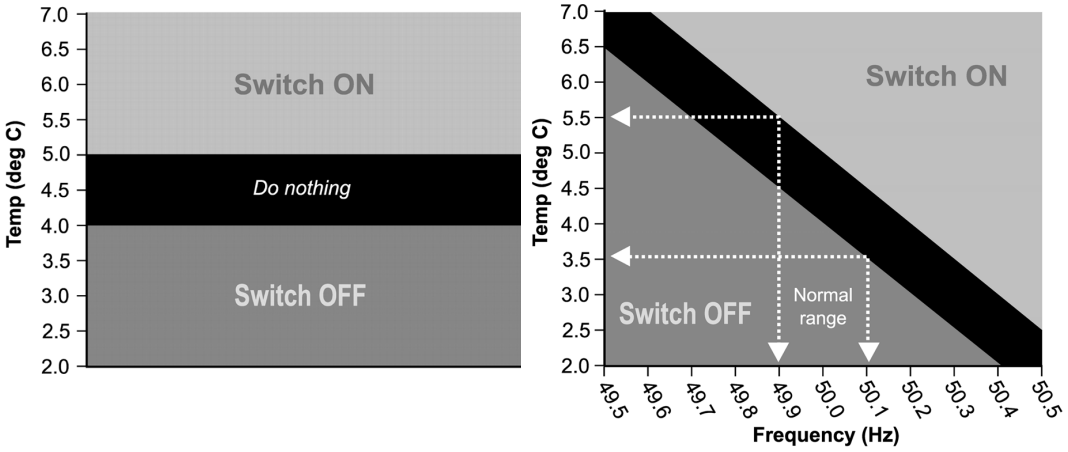

Figure 2.5: Taken from[69]. Normal fridge switch on/off rules (left), linearly frequency-sensitive switching rules proposed in [69] (right).

The challenges with this type of control are the aforementioned potential synchronisation issues, and in our work we attempt to fully explore these issues and look to solve them through the addition of heterogeneity to the TCL population.

Stochastic temperature set point control

In order to prevent synchronisation in a population of TCLs with decentralised control, many papers introduce stochasticity into the control scheme. Typically this takes the form of randomising switch on times following a response action or randomly switching a TCL on or off in addition to the normal control rules. For example, Xu *et al.* [47] simulate a heterogeneous population of electric heaters in the Nordic power grid using fixed frequency threshold response and the deterministic control proposed in [69], with the addition of stochasticity in two of the control parameters. They uniformly distribute the frequency switch-off threshold $f_{\texttt{off}}$ between 49.85 and 49.90 Hz and uniformly distribute the time to switch back on following a drop in frequency below $f_{\texttt{off}}$ between 4 and 6 minutes.

Molina-García *et al.* [66] use a distributed frequency-threshold control approach to model a heterogeneous population of different types of TCL. Figure 2.6 indicates the control approach - frequency deviations Δf are allowed to exist without response for a short period of time τ. Larger deviations cause response more quickly than small deviations, and depending on the type of TCL different threshold limits can be applied. TCL protection rules prevent devices from remaining switched off for too long or switching off too soon after a TCL switches back on following response. After the minimum recovery time the time of the next switch off is randomised to prevent TCL synchronisation.

In their 2012 paper [53] Angeli and Kountouriotis model domestic fridges as Markov-jump linear systems where the on/off switching is governed by transition probability rates rather than temperature set points. These rates are determined by choosing the desired population average temperature or duty cycle and the temperature probability density is steered towards a desired distribution. The authors show that their algorithm "yields a locally asymptotically stable closed-loop system, regardless of parameter values and control gains" [53]. They also eliminate the 'payback' phase (overshoots from fridges recovering lost energy following response actions). However, as noted in [72], in fully eliminating the payback phase the recovery time is longer for each device and rapid response is less feasible. In their 2013 paper Aunedi *et al.* [54] (including the authors of [53]) assess the economic and environmental ben-

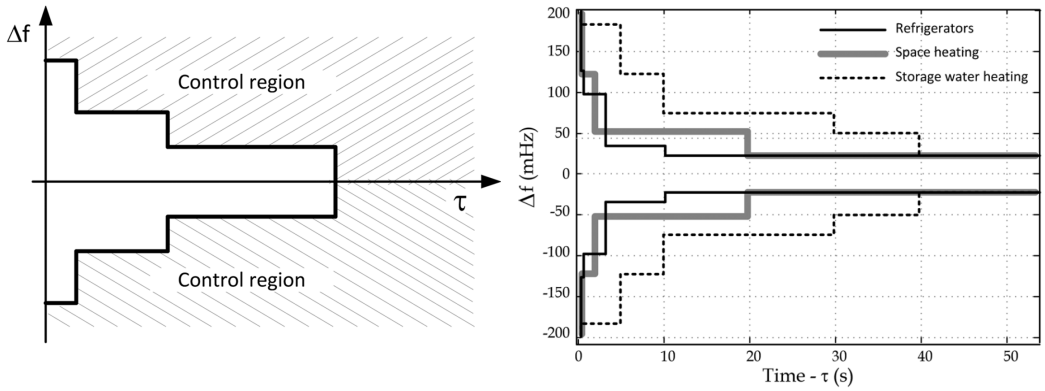

Figure 2.6: Individual load controller Δf-time characteristic (left), average characteristics for different types of TCL used in simulations (right), reproduced from [66].

efits of frequency response under the control scheme proposed in [53] in which the switching probabilities are optimised to prevent overshoots and instabilities. Additional hybrid control schemes are proposed, such as introducing safety temperature thresholds to prevent the fridges from exceeding their preferred temperature range, and making these thresholds frequency-dependent, to increase response speed for large frequency deviations.

Trovato, Tindemans and Strbac have also published a number of papers on stochastic control of TCLs for frequency response. For example, in their 2013 paper [72] the authors choose to let temperature set points depend on both frequency deviation and the rate of change of frequency (RoCoF), which helps speed up the response following a major loss. The deterministic scheme from [69] (with RoCoF included) and the stochastic control in [53] are compared for simulations of a very large (1.8GW) generator loss. In their later paper [73] the authors note the disadvantages of this approach, namely that particular scenarios require carefully-tuned parameters and that beyond the short-term, control over the power profile is limited. In their 2015 paper [73] the authors model a heterogeneous population of TCLs, each independently targeting a reference power profile. In this novel approach, the (estimated) net heating rate is used as a control parameter, which when combined with grid frequency, allows each appliance to compute the reference power profile. The control framework is simple enough to be implemented and simulations demonstrate a number of benefits compared with other approaches. A few issues remain outstanding, such as the need to prevent devices from switching too soon following one switch, due to the stochasticity of the control, and the lack of optimal choice for the reference power profile.

A very different approach to controlling TCLs for frequency response that still makes use of stochasticity is the use of mean-field game theory. For example, in [55] Bagagiolo and Bauso assign a cost function to each TCL (or 'agent') to incentivise preferable behaviour from the appliance perspective in addition to frequency-responsive behaviour. Synchronisation issues are bypassed by introducing a switching probability of $\frac{1}{2}$ when the frequency requires no response. Further work on stochastic models of TCL populations for frequency response can be found in [89, 90] whose stochastic dynamic model is based on formal abstractions.

Fuzzy logic control

A number of papers employ fuzzy logic control to implement a demand-side control scheme. A fuzzy logic controller (FLC) "provides an algorithm which can convert the linguistic control strategy based on on expert knowledge into an automatic control strategy [...] in particular, the methodology of the FLC appears very useful when the processes are too complex for analysis by conventional quantitative techniques or when the available sources of information are interpreted qualitatively, inexactly, or uncertainly" [91]. FLCs are known to work well for nonlinear systems [92], such as the electricity grid, and avoid the computational intensity required for some other types of control. For example, in 1996 Bhattacharyya and Crow [93], motivated by increasing competition in the electricity market and anticipated growth in demand, proposed a fuzzy logic approach to use air conditioners for peak load shaving. Their scheme optimised both consumer comfort preferences and utility unit commitment savings. More recently, Goel *et al.* [94] have taken a similar approach that also considers transmission network reliability. They implement fuzzy dynamic programming to optimise a trade-off between "peak load shaving, operating cost reduction and system reliability improvement".

Fuzzy logic control for frequency response has also been explored, in particular for islanded power systems (small systems separated from a national, or much larger, system). For example, frequency control in interconnected two-area power systems using FLC is presented in [92, 95]. Pandiaraj *et al.* [96] use both electricity grid frequency and voltage as input variables for their FLC. The authors test their approach in a laboratory, creating an islanded 18kW power system consisting of water-heating loads and different amounts of wind power. They find that in general the load controllers were able to maintain frequency and voltage to within the required limits. Simulations suggest that on a larger system higher levels of control would be possible.

Price Signals

An alternative to direct instructions and frequency signals is the use of a price signal that TCLs could respond to. The advantages of price signals are that it is possible to measure the financial benefits to consumers of DSR participation, and individual consumers could potentially make their own choices about the value they place on service disruption at, say, given times of the day. However, current price signals typically change on half-hourly or at least several-minute time scales, which makes them ill-suited for dynamic frequency response. Reviews on the use of price signals for demand response can be found in references [97–99].

It is interesting to note that, just as with grid frequency-based control, demand-dependent price controls can also lead to unwanted oscillations in load response. For example, it is shown in simulations that a population of plug-in electric vehicles (PEVs) can exhibit "spontaneous emergence of significant oscillations" [46]. The oscillations are not guaranteed due to the randomised initial conditions of the PEVs, but the likelihood increases significantly with population size (see Figure 2.7).

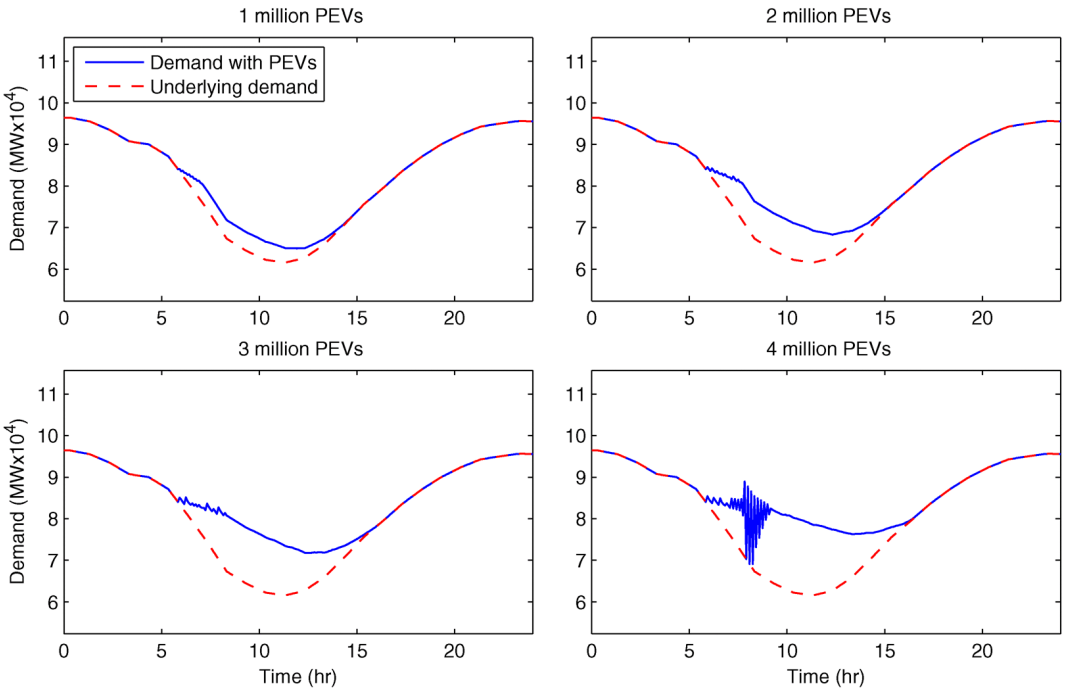

Figure 2.7: Total load demand due to price-based control of varying numbers of PEV loads, reproduced from [46].

An approach far better-suited to frequency response provision is proposed by Schäfer *et al.* [100]. Rather than receiving prices from a centralised controller, the authors

take a decentralised approach and each device calculates the price directly from grid frequency. Different functions for converting frequency into prices are considered, along with the effects of time delays on efficacy and instabilities. Oscillations and instabilities are found to be possible, but the authors argue that a well-chosen design for the controller and frequency-price coupling may allow these risks to be mitigated.

The potential for synchronisation and instability with price-based demand response is one of the two "major drawbacks" remarked upon in [35]. The other is the controversial nature of "exposing customers to price volatility". Willingness of consumers to participate in these sort of schemes is vital for success, and any hint that participation could increase energy bills would be likely to prevent the large-scale roll-out required. For our non-dynamic pricing approach we consider that DSR participants would either be incentivised through some kind of regular payment/utility bill discount, or be required by law to participate (provided that the end-user can be guaranteed not to be adversely affected).

2.4.4 Summary

The last ten years have seen a wealth of research develop on the use of TCLs for demand-side response, driven largely by the challenges of integrating renewable energy sources, and the opportunities of a more 'smart grid' approach to electricity grid operation and design. The potential benefits and challenges of using TCLs with decentralised control for frequency response are summarised in Table 2.2. TCLs have the potential to provide a valuable service to the System Operator, but several obstacles must be overcome in order to achieve a large-scale, cost-effective roll-out. A number of studies have anticipated or demonstrated through simulations the potential for TCLs to synchronise and cause problems on the network. In [53] Angeli and Kountouriotis offer theoretical arguments for the long-term tendency of the system towards TCL synchronisation. We concur with the mathematical reasoning presented, nevertheless, we believe that further reasoning and inquiry is required for a more complete understanding of this phenomenon.

Although stochastic controls have been widely proposed to prevent synchronisation, we consider the potential unpopularity of randomness in domestic appliance operation, and reduced mathematical tractability sufficient reasons to focus on deterministic control schemes. In this thesis we develop a mathematically rigorous treatment of the homogeneous case, and explore the potential for the natural heterogeneity in a population of TCLs to prevent synchronisation issues through simulations based

on real system data.

Table 2.2: Summary of the potential benefits and challenges of using TCLs with decentralised control for frequency response [101].

Benefits	**Challenges**
• Low-cost system stability improvements	• Achieving sufficient consumer participation
• May increase the amount of renewable generation that can be safely incorporated onto the system - environmental benefits	• Eliminating undesirable effects on grid stability during the 'payback' phase such as overshoots and synchronisation
• May reduce the number of fossil-fuel generators to run part-loaded on the system for frequency response	• Preventing detrimental or noticeable effects on end-user experience
	• Determining the optimal control implementation

"Nothing in life is to be feared, it is only to be understood. Now is the time to understand more, so that we may fear less."

Marie Curie

3

Model and Stability Analysis

3.1 Introduction

Under what conditions will a population of thermostatically-controlled loads (TCLs) cause problems for the electricity grid through partial or total synchronisation? If a population of TCLs is homogeneous (all with identical properties and operating rules), will synchronisation always occur?

We can think of a population of frequency-sensitive TCLs on the electricity grid as a system of coupled oscillators. Each moves through its temperature cycle, interacting with every other TCL through their combined effect on the electricity grid frequency. The Kuramoto framework was developed [102, 103] which elegantly describes basic features of this type of system and allows for stability analysis. It has been used to study a variety of coupled oscillator systems, such as neurons, fireflies, and more recently crowd-synchronisation on the Millennium Bridge [104]. The Kuramoto model is governed by the equation

$$\dot{\theta}_i = \omega_i + \frac{K}{N}\sum_{j=1}^{N}\sin(\theta_j - \theta_i), \qquad i = 1, ..., N \tag{3.1}$$

where θ_i is the phase of the ith oscillator, ω_i is its natural frequency, $K \geq 0$ is the coupling strength, and N is the number of oscillators [105]. The frequency of each oscillator is equally influenced by the frequencies of all of the other oscillators (equal coupling). Kuramoto defined the following complex order parameter which is a measure of the synchronisation of the population,

$$re^{i\psi} = \frac{1}{N}\sum_{j=1}^{N} e^{-\theta_j}. \tag{3.2}$$

Figure 3.1 illustrates the Kuramoto model and the significance of the order parameter. $r(t) \geq 0$ is a measure of phase coherence and $\psi(t)$ measures the average phase. These are mean-field quantities, and it can be shown that the oscillators are coupled only through r and ψ. The mean-field nature of the system allowed Kuramoto to solve (3.1) exactly in the infinite-N limit [102]. For this case Kuramoto found the critical value of the coupling strength in terms of the width of the distribution of natural frequencies ω_i, above which the system exhibits partial synchronisation ($r > 0$). We will return to this threshold in the last part of this thesis.

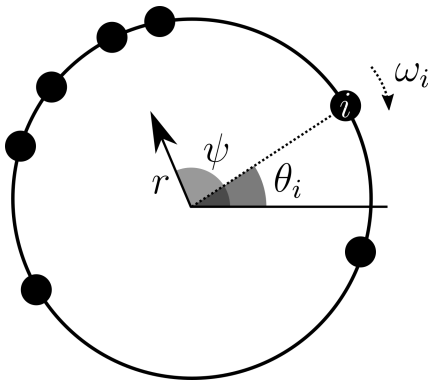

Figure 3.1: Illustration of the Kuramoto model

Our work takes inspiration from the Kuramoto model. We can think of the TCLs as a population of oscillators, moving around the temperature cycle. They are coupled via the grid frequency signal. However, there are several key differences between the coupled oscillators of the Kuramoto model and our system, which make modelling our TCL population more difficult. In the Kuramoto model each oscillator is equally affected by every other oscillator at all times. In contrast, only the proportion of TCLs switched on (rather than their temperatures or temperature derivatives) affects a TCL. Also, the TCLs in the middle of their on or off phase will take longer to be affected by the frequency than those close to the temperature set points,

which may have to change their behaviour as the set points move. In the Kuramoto model, oscillators are modelled as moving around a circle, and with zero coupling would move according to their natural frequencies (at constant speed). If we were mapping the temperature cycles onto a circle then we would need the circle to be able to change in length as the temperature set points change. The dynamics would also be non-smooth at the switch on and off points. I considered many options for altering the circle in Figure 3.1 to create a simple model for our system comparable with the Kuramoto system. For example, mapping the temperature cycling to an ellipse, mapping the on and off portions of the cycle each to one half of two different ellipses (due to different on and off durations) with discontinuities at the joins, and maps to rectangles were all considered. Any successful model would need to account for the nonlinear 'natural frequencies' (rate of change of temperature), the changing temperature set points, and the coupling with only the switched on TCLs.

With these challenges in mind and inspired by results for the Kuramoto model, in this chapter we propose a new modelling framework for TCLs and present a mathematical analysis of the stability of our system. In Section 3.2 we set out our model. In Section 3.3 we analyse the stability of the system close to the nominal frequency. The final part of this chapter, Section 3.4, solves for the behaviour of one and then two synchronised groups of TCLs, simulates the behaviour of three groups, and proposes how a group of N synchronised groups would behave.

3.2 The Model

We begin by establishing our model which we use throughout the thesis. The modelling is kept appliance-neutral where possible, but it is set up for cooling devices such as fridges, (fridge-)freezers and air-conditioners, and would need to be altered in minor ways to be adapted to other appliances like heat pumps or hot water tanks. For the simulations that follow and in all specific examples given, we consider a typical fridge as our TCL appliance of choice. Our modelling assumptions can be summarised as follows:

3.2.1 Assumptions

(i) Electricity grid frequency is the same everywhere on the network and there are no inter-area oscillations [80] (therefore all machines are assumed to rotate in synchrony)

(ii) All TCLs sense frequency deviations with negligible measurement delay or measurement error

(iii) All system parameters remain constant over time (defined in Table 3.1)

(iv) Fridges and freezers are not affected by the fridge/freezer door being opened, or by the addition or removal of food (in effect we assume this never occurs)

(v) TCLs have continuous thermostat control (in temperature and time) and can therefore sense and implement temperature/set point changes with infinite precision

(vi) TCLs consume constant power when on, and zero power when off, and are controlled only by the rules outlined in the model.

These assumptions allow us to create a tractable model for analytic study. Assumptions (iii) and (iv) are probably the easiest and most natural to relax first, and could be relaxed by adding time-dependent forcing effects. For most of this thesis I consider a population of identical TCLs, but our formulation can be extended easily to an inhomogeneous population and I will give evidence that the effects of sufficient diversity will be stabilising, as supported by our final simulations.

3.2.2 Individual TCLs

For the temperature cycling of a TCL we adopt the linear model and notation presented in [53]. Let the temperature of a TCL at time t be denoted by $T(t)$, the cooling/heating coefficient by α, and the asymptotic temperatures that the TCL would reach if left on/off indefinitely by T_{ON} and T_{OFF}, respectively. Then

$$\dot{T}(t) = \begin{cases} \alpha\big(T_{\text{ON}} - T(t)\big) & \text{when the TCL is on} \\ \alpha\big(T_{\text{OFF}} - T(t)\big) & \text{when the TCL is off.} \end{cases} \tag{3.3}$$

A (cooling) TCL will switch off when the temperature reaches its lower temperature set point T_- and switch on when it reaches its upper temperature set point T_+. We choose to make these set points sensitive to system frequency deviations away from 50Hz, denoted $f(t)$ (*i.e.* $f(t) = \text{Frequency}(t) - 50\text{Hz}$). Insufficient generation to meet demand causes $f < 0$ and so we need the TCLs to reduce their power consumption to bring f back to zero. We implement this by increasing the temperature set points so that the TCLs switch off sooner/stay off for longer. Over-supply of electricity to the grid causes $f > 0$, and so in this case we decrease the temperature set

points to increase overall power consumption. Thus we define our frequency-sensitive temperature set points,

$$T_-\big(f(t)\big) := T_-^0 - \beta_- f(t) \qquad \text{lower (switch off) set point} \tag{3.4a}$$

$$T_+\big(f(t)\big) := T_+^0 - \beta_+ f(t) \qquad \text{upper (switch on) set point} \tag{3.4b}$$

where β_-, β_+ are positive constants that determine the sensitivity of the lower and upper temperature set points to frequency deviations. T_-^0 and T_+^0 are the uncoupled[1] temperature set points, which we typically take to be 2°C and 7°C respectively. This framework is very similar to that suggested in [69], although we allow the upper and lower temperature set points to have different sensitivities to the frequency (β_- and β_+).

We can solve (3.3) for the temperature of a TCL at time t. If a TCL has temperature T_0 at time t_0 and does not switch on/off before time t then the temperature $T(t)$ is given by

$$T(t) = (T_0 - T_{\text{ON}})e^{-\alpha(t-t_0)} + T_{\text{ON}} \qquad \text{when on} \tag{3.5a}$$

$$T(t) = (T_0 - T_{\text{OFF}})e^{-\alpha(t-t_0)} + T_{\text{OFF}} \qquad \text{when off.} \tag{3.5b}$$

We can rearrange (3.5a) and (3.5b) and solve for the on and off durations τ_{ON} and τ_{OFF} respectively, assuming constant grid frequency:

$$\tau_{\text{ON}}(f) = \frac{1}{\alpha}\log\left(\frac{T_+(f) - T_{\text{ON}}}{T_-(f) - T_{\text{ON}}}\right) \tag{3.6a}$$

$$\tau_{\text{OFF}}(f) = \frac{1}{\alpha}\log\left(\frac{T_{\text{OFF}} - T_-(f)}{T_{\text{OFF}} - T_+(f)}\right). \tag{3.6b}$$

These variables will be useful when we consider the equilibrium of the system, in which the temperature set points become fixed. In the traditional case when TCLs are uncoupled from the grid (or the special case $f \equiv 0$) their 'natural' on and off cycle durations, τ_{ON}^0 and τ_{OFF}^0, are given by

$$\tau_{\text{ON}}^0 = \frac{1}{\alpha}\log\left(\frac{T_+^0 - T_{\text{ON}}}{T_-^0 - T_{\text{ON}}}\right) \tag{3.7a}$$

$$\tau_{\text{OFF}}^0 = \frac{1}{\alpha}\log\left(\frac{T_{\text{OFF}} - T_-^0}{T_{\text{OFF}} - T_+^0}\right). \tag{3.7b}$$

Note that when a TCL population is not frequency sensitive, the expected proportion

[1] A fridge is 'uncoupled' from the grid frequency if $\beta_- = \beta_+ = 0$.

of TCLs switched on is given by

$$\rho_0 = \frac{\tau^0_{\text{ON}}}{\tau^0_{\text{ON}} + \tau^0_{\text{OFF}}}. \tag{3.8}$$

In order for the TCLs to operate properly they need to cycle on and off, and so we require that

$$T_{\text{ON}} < T_-\big(f(t)\big) < T_+\big(f(t)\big) < T_{\text{OFF}} \quad \forall \quad t. \tag{3.9}$$

We also need a TCL to respond 'appropriately' to a change in frequency, that is to say, for the average power consumption over one cycle to increase when the frequency decreases, and decrease when the frequency increases. It is shown in Appendix A that a sufficient condition to ensure this is

$$\frac{\beta_+}{\beta_-} \in \left(\frac{T_{\text{OFF}} - T_+}{T_{\text{OFF}} - T_-}, \frac{T_+ - T_{\text{ON}}}{T_- - T_{\text{ON}}}\right). \tag{3.10}$$

which is a non-empty interval (notably containing $\{1\}$).

3.2.3 Electricity grid frequency

A simplified equation for the frequency F of a power system can be determined by Newton's 2nd Law of Motion or the derived equation for energy. If we let $f := F - F_0$, where F_0 is the nominal grid frequency (50Hz in Europe), and linearise about F_0 then we obtain [66]

$$M\frac{\mathrm{d}f}{\mathrm{d}t} + Df(t) = \Delta P_g - \Delta P_l \tag{3.11}$$

and for brevity we introduce new variables along with explicit consideration of TCL power consumption,

$$\frac{\mathrm{d}f}{\mathrm{d}t}(t) = c\big(\Delta P - \rho(t)P_c\big) - \gamma f(t) \tag{3.12}$$

where

$M := 4\pi^2 I F_0$	stands for 2π times nominal angular momentum of the rotating masses in the system
I	stands for total inertia of the rotating masses of the system

D	stands for damping factor representing the natural frequency dependence of the load alongside the damping provided by synchronous generator damper windings
ΔP_g	stands for change in total active power generation, compared to a reference level
ΔP_l	stands for change in total active power load, compared to a reference level
$c := \frac{1}{M}$	stands for inverse nominal angular momentum, introduced for brevity
ΔP	stands for 'surplus power generation for the TCLs', total system active power generation minus total system active power load, excluding TCL power consumption
ρ	stands for proportion of TCLs switched on
P_c	stands for power consumed by TCL population when all switched on
$\gamma := \frac{D}{M}$	is a variable introduced for brevity.

In this chapter we make the simplifying assumption that the 'surplus' power generation on the system for TCL consumption ΔP is a constant. We use the '$*$' notation to denote equilibrium values. In equilibrium

$$c\big(\Delta P - \rho^* P_c\big) - \gamma f^* = 0 \tag{3.13}$$

hence

$$f^* = \frac{c}{\gamma}\big(\Delta P - \rho^* P_c\big), \tag{3.14}$$

therefore we can rewrite our equation for $\dot{f}$ in terms of deviations from equilibrium values:

$$\dot{\tilde{f}}(t) = cP_c\big(\rho^* - \rho(t)\big) - \gamma\tilde{f} \tag{3.15}$$

where

$$\tilde{f} := f - f^*. \tag{3.16}$$

3.2.4 Parameter Choices

We take as reference the Great Britain (GB) electricity system. This covers mainland England, Scotland and Wales. In 2015 approximately 10.4m households in the UK, which also includes Northern Ireland, owned a fridge and 19.1m households owned a fridge-freezer [106]. In the same year approximately 2.8% of the population lived in Northern Ireland [107]. If we assume that the average number

of people per household is the same in Northern Ireland and in GB, and an even distribution of fridge and fridge-freezer ownership, then approximately 10.1m and 18.6m households in GB owned a fridge and fridge-freezer, respectively. If using TCLs for frequency response became standard practice, that would mean a very large number of appliances could participate in frequency response. We model the case of 1 million fridges participating in frequency response, which corresponds to roughly 10% of fridges in GB. We take the power consumed by an individual fridge when switched on, p, to be 70W, as assumed in [71] and [72]. This means that we let $p = 7 \times 10^{-5}$MW and the total power consumption if all fridges were switched on, $P_c = 7 \times 10^{-5} \times 10^6 = 70$MW.

Using our approximation for $\dot{f}(t)$ [1], $c = \frac{50}{2E_k}$, where E_k is total stored kinetic energy, related to system inertia. Our GB system data (discussed later) gives an approximate average value for E_k, $E_k = 2.5 \times 10^5$MVAs (note that MVAs=MJ), and so $c = 1 \times 10^{-4}$. We let ρ^* vary between 0 and 1 by changing ΔP. When the rest of the system is perfectly balanced, ΔP corresponds to the expected power consumption of the population. When the TCLs are identical, as in our case, this is the same as the duty cycle multiplied by P_c [73]. In the literature, duty cycles for fridges are typically assumed to be around 30%. Examples in simulations and experiments include fridge duty cycles of 22% [54], 25% [53], 32% [41] and 33.3% [74]. The lower the duty cycle, the greater the efficiency of the TCL. We take $T_{\text{ON}} = -26°$C for a duty cycle of approximately 33.3% after taking T_{OFF}, T_-^0 and T_+^0 from [72]. Parameter α is chosen to achieve a total cycle of approximately 45 minutes, similar to [74] which assumes 42 minutes. Our parameters are summarised in Table 3.1, and throughout this thesis we take these values unless stated otherwise.

3.3 Stability of a uniform distribution at 50Hz

The ideal conditions for the stable and efficient operation of the electricity grid would be (among other things) when grid frequency is exactly at the nominal frequency (we use the European nominal frequency, 50Hz). This is because the power plants and other system components are designed to work optimally at this frequency, and deviations away from 50Hz can cause huge instabilities and even power outages in extreme cases. In our model when a population of TCLs is consuming its expected power level[2] and the frequency is 50Hz, we have $\frac{\mathrm{d}f}{\mathrm{d}t} = 0$. It is this 'ideal' state

[2]The 'expected power level' is the expected power consumption of the population when uncoupled from grid frequency.

Table 3.1: Parameter values assumed, unless stated otherwise

Parameter	**Value**	**Units**
T_{OFF}	20	°C
T_{ON}	-26	°C
T_{-}^{0}	2	°C
T_{+}^{0}	7	°C
α	1.808×10^{-4}	s^{-1}
β_{+}	2.4	$°\text{C.Hz}^{-1}$
β_{-}	2.4	$°\text{C.Hz}^{-1}$
c	1×10^{-4}	Hz(MVAs)^{-1}
γ	0	s^{-1}
p	7×10^{-5}	MW
P_c	70	MW
ρ_0	0.3355	-
ΔP	23.485	MW

that we study in this section (of course in reality, even under normal operation the electricity grid is subject to noise, and so the frequency fluctuates in a small interval around 50Hz).

We begin by studying the stability of a population of TCLs uniformly distributed in phase (meaning the time since last switch on). This means that under constant temperature set point conditions the TCLs would switch on at a constant rate, and switch off at a (possibly different) constant rate[3]. In the context of the Kuramoto model this is usually referred to as the 'incoherent solution,' for example [103, 105]. Just as in Strogatz and Mirollo's treatment of the Kuramoto model [105], we model the infinite-N limit of a population of TCLs as a continuum of TCLs distributed over an interval with periodic boundary conditions.

In order to obtain a tractable model, comparable to the Kuramoto model, three key challenges must be addressed. Firstly, the TCL temperature cycling is described by the piecewise-smooth nonlinear function (see (3.5a) and (3.5b)), with non-differentiability at each temperature set point. Secondly, these set points are continuously changing with grid frequency, and so any map to a periodic regime must be sufficiently flexible to accommodate this. Finally, in order to know a TCL's rate of change of temperature at any time, one needs to know both its current temperature, and its current (on/off) state. We therefore propose a new modelling

[3]Note that since TCLs heat (or cool) at different rates depending on their current temperature, uniformly distributing the TCLs within each part of the cycle does not correspond to uniformly distributing the population over the temperature scale.

framework to overcome these challenges and permit stability analysis for the model.

We map each TCL with temperature and on/off state to a point θ on the interval $[-1, 1)$, in such a way that θ dictates both the temperature and the state of a TCL. The switched off TCLs are mapped to the interval $[-1, 0)$ and the switched on TCLs are mapped to $[0, 1)$. Then we define the position $\theta(t)$ of a TCL at time t with temperature $T(t)$ and state on or off by

$$\theta(t) = \begin{cases} \theta_{\text{ON}}(t) = \dfrac{1}{\alpha\tau_{\text{ON}}\big(f(t)\big)} \log\left(\dfrac{T_+\big(f(t)\big) - T_{\text{ON}}}{T(t) - T_{\text{ON}}}\right) \in [0, 1) & \text{if on} \\ \theta_{\text{OFF}}(t) = \dfrac{1}{\alpha\tau_{\text{OFF}}\big(f(t)\big)} \log\left(\dfrac{T_{\text{OFF}} - T_+\big(f(t)\big)}{T_{\text{OFF}} - T(t)}\right) \in [-1, 0) & \text{if off.} \end{cases} \tag{3.17}$$

Note that the model implicitly assumes that the temperature set points never change fast enough to leave a TCL outside of the interval $[T_-\big(f(t)\big), T_+\big(f(t)\big)]$. Since in this thesis we use this model for only linear stability analysis about the equilibrium, we consider this to be a reasonable assumption. Our choice of θ means that uniformly distributing a population of TCLs over each part of the temperature cycle (as discussed above) corresponds to a uniform distribution of on and off TCLs in their respective halves of θ-space. Figure 3.2(a) illustrates our map from temperature space to θ-space. In temperature space we need two pieces of information to know how the temperature of a TCL is changing; its temperature and its state. Our mapping reduces the required information to just the value of θ, since the sign of θ gives its on/off state. Figure 3.2(b) shows what we mean by 'uniform distribution'. In each half of θ-space the density of TCLs is uniform, and the proportion in each half corresponds to the proportion of time spent on/off during its cycle. We introduce the variable u^* below. Note that the areas of the two rectangles always sum to one.

As in [105], we consider the population density in θ-space. Let $u(\theta, t)\mathrm{d}\theta$ denote the fraction of TCLs that lie between θ and $\theta + \mathrm{d}\theta$ at time t. Then u is non-negative, with period length 2 in θ and satisfies the normalisation

$$\int_{-1}^{+1} u(\theta, t)\mathrm{d}\theta = 1 \tag{3.18}$$

for all t. The evolution of u is governed by the continuity equation [108]

$$\frac{\partial u}{\partial t} + \frac{\partial}{\partial \theta}(uv) = 0 \tag{3.19}$$

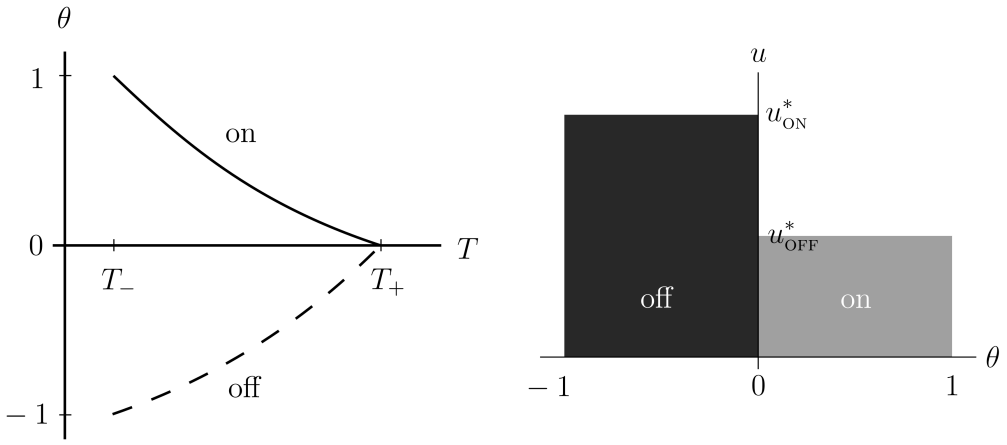

(a) map from T to θ (b) 'uniform distribution' of θ

Figure 3.2: Illustration of the mapping from temperature-space to θ-space (a), and a 'uniform distribution' of TCLs in phase (b), where the proportions switched on/off are the proportions in equilibrium, and the areas of the rectangles sum to one.

where v is the velocity of a TCL in θ-space, $v(\theta,t) := \dot{\theta}(t)$. Differentiating (3.17) gives

$$v_{\text{ON}}(\theta,t) = \frac{1}{\tau_{\text{ON}}\big(f(t)\big)}\Big(1+\frac{1}{\alpha}\Big[\phi_{\text{ON}}\big(f(t)\big)\theta - \frac{\beta_+}{T_+\big(f(t)\big)-T_{\text{ON}}}\Big]\dot{f}(t)\Big) \tag{3.20a}$$

$$v_{\text{OFF}}(\theta,t) = \frac{1}{\tau_{\text{OFF}}\big(f(t)\big)}\Big(1+\frac{1}{\alpha}\Big[\phi_{\text{OFF}}\big(f(t)\big)\theta + \frac{\beta_+}{T_{\text{OFF}}-T_+\big(f(t)\big)}\Big]\dot{f}(t)\Big) \tag{3.20b}$$

where

$$\phi_{\text{ON}}\big(f(t)\big) := \frac{\beta_+}{T_+\big(f(t)\big)-T_{\text{ON}}} - \frac{\beta_-}{T_-\big(f(t)\big)-T_{\text{ON}}} \tag{3.21a}$$

$$\phi_{\text{OFF}}\big(f(t)\big) := \frac{\beta_+}{T_{\text{OFF}}-T_+\big(f(t)\big)} - \frac{\beta_-}{T_{\text{OFF}}-T_-\big(f(t)\big)}. \tag{3.21b}$$

Note that for $\frac{\beta_+}{\beta_-}$ satisfying (3.10), $\phi_{\text{ON}}\big(f(t)\big) < 0$ and $\phi_{\text{OFF}}\big(f(t)\big) > 0$. Under a constant grid frequency, $\dot{\theta}_{\text{ON}}$ and $\dot{\theta}_{\text{OFF}}$ are constants. In equilibrium u^* we have $\dot{u}^* = 0$, and therefore (3.19) implies

$$u^*_{\text{ON}}(\theta) = \frac{k_0}{v^*_{\text{ON}}(\theta)}; \qquad\qquad u^*_{\text{OFF}}(\theta) = \frac{k_0}{v^*_{\text{OFF}}(\theta)},$$

for some constant k_0. Since $\dot{f}^* = 0$, from (3.20a) and (3.20b) we have

$$v^*_{\text{ON}} = \frac{1}{\tau^*_{\text{ON}}}; \qquad\qquad v^*_{\text{OFF}} = \frac{1}{\tau^*_{\text{OFF}}}.$$

Then for all $\theta \in [-1, 0), [0, 1)$ respectively,

$$u^*_{\text{ON}}(\theta) = k_0\tau^*_{\text{ON}} \qquad\qquad u^*_{\text{OFF}}(\theta) = k_0\tau^*_{\text{OFF}}$$

and k_0 is determined by the normalisation criterion (3.18),

$$\int_{-1}^{1} u^* \mathrm{d}\theta = k_0(\tau^*_{\text{ON}} + \tau^*_{\text{OFF}}) = 1 \tag{3.22}$$

$$k_0 = \frac{1}{\tau^*_{\text{ON}} + \tau^*_{\text{OFF}}}. \tag{3.23}$$

The proportion of TCLs switched on, $\rho(t)$, is given by

$$\rho(t) = \int_0^1 u(\theta, t)\mathrm{d}\theta. \tag{3.24}$$

In equilibrium $\rho(t) = \rho^*$ (3.15), therefore

$$\rho^* = \int_0^1 u^*(\theta, t)\mathrm{d}\theta \tag{3.25}$$

$$\rho^* = \frac{\tau^*_{\text{ON}}}{\tau^*_{\text{ON}} + \tau^*_{\text{OFF}}} \tag{3.26}$$

where for any function $g\big(f(t)\big)$ the notation g^* denotes $g(f^*)$.

We introduce the notation '$_\bullet$' to imply that an equation holds for the variable with either of two values, 'on' or 'off'. Our approach is to perturb the system about the equilibrium (u^*, f^*) by a small amount $\tau^*_\bullet\eta(\theta, t)$, and to consider the evolution of the perturbation. By (3.18) the perturbation satisfies

$$\int_{-1}^{+1} \tau^*_\bullet\eta(\theta, t)\mathrm{d}\theta = 0. \tag{3.27}$$

We write

$$u_\bullet = \big(k_0 + \eta(\theta, t)\big)\tau^*_\bullet \tag{3.28}$$

$$v_\bullet = \frac{1}{\tau^*_\bullet}\big(1 + w(\theta, t)\big) \tag{3.29}$$

so that (3.19) becomes

$$\tau_\bullet^* \frac{\partial}{\partial t}[\eta] + \frac{\partial}{\partial \theta}[k_0 + k_0 w + \eta + \eta w] = 0. \tag{3.30}$$

Taking the first order approximation yields

$$\tau_\bullet^* \frac{\partial}{\partial t}[\eta] + k_0 \frac{\partial}{\partial \theta}[w] + \frac{\partial}{\partial \theta}[\eta] = 0. \tag{3.31}$$

Rearranging (3.29) for w and substituting (3.20a, 3.20b) for $v_\bullet$ gives

$$w_{\text{ON}} = \frac{1}{\alpha}\left(\phi_{\text{ON}}^* \theta - \frac{\beta_+}{T_+^* - T_{\text{ON}}}\right)\dot{f}(t) - \frac{\delta\tau_{\text{ON}}(t)}{\tau_{\text{ON}}^*} \tag{3.32a}$$

$$w_{\text{OFF}} = \frac{1}{\alpha}\left(\phi_{\text{OFF}}^* \theta + \frac{\beta_+}{T_{\text{OFF}} - T_+^*}\right)\dot{f}(t) - \frac{\delta\tau_{\text{OFF}}(t)}{\tau_{\text{OFF}}^*} \tag{3.32b}$$

and

$$\delta\tau_{\text{ON}}(t) = -\frac{\phi_{\text{ON}}^* \tilde{f}(t)}{\alpha}; \qquad \delta\tau_{\text{OFF}}(t) = -\frac{\phi_{\text{OFF}}^* \tilde{f}(t)}{\alpha}.$$

Hence

$$\begin{aligned}\frac{\partial}{\partial \theta}[w_\bullet(t)] &= \phi_\bullet^* \frac{\dot{f}}{\alpha} + \left(w(t)\Big|_{\theta=0^+} - w(t)\Big|_{\theta=0^-}\right)\delta(\theta) + \\ &\qquad + \left(w(t)\Big|_{\theta=-1} - w(t)\Big|_{\theta=1}\right)\delta(\theta - 1) \\ \frac{\partial}{\partial \theta}[w_\bullet(t)] &= \frac{1}{\alpha}\left[\phi_\bullet^* \dot{f} - \nu_0 \delta(\theta) + \nu_1 \delta(\theta - 1)\right]\dot{f}(t) + \frac{\mu}{\alpha}\left[\delta(\theta - 1) - \delta(\theta)\right]\tilde{f}\end{aligned}$$

where we have defined

$$\nu_0 := \frac{\beta_+}{T_+^* - T_{\text{ON}}} + \frac{\beta_+}{T_{\text{OFF}} - T_+^*} > 0 \tag{3.33a}$$

$$\nu_1 := \frac{\beta_-}{T_-^* - T_{\text{ON}}} + \frac{\beta_-}{T_{\text{OFF}} - T_-^*} > 0 \tag{3.33b}$$

$$\mu := \frac{\phi_{\text{OFF}}^*}{\tau_{\text{OFF}}^*} - \frac{\phi_{\text{ON}}^*}{\tau_{\text{ON}}^*} > 0 \quad \text{if } \frac{\beta_+}{\beta_-} \text{ satisfies (3.10) with } T_\pm^*. \tag{3.33c}$$

We have a time-invariant linear system (3.31), and so it is natural to look for solutions for which the time dependence of our variables $\tilde{f}$ and η is $e^{\lambda t}$; $\lambda \in \mathbb{C}$ is called

an eigenvalue of the system. Defining $k := \frac{k_0}{\alpha}$ and renaming $\tilde{f}$ to f, (3.31) becomes

$$\tau_\bullet^* \lambda \eta + \frac{\partial \eta}{\partial \theta} + k\big[\phi_\bullet^* - \nu_0 \delta(\theta) + \nu_1 \delta(\theta - 1)\big]\lambda f + k\mu[\delta(\theta - 1) - \delta(\theta)]f = 0. \tag{3.34}$$

We introduce an integrating factor so that on the open intervals $(-1, 0) \cup (0, 1)$ we can find an expression for $\eta(\theta)$:

$$\begin{aligned}
\frac{\partial}{\partial \theta}\big(e^{\lambda \tau_\bullet^* \theta}\eta\big) + k\phi_\bullet \lambda f e^{\lambda \tau_\bullet^* \theta} &= 0 \\
e^{\lambda \tau_\bullet^* \theta}\eta &= \eta_\bullet(0) - k\phi_b ullet^* \lambda f \int_0^\theta e^{\lambda \tau_\bullet^* \theta'} \mathrm{d}\theta' \\
&= \eta_b ullet(0) - \frac{k\phi_b ullet^* f}{\tau_b ullet^*}\big(e^{\lambda \tau_b ullet^* \theta} - 1\big) \\
\therefore \quad \eta(\theta) &= \left(\eta_\bullet(0) + kf\frac{\phi_\bullet^*}{\tau_\bullet^*}\right)e^{-\lambda \tau_\bullet^* \theta} - kf\frac{\phi_\bullet^*}{\tau_\bullet^*}.
\end{aligned} \tag{3.35}$$

At the discontinuities $\theta = 0$ and $\theta = \pm 1$,

$$\eta_{\mathrm{ON}}(0) - \eta_{\mathrm{OFF}}(0) = kf(\lambda \nu_0 + \mu) \tag{3.36a}$$

$$\eta_{\mathrm{OFF}}(-1) - \eta_{\mathrm{ON}}(1) = -kf(\lambda \nu_1 + \mu). \tag{3.36b}$$

We can use (3.35) to find expressions for $\eta(-1)$ and $\eta(1)$, and substitute these into (3.36b). After substitution for $\eta_{\mathrm{OFF}}(0)$ (or $\eta_{\mathrm{ON}}(0)$) using (3.36a) and rearrangement we arrive at

$$\eta_{\mathrm{ON}}(0)g(\lambda) = -kf\left(\frac{\phi_{\mathrm{ON}}^*}{\tau_{\mathrm{ON}}^*}g(\lambda) + \lambda\big(\nu_1 - \nu_0 e^{\lambda \tau_{\mathrm{OFF}}^*}\big)\right) \tag{3.37a}$$

$$\eta_{\mathrm{OFF}}(0)g(\lambda) = -kf\left(\frac{\phi_{\mathrm{OFF}}}{\tau_{\mathrm{OFF}}^*}g(\lambda) + \lambda\big(\nu_1 - \nu_0 e^{-\lambda \tau_{\mathrm{ON}}^*}\big)\right). \tag{3.37b}$$

where
$$g(\lambda) = e^{\lambda \tau_{\mathrm{OFF}}^*} - e^{-\lambda \tau_{\mathrm{ON}}^*}. \tag{3.37c}$$

It is possible to have $g(\lambda) = 0$, namely, whenever $\lambda = \frac{2n\pi}{\tau_{\mathrm{ON}}^* + \tau_{\mathrm{OFF}}^*} i$ for any $n \in \mathbb{Z}$, and therefore we do not divide through by $g(\lambda)$. Rewriting our equation for the rate of change of grid frequency near the equilibrium (3.15) as

$$\dot{f}(t) = -\gamma f(t) - cP_c \tau_{\mathrm{ON}}^* \int_0^1 \eta(\theta, t)\mathrm{d}\theta \tag{3.38}$$

and setting $\dot{f} = \lambda f$ gives

$$\int_0^1 \eta(\theta, t) \mathrm{d}\theta = -\frac{(\lambda + \gamma) f}{c P_c \tau^*_{\mathrm{ON}}}. \tag{3.39}$$

Integrating (3.35) over $[0, 1)$ in θ (the switched on TCLs), setting the resulting expression equal to the right hand side of (3.39), and substituting our expression in (3.37a) for $\eta_{\mathrm{ON}}(0)$ establishes the following implicit equation for λ:

$$(\lambda + \gamma - Z\phi^*_{\mathrm{ON}}) g(\lambda) = Z(\nu_1 - \nu_0 e^{\lambda \tau^*_{\mathrm{OFF}}})(1 - e^{-\lambda \tau^*_{\mathrm{ON}}}) \tag{3.40}$$

where we have defined $Z := kcP_c$, which reflects the strength of the effect of the TCLs on grid frequency.

When $Z = 0$ (no effect of the TCLs on the grid frequency) the eigenvalue equation (3.40) reduces to $(\lambda + \gamma) g(\lambda) = 0$, so the eigenvalues are $\lambda = -\gamma$ and $\lambda = \frac{2n\pi i}{\tau^*_{\mathrm{ON}} + \tau^*_{\mathrm{OFF}}}$ for $n \in \mathbb{Z}$ (the roots of $g(\lambda) = 0$). It can also be seen from (3.40) that for all Z there is an eigenvalue $\lambda = 0$. It corresponds to conservation of the number of TCLs. This eigenvalue 0 is removed by the normalisation condition (3.27). The real and imaginary parts of λ that solve (3.40) can be solved for numerically, using for example [109]. Figure 3.3 shows numerical solutions for the first five eigenvalues above (or on) the real axis for the parameter values given in Table 3.1 in Section 3.2.4, and allowing Z to vary from its value Z_0 derived from the table, by $Z = hZ_0$. There is an infinite sequence of eigenvalues going upwards, and their reflections in the real axis. Increasing Z from zero by powers of 10 is seen to decrease the real part of the eigenvalues from zero and therefore the system is stable to small perturbations.

This is a surprising result because intuitively identical TCLs are vulnerable to synchronisation which would cause instabilities on the system, which is the general view in the literature as discussed previously. The result is not due to the damping constant γ, because we chose $\gamma = 0$ so as not to mask the effect of the TCLs. What the analysis does not tell us is how small any perturbations would have to be for a population of TCLs to have a stabilising effect on grid frequency. It might be that a larger perturbation than valid for linearisation leads to instability. In Section 4.2 we study the effects of different sized perturbations using simulations, and indeed find growth of synchronisation. In the next section we consider the behaviour of a population of TCLs under the opposite type of perturbation - namely all TCLs synchronised into one or two groups.

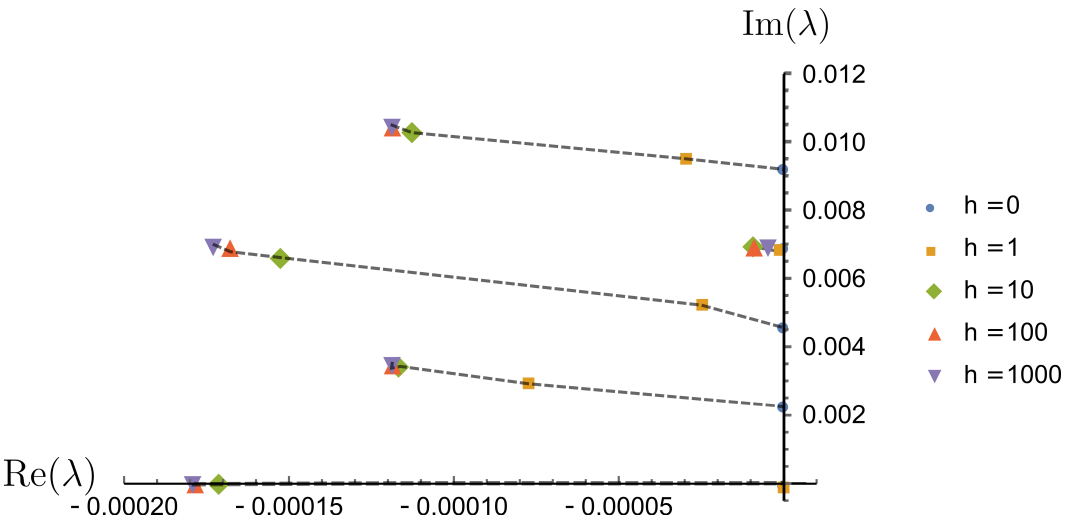

Figure 3.3: Numerical solutions for the first five eigenvalues above the real axis (there is an infinite sequence going further along the imaginary axis, and they are reflected in the real axis). We use multiplier h to increase Z, and the real part of each eigenvalue we have followed decreases from 0 as Z increases from 0.

3.4 Stability of synchronised groups of TCLs

In the previous section we studied the stability of a uniformly distributed (continuum) population of TCLs at the 50Hz equilibrium and found it to be stable almost everywhere in parameter space. In this section we consider the opposite extreme of possible TCL distributions, the Dirac delta distribution. This is to say, we explore the behaviour of a fully-synchronised population of TCLs, all switching on and off at the same time, all with the same temperature and (again) identical parameters. This is equivalent to imagining just one TCL with the power consumption of the whole population. We introduce the following definition.

Definition 3.4.1. *TCLs A and B are* ***synchronised*** *(or equivalently,* ***in the same group****) at time t if $T_{\mathrm{A}}(t) = T_{\mathrm{B}}(t)$ and $S_{\mathrm{A}}(t) = S_{\mathrm{B}}(t)$ where $S_{\mathrm{I}}(t)$ is the on/off state of TCL I at time t.*

Note that since all TCLs obey the same deterministic rules, if two TCLs are synchronised at time t' then they remain synchronised for all time thereafter ($\forall t \geq t'$).

We begin this section by studying the periodic solution of the single group and then explore the behaviour of two groups, ultimately asking whether the single group is stable to splitting into two.

3.4.1 Mapping the switch times of the fully-synchronised population

We begin by constructing a map from one (whole population) switch on event to the next. We show that under certain conditions such a mapping is a contraction. Let the subscript n denote the nth switch on and nth switch off event. Without loss of generality, suppose that after our initial start time t_0 the next switch event is the population switching on. This implies that for all $n \in \mathbb{N}$, $t_n^{\text{OFF}} > t_n^{\text{ON}}$. Figure 3.4 illustrates the notation. Hence the amount of time the population spends switched on following the nth switch on event is given by

$$t_n^{\text{OFF}} - t_n^{\text{ON}} = \frac{1}{\alpha} \log\left(\frac{T_+^0 - \beta_+ f_n^{\text{ON}} - T_{\text{ON}}}{T_-^0 - \beta_- f_n^{\text{OFF}} - T_{\text{ON}}} \right), \tag{3.41a}$$

where $f_n^{\text{ON}}, f_n^{\text{OFF}}$ are the frequencies at the nth switch on and off times. The amount of time spent switched off following the nth switch off is given by

$$t_{n+1}^{\text{ON}} - t_n^{\text{OFF}} = \frac{1}{\alpha} \log\left(\frac{T_{\text{OFF}} - T_-^0 + \beta_- f_n^{\text{OFF}}}{T_{\text{OFF}} - T_+^0 + \beta_+ f_{n+1}^{\text{ON}}} \right). \tag{3.41b}$$

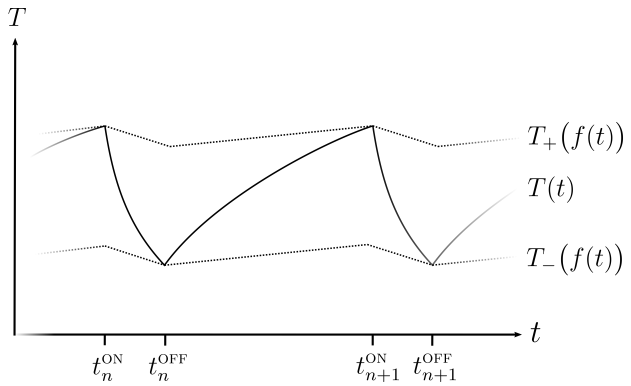

Figure 3.4: Illustration of the nth and $n+1$th switching events of the fully synchronised population and the frequency-sensitive temperature set points $T_-\big(f(t)\big)$ and $T_+\big(f(t)\big)$.

Assuming, as for the numerical analysis in Section 3.3, that the system has no damping, we set $\gamma = 0$ in equation (3.15) for $\dot{f}(t)$. In a synchronised population, at time t all TCLs are either on ($\rho(t) = 1$) or all are off ($\rho(t) = 0$). Then we can define

constants $c_{\text{ON}}, c_{\text{OFF}} > 0$ such that

$$\dot{f} = \begin{cases} -c_{\text{ON}} & := cP_c(\rho^* - 1) \text{ when the population is on} \\ +c_{\text{OFF}} & := cP_c\rho^* \text{ when the population is off.} \end{cases} \tag{3.42}$$

Hence the values of f at the switch off and on times are given by the piecewise-linear functions

$$f_n^{\text{OFF}} = f_n^{\text{ON}} - c_{\text{ON}}(t_n^{\text{OFF}} - t_n^{\text{ON}}) \tag{3.43a}$$

$$f_{n+1}^{\text{ON}} = f_n^{\text{OFF}} + c_{\text{OFF}}(t_{n+1}^{\text{ON}} - t_n^{\text{OFF}}) \tag{3.43b}$$

which after substituting for the switching times using (3.41a) and (3.41b) become

$$f_n^{\text{OFF}} - f_n^{\text{ON}} = -\frac{c_{\text{ON}}}{\alpha} \log\left(\frac{T_+^0 - \beta_+ f_n^{\text{ON}} - T_{\text{ON}}}{T_-^0 - \beta_- f_n^{\text{OFF}} - T_{\text{ON}}}\right) \tag{3.44a}$$

$$f_{n+1}^{\text{ON}} - f_n^{\text{OFF}} = \frac{c_{\text{OFF}}}{\alpha} \log\left(\frac{T_{\text{OFF}} - T_-^0 + \beta_- f_n^{\text{OFF}}}{T_{\text{OFF}} - T_+^0 + \beta_+ f_{n+1}^{\text{ON}}}\right) \tag{3.44b}$$

which can be rearranged into

$$f_n^{\text{OFF}} - \frac{c_{\text{ON}}}{\alpha} \log(T_-^0 - \beta_- f_n^{\text{OFF}} - T_{\text{ON}}) = f_n^{\text{ON}} - \frac{c_{\text{ON}}}{\alpha} \log(T_+^0 - \beta_+ f_n^{\text{ON}} - T_{\text{ON}}) \tag{3.45a}$$

$$f_{n+1}^{\text{ON}} + \frac{c_{\text{OFF}}}{\alpha} \log(T_{\text{OFF}} - T_+^0 + \beta_+ f_{n+1}^{\text{ON}}) = f_n^{\text{OFF}} + \frac{c_{\text{OFF}}}{\alpha} \log(T_{\text{OFF}} - T_-^0 + \beta_- f_n^{\text{OFF}}). \tag{3.45b}$$

Now since each side of (3.45a) and (3.45b) are functions of only one of the $f_n^\bullet$ variables, we can explicitly name them as such:

$$\phi_{\text{ON}}^-(f_n^{\text{OFF}}) := f_n^{\text{OFF}} - \frac{c_{\text{ON}}}{\alpha} \log(T_-^0 - \beta_- f_n^{\text{OFF}} - T_{\text{ON}}) \tag{3.46a}$$

$$\phi_{\text{ON}}^+(f_n^{\text{ON}}) := f_n^{\text{ON}} - \frac{c_{\text{ON}}}{\alpha} \log(T_+^0 - \beta_+ f_n^{\text{ON}} - T_{\text{ON}}) \tag{3.46b}$$

$$\phi_{\text{OFF}}^-(f_n^{\text{OFF}}) := f_n^{\text{OFF}} + \frac{c_{\text{OFF}}}{\alpha} \log(T_{\text{OFF}} - T_-^0 + \beta_- f_n^{\text{OFF}}) \tag{3.46c}$$

$$\phi_{\text{OFF}}^+(f_{n+1}^{\text{ON}}) := f_{n+1}^{\text{ON}} + \frac{c_{\text{OFF}}}{\alpha} \log(T_{\text{OFF}} - T_+^0 + \beta_+ f_{n+1}^{\text{ON}}). \tag{3.46d}$$

Each of the four ϕ functions is increasing and therefore invertible, and so we can

write

$$f_n^{\mathrm{OFF}} = \phi_{\mathrm{ON}}^{-^{-1}}\phi_{\mathrm{ON}}^{+}(f_n^{\mathrm{ON}}) \tag{3.47a}$$

$$f_{n+1}^{\mathrm{ON}} = \phi_{\mathrm{OFF}}^{+^{-1}}\phi_{\mathrm{OFF}}^{-}(f_n^{\mathrm{OFF}}) \tag{3.47b}$$

and therefore

$$f_{n+1}^{\mathrm{ON}} = \phi_{\mathrm{OFF}}^{+^{-1}}\phi_{\mathrm{OFF}}^{-}\phi_{\mathrm{ON}}^{-^{-1}}\phi_{\mathrm{ON}}^{+}(f_n^{\mathrm{ON}}), \tag{3.47c}$$

which is a mapping from the frequency at one switch on event to the frequency at the next. The mapping is a contraction *iff*

$$\left|\left(\phi_{\mathrm{OFF}}^{+^{-1}}\phi_{\mathrm{OFF}}^{-}\phi_{\mathrm{ON}}^{-^{-1}}\phi_{\mathrm{ON}}^{+}\right)'\right| < 1 \tag{3.48}$$

iff

$$\left|\frac{(\phi_{\mathrm{OFF}}^{-})'}{(\phi_{\mathrm{OFF}}^{+})'}\frac{(\phi_{\mathrm{ON}}^{+})'}{(\phi_{\mathrm{ON}}^{-})'}\right| < 1 \tag{3.49}$$

(evaluated at the appropriate places).

Note that

$$\frac{(\phi_{\mathrm{OFF}}^{-})'}{(\phi_{\mathrm{OFF}}^{+})'} = \frac{1+\frac{\beta_- c_{\mathrm{OFF}}}{\alpha(T_{\mathrm{OFF}}-T_n^-)}}{1+\frac{\beta_+ c_{\mathrm{OFF}}}{\alpha(T_{\mathrm{OFF}}-T_{n+1}^+)}} < 1 \tag{3.50}$$

iff

$$\frac{\beta_+}{\beta_-} > \frac{T_{\mathrm{OFF}}-T_{n+1}^+}{T_{\mathrm{OFF}}-T_n^-}. \tag{3.51}$$

Similarly

$$\frac{(\phi_{\mathrm{ON}}^{+})'}{(\phi_{\mathrm{ON}}^{-})'} = \frac{1+\frac{\beta_+ c_{\mathrm{ON}}}{\alpha(T_n^+-T_{\mathrm{ON}})}}{1+\frac{\beta_- c_{\mathrm{ON}}}{\alpha(T_n^--T_{\mathrm{ON}})}} < 1 \tag{3.52}$$

iff

$$\frac{\beta_+}{\beta_-} < \frac{T_n^+-T_{\mathrm{ON}}}{T_n^--T_{\mathrm{ON}}}. \tag{3.53}$$

Therefore a sufficient condition for the mapping to be a contraction is that

$$\frac{\beta_+}{\beta_-} \in \left(\frac{T_{\mathrm{OFF}}-T_{n+1}^+}{T_{\mathrm{OFF}}-T_n^-}, \frac{T_n^+-T_{\mathrm{ON}}}{T_n^--T_{\mathrm{ON}}}\right) \tag{3.54}$$

which is a non-empty interval (containing $\{1\}$), so long as $T_{\mathrm{ON}} < T_n^- < T_n^+ < T_{\mathrm{OFF}}$ and $T_n^- < T_{n+1}^+$ for all n. It is worth recalling our earlier condition on the values of $\beta_\pm$ (3.10) which also imposed that $\frac{\beta_+}{\beta_-}$ belong to an open interval containing $\{1\}$.

3.4.2 Solving for the periodic solution of the fully-synchronised population

The contraction property of the mapping $f_n^{\text{ON}} \mapsto f_{n+1}^{\text{ON}}$ (3.47c) under the above conditions implies that there is an attracting fixed point so long as $T_{\text{ON}} < T_n^- < T_n^+ < T_{\text{OFF}}$, and hence a periodic solution for the synchronised population. We now seek to solve for this periodic solution. Denote by l_{ON} and l_{OFF} the amount of time spent on and off during one (periodic) cycle, respectively. Since power consumption for the population is constant during each on/off phase, the frequency moves linearly between upper and lower values which we denote by f_+ and f_-. Therefore the temperature of the population will cycle between upper and lower set points, given by $T_+^0 - \beta_+ f_+$ and $T_-^0 - \beta_- f_-$, respectively. Equations (3.43a) and (3.43b) show us that

$$f_- = f_+ - c_{\text{ON}} l_{\text{ON}} \tag{3.55a}$$
$$f_+ = f_- + c_{\text{OFF}} l_{\text{OFF}}. \tag{3.55b}$$

The temperature evolution equations (3.5a, 3.5b) allow us to express the switch on and switch off temperatures as follows:

$$T_+^0 - \beta_+ f_+ = (T_-^0 - \beta_- f_- - T_{\text{OFF}}) e^{-\alpha l_{\text{OFF}}} + T_{\text{OFF}} \tag{3.56a}$$
$$T_-^0 - \beta_- f_- = (T_+^0 - \beta_+ f_+ - T_{\text{ON}}) e^{-\alpha l_{\text{ON}}} + T_{\text{ON}} \tag{3.56b}$$

which after substituting for f_- using (3.55a) and rearranging, become

$$f_+(\beta_- e^{-\alpha l_{\text{OFF}}} - \beta_+) = (T_-^0 - T_{\text{OFF}} + \beta_- c_{\text{ON}} l_{\text{ON}}) e^{-\alpha l_{\text{OFF}}} + T_{\text{OFF}} - T_+^0 \tag{3.57a}$$
and $$f_+(\beta_+ e^{-\alpha l_{\text{ON}}} - \beta_-) = (T_+^0 - T_{\text{ON}}) e^{-\alpha l_{\text{ON}}} + T_{\text{ON}} - T_-^0 - \beta_- c_{\text{ON}} l_{\text{ON}}. \tag{3.57b}$$

Now we have two equations in terms of f_+, l_{ON} and l_{OFF} that we can combine into one equation and eliminate f_+,

$$\begin{aligned}(\beta_+ e^{-\alpha l_{\text{ON}}} - \beta_-) &\left[(T_-^0 - T_{\text{OFF}} + \beta_- c_{\text{ON}} l_{\text{ON}}) e^{-\alpha l_{\text{OFF}}} + T_{\text{OFF}} - T_+^0 \right] \\ &= (\beta_- e^{-\alpha l_{\text{OFF}}} - \beta_+) \left[(T_+^0 - T_{\text{ON}}) e^{-\alpha l_{\text{ON}}} + T_{\text{ON}} - T_-^0 - \beta_- c_{\text{ON}} l_{\text{ON}} \right].\end{aligned} \tag{3.58}$$

We can also express l_{OFF} in terms of l_{ON} by summing (3.55a) and (3.55b) to give

$$c_{\text{ON}} l_{\text{ON}} = c_{\text{OFF}} l_{\text{OFF}} \qquad \text{or, equivalently,} \qquad (1 - \rho^*) l_{\text{ON}} - \rho^* l_{\text{OFF}} = 0 \tag{3.59}$$

and so equations (3.57b) and (3.59) form a pair of coupled equations for l_{ON} and l_{OFF}, which can be solved numerically.

Figure 3.5 shows one temperature cycle for the single group under different choices for ρ^*. Denote by ρ_0 the value of ρ when $f = 0$. As ρ^* gets further away from ρ_0 the solutions drift further from the uncoupled temperature range (2-7°C). The cycle lengths are symmetric about $\rho^* = \frac{1}{2}$ but the TCLs consume more power per cycle as ρ^* increases.

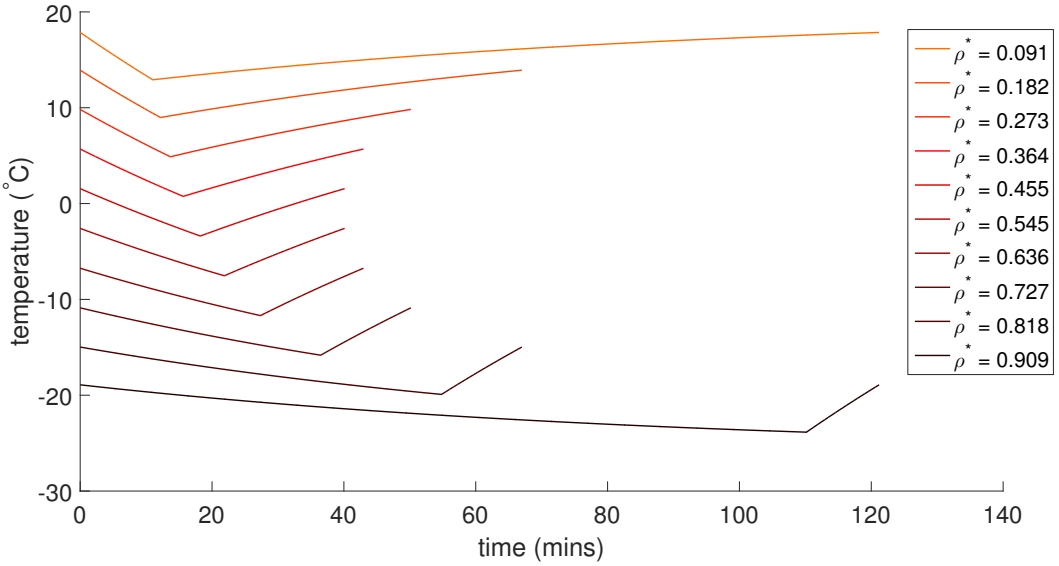

Figure 3.5: One cycle of the single group solution for different values of ρ^* when $\rho_0 \approx 0.3355$. They include values that lead to unrealistic results for real fridges, but are there to illustrate the effect.

It is interesting to note that the on and off cycle durations are affected by each of β, c and P_c equally (when $\beta_- = \beta_+ := \beta$). Taking (3.58) and dividing through by β gives

$$\begin{aligned}(e^{-\alpha l_{\text{ON}}} - 1)\Big[(T_-^0 - T_{\text{OFF}} + \beta c P_c(1-\rho^*) l_{\text{ON}})e^{-\alpha l_{\text{OFF}}} + T_{\text{OFF}} - T_+^0\Big] \\ = (e^{-\alpha l_{\text{OFF}}} - 1)\Big[(T_+^0 - T_{\text{ON}})e^{-\alpha l_{\text{ON}}} + T_{\text{ON}} - T_-^0 - \beta c P_c(1-\rho^*) l_{\text{ON}}\Big] \qquad (3.60)\end{aligned}$$

in which the terms β, c and P_c only occur in the form of the product $\beta c P_c$ and hence our claim is true. Parameter β is the sensitivity of the TCLs to the frequency, c is inversely proportional to system inertia, and P_c is the maximum power consumption possible from the TCL population. Figure 3.6 shows the impact of changing $\beta c P_c$ (collectively) on the duration of the on and off portions of the temperature

cycle. We choose a log-linear plot to scale up (and down) from our standard value ($\beta c P_c = 0.0168$) by factors of ten, since there could be a very large variation in the number of TCLs in frequency-sensitive mode. We can think of the collective term $\beta c P_c$ as a measure of overall sensitivity. Clearly increasing β increases the sensitivity of each TCL to the frequency. Increasing c decreases system inertia, which in turn makes frequency more sensitive to supply-demand imbalance fluctuations. Finally, increasing P_c increases the availability of the demand-side to respond to the frequency (more TCLs in frequency-sensitive mode), and so the population as a whole can be thought of as becoming more sensitive. The single group case is an extreme that we would never want to see on the real system, but it can give insights into the properties of the solutions for more groups. Naturally, as sensitivity increases, the effect on fridge cycling becomes more severe, something we would like to keep fairly minimal.

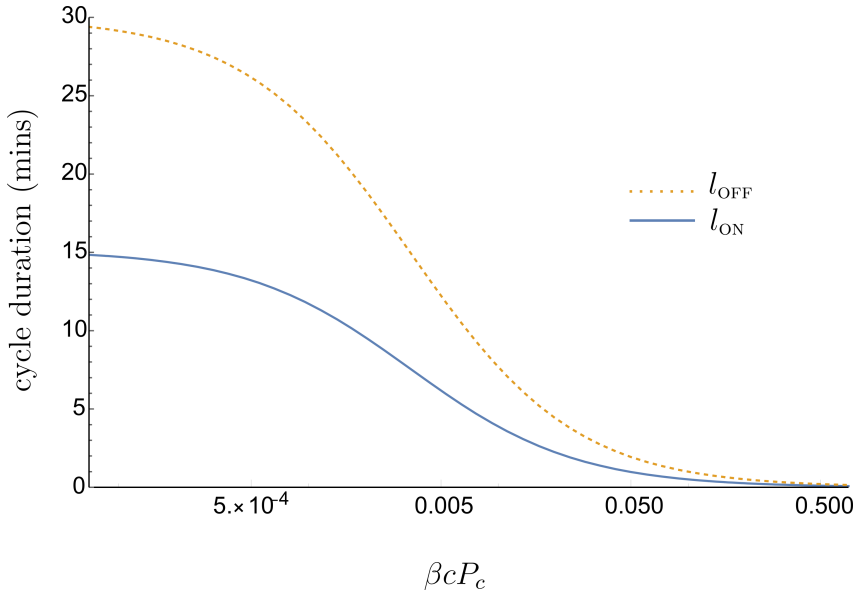

Figure 3.6: Effect changing of $\beta c P_c$ on the on and off cycle durations

3.4.3 The importance of nonlinearity

Before we move on to the more complicated case of two synchronised groups of TCLs, let us take a moment to ask whether linearising the temperature dynamics of the TCLs would be a valid simplification of the system. By this, we mean that the temperature time derivative of each TCL is a constant (rather than being temperature dependent). Note that this is not to be confused with our original linear

model, which gives rise to exponential, rather than linear temperature dynamics, as we assume now. Such a simplification could make our analysis of two or more groups of TCLs significantly easier, but would it be able to capture the important aspects of our system?

Suppose that the temperature evolution of a TCL is linear, and denote the constant temperature derivative with respect to time $\dot{T}(t)$, by

$$\dot{T}(t) = \begin{cases} -T'_{\text{ON}} & \text{if the population is switched on} \\ T'_{\text{OFF}} & \text{if the population is switched off.} \end{cases}$$

As in Section 3.4.1, we use the notation t_n^{ON} and t_n^{OFF} to denote the nth switch on and switch off times of the population, where, without loss of generality, we let the first switch be a switch on. We also repeat the notation f_n^{ON} and f_n^{OFF} to denote the grid frequency at times t_n^{ON} and t_n^{OFF}. Assume that the temperature set point sensitivities to frequency $\beta_- = \beta_+ =: \beta$, then

$$T_n^{\text{ON}} = T_+^0 - \beta f_n^{\text{ON}} \tag{3.61a}$$
$$T_n^{\text{OFF}} = T_-^0 - \beta f_n^{\text{OFF}}. \tag{3.61b}$$

Equating two expressions for the temperature at the nth switch on and off times gives relations for the on and off durations. When switching on,

$$T_n^{\text{OFF}} + (t_{n+1}^{\text{ON}} - t_n^{\text{OFF}})T'_{\text{OFF}} = T_+^0 - \beta f_{n+1}^{\text{ON}} \tag{3.62}$$
$$\therefore \qquad t_{n+1}^{\text{ON}} - t_n^{\text{OFF}} = \frac{T_+^0 - T_-^0 - \beta(f_{n+1}^{\text{ON}} - f_n^{\text{OFF}})}{T'_{\text{OFF}}} \tag{3.63}$$

and when switching off,

$$T_n^{\text{ON}} - (t_n^{\text{OFF}} - t_n^{\text{ON}})T'_{\text{ON}} = T_-^0 - \beta f_n^{\text{OFF}} \tag{3.64}$$
$$\therefore \qquad t_n^{\text{OFF}} - t_n^{\text{ON}} = \frac{T_+^0 - T_-^0 - \beta(f_n^{\text{ON}} - f_n^{\text{OFF}})}{T'_{\text{ON}}}. \tag{3.65}$$

Taking $\gamma = 0$ in the frequency derivative equation (3.12),

$$\dot{f} = \begin{cases} -c(P_c - \Delta P) & \text{when the population is on} \\ c\Delta P & \text{when the population is off} \end{cases} \tag{3.66}$$

and so

$$f_n^{\text{OFF}} = f_n^{\text{ON}} - c(P_c - \Delta P)(t_n^{\text{OFF}} - t_n^{\text{ON}}) \tag{3.67a}$$

$$f_{n+1}^{\text{ON}} = f_n^{\text{OFF}} + c\Delta P(t_{n+1}^{\text{ON}} - t_n^{\text{OFF}}). \tag{3.67b}$$

We use (3.67b) to substitute for the f terms in (3.63) and we use (3.67a) to substitute for the f terms in (3.65):

$$t_{n+1}^{\text{ON}} - t_n^{\text{OFF}} = \frac{T_+^0 - T_-^0 - \beta c\Delta P(t_{n+1}^{\text{ON}} - t_n^{\text{OFF}})}{T'_{\text{OFF}}} \tag{3.68}$$

$$= \frac{T_+^0 - T_-^0}{T'_{\text{OFF}} + \beta c\Delta P} \tag{3.69}$$

and

$$t_n^{\text{OFF}} - t_n^{\text{ON}} = \frac{T_+^0 - T_-^0 - \beta c(P_c - \Delta P)(t_n^{\text{OFF}} - t_n^{\text{ON}})}{T'_{\text{ON}}} \tag{3.70}$$

$$= \frac{T_+^0 - T_-^0}{T'_{\text{ON}} + \beta c(P_c - \Delta P)}. \tag{3.71}$$

In both cases the duration between successive switches is a positive constant with no dependence on n, assuming constant $\Delta P < P_c$ (as we do throughout).

Next we turn our attention to the frequency at each switch event. How does the frequency at the switch on (or switch off) events change over time? We sum (3.67a) and (3.67b) to give

$$f_{n+1}^{\text{ON}} - f_n^{\text{ON}} = c\Delta P(t_{n+1}^{\text{ON}} - t_n^{\text{OFF}}) - c(P_c - \Delta P)(t_n^{\text{OFF}} - t_n^{\text{ON}}) \tag{3.72}$$

$$= c(T_+^0 - T_-^0)\left(\frac{\Delta P}{T'_{\text{OFF}} + \beta c\Delta P} - \frac{P_c - \Delta P}{T'_{\text{ON}} + \beta c(P_c - \Delta P)}\right) \tag{3.73}$$

$$= c(T_+^0 - T_-^0)\left(\frac{T'_{\text{ON}}\Delta P - T'_{\text{OFF}}(P_c - \Delta P)}{(T'_{\text{OFF}} + \beta c\Delta P)(T'_{\text{ON}} + \beta c(P_c - \Delta P))}\right). \tag{3.74}$$

We are assuming that $P_c \geq \Delta P$ and therefore the sign of $(f_{n+1}^{\text{ON}} - f_n^{\text{ON}})$ depends exclusively on the sign of denominator.

$$T'_{\text{ON}}\Delta P - T'_{\text{OFF}}(P_c - \Delta P) = 0 \tag{3.75}$$

$$\text{iff} \qquad \Delta P = \frac{T'_{\text{OFF}}}{T'_{\text{OFF}} - T'_{\text{ON}}} P_c \tag{3.76}$$

$$= \frac{\tau_{\text{ON}}^0}{\tau_{\text{ON}}^0 + \tau_{\text{OFF}}^0} P_c \tag{3.77}$$

which is the expected nominal power consumption of the population (*i.e.* when the TCLs operate without frequency sensitivity). When P_c is equal to the nominal power consumption of the TCLs there is no imbalance on the system. Therefore there cannot be a periodic solution for the synchronised group if there is any system imbalance. By (3.67a) and (3.67b) and our result that the on and off durations are constants, the same condition holds for the sign of $(f_{n+1}^{\text{OFF}} - f_n^{\text{OFF}})$. Therefore the frequency at the switch times will increase or decrease indefinitely. By (3.61a) and (3.61b), the temperature of the TCLs at each switch will also increase or decrease indefinitely.

This reveals the value (and necessity for our purposes) of the exponential heating and cooling of the TCLs. If the temperature evolution is linear, a synchronised population will be incapable of assisting with power imbalance. On the contrary, the exponential temperature evolution means that the duty cycle, and therefore the average power consumption of the population, change as the temperature operating range changes.

We can elicit this mathematically by differentiating the nominal duty cycle with respect to the lower temperature set point when the temperature operating range is fixed. Let $\Delta T := T_+^0 - T_-^0$. If the temperature evolution is linear, since $T'_{\text{OFF}} = \frac{\Delta T}{\tau_{\text{OFF}}^0}$, $T'_{\text{ON}} = \frac{\Delta T}{\tau_{\text{ON}}^0}$,

$$\begin{aligned}\frac{\partial}{\partial T_-^0}\left(\frac{\tau_{\text{ON}}^0}{\tau_{\text{ON}}^0 + \tau_{\text{OFF}}^0}\right) &= \frac{\partial}{\partial T_-^0}\left(\frac{T'_{\text{OFF}}}{T'_{\text{OFF}} + T'_{\text{ON}}}\right) \\ &= 0.\end{aligned}$$

However, when the temperature evolution is nonlinear, as in our original model,

$$\begin{aligned}\frac{\partial}{\partial T_-^0}\left(\frac{\tau_{\text{ON}}^0}{\tau_{\text{ON}}^0 + \tau_{\text{OFF}}^0}\right) &= \frac{-\Delta T}{\alpha(\tau_{\text{ON}}^0 + \tau_{\text{OFF}}^0)^2}\left(\frac{\tau_{\text{ON}}^0}{(T_{\text{OFF}} - T_-^0)(T_{\text{OFF}} - T_+^0)} + \right. \\ &\qquad \left. + \frac{\tau_{\text{OFF}}^0}{(T_+^0 - T_{\text{ON}})(T_-^0 - T_{\text{ON}})}\right) \qquad (3.78) \\ &< 0. \qquad (3.79)\end{aligned}$$

We conclude that the exponential heating and cooling of the TCLs is key to their value as a demand-side resource for supporting the electricity grid frequency. In addition, the linearisation of the temperature evolution cannot help us to analyse the dynamics of a population, since the properties in the two cases are significantly different. With this in mind, we return to our model and analysis of the fully syn-

chronised group, posing the question: given a population split into two synchronised groups, will the groups merge into one fully synchronised population, or will they remain distinct indefinitely?

3.4.4 Two synchronised groups: Simulations

Introduction

Having studied the behaviour of a fully synchronised population we now ask what would happen if a population comprised two groups of TCLs (recall the definition of a synchronised group of TCLs in at the beginning of Section 3.4 on page 49). The key difference between the model for two groups and the model for a single population is in the equation for $\dot{f}(t)$. Suppose that the population is divided such that proportion σ belongs to the group A, G_A, and proportion $1-\sigma$ belongs to the group B, G_B. Then depending on which of the two groups is switched on at time t, $\dot{f}(t)$ will take one of four possible values:

$$\dot{f}(t) = \begin{cases} -cP_c(\sigma - \rho^*) & \text{if only } G_A \text{ is on} \\ -cP_c(1-\sigma-\rho^*) & \text{if only } G_B \text{ is on} \\ -cP_c(1-\rho^*) & \text{if both } G_A \text{ and } G_B \text{ are on} \\ -cP_c(-\rho^*) & \text{if both } G_A \text{ and } G_B \text{ are off.} \end{cases} \tag{3.80}$$

Although this difference may seem fairly simple, moving from one to two groups of TCLs brings a significant complication when it comes to analysing the model. There are now multiple possibilities for the order in which switching on and off occurs and this order can change over time. Simply presupposing the existence of a periodic solution and solving for it is no longer an option. The groups may always merge into one (this can happen under certain parameters), and if they do tend towards separate periodic solutions, the switching order is not obvious, nor easy to solve for. That is why we begin our study with numerical simulations to gain insights into the long-term behaviour of two groups under a range of conditions. In the following subsection we take an in-depth look at the switching events and derivation of the equations underpinning two-group behaviour. Finally in Section 3.4.6 we linearise about the single group solution and analytically study the stability of the fully synchronised population to splitting into two groups.

Phase difference and long-term behaviour

We would like to know whether two distinct groups can co-exist long term or whether they will ultimately merge into the single population solution described in Section 3.4.2. We begin by simulating the temperature cycling of two groups to acquire some intuition.

In our simulations the temperatures of the two groups of TCLs are updated each time step (length one second) along with the grid frequency and if either TCL hits the temperature set point it switches on/off (see Appendix B for details). Our parameters correspond to fridges and are given in Table 3.1. In order to observe the merging/separating of the two groups we need a way to measure the difference between them. A natural way to do this is to consider the difference between the switch on times of the two groups. We define the 'nth normalised phase difference' θ_n, for $n > 0$, as follows:

$$\theta_n = \frac{n\text{th switch on time of } G_A - n\text{th switch on time of } G_B}{\text{most recent cycle duration of } G_A} \tag{3.81a}$$

$$\theta_n = \frac{t_n^{\mathrm{ON}}(\mathrm{A}) - t_n^{\mathrm{ON}}(\mathrm{B})}{t_n^{\mathrm{ON}}(\mathrm{A}) - t_{n-1}^{\mathrm{ON}}(\mathrm{A})}. \tag{3.81b}$$

The normalisation is to counter the changing cycle lengths of the groups, and keeps $\theta_n \in [-1, 1]$. The sign of θ_n depends entirely on the initial conditions of the system, namely which group switches on first. If $\lim_{n\to+\infty} \theta_n \in \{1, 0, -1\}$ then the groups have synchronised[4] since

$$\lim_{n\to+\infty} \theta_n = 1 \quad \Rightarrow \quad t_n^{\mathrm{ON}}(\mathrm{B}) = t_{n-1}^{\mathrm{ON}}(\mathrm{A}) \tag{3.82a}$$

$$\lim_{n\to+\infty} \theta_n = 0 \quad \Rightarrow \quad t_n^{\mathrm{ON}}(\mathrm{B}) = t_n^{\mathrm{ON}}(\mathrm{A}) \tag{3.82b}$$

$$\lim_{n\to+\infty} \theta_n = -1 \quad \Rightarrow \quad t_n^{\mathrm{ON}}(\mathrm{B}) = \left(t_n^{\mathrm{ON}}(\mathrm{A}) - t_{n-1}^{\mathrm{ON}}(\mathrm{A})\right) + t_n^{\mathrm{ON}}(\mathrm{A})$$

which, assuming constant cycle duration at the limit,

$$= \left(t_{n+1}^{\mathrm{ON}}(\mathrm{A}) - t_n^{\mathrm{ON}}(\mathrm{A})\right) + t_n^{\mathrm{ON}}(\mathrm{A})$$
$$= t_{n+1}^{\mathrm{ON}}(\mathrm{A}). \tag{3.82c}$$

[4]For the case $\lim_{n\to+\infty} \theta_n = -1$ we also have to assume that the cycle duration of G_A has become constant in order for the limit to imply synchronisation. This can be easily checked simply by interchanging G_A and G_B and checking if the limit is now 1.

In the penultimate line above we have assumed periodic behaviour for G_A to make the cycle duration substitution. It would be preferable not to have to make this assumption, however since our initial choice of start time is arbitrary we can simply choose a time such that G_B switches on first and then synchronisation will occur *iff* $\lim_{n\to+\infty}\theta_n \in \{0,1\}$. If $\lim_{n\to+\infty}\theta_n \in \{(-1,1)\setminus\{0\}\}$ the two groups remain distinct from one another since the phase difference is not a multiple of the cycle duration of G_A.

Figures 3.7-3.10 show eight different possibilities for the long-term behaviour of two groups. The left-hand plots show how the phase difference θ changes from one switch on event of G_A to the next for different initial switching orders of the two groups and for two different values of σ. For these figures $\rho^* \approx 0.1174$ (achieved with the values in Table 3.1 and using $T_{\text{ON}} = -100$. The right-hand plots show the temperature profiles over time for the two groups over three cycles towards the end of the simulation, along with the upper and lower temperature set points.

Figures 3.7 and 3.8 show examples of two groups merging into one. When G_B is larger than G_A ($\sigma < 0.5$) as in Figure 3.7, the phase difference decreases which signifies that the switch on times of B and the subsequent switch on times of G_A are getting closer together. When G_A is larger ($\sigma > 0.5$) as in Figure 3.8 the phase difference increases which signifies that the switch on times of B and the previous switch on times of G_A are getting closer together. In the long-term the groups synchronise in both cases, as is clear from asymptotic values of θ and by noting that the temperature cycles have become indistinguishable. It is, however, possible for the two groups to co-exist distinctly long-term.

Figures 3.9 and 3.10 show the long-term behaviour of two groups in exactly the same way as in the previous figures but with different values for σ (importantly, much closer to $\sigma = 0.5$). In these four examples the normalised phase difference θ settles down to a value in $(0,1)$ or $(-1,0)$ and the two groups do not merge into one. This is seen most clearly by comparing the eventual temperature cycling (the right hand plots) in Figures 3.7 and 3.8 with those in Figures 3.9 and 3.10.

We can find the asymptotic behaviour of the normalised phase difference for any value of $\sigma \in (0,1)$, and through repeated simulations, can discern the bifurcation diagram. We find that the two groups can coexist for values of σ very close to 0.5 (between about 0.48 and 0.52 depending on the other parameters). Figure 3.11 shows the results of repeated simulations which show the full bifurcation picture. For ease of reading, the narrow range around $\sigma = 0.5$ has been magnified. We

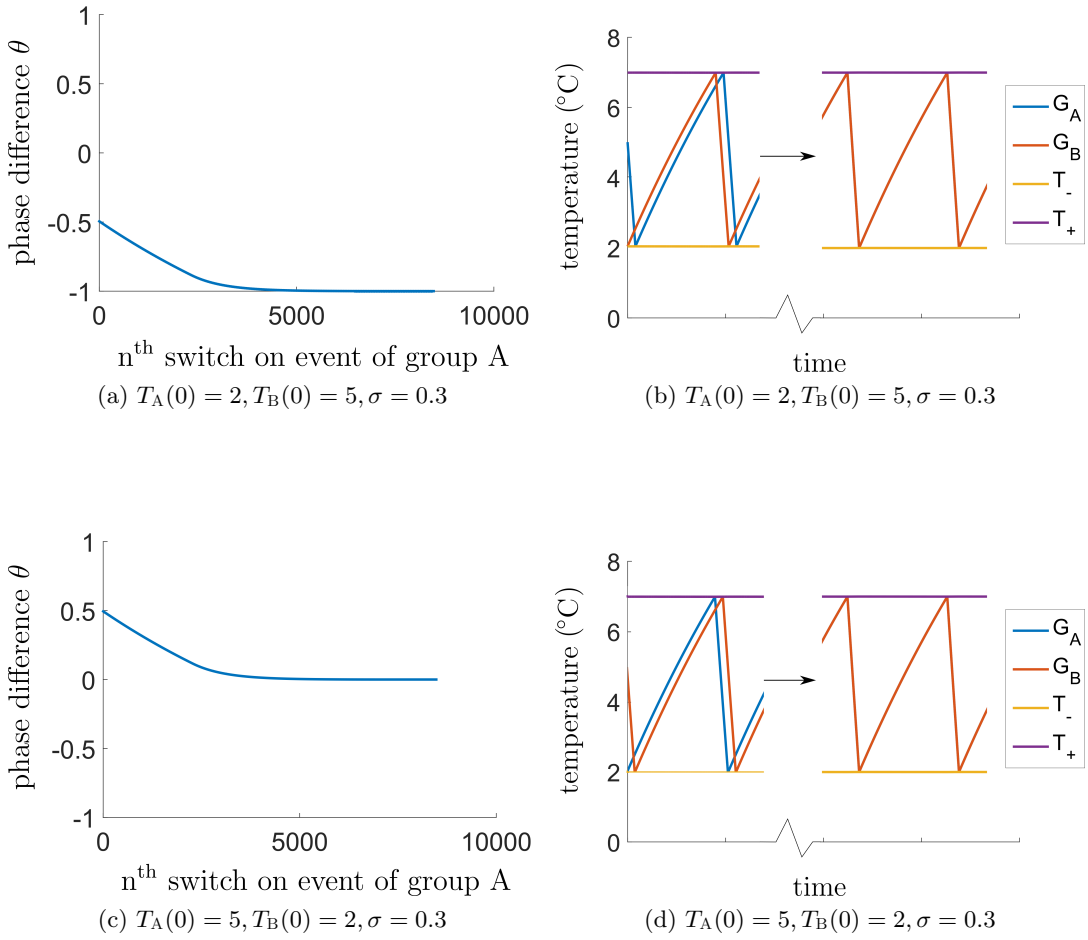

(a) $T_A(0) = 2, T_B(0) = 5, \sigma = 0.3$

(b) $T_A(0) = 2, T_B(0) = 5, \sigma = 0.3$

(c) $T_A(0) = 5, T_B(0) = 2, \sigma = 0.3$

(d) $T_A(0) = 5, T_B(0) = 2, \sigma = 0.3$

Figure 3.7: Each row shows the results from one simulation for parameter values shown and $\rho^* \approx 0.1174$, all others as in Table 3.1. Left-hand figures show phase difference against group A switch on events (see (3.81b)). Right-hand figures show temperature against time for G_A and G_B (not distinct from one another due to synchronisation) for a subset of the time window near the end of the simulation.

find that even if the switch on times of two groups start negligibly close to one another, given certain values of σ, they can move apart. The intuition behind these results is that when one group is more than a little larger than the other it will have a dominating effect and 'pull' the smaller group towards it. If, however, the two groups are of almost identical size, there is no dominant group and they will remain separate.

We can also explore the effect of varying the parameter ρ^*, which we do by varying

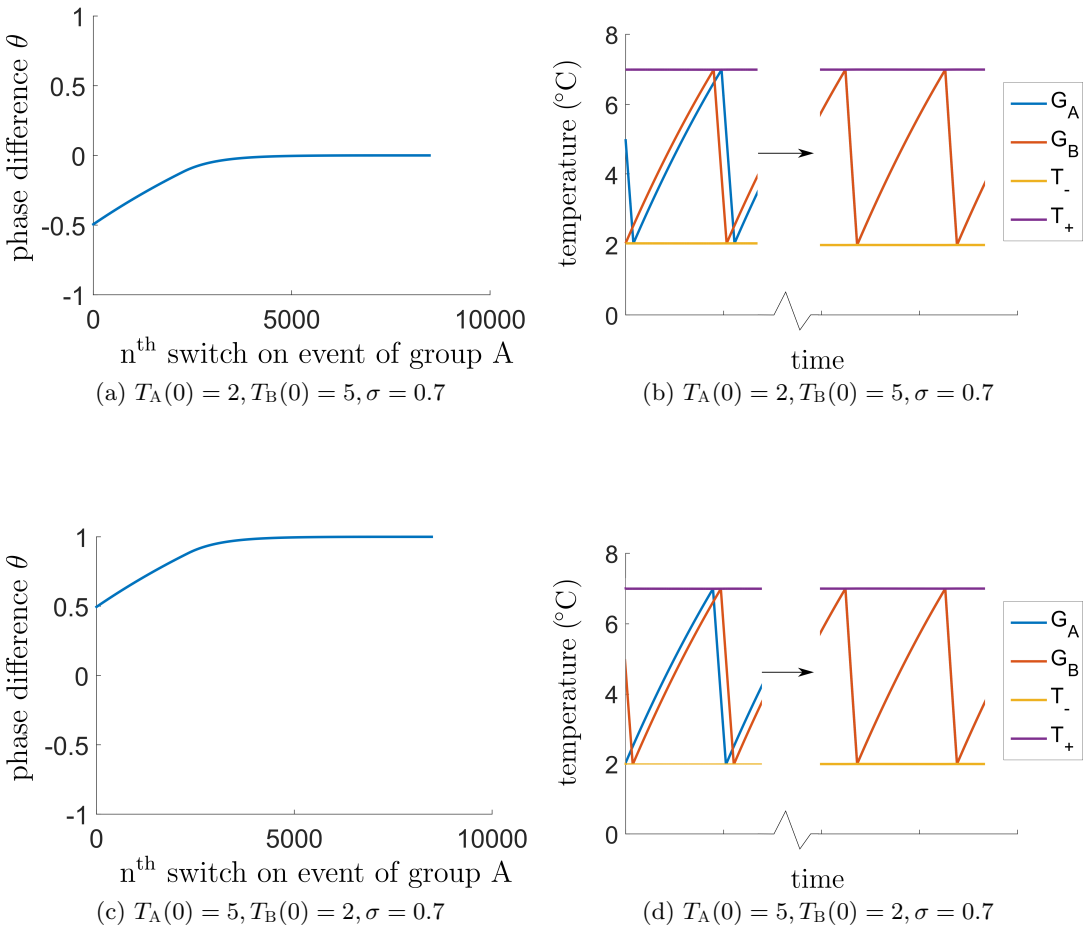

(a) $T_A(0) = 2, T_B(0) = 5, \sigma = 0.7$

(b) $T_A(0) = 2, T_B(0) = 5, \sigma = 0.7$

(c) $T_A(0) = 5, T_B(0) = 2, \sigma = 0.7$

(d) $T_A(0) = 5, T_B(0) = 2, \sigma = 0.7$

Figure 3.8: Each row shows the results from one simulation for parameter values shown and $\rho^* \approx 0.1174$, all others as in Table 3.1. Left-hand figures show phase difference against group A switch on events (see (3.81b)). Right-hand figures show temperature against time for G_A and G_B (not distinct from one another due to synchronisation) for a subset of the time window near the end of the simulation.

T_{ON}. Repeated simulations for different values allow us to construct a diagram to show the regions in (σ, ρ^*)-space that will lead to synchronisation, and those that will keep two distinct groups forever apart. We omit this diagram for the time being, as it matches the bifurcation diagram derived in Section 3.4.6.

Our approach so far has been to consider the system in terms of the continuous time dynamics. It can take a long time for groups to settle down to their steady-state behaviour when simulations have to update using small time steps to reduce numerical errors. An alternative is to model the system as a sequence of discrete

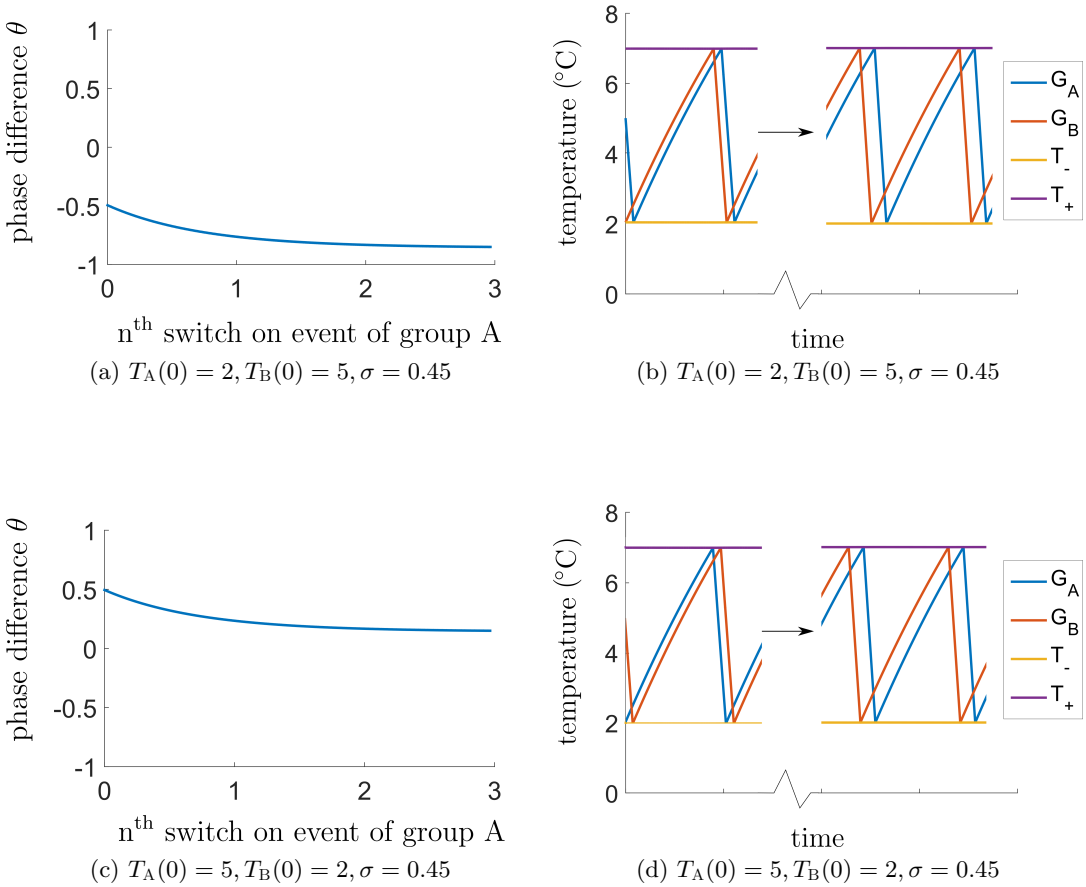

(a) $T_A(0) = 2, T_B(0) = 5, \sigma = 0.45$

(b) $T_A(0) = 2, T_B(0) = 5, \sigma = 0.45$

(c) $T_A(0) = 5, T_B(0) = 2, \sigma = 0.45$

(d) $T_A(0) = 5, T_B(0) = 2, \sigma = 0.45$

Figure 3.9: Each row shows the results from one simulation for parameter values shown and $\rho^* \approx 0.1174$, all others as in Table 3.1. Left-hand figures show phase difference against group A switch on events (see (3.81b)). Right-hand figures show temperature against time for G_A and G_B (not distinct from one another due to synchronisation) for a subset of the time window near the end of the simulation.

switching events. This will be the focus of the next section.

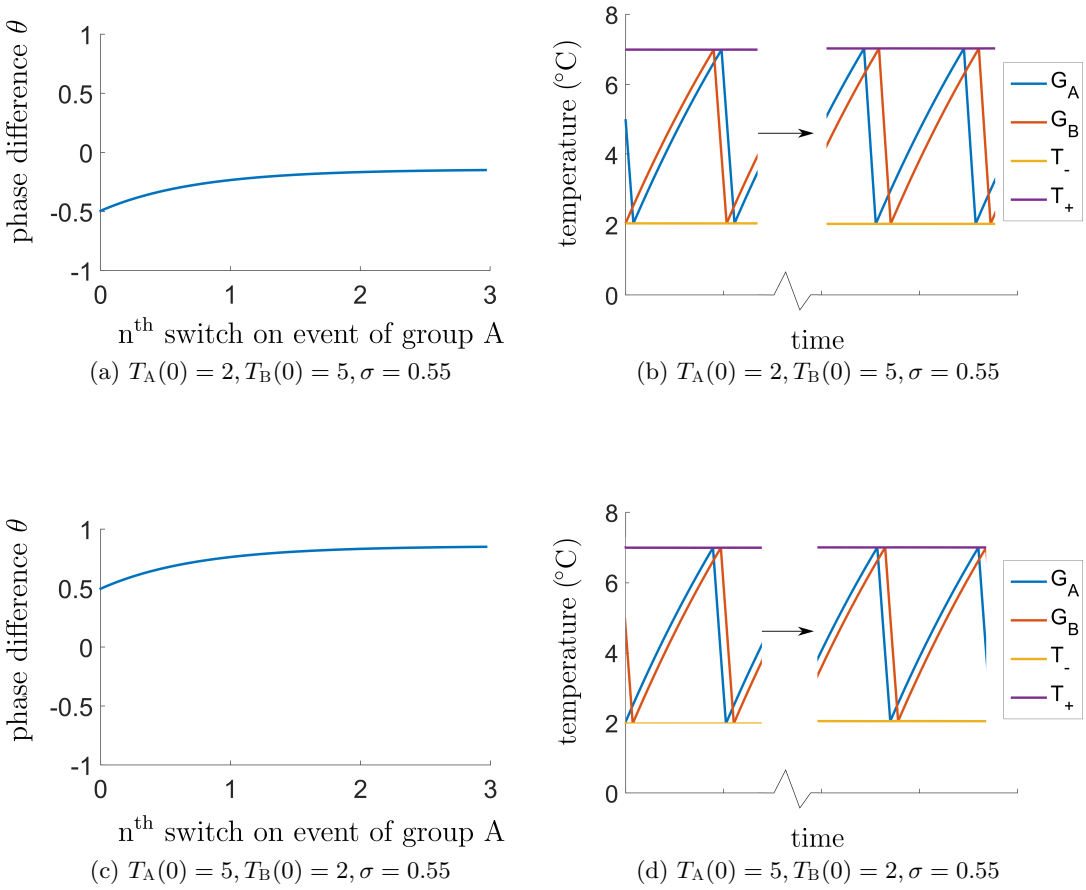

(a) $T_{\mathrm{A}}(0) = 2, T_{\mathrm{B}}(0) = 5, \sigma = 0.55$

(b) $T_{\mathrm{A}}(0) = 2, T_{\mathrm{B}}(0) = 5, \sigma = 0.55$

(c) $T_{\mathrm{A}}(0) = 5, T_{\mathrm{B}}(0) = 2, \sigma = 0.55$

(d) $T_{\mathrm{A}}(0) = 5, T_{\mathrm{B}}(0) = 2, \sigma = 0.55$

Figure 3.10: Each row shows the results from one simulation for parameter values shown and $\rho^* \approx 0.1174$, all others as in Table 3.1. Left-hand figures show θ against A switching events (see (3.81b)). Right hand figures show temperature against time for G_A and G_B for a subset of the time window near the end of the simulation.

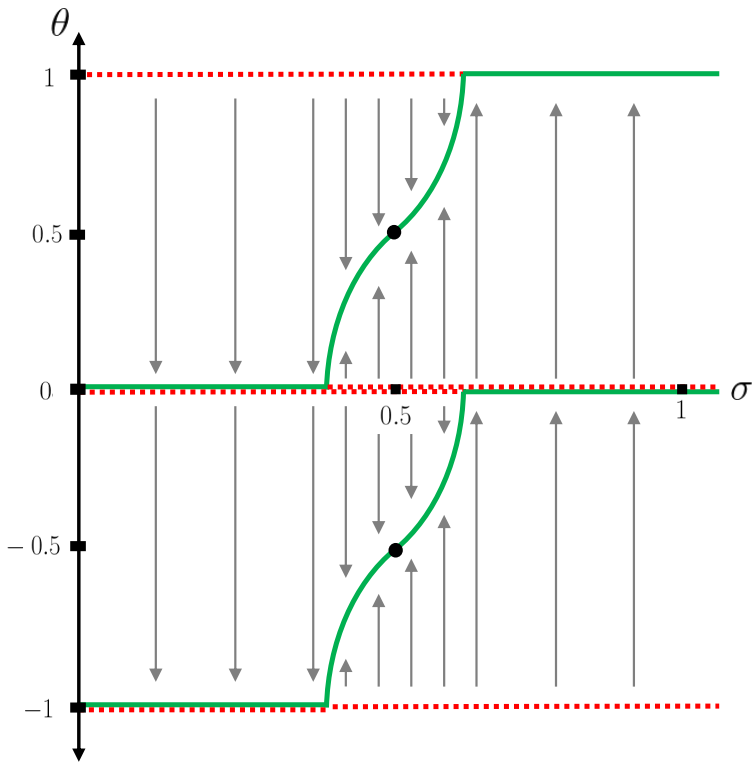

Figure 3.11: Bifurcation diagram for the phase difference between two groups of TCLs. Green solid lines represent stable fixed points, red dashed lines represent unstable fixed points. Two groups can co-exist for $\sigma \approx 0.5$. The range has been expanded for diagram, narrower than presented here (approximately ± 0.2 around 0.5).

3.4.5 Possible two-group switching behaviour

Switching event orders

To model the temperature cycling behaviour of two groups requires greater consideration than was required for the fully synchronised population (one group). This is because there are more types of switching events, for which the order is unclear. The two groups can switch simultaneously or separately, and simply knowing which group

switched last does not tell us which group will switch next. There are four on/off state combinations (S_A, S_B) of the system; $(S_A, S_B) \in \{(1,1),(0,0),(1,0),(0,1)\}$. Figure 3.12 shows these four system states and labels the 12 switching events between them (labelled with arrows A-L). The goal is to discover the long-term behaviour of a population, and one way of analysing this is to study the progression of switching events. Do we find that for given parameters and initial conditions a population will settle down to a certain switching pattern? It is clear that if switch event K $((0,0) \to (1,1))$ or L $((1,1) \to (0,0))$ is reached then the populations have synchronised into one group, and so the switching pattern will remain as the loop KL thereafter. Are there other possibilities?

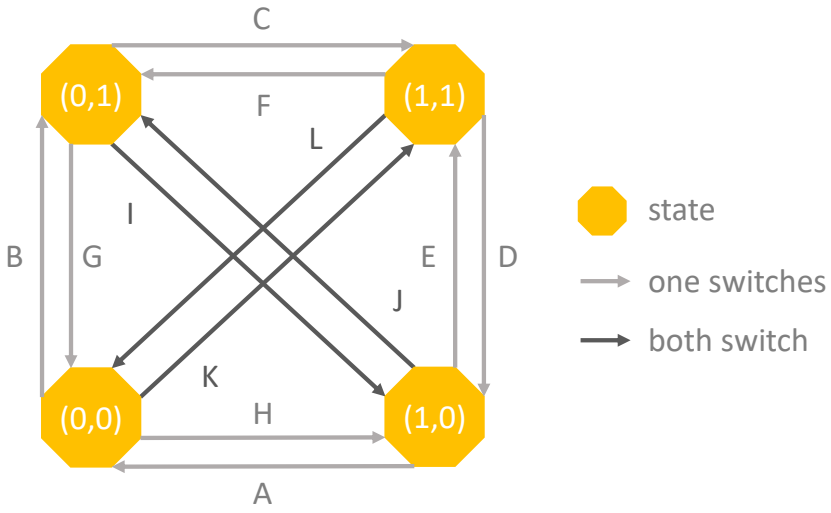

Figure 3.12: The 4 system states and 12 switch events for 2 groups. Octagons show the 4 possible system states (S_A, S_B). Light arrows show single switch events, dark arrows show double switch events (both groups switch simultaneously).

To understand the possible orders in which switching events can occur we create a new diagram (Figure 3.13) formed from nodes representing the arrows in Figure 3.12. One event can follow another if and only if the end state of the first event is the same as the starting state of the second. In Figure 3.13 all possible switch event progressions are shown with arrows. This diagram shows the full set of possible event transitions. Given the initial states and temperatures of the two groups we would like to analyse the progression of switch events and discover the long-term behaviour of the system. This requires solving for the time at which each successive switch occurs, and the temperatures and states of the groups at each switch.

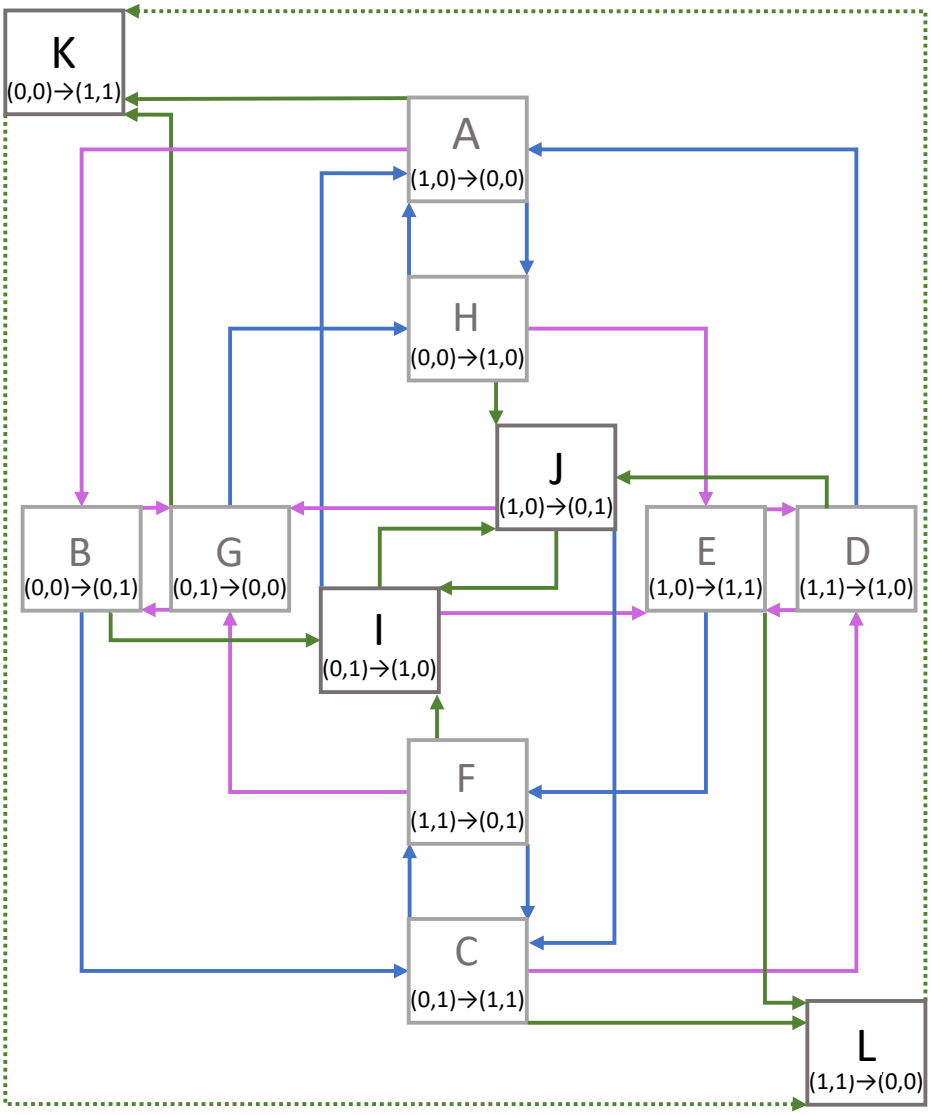

Figure 3.13: Rectangles show switching events, arrows represent all possible switching event progressions. G_A switches then G_B switches (blue), G_B switches then G_A (pink), one of the switches is simultaneous (green), both switches simultaneous (dashed green).

Solving for the two-group switching behaviour

Suppose that when a switch occurs (at time, say, $t = 0$) we know the temperatures of the two groups, $\big(T_{\mathrm{A}}(0), T_{\mathrm{A}}(0)\big)$ and their on/off states $\big(S_{\mathrm{A}}(0), S_{\mathrm{B}}(0)\big)$. In order to know which group will switch next we solve for the switch time in each case, G_A switching next and G_B switching next, and compare the two times. Whichever

group has the soonest switch time will switch next. If the switch times are the same then we have a simultaneous switch event.

The general method for solving for the switch times is as follows. Suppose group I switches at time $t = 0$ and test the hypothesis that group J switches next (I and J could be the same group). Then if this next switch occurs at time t,

$$T_{\mathrm{J}}(t) = T_{\bullet}^{0} - \beta_{\bullet} f(t) \tag{3.83}$$

$$f(t) = f(0) + t\dot{f}(t) \tag{3.84}$$

$$\therefore T_{\mathrm{J}}(t) = T_{\bullet}^{0} - \beta_{\bullet}[f(0) + t\dot{f}(t)] \tag{3.85}$$

where subscript '$\bullet$' signifies '$+$' if group J is switching on at time t and '$-$' if group J is switching off at time t. Now our information about the switch at time $t = 0$ tells us that

$$T_{\mathrm{I}}(0) = T_{\circ}^{0} - \beta_{\circ} f(0) \tag{3.86}$$

$$\therefore f(0) = \frac{T_{\circ}^{0} - T_{\mathrm{I}}(0)}{\beta_{\circ}} \tag{3.87}$$

$$\therefore T_{\mathrm{J}}(t) = T_{\bullet}^{0} - \beta_{\bullet}[\frac{T_{\circ}^{0} - T_{\mathrm{I}}(0)}{\beta_{\circ}} + t\dot{f}(t)] \tag{3.88}$$

where '$\circ$' signifies '$+$' if G_{I} is switching on at time 0 and '$-$' if G_{I} is switching off at time 0. For each hypothetical switching event progression of the form XY[5] the

[5] In the switch progression XY switch X occurs at time 0 and switch Y occurs at time t. For example, if XY is the switch event progression CD, then group A switches on at time 0 and group B switches off at time t.

exact form of equation 3.88 for each possible event progression is as follows.

$$AH, AK, LK \quad T_{\mathrm{A}}(t) = T_+^0 \quad - \beta_+ cp\rho^* t - \tfrac{\beta_+}{\beta_-}\big(T_-^0 - T_{\mathrm{A}}(0)\big) \tag{3.89a}$$

$$BC, BI, JC \quad T_{\mathrm{A}}(t) = \quad + \beta_+ cp(1-\sigma-\rho^*)t + T_{\mathrm{B}}(0) \tag{3.89b}$$

$$CF, CL, KL \quad T_{\mathrm{A}}(t) = T_-^0 \quad + \beta_- cp(1-\rho^*)t - \tfrac{\beta_-}{\beta_+}\big(T_+^0 - T_{\mathrm{A}}(0)\big) \tag{3.89c}$$

$$DA, DJ, IA, IJ \quad T_{\mathrm{A}}(t) = \quad + \beta_- cp(\sigma-\rho^*)t + T_{\mathrm{B}}(0) \tag{3.89d}$$

$$EF, EL, KL \quad T_{\mathrm{A}}(t) = T_-^0 \quad + \beta_- cp(1-\rho^*)t - \tfrac{\beta_-}{\beta_+}\big(T_+^0 - T_{\mathrm{B}}(0)\big) \tag{3.89e}$$

$$FC, FI, JC \quad T_{\mathrm{A}}(t) = T_+^0 \quad + \beta_+ cp(1-\sigma-\rho^*)t - \tfrac{\beta_+}{\beta_-}\big(T_-^0 - T_{\mathrm{A}}(0)\big) \tag{3.89f}$$

$$GH, GK, LK \quad T_{\mathrm{A}}(t) = T_+^0 \quad - \beta_+ cp\rho^* t - \tfrac{\beta_+}{\beta_-}\big(T_-^0 - T_{\mathrm{B}}(0)\big) \tag{3.89g}$$

$$HA, HJ, IA, IJ \quad T_{\mathrm{A}}(t) = T_-^0 \quad + \beta_- cp(\sigma-\rho^*)t - \tfrac{\beta_-}{\beta_+}\big(T_+^0 - T_{\mathrm{A}}(0)\big) \tag{3.89h}$$

$$AB, AK, LK \quad T_{\mathrm{B}}(t) = T_+^0 \quad - \beta_+ cp\rho^* t - \tfrac{\beta_+}{\beta_-}\big(T_-^0 - T_{\mathrm{A}}(0)\big) \tag{3.89i}$$

$$BG, BI, JG \quad T_{\mathrm{B}}(t) = T_-^0 \quad + \beta_- cp(1-\sigma-\rho^*)t - \tfrac{\beta_-}{\beta_+}\big(T_+^0 - T_{\mathrm{B}}(0)\big) \tag{3.89j}$$

$$CD, CL, KL \quad T_{\mathrm{B}}(t) = T_-^0 \quad + \beta_- cp(1-\rho^*)t - \tfrac{\beta_-}{\beta_+}\big(T_+^0 - T_{\mathrm{A}}(0)\big) \tag{3.89k}$$

$$DE, DJ, IE, IJ \quad T_{\mathrm{B}}(t) = T_+^0 \quad + \beta_+ cp(\sigma-\rho^*)t - \tfrac{\beta_+}{\beta_-}\big(T_-^0 - T_{\mathrm{B}}(0)\big) \tag{3.89l}$$

$$ED, EL, KL \quad T_{\mathrm{B}}(t) = T_-^0 \quad + \beta_- cp(1-\rho^*)t - \tfrac{\beta_-}{\beta_+}\big(T_+^0 - T_{\mathrm{B}}(0)\big) \tag{3.89m}$$

$$FG, FI, JG \quad T_{\mathrm{B}}(t) = \quad + \beta_- cp(1-\sigma-\rho^*)t + T_{\mathrm{A}}(0) \tag{3.89n}$$

$$GB, GK, LK \quad T_{\mathrm{B}}(t) = T_+^0 \quad - \beta_+ cp\rho^* t - \tfrac{\beta_+}{\beta_-}\big(T_-^0 - T_{\mathrm{B}}(0)\big) \tag{3.89o}$$

$$HE, HJ, IE, IJ \quad T_{\mathrm{B}}(t) = \quad + \beta_+ cp(\sigma-\rho^*)t + T_{\mathrm{A}}(0). \tag{3.89p}$$

Note that switch progressions involving a simultaneous switch have multiple valid equations.

We can equate our equation for $T_{\mathrm{J}}(t)$ with the temperature evolution equation (3.5a) if on or (3.5b) if off and solve (numerically) for t. Once we have the switch time t the temperatures of the two groups at time t follow easily. The temperature evolution equations tell us that for event progressions of the form:

$$\text{AX, BX, FX, GX JX, LX:} \quad T_{\mathrm{A}}(t) = (T_{\mathrm{A}}(0) - T_{\mathrm{OFF}})e^{-\alpha t} + T_{\mathrm{OFF}} \tag{3.90a}$$

$$\text{CX, DX, EX, HX, IX, KX:} \quad T_{\mathrm{A}}(t) = (T_{\mathrm{A}}(0) - T_{\mathrm{ON}})e^{-\alpha t} + T_{\mathrm{ON}} \tag{3.90b}$$

$$\text{AX, DX, GX, HX, IX, LX:} \quad T_{\mathrm{B}}(t) = (T_{\mathrm{B}}(0) - T_{\mathrm{OFF}})e^{-\alpha t} + T_{\mathrm{OFF}} \tag{3.90c}$$

$$\text{BX, CX, EX, FX, JX, KX:} \quad T_{\mathrm{B}}(t) = (T_{\mathrm{B}}(0) - T_{\mathrm{ON}})e^{-\alpha t} + T_{\mathrm{ON}}. \tag{3.90d}$$

where 'X' represents any possible switching event directly following the first event in the pair. These allow us to solve for the switch time and then to find the temperature

of each group when the switch occurs.

The $G_A \sim G_B$ group symmetry means that the following pairs of (memoryless) switch events are symmetric in G_A and G_B: A∼G, B∼H, C∼E, D∼F and I∼J. Therefore any information learned/equations solved for a switch event progression can be applied to the event progression in its symmetric pair by 1) replacing the each of the two letters in the event name by their symmetric pairs, 2) swapping T_A and T_B in the results/equations, and 3) swapping σ and $1-\sigma$ in the equations.

Given the on/off states of the groups at time 0, the space of initial temperatures of the two groups, $(T_{\mathrm{ON}}, T_{\mathrm{OFF}})^2$, can be split into regions of initial conditions that map to each possible subsequent switch event. On the boundaries of the regions simultaneous switching occurs. We begin our exploration of these regions by solving for simultaneous switching in each of the four system states.

Case 1: $\big(\mathbf{S}_\mathrm{A}(\mathbf{0}), \mathbf{S}_\mathrm{B}(\mathbf{0})\big) = (\mathbf{1}, \mathbf{1})$
Both groups are switched on and therefore

$$T_\mathrm{A}(t) = (T_\mathrm{A}(0) - T_{\mathrm{ON}})e^{-\alpha t} + T_{\mathrm{ON}} \tag{3.91a}$$
$$T_\mathrm{B}(t) = (T_\mathrm{B}(0) - T_{\mathrm{ON}})e^{-\alpha t} + T_{\mathrm{ON}}. \tag{3.91b}$$

Both groups are cooling down to reach the lower temperature set point and so whichever started off coolest will switch off first. The groups will switch simultaneously if and only if $T_\mathrm{A}(t) = T_\mathrm{B}(t)$ which occurs if and only if $T_\mathrm{A}(0) = T_\mathrm{B}(0)$.

Case 2: $\big(\mathbf{S}_\mathrm{A}(\mathbf{0}), \mathbf{S}_\mathrm{B}(\mathbf{0})\big) = (\mathbf{0}, \mathbf{0})$
Both groups are switched off and therefore

$$T_\mathrm{A}(t) = (T_\mathrm{A}(0) - T_{\mathrm{OFF}})e^{-\alpha t} + T_{\mathrm{OFF}} \tag{3.92a}$$
$$T_\mathrm{B}(t) = (T_\mathrm{B}(0) - T_{\mathrm{OFF}})e^{-\alpha t} + T_{\mathrm{OFF}} \tag{3.92b}$$

and so as in case 1 the groups will switch on simultaneously *iff* $T_\mathrm{A}(0) = T_\mathrm{B}(0)$. If they start at different temperatures the next group to switch on will be the group with the highest initial temperature. The results for cases 1 and 2 are shown graphically in Figure 3.14. Note that the results do not depend on which group switched at $t = 0$.

Case 3: $\big(\mathbf{S}_\mathrm{A}(\mathbf{0}), \mathbf{S}_\mathrm{B}(\mathbf{0})\big) = (\mathbf{1}, \mathbf{0})$
When G_A is on and G_B is off they will switch simultaneously *iff* G_A reaches its lower set point at the same time t that G_B reaches its upper set point. The temperatures

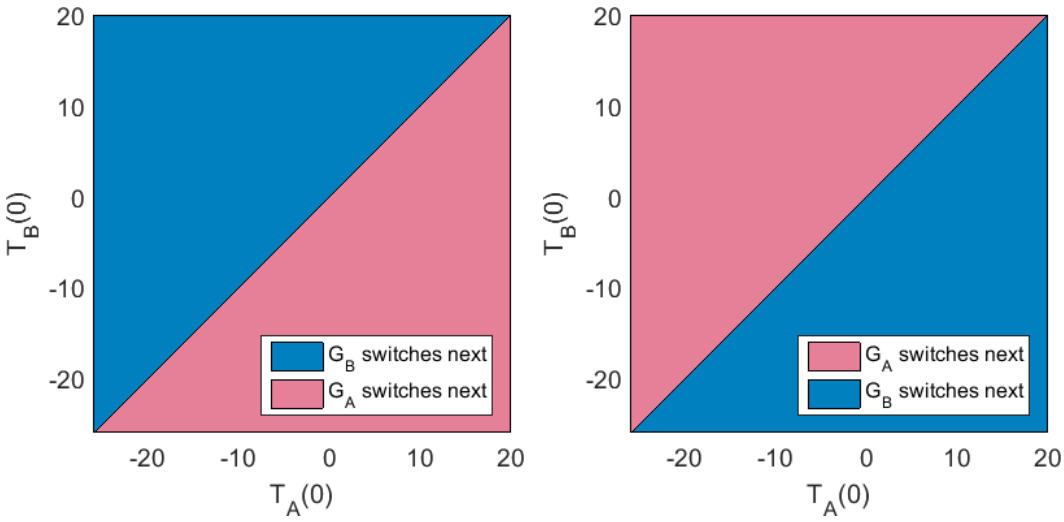

(a) $\big(S_{\mathrm{A}}(0), S_{\mathrm{B}}(0)\big) = (1, 1)$ (b) $\big(S_{\mathrm{A}}(0), S_{\mathrm{B}}(0)\big) = (0, 0)$

Figure 3.14: Figures showing which group will be the next to switch given initial temperatures for cases 1 and 2. The dividing lines indicate simultaneous switching. For these figures $\sigma = 0.7$ and all other parameters are as given in Table 3.1.

of each group at this simultaneous switch are therefore given by

$$T_{\mathrm{A}}(t) = (T_{\mathrm{A}}(0) - T_{\mathrm{ON}})e^{-\alpha t} + T_{\mathrm{ON}} \qquad = T_{-}^{0} - \beta_{-} f(t) \tag{3.93a}$$

$$T_{\mathrm{B}}(t) = (T_{\mathrm{B}}(0) - T_{\mathrm{OFF}})e^{-\alpha t} + T_{\mathrm{OFF}} \qquad = T_{+}^{0} - \beta_{+} f(t) \tag{3.93b}$$

which we can write in matrix form as

$$\begin{pmatrix} T_{\mathrm{A}}(0) - T_{\mathrm{ON}} & \beta_{-} \\ T_{\mathrm{B}}(0) - T_{\mathrm{OFF}} & \beta_{+} \end{pmatrix} \begin{pmatrix} e^{-\alpha t} \\ f(t) \end{pmatrix} = \begin{pmatrix} T_{-}^{0} - T_{\mathrm{ON}} \\ T_{+}^{0} - T_{\mathrm{OFF}} \end{pmatrix} \tag{3.94}$$

which gives

$$\begin{pmatrix} e^{-\alpha t} \\ f(t) \end{pmatrix} = \frac{1}{\Delta} \begin{pmatrix} \beta_{+} & -\beta_{-} \\ -(T_{\mathrm{B}}(0) - T_{\mathrm{OFF}}) & T_{\mathrm{A}}(0) - T_{\mathrm{ON}} \end{pmatrix} \begin{pmatrix} T_{-}^{0} - T_{\mathrm{ON}} \\ T_{+}^{0} - T_{\mathrm{OFF}} \end{pmatrix} \tag{3.95}$$

where determinant

$$\Delta := \beta_{+}(T_{\mathrm{A}}(0) - T_{\mathrm{ON}}) - \beta_{-}(T_{\mathrm{B}}(0) - T_{\mathrm{OFF}}) > 0.$$

Therefore we can write

$$e^{-\alpha t} = g\big(T_{\mathrm{A}}(0), T_{\mathrm{B}}(0)\big) \tag{3.96}$$

$$f(t) = h\big(T_{\mathrm{A}}(0), T_{\mathrm{B}}(0)\big) \tag{3.97}$$

where h and g are functions given by the matrix multiplication in (3.95).

The frequency at the next switch time t depends on the previous switch event:

$$f(t) = \begin{cases} \frac{T_+^0 - T_{\mathrm{A}}(0)}{\beta_+} - cp(\sigma - \rho^*)t & \text{if } G_A \text{ switched most recently} \\ \\ \frac{T_-^0 - T_{\mathrm{B}}(0)}{\beta_-} - cp(\sigma - \rho^*)t & \text{if } G_B \text{ switched most recently.} \end{cases} \tag{3.98}$$

To find the simultaneous switch curve in $\big(T_{\mathrm{A}}(0), T_{\mathrm{B}}(0)\big)$ space we combine the previous three equations into one equation that we use to solve for $T_{\mathrm{B}}(0)$ in terms of $T_{\mathrm{A}}(0)$:

$$\begin{aligned} h\big(T_{\mathrm{A}}(0), T_{\mathrm{B}}(0)\big) = \frac{cp}{\alpha}(\sigma - \rho^*) \log g\big(T_{\mathrm{A}}(0), T_{\mathrm{B}}(0)\big) + \\ + \begin{cases} \frac{T_+^0 - T_{\mathrm{A}}(0)}{\beta_+} & \text{if A switched most recently} \\ \\ \frac{T_-^0 - T_{\mathrm{B}}(0)}{\beta_-} & \text{if B switched most recently.} \end{cases} \end{aligned} \tag{3.99}$$

where

$$h\big(T_{\mathrm{A}}(0), T_{\mathrm{B}}(0)\big) := \frac{(T_{\mathrm{A}}(0) - T_{\mathrm{ON}})(T_+^0 - T_{\mathrm{OFF}}) - (T_{\mathrm{B}}(0) - T_{\mathrm{OFF}})(T_-^0 - T_{\mathrm{ON}})}{\beta_+(T_{\mathrm{A}}(0) - T_{\mathrm{ON}}) - \beta_-(T_{\mathrm{B}}(0) - T_{\mathrm{OFF}})}$$

$$g\big(T_{\mathrm{A}}(0), T_{\mathrm{B}}(0)\big) := \frac{\beta_+(T_-^0 - T_{\mathrm{ON}}) - \beta_-(T_+^0 - T_{\mathrm{OFF}})}{\beta_+(T_{\mathrm{A}}(0) - T_{\mathrm{ON}}) - \beta_-(T_{\mathrm{B}}(0) - T_{\mathrm{OFF}})}.$$

The solution of (3.99) is shown by the dividing line between the two regions in Figure 3.15 (a and b) for the parameters in Table 3.1. We find that changing the parameters has negligible impact on the shape of each region.

Case 4: $\big(\mathbf{S}_{\mathrm{A}}(\mathbf{0}), \mathbf{S}_{\mathrm{B}}(\mathbf{0})\big) = (\mathbf{0}, \mathbf{1})$

Case 4 is just case 3 where groups A and B have been swapped. There is nothing that marks the groups as different apart from their starting temperatures and the most recent group to switch therefore the equation to solve is the same as in case 3 only with A in the place of B. The solution of this equation is shown by the dividing line between the two regions in Figure 3.15 (c and d).

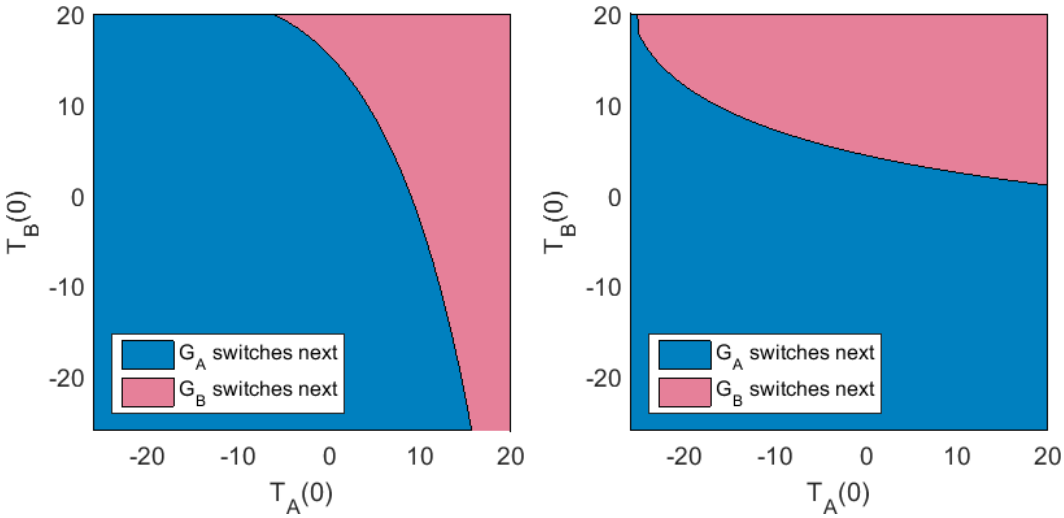

(a) $\big(S_{\mathrm{A}}(0), S_{\mathrm{B}}(0)\big) = (1, 0)$, A switched last

(b) $\big(S_{\mathrm{A}}(0), S_{\mathrm{B}}(0)\big) = (1, 0)$, B switched last

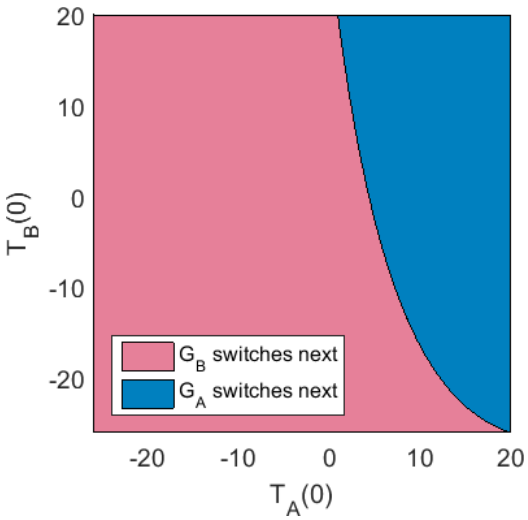

(c) $\big(S_{\mathrm{A}}(0), S_{\mathrm{B}}(0)\big) = (0, 1)$, A switched last

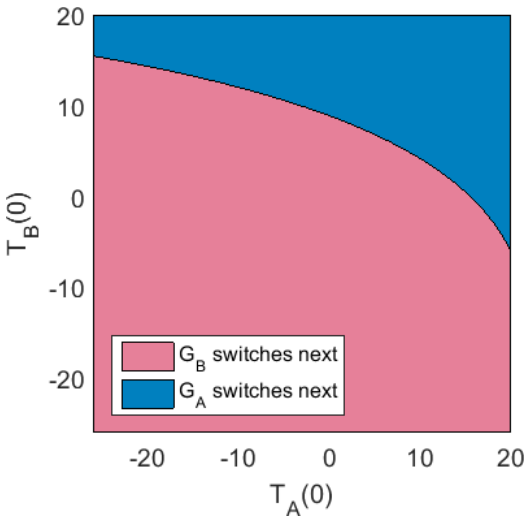

(d) $\big(S_{\mathrm{A}}(0), S_{\mathrm{B}}(0)\big) = (0, 1)$, B switched last

Figure 3.15: Figures showing which group will be the next to switch given initial temperatures and which group was the last to switch for cases 3 and 4. The dividing line indicates simultaneous switching and solve equation (3.99). For these figures $\sigma = 0.7$ and all other parameters are as given in Table 3.1.

For each event A, B, ..., L we can consider which regions in the space of initial temperatures $(T_{\text{ON}}, T_{\text{OFF}})^2$ will map to which next switch event. For some events not every initial temperature combination $\big(T_{\text{A}}(0), T_{\text{B}}(0)\big)$ will be possible. Solving for the next switch event for each initial pair of temperatures will result in the time until the next switch, t. If t is found to be negative then the initial condition is infeasible.

Eliminating infeasible initial conditions

Setting $t = 0$ in the switch event equations and setting $\beta_- \approx \beta_+$ gives:

AB	$T_{\text{B}}(0) \approx T_{\text{A}}(0) + T_+^0 - T_-^0$	straight line, slope 1
CD	$T_{\text{B}}(0) \approx T_{\text{A}}(0) - (T_+^0 - T_-^0)$	straight line, slope 1
EF	$T_{\text{B}}(0) \approx T_{\text{A}}(0) + T_+^0 - T_-^0$	straight line, slope 1
GH	$T_{\text{B}}(0) \approx T_{\text{A}}(0) - (T_+^0 - T_-^0)$	straight line, slope 1

for BC, DA, HE, FG:

$T_{\text{A}}(0) = T_{\text{B}}(0)$	straight line, slope 1

for AH, BG, CF, DE, ED, FC, GB, HA, IA, IE, IJ, JC, JG, JI, LK, KL:

$T_+^0 \approx T_-^0$	not possible.

This allows us to eliminate certain regions of the initial temperature space as we cannot allow negative time until the next switch. Additionally, for some events it is implicit that the initial temperature of one group be higher than the other:

- Event B: both off when G_B switches on therefore G_B must be hotter when it switches
- Event D: both on when G_B switches off therefore G_B must be cooler when it switches
- Event F: both on when G_A switches off therefore G_A must be cooler when it switches
- Event H: both off when G_A switches on therefore G_A must be hotter when it switches

and so for these events half of the state space is eliminated as infeasible.

Events I, J, K and L have special properties, being the four events in which the two groups switching simultaneously. Event I is the switch $(0,1) \to (1,0)$ and therefore no matter which switch happens next, we know that

$$T_{\mathrm{A}}(0) = T_{+}^{0} - \beta_{+} f(0)$$
$$T_{\mathrm{B}}(0) = T_{-}^{0} - \beta_{-} f(0)$$

and therefore

$$T_{\mathrm{B}}(0) = T_{-}^{0} - \tfrac{\beta_{-}}{\beta_{+}}\left(T_{+}^{0} - T_{\mathrm{A}}(0)\right)$$
$$T_{\mathrm{B}}(0) = \frac{\beta_{-}}{\beta_{+}} T_{\mathrm{A}}(0) - \left(\tfrac{\beta_{-}}{\beta_{+}} T_{+}^{0} - T_{0}^{0}\right)$$

which is a straight line with slope 1. Due to the symmetrical nature of the two groups we can interchange A and B in this equation to get the equivalent result for event J:

$$T_{\mathrm{B}}(0) = \tfrac{\beta_{-}}{\beta_{+}} T_{\mathrm{A}}(0) + \tfrac{\beta_{-}}{\beta_{+}} T_{+}^{0} - T_{-}^{0}.$$

For events K and L the identical switching behaviour of the two groups tells us that they have synchronised (merged into one group) and therefore the valid initial conditions are exactly the line $T_{\mathrm{A}}(0) = T_{\mathrm{B}}(0)$.

All of this information allows us to summarise the valid initial conditions for each event and identify which regions within initial temperature space map to which next event. The results are shown in Figure 3.16. The position of each square corresponds to the position of the first event in the pair in Figure 3.13. After the initial switch event (X in the XY pair), G_A switching next is shown in pink, G_B switching next in blue, both switching in green and infeasible initial conditions in white. The vector fields show the direction in which the pair of temperatures will move following the initial switch (event X in each event progression XY shown). The trajectory of the temperatures starting at $\big(T_{\mathrm{A}}(0), T_{\mathrm{B}}(0)\big)$ is a straight line in $(T_{\mathrm{A}}, T_{\mathrm{B}})$-space.

To see this define notation

$$T_{\bullet}(I) := \begin{cases} T_{\mathrm{ON}} & \text{if } G_{\mathrm{I}} \text{ is switched on} \\ T_{\mathrm{OFF}} & \text{if } G_{\mathrm{I}} \text{ is switched off.} \end{cases}$$

Then by (3.3) we can write the rate of change of temperature of group I as:

$$\dot{T}_{\mathrm{I}}(t) = \alpha\big(T_{\bullet}(I) - T_{\mathrm{I}}(t)\big)$$

and therefore

$$\begin{aligned}
\frac{\mathrm{d}}{\mathrm{d}t}\left(\frac{\dot{T}_{\mathrm{A}}}{\dot{T}_{\mathrm{B}}}\right)(t) &= \frac{\mathrm{d}}{\mathrm{d}t}\left(\frac{\alpha\big(T_{\bullet}(A) - T_{\mathrm{A}}(t)\big)}{\alpha\big(T_{\bullet}(B) - T_{\mathrm{B}}(t)\big)}\right) \\
&= \frac{-\dot{T}_{\mathrm{A}}(t)\big(T_{\bullet}(B) - T_{\mathrm{B}}(t)\big) + \dot{T}_{\mathrm{B}}(t)\big(T_{\bullet}(A) - T_{\mathrm{A}}(t)\big)}{\big(T_{\bullet}(B) - T_{\mathrm{B}}(t)\big)^2} \\
&= \frac{-\alpha\big(T_{\bullet}(A) - T_{\mathrm{A}}(t)\big)\big(T_{\bullet}(B) - T_{\mathrm{B}}(t)\big) + \alpha\big(T_{\bullet}(B) - T_{\mathrm{B}}(t)\big)\big(T_{\bullet}(A) - T_{\mathrm{A}}(t)\big)}{\big(T_{\bullet}(B) - T_{\mathrm{B}}(t)\big)^2} \\
&= 0.
\end{aligned}$$

Knowing the shape of the trajectories is useful for considering how the valid regions shown in Figure 3.16 will change when they map to the temperature space of the next event. The complications arise from the switch times. Whilst two points in $\big(T_{\mathrm{A}}(0), T_{\mathrm{B}}(0)\big)$-space might be very close to one another, heading along nearby linear trajectories towards their temperatures at the next switch, they will take different amounts of time to reach their destination. The time taken to switch is a nonlinear (implicit) function of the initial temperatures and so if a region of initial temperatures were to be mapped to their corresponding temperatures at the next switch event, the region would likely undergo a nonlinear transformation.

Our simulations (such as those presented in Figures 3.9 and 3.10) suggest that for certain values of σ and ρ^* the groups will remain separate for all time and settle down to periodic temperature cycling. We would like to know what event progressions are possible in the long run. For example, perhaps a trajectory could settle on the event loop ABGH. If we were to map the region AB (the pink isosceles trapezium in event square A in Figure 3.16) to its image in the event B square, the vector field arrows indicate that the new region would be a smaller shape shifted more densely into the upper right-hand corner. We could imagine that the new region is likely to intersect the pink region BG, the green line BI and the blue region BC. Therefore only a portion of the original region could continue on to the next event in the loop, BG. If ABGH is truly a loop that can exist indefinitely then there exists at least one point in the AB region that will map back round to itself following one loop.

To explore the potential long-term behaviour of two groups we can solve for their temperatures and the grid frequency using the switching event equations, mapping

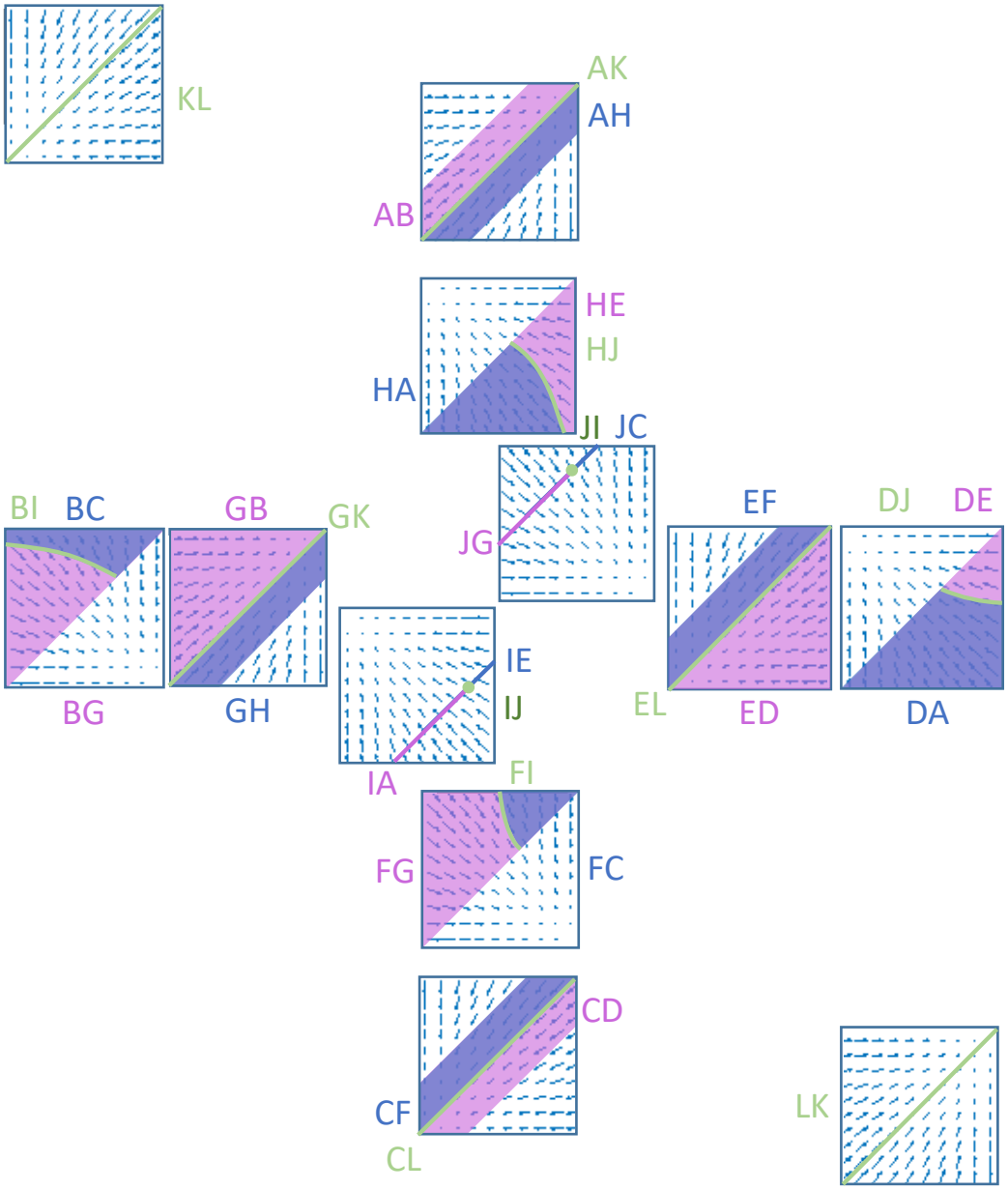

Figure 3.16: Initial condition regions for switching event progression of two groups of TCLs. For each event X in Figure 3.13 the space of initial conditions that map to the next switch event Y are labelled XY. G_A switches next (pink), G_B switches next (blue), both switch next (green), invalid initial condition (white). Vector field arrows indicate how initial temperatures will change before the next switch. Connecting arrows between squares removed for ease of reading, shown in Figure 3.13.

each switch event to the next. Figure 3.17 shows the behaviour of two groups of TCLs. In the left-hand figures (a, c, e), $\rho^* \approx 0.27$; in the right-hand figures (b,

d, f), $\rho^* \approx 0.79$. All other parameters are the same for the two simulations, and $\sigma = 0.48$. Figures (a) and (b) show the path through the switch events A-L. Figures (c) and (d) show these same paths, with the addition of the vertical (time) axis, which allows us to see the order in which the switch events occur. For example, Figure (c) indicates that the left-hand simulation initially loops through events A-B-C-D repeatedly, before changing to loop A-B-G-H. Figures (e) and (f) show the temperature progressions of the two groups for each choice of parameter values. The blue numbers next to the circled data points show the temperature pairs at each of the first four switch events. The fifth temperature pair will be the next point along the blue line (of points) next to circle 1. The sixth will be the point next to the circle two on the red line (of points). This continues until the final four points, marked by a cross at the end of each of the coloured lines. The $(T_\mathrm{A}, T_\mathrm{B})$ coordinates at each of these final points are labelled as a vector pair. Some of the lines (points in order of the same colour) have a distinct change in gradient, such as the purple line in Figure (e) and the blue line in Figure (f). These occur when the switching event progression loop changes. The $T_\mathrm{A} = T_\mathrm{B}$ line is shown to highlight whether the temperature cycles of the two groups are getting closer together. Synchronised groups would result in two distinct points on this diagonal line. Figures 3.18 and 3.19 show further examples of initial conditions that end with periodic behaviour in the A-B-G-H loop, for $\sigma = 0.48$ and $\rho^* \approx 0.27$.

To show the difference between synchronising and non-synchronising groups, Figure 3.20 shows the results for the same two choices of parameters as in Figure 3.17, except with $\sigma = 0.2$ (for both). Note that the four initial switch events (A-B-C-D) go through multiple different event loops before ultimately reaching the absorbing K-L loop when the two groups merge into one.

Visualising the switch events progressions for different choices of parameters and initial conditions is helpful to gain intuition about how two groups can be behave. In the next section we take an analytic approach to analysing under what conditions two groups will merge or separate.

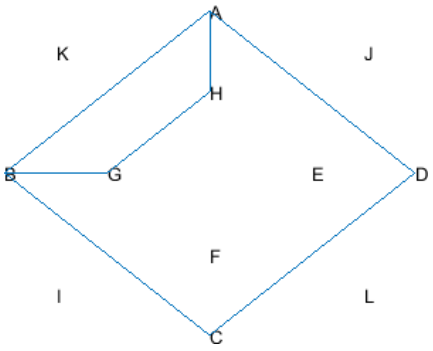

(a) Switch event paths

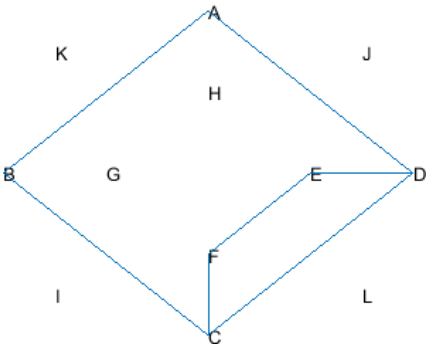

(b) Switch event paths

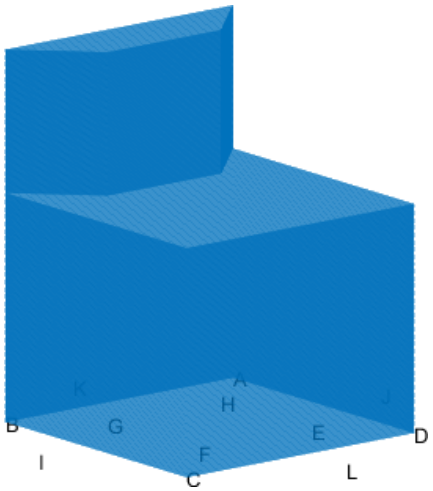

(c) Switch event paths through time (z-axis)

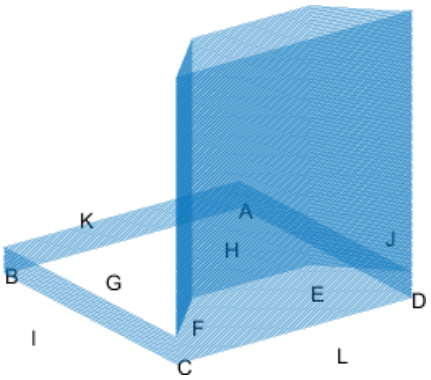

(d) Switch event paths through time (z-axis)

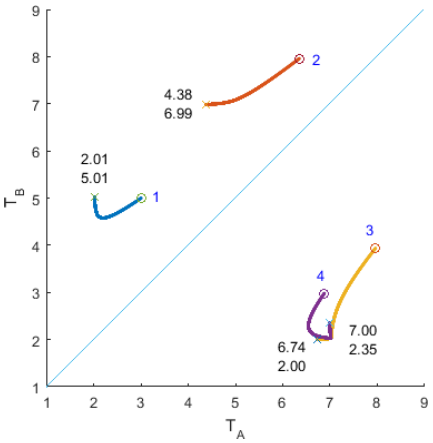

(e) Temperature progression

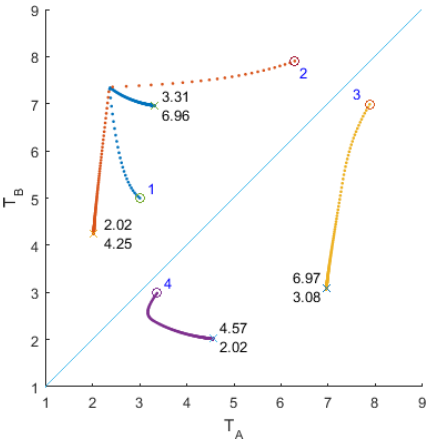

(f) Temperature progression

Figure 3.17: Tracking initial temperature pair (3,5) from event A through switch events over time, with $\sigma = 0.48$. $\rho^* \approx 0.27$ for (a,c,e), $\rho^* \approx 0.79$ for (b,d,f). First four temperature pairs labelled 1-4 in (e) and (f), continue down the coloured lines in that order to labelled points. For an expanded explanation see text above.

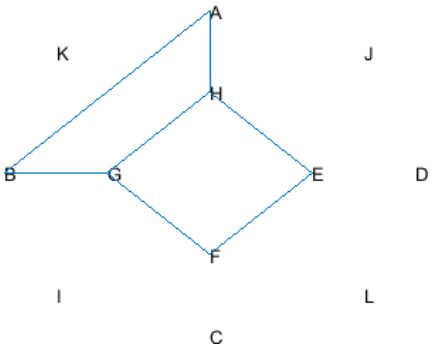

(a) Switch event paths

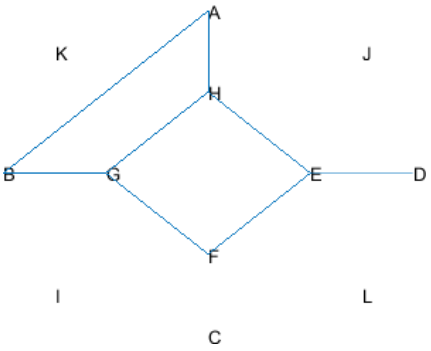

(b) Switch event paths

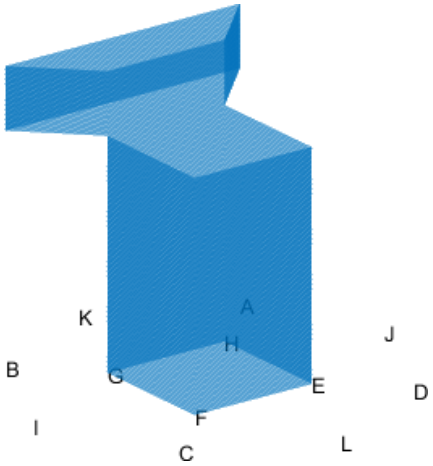

(c) Switch event paths through time (z-axis)

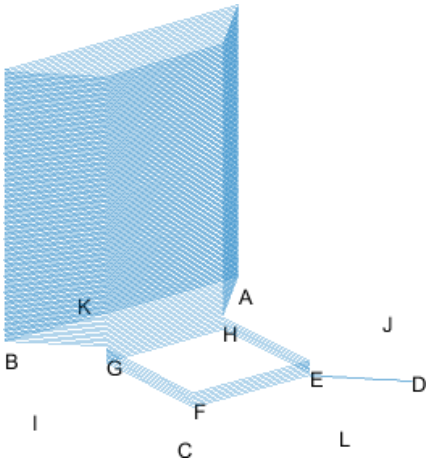

(d) Switch event paths through time (z-axis)

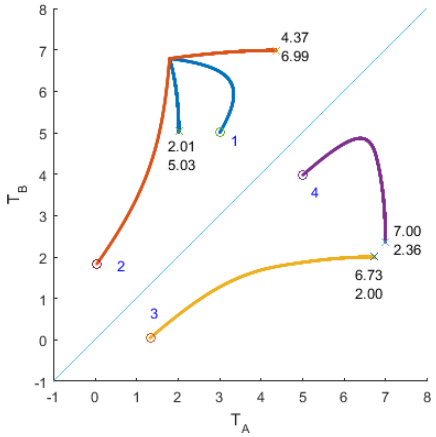

(e) Temperature progression

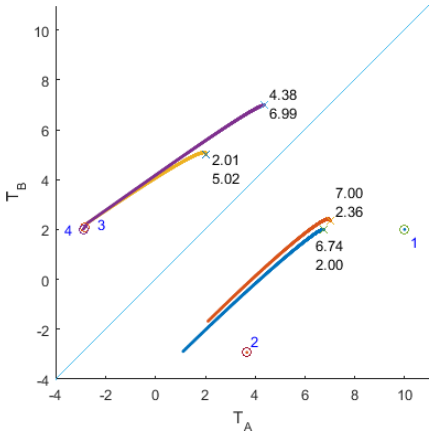

(f) Temperature progression

Figure 3.18: Tracking initial temperature pairs (3,5) (a,c,e) and (10,2) (b,d,f) from event E through switch events over time. First four temperature pairs labelled 1-4 in (e) and (f), continue down the coloured lines in that order to labelled points.

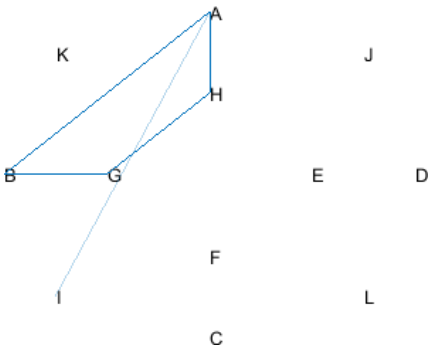

(a) Switch event paths

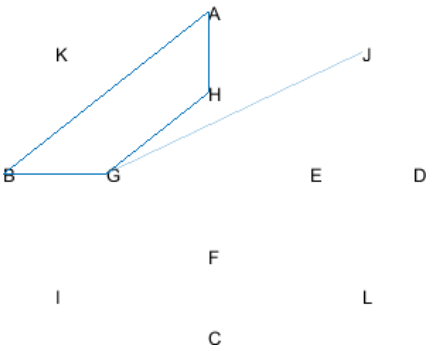

(b) Switch event paths

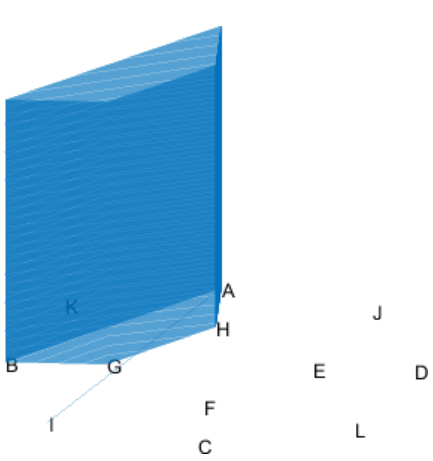

(c) Switch event paths (2,7) (from J)

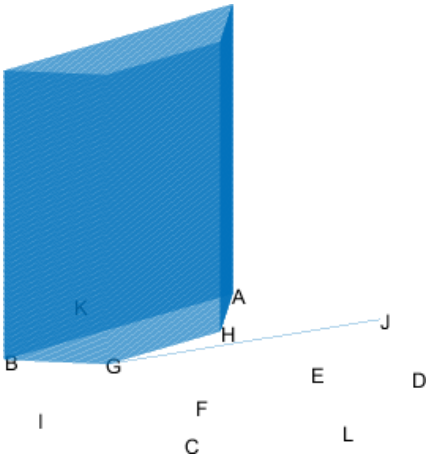

(d) Switch event paths (2,7) (from J)

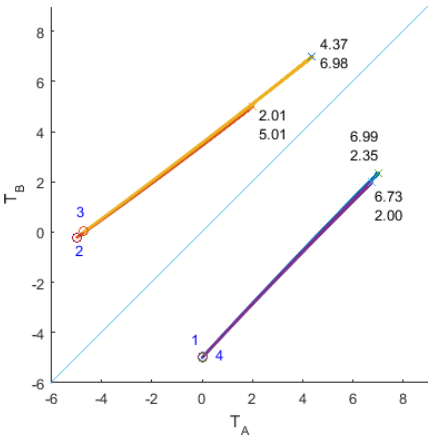

(e) Temperature progression

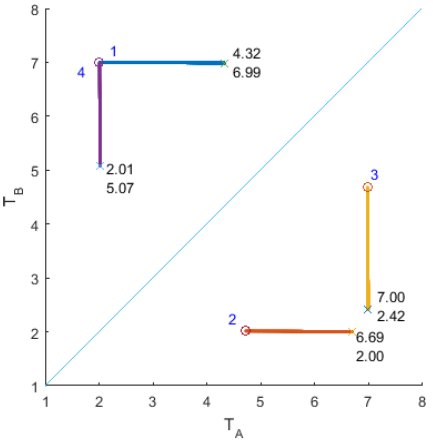

(f) Temperature progression

Figure 3.19: Tracking initial temperature pairs (0,-5) (from I) (a,c,e) and (2,7) (from J) (b,d,f) through switch events over time. First four temperature pairs labelled 1-4 in (e) and (f), continue down the coloured lines in that order to labelled points.

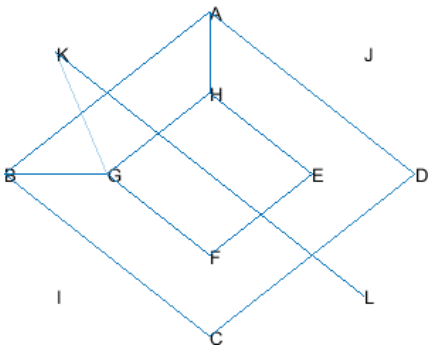

(a) Switch event paths

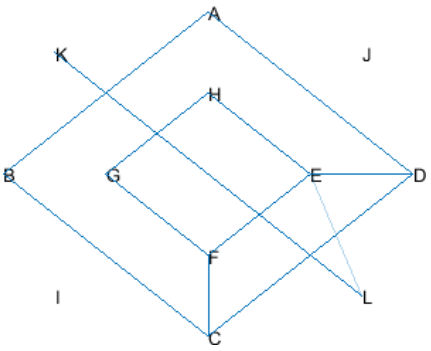

(b) Switch event paths

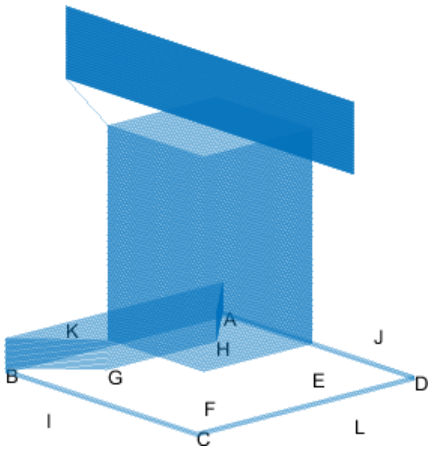

(c) Switch event paths through time (z-axis)

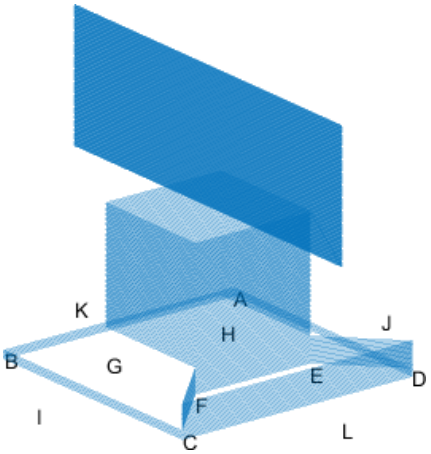

(d) Switch event paths through time (z-axis)

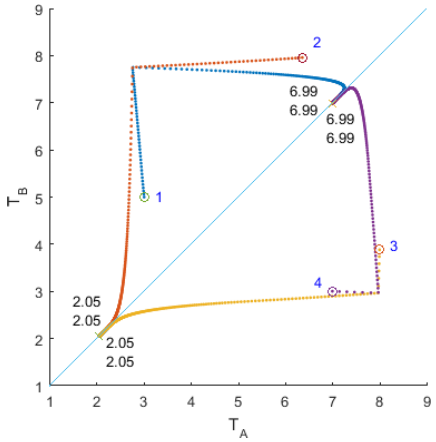

(e) Temperature progression

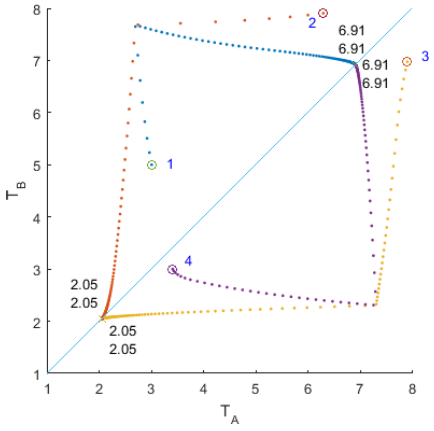

(f) Temperature progression

Figure 3.20: Tracking initial temperature pair (3,5) from event A through switch events over time, with $\sigma = 0.2$. $\rho^* \approx 0.27$ for (a,c,e), $\rho^* \approx 0.79$ for (b,d,f). First four temperature pairs labelled 1-4 in (e) and (f), continue down the coloured lines in that order to labelled points. For an expanded explanation see text above.

3.4.6 Linearising about the single group solution

In the previous sections our simulations and switch event mappings suggested that eventually two groups of TCLs will settle down to periodic solutions. In this section we use our knowledge of the single group periodic solution from Section 3.4.2 and the equations for the switching events to ask under what conditions two groups will merge or remain distinct. Suppose we have a population of frequency-sensitive TCLs that are split into two synchronised groups. We would like to understand the dynamics of the switch times, and we ask whether, given sufficient time, the groups will merge, or whether they will remain distinct, possibly settling down to separated periodic solutions. In particular, we consider the initial difference between the switch on times Δ_t to be very small and the switch on temperatures very close to the single group periodic solution from the previous subsection.

Let Γ denote the single group periodic solution, which cycles periodically through temperature space with temperature $T_\Gamma(t)$. As before, we denote the switched on duration in this solution by l_{ON} and the switched off duration by l_{OFF}. Suppose that the population is split into two groups A and B, such that proportion σ belongs to group A, and proportion $1-\sigma$ belongs to group B. Suppose also that group B switches on at time $t = 0$, followed soon after by group A switching on, at time $t_1 > 0$. Then after a time period of length similar to l_{ON} group B switches off, which is again followed shortly after by group A switching off. After a time period similar to l_{OFF} each of the groups then switch back on. We shall assume that the switching order does not change, since if they to swap, we need only repeat this process with σ replaced by $1-\sigma$. Simulations show that the switching order will not continue to change indefinitely.

We would like to compare the temperature cycles of these two groups with the single group periodic solution Γ. Without loss of generality suppose that group B initially switches on at the same time as a fully synchronised population solution. We compare the cycling of the groups A and B using the following measures, along with all those shown in Figure 3.21. Let $\Delta_T := T_{\text{B}}(0) - T_{\text{A}}(0)$ and $\Delta'_T := T_{\text{B}}(t_4) - T_{\text{A}}(t_4)$, the temperature difference when B switches on the first and second times, respectively. In addition, let $\Delta_t := t_1 - 0 = t_1 = \epsilon_1$ and $\Delta'_t := t_5 - t_4$, the time difference between the two groups switching on the first, and second times respectively. Further notation is shown in Figure 3.21.

In order to calculate Δ'_T and Δ'_t we need to calculate the switch times and temperatures of the two groups at each switch event leading up to t_5. Solving for the switch

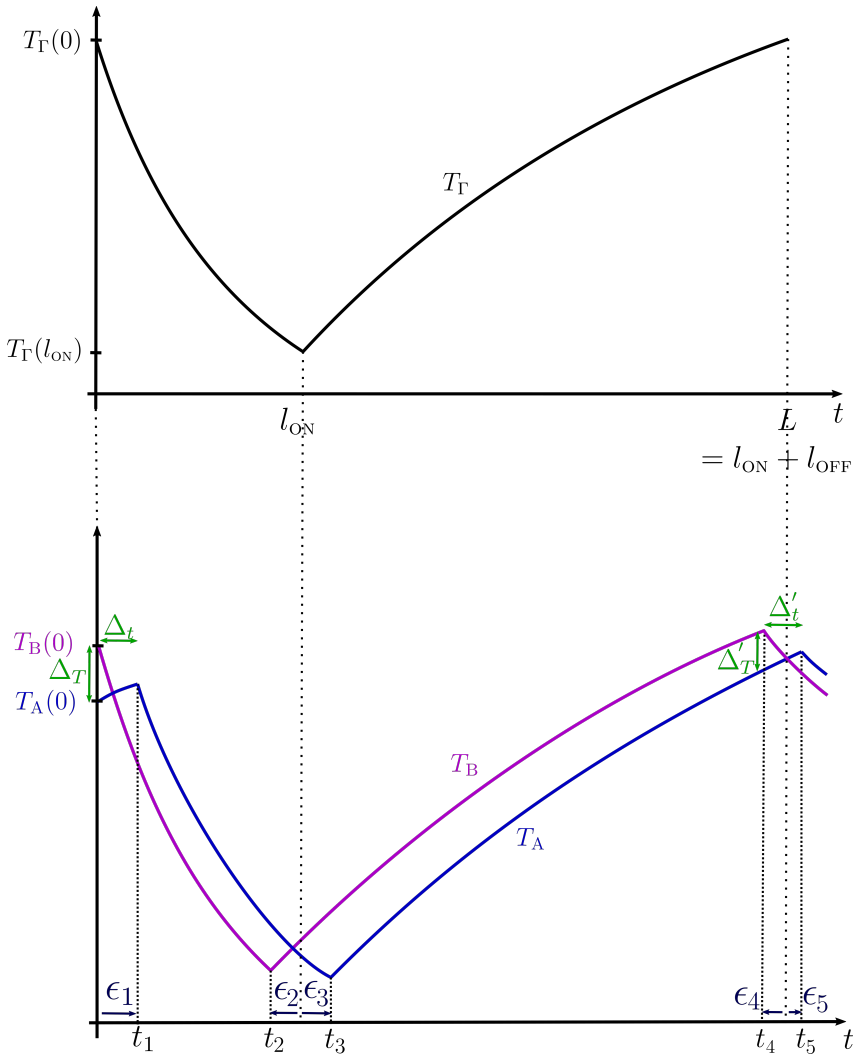

Figure 3.21: Linearisation about the single-group solution. Upper diagram: single group solution $T_\Gamma(t)$. Lower diagram: temperature cycling of groups A and B close to the single-group solution.

times and temperatures when there are two groups is a little more complicated than for the fully synchronised case. It requires solving the temperature set point equations using the system conditions at the previous switch and the equation for $\dot{f}$ which now takes one of four values depending on which combination of groups are switched on (both, neither, A only, or B only). We begin by making the simplifying assumption $\beta_- = \beta_+ := \beta$. Now since group A is switching on at time t_1 and group

B switched off at time 0,

$$\begin{aligned} T_{\mathrm{A}}(t_1) &= T_+^0 - \beta f(t_1) \\ f(t_1) &= f(0) - cP_c(1-\sigma-\rho^*)t_1 \\ f(0) &= \frac{1}{\beta}\big(t_+^0 - T_{\mathrm{B}}(0)\big) \\ \therefore T_{\mathrm{A}}(t_1) &= T_{\mathrm{B}}(0) + \beta cP_c(1-\sigma-\rho^*)t_1. \end{aligned} \tag{3.100a}$$

In addition, by the temperature evolution equations,

$$T_{\mathrm{A}}(t_1) = (T_{\mathrm{A}}(0) - T_{\mathrm{OFF}})e^{-\alpha t_1} + T_{\mathrm{OFF}}. \tag{3.100b}$$

Equating (3.100a) and (3.100b) and introducing our new notation gives

$$\beta cP_c(1-\sigma-\rho^*)\Delta_t + \Delta_T = (T_{\mathrm{A}}(0) - T_{\mathrm{OFF}})(e^{-\alpha\Delta_t} - 1). \tag{3.101}$$

If we write $T_{\mathrm{A}}(0) = T_\Gamma(0) + \delta T_{\mathrm{A}}(0)$ and take $\delta T_{\mathrm{A}}(0)$ and Δ_t small, then

$$\Delta_T = (T_\Gamma(0) + \delta T_{\mathrm{A}}(0) - T_{\mathrm{OFF}})(e^{-\alpha\Delta_t} - 1) - \beta cP_c(1-\sigma-\rho^*)\Delta_t$$

and linearising in Δ_t gives

$$\Delta_T \approx \xi\Delta_t \tag{3.102}$$

where

$$\xi := \alpha\big(T_{\mathrm{OFF}} - T_\Gamma(0)\big) - \beta cP_c(1-\sigma-\rho^*). \tag{3.103}$$

More generally, at each switch event we have the temperature evolution equations that describe the temperature of each group as a function of their temperature at the previous switch (such as (3.100b)), and an additional equation for the temperature of the switching group, using the temperature set point equations (such as (3.100a)).

The temperature evolution equations tell us that:

$$T_{\mathrm{A}}(t_1) = (T_{\mathrm{A}}(0) - T_{\mathrm{OFF}})e^{-\alpha t_1} + T_{\mathrm{OFF}} \tag{3.104a}$$
$$T_{\mathrm{B}}(t_1) = (T_{\mathrm{B}}(0) - T_{\mathrm{ON}})e^{-\alpha t_1} + T_{\mathrm{ON}} \tag{3.104b}$$
$$T_{\mathrm{A}}(t_2) = (T_{\mathrm{A}}(t_1) - T_{\mathrm{ON}})e^{-\alpha(t_2-t_1)} + T_{\mathrm{ON}} \tag{3.104c}$$
$$T_{\mathrm{B}}(t_2) = (T_{\mathrm{B}}(t_1) - T_{\mathrm{ON}})e^{-\alpha(t_2-t_1)} + T_{\mathrm{ON}} \tag{3.104d}$$
$$T_{\mathrm{A}}(t_3) = (T_{\mathrm{A}}(t_2) - T_{\mathrm{ON}})e^{-\alpha(t_3-t_2)} + T_{\mathrm{ON}} \tag{3.104e}$$
$$T_{\mathrm{B}}(t_3) = (T_{\mathrm{B}}(t_2) - T_{\mathrm{OFF}})e^{-\alpha(t_3-t_2)} + T_{\mathrm{OFF}} \tag{3.104f}$$
$$T_{\mathrm{A}}(t_4) = (T_{\mathrm{A}}(t_3) - T_{\mathrm{OFF}})e^{-\alpha(t_4-t_3)} + T_{\mathrm{OFF}} \tag{3.104g}$$
$$T_{\mathrm{B}}(t_4) = (T_{\mathrm{B}}(t_3) - T_{\mathrm{OFF}})e^{-\alpha(t_4-t_3)} + T_{\mathrm{OFF}}. \tag{3.104h}$$

The temperature set point equations provide us with:

$$T_{\mathrm{A}}(t_1) = T_{\mathrm{B}}(0) + \beta c P_c(1 - \sigma - \rho^*)t_1 \tag{3.105a}$$
$$T_{\mathrm{B}}(t_2) = T_{\mathrm{A}}(t_1) + \beta c P_c(1 - \rho^*)(t_2 - t_1) - (T_+^0 - T_-^0) \tag{3.105b}$$
$$T_{\mathrm{A}}(t_3) = T_{\mathrm{B}}(t_2) + \beta c P_c(\sigma - \rho^*)(t_3 - t_2) \tag{3.105c}$$
$$T_{\mathrm{B}}(t_4) = T_{\mathrm{A}}(t_3) - \beta c P_c \rho^*(t_4 - t_3) + T_+^0 - T_-^0. \tag{3.105d}$$

Equations (3.104a) and (3.105a) determine t_1 in terms of $T_{\mathrm{A}}(0)$ and $T_{\mathrm{B}}(0)$. Equations (3.104a) and (3.104b) determine $T_{\mathrm{A}}(t_1), T_{\mathrm{B}}(t_1)$, and so forth, and hence $T_{\mathrm{A}}(t_4), T_{\mathrm{B}}(t_4)$ are determined by $T_{\mathrm{A}}(0), T_{\mathrm{B}}(0)$. To analyse the linear stability of the fixed point of this map corresponding to the one group solution T_Γ (Section 3.4.2) we find that $\Delta_T' := T_{\mathrm{B}}(t_4) - T_{\mathrm{A}}(t_4)$ depends only on ΔT and some differences of switching times, by eliminating the temperatures at the intermediary switch times.

$$\begin{aligned}\Delta_T' = {} & \big(T_{\mathrm{B}}(0) - T_{\mathrm{A}}(0)\big)e^{-\alpha(t_4-t_1)} + \\ & + (T_{\mathrm{OFF}} - T_{\mathrm{ON}})(e^{-\alpha(t_4-t_3)} - e^{-\alpha(t_4-t_2)} - e^{-\alpha(t_4-t_1)} + e^{-\alpha(t_4)}).\end{aligned} \tag{3.106}$$

Defining $L := l_{\mathrm{ON}} + l_{\mathrm{OFF}}$ and linearising about the single group solution using the ϵ_i notation from Figure 3.21 (signed displacement from the single group switch times) gives

$$\Delta_T' \approx e^{-\alpha L}\Delta_T + \alpha(T_{\mathrm{OFF}} - T_{\mathrm{ON}})[(\epsilon_3 - \epsilon_2)e^{-\alpha l_{\mathrm{OFF}}} - e^{-\alpha L}\Delta_t]. \tag{3.107}$$

Since (3.104a) and (3.105a) are two equations for $T_{\mathrm{A}}(t_1)$, (3.104d) and (3.105b) are two equations for $T_{\mathrm{B}}(t_2)$, (3.104e) and (3.105c) are two equations for $T_{\mathrm{A}}(t_3)$, and

(3.104h) and (3.105d) are two equations for $T_{\mathrm{B}}(t_4)$, we have

$$(T_{\mathrm{A}}(0) - T_{\mathrm{OFF}})e^{-\alpha t_1} + T_{\mathrm{OFF}} = T_{\mathrm{B}}(0) + \beta c P_c(1 - \sigma - \rho^*)t_1 \tag{3.108a}$$

$$(T_{\mathrm{B}}(t_1) - T_{\mathrm{ON}})e^{-\alpha(t_2 - t_1)} + T_{\mathrm{ON}} = T_{\mathrm{A}}(t_1) + \beta c P_c(1 - \rho^*)(t_2 - t_1) - (T_+^0 - T_-^0) \tag{3.108b}$$

$$(T_{\mathrm{A}}(t_2) - T_{\mathrm{ON}})e^{-\alpha(t_3 - t_2)} + T_{\mathrm{ON}} = T_{\mathrm{B}}(t_2) + \beta c P_c(\sigma - \rho^*)(t_3 - t_2) \tag{3.108c}$$

$$(T_{\mathrm{B}}(t_3) - T_{\mathrm{OFF}})e^{-\alpha(t_4 - t_3)} + T_{\mathrm{OFF}} = T_{\mathrm{A}}(t_3) - \beta c P_c \rho^*(t_4 - t_3) + T_+^0 - T_-^0. \tag{3.108d}$$

We used (3.108a) already to determine t_1 in terms of ΔT to first order (3.102). Denote $\tau := \epsilon_3 - \epsilon_2$, then to find τ to first order we linearise (3.108c) to obtain

$$\begin{aligned}
&\beta c p(\sigma - \rho^*)\tau + T_\Gamma(l_{\mathrm{ON}}) + \big(T_{\mathrm{B}}(t_2) - T_\Gamma(l_{\mathrm{ON}})\big) \\
&\qquad = \Big(T_\Gamma(l_{\mathrm{ON}}) + \big(T_{\mathrm{A}}(t_2) - T_\Gamma(l_{\mathrm{ON}})\big)\Big)e^{-\alpha\tau} + T_{\mathrm{ON}}(1 - e^{-\alpha\tau}) \\
&\beta c p(\sigma - \rho^*)\tau + T_\Gamma(l_{\mathrm{ON}}) + \big(T_{\mathrm{B}}(t_2) - T_\Gamma(l_{\mathrm{ON}})\big) \\
&\qquad = T_\Gamma(l_{\mathrm{ON}}) + T_{\mathrm{A}}(t_2) - T_\Gamma(l_{\mathrm{ON}}) - \alpha\tau[T_\Gamma(l_{\mathrm{ON}}) + \big(T_{\mathrm{A}}(t_2) - T_\Gamma(l_{\mathrm{ON}})\big)] + \\
&\qquad\qquad + T_{\mathrm{ON}}(1 - 1 + \alpha\tau)
\end{aligned}$$

which gives

$$[\beta c p(\sigma - \rho^*) + \alpha(T_\Gamma(l_{\mathrm{ON}}) - T_{\mathrm{ON}})]\tau = T_{\mathrm{A}}(t_2) - T_{\mathrm{B}}(t_2). \tag{3.109}$$

Now we can find a substitution for $T_{\mathrm{A}}(t_2)$ and $T_{\mathrm{B}}(t_2)$:

$$\begin{aligned}
T_{\mathrm{A}}(t_2) - T_{\mathrm{B}}(t_2) &= T_{\mathrm{A}}(0)e^{-\alpha t_2} + T_{\mathrm{OFF}}(e^{-\alpha(t_2 - t_1)} - e^{-\alpha t_2}) + \\
&\quad + T_{\mathrm{ON}}(1 - e^{-\alpha(t_2 - t_1)}) - (T_{\mathrm{B}}(0) - T_{\mathrm{ON}})e^{-\alpha t_2} - T_{\mathrm{ON}} \\
&= -\big(T_{\mathrm{B}}(0) - T_{\mathrm{A}}(0)\big)e^{-\alpha(l_{\mathrm{ON}} + \epsilon_2)} + T_{\mathrm{OFF}}(e^{-\alpha(l_{\mathrm{ON}} + \epsilon_2 - \epsilon_1)} - e^{-\alpha(l_{\mathrm{ON}} + \epsilon_2)}) + \\
&\quad + T_{\mathrm{ON}}(e^{-\alpha(l_{\mathrm{ON}} + \epsilon_2)} - e^{-\alpha(l_{\mathrm{ON}} + \epsilon_2 - \epsilon_1)}) \\
&= -\Delta_T e^{-\alpha l_{\mathrm{ON}}} + T_{\mathrm{OFF}}\alpha\epsilon_1 e^{-\alpha l_{\mathrm{ON}}} - T_{\mathrm{ON}}\alpha\epsilon_1 e^{-\alpha l_{\mathrm{ON}}} \\
&= (\alpha(T_{\mathrm{OFF}} - T_{\mathrm{ON}})\Delta_t - \Delta_T)e^{-\alpha l_{\mathrm{ON}}}
\end{aligned}$$

and we can use this substitution to arrive at

$$\tau = \epsilon_3 - \epsilon_2 = \frac{(\alpha(T_{\mathrm{OFF}} - T_{\mathrm{ON}})\Delta_t - \Delta_T)e^{-\alpha l_{\mathrm{ON}}}}{\beta c P_c(\sigma - \rho^*) + \alpha(T_\Gamma(l_{\mathrm{ON}}) - T_{\mathrm{ON}})}. \tag{3.110}$$

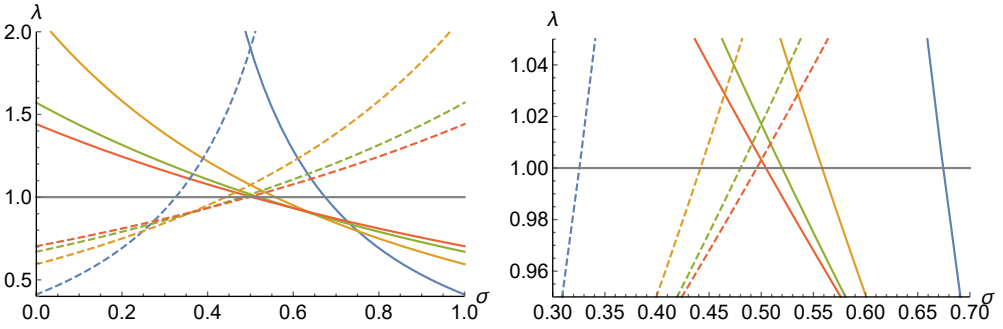

(a) Full interval (b) Enlargement

Figure 3.22: Solutions for λ (Eq (3.112)) (solid lines) for different values of ρ^*. Dashed lines show reflection in $\sigma = \frac{1}{2}$ to show the effect of reversing the switching order of the groups. Blue: $\rho^* = 0.1$, yellow: $\rho^* = 0.2$, green: $\rho^* = 0.3$, red: $\rho^* = 0.4$. Black line shows the boundary of stability (stable below, unstable above). The results are identical when ρ^* is replaced by $1 - \rho^*$. Figure (b) shows an enlargement centred at $\sigma = \frac{1}{2}$, showing that either switching order of the groups leads to $\lambda_2 > 1$ on a small interval of σ. In this case the groups never merge and in all other cases they will.

With our expression for τ and for Δ_t using (3.102), we arrive at

$$\Delta_T' = \lambda \Delta_T \tag{3.111}$$

where

$$\begin{aligned}\lambda :=& \left(1 - \frac{\alpha(T_{\text{OFF}} - T_{\text{ON}})}{\alpha\big(T_{\text{OFF}} - T_\Gamma(0)\big) - \beta c P_c(1 - \sigma - \rho^*)}\right) \cdot \\ & \cdot \left(1 - \frac{\alpha(T_{\text{OFF}} - T_{\text{ON}})}{\alpha(T_\Gamma(l_{\text{ON}}) - T_{\text{ON}}) + \beta c P_c(\sigma - \rho^*)}\right) e^{-\alpha L}.\end{aligned} \tag{3.112}$$

So $[-1, +1]$ is a left eigenvector of the linearised map in the space of $\begin{pmatrix}\delta T_{\text{A}} \\ \delta T_{\text{B}}\end{pmatrix}$ with eigenvalue λ. We can plot λ against σ for various ρ^* to see whether $|\lambda| < 1$ (in which case the two groups merge into one) or whether $|\lambda| > 1$ (they move apart). The results are shown in Figure 3.22.

Next we derive bounds on the second eigenvalue, and find that it is insignificant for determining the stability of the system. The temperature cycles of groups A and B are very close to the single group temperature cycle T_Γ and therefore, for $I \in \{A, B\}$

we write

$$\begin{aligned}
T_{\mathrm{I}}(0) &= T_{\Gamma}(0) + \delta T_{\mathrm{I}}(0) \\
T_{\mathrm{I}}(t_1) &= T_{\Gamma}(0) + \delta T_{\mathrm{I}}(t_1) \\
T_{\mathrm{I}}(t_2) &= T_{\Gamma}(l_{\mathrm{ON}}) + \delta T_{\mathrm{I}}(t_2) \\
T_{\mathrm{I}}(t_3) &= T_{\Gamma}(l_{\mathrm{ON}}) + \delta T_{\mathrm{I}}(t_3) \\
T_{\mathrm{I}}(t_4) &= T_{\Gamma}(0) + \delta T_{\mathrm{I}}(t_4).
\end{aligned}$$

Our approach is to seek a map M such that

$$\begin{pmatrix} \delta T_{\mathrm{A}}(t_4) \\ \delta T_{\mathrm{B}}(t_4) \end{pmatrix} = M \begin{pmatrix} \delta T_{\mathrm{A}}(0) \\ \delta T_{\mathrm{B}}(0) \end{pmatrix}.$$

Taking linear approximations as in Section 3.4.6, (3.108a) approximates to

$$\begin{aligned}
T_{\Gamma}(0) + \delta T_{\mathrm{A}}(0) - \alpha t_1 (T_{\Gamma}(0) - T_{\mathrm{OFF}}) &\approx T_{\Gamma}(0) + \delta T_{\mathrm{B}}(0) + \beta c P_c (1 - \sigma - \rho^*) t_1 \\
t_1 &\approx \frac{\delta T_{\mathrm{B}}(0) - \delta T_{\mathrm{A}}(0)}{\xi_1} \qquad (3.113)
\end{aligned}$$

$$\text{where} \qquad \xi_1 := \alpha\big(T_{\mathrm{OFF}} - T_{\Gamma}(0)\big) - \beta c P_c (1 - \sigma - \rho^*). \qquad (3.114)$$

We can use this expression for t_1 and take a first order approximation of (3.104a) to find an expression for $\delta T_{\mathrm{A}}(t_1)$ in terms of $\delta T_{\mathrm{A}}(0)$:

$$\begin{aligned}
T_{\Gamma}(0) + \delta T_{\mathrm{A}}(t_1) &= (T_{\Gamma}(0) + \delta T_{\mathrm{A}}(0) - T_{\mathrm{OFF}}) e^{-\alpha t_1} + T_{\mathrm{OFF}} \\
\delta T_{\mathrm{A}}(t_1) &\approx \delta T_{\mathrm{A}}(0) - \alpha t_1 (T_{\Gamma}(0) - T_{\mathrm{OFF}}) \\
\delta T_{\mathrm{A}}(t_1) &\approx \delta T_{\mathrm{A}}(0) + \frac{\alpha}{\xi_1}\big(T_{\mathrm{OFF}} - T_{\Gamma}(0)\big)\big(\delta T_{\mathrm{B}}(0) - \delta T_{\mathrm{A}}(0)\big). \qquad (3.115)
\end{aligned}$$

Similarly, using (3.104b) we find that

$$\delta T_{\mathrm{B}}(t_1) \approx \delta T_{\mathrm{B}}(0) - \frac{\alpha}{\xi_1}(T_{\Gamma}(0) - T_{\mathrm{ON}})\big(\delta T_{\mathrm{B}}(0) - \delta T_{\mathrm{A}}(0)\big). \qquad (3.116)$$

We repeat this process to find expressions for each time interval[6] $(\epsilon_i - \epsilon_{i-1})$ for

[6] Recall that $t_1 = \epsilon_1 - 0$ is the first interval between switch times.

$i \in \{2,3,4\}$ and each subsequent $\delta T_{\mathrm{A}}(t_i)$ and $\delta T_{\mathrm{B}}(t_i)$. We use (3.108b) to find

$$\epsilon_2 - \epsilon_1 \approx \frac{\delta T_{\mathrm{B}}(t_1)e^{-\alpha l_{\mathrm{ON}}} - \delta T_{\mathrm{A}}(t_1)}{\xi_2} \tag{3.117}$$

$$\text{where} \qquad \xi_2 := \alpha(T_\Gamma(0) - T_{\mathrm{ON}})e^{-\alpha l_{\mathrm{ON}}} + \beta c P_c(1-\rho^*). \tag{3.118}$$

Equations (3.104c) and (3.104d) thus yield

$$\delta T_{\mathrm{A}}(t_2) \approx \delta T_{\mathrm{A}}(t_1)e^{-\alpha l_{\mathrm{ON}}} - \frac{\alpha}{\xi_2}(T_\Gamma(0) - T_{\mathrm{ON}})\big(\delta T_{\mathrm{B}}(t_1)e^{-\alpha l_{\mathrm{ON}}} - \delta T_{\mathrm{A}}(t_1)\big)e^{-\alpha l_{\mathrm{ON}}} \tag{3.119}$$

$$\delta T_{\mathrm{B}}(t_2) \approx \delta T_{\mathrm{B}}(t_1)e^{-\alpha l_{\mathrm{ON}}} - \frac{\alpha}{\xi_2}(T_\Gamma(0) - T_{\mathrm{ON}})\big(\delta T_{\mathrm{B}}(t_1)e^{-\alpha l_{\mathrm{ON}}} - \delta T_{\mathrm{A}}(t_1)\big)e^{-\alpha l_{\mathrm{ON}}}. \tag{3.120}$$

Using (3.108c) we find

$$\epsilon_3 - \epsilon_2 \approx \frac{\delta T_{\mathrm{A}}(t_2) - \delta T_{\mathrm{B}}(t_2)}{\xi_3} \tag{3.121}$$

$$\text{where} \qquad \xi_3 := \alpha(T_\Gamma(l_{\mathrm{ON}}) - T_{\mathrm{ON}}) + \beta c P_c(\sigma - \rho^*). \tag{3.122}$$

Equations (3.104e) and (3.104f) yield

$$\delta T_{\mathrm{A}}(t_3) \approx \delta T_{\mathrm{A}}(t_2) - \frac{\alpha}{\xi_3}(T_\Gamma(l_{\mathrm{ON}}) - T_{\mathrm{ON}})\big(\delta T_{\mathrm{A}}(t_2) - \delta T_{\mathrm{B}}(t_2)\big) \tag{3.123}$$

$$\delta T_{\mathrm{B}}(t_3) \approx \delta T_{\mathrm{B}}(t_2) + \frac{\alpha}{\xi_3}\big(T_{\mathrm{OFF}} - T_\Gamma(l_{\mathrm{ON}})\big)\big(\delta T_{\mathrm{A}}(t_2) - \delta T_{\mathrm{B}}(t_2)\big). \tag{3.124}$$

Finally (3.108d) gives

$$\epsilon_4 - \epsilon_3 \approx \frac{\delta T_{\mathrm{A}}(t_3) - \delta T_{\mathrm{B}}(t_3)e^{-\alpha l_{\mathrm{OFF}}}}{\xi_4} \tag{3.125}$$

$$\text{where} \qquad \xi_4 := \alpha(T_{\mathrm{OFF}} - T_\Gamma\big(l_{\mathrm{ON}}\big))e^{-\alpha l_{\mathrm{OFF}}} + \beta c P_c \rho^* \tag{3.126}$$

and (3.104g) and (3.104h) give

$$\delta T_{\mathrm{A}}(t_4) \approx \delta T_{\mathrm{A}}(t_3)e^{-\alpha l_{\mathrm{OFF}}} + \frac{\alpha}{\xi_4}(T_{\mathrm{OFF}} - T_{\Gamma}\big(l_{\mathrm{ON}}\big))(\delta T_{\mathrm{A}}(t_3) - \delta T_{\mathrm{B}}(t_3)e^{-\alpha l_{\mathrm{OFF}}})e^{-\alpha l_{\mathrm{OFF}}} \tag{3.127}$$

$$\delta T_{\mathrm{B}}(t_4) \approx \delta T_{\mathrm{B}}(t_3)e^{-\alpha l_{\mathrm{OFF}}} + \frac{\alpha}{\xi_4}(T_{\mathrm{OFF}} - T_{\Gamma}\big(l_{\mathrm{ON}}\big))(\delta T_{\mathrm{A}}(t_3) - \delta T_{\mathrm{B}}(t_3)e^{-\alpha l_{\mathrm{OFF}}})e^{-\alpha l_{\mathrm{OFF}}}. \tag{3.128}$$

For each $i \in \{1, 2, 3, 4\}$ we can write

$$\begin{pmatrix} \delta T_{\mathrm{A}}(t_i) \\ \delta T_{\mathrm{B}}(t_i) \end{pmatrix} = M_i \begin{pmatrix} \delta T_{\mathrm{A}}(t_{i-1}) \\ \delta T_{\mathrm{B}}(t_{i-1}) \end{pmatrix}$$

and so

$$\begin{pmatrix} \delta T_{\mathrm{A}}(t_4) \\ \delta T_{\mathrm{B}}(t_4) \end{pmatrix} = M \begin{pmatrix} \delta T_{\mathrm{A}}(0) \\ \delta T_{\mathrm{B}}(0) \end{pmatrix}$$

where

$$M := M_4 M_3 M_2 M_1.$$

We introduce the following simplifying notation before defining each matrix M_i. Let

$$\mathcal{A} = \alpha\big(T_{\mathrm{OFF}} - T_{\Gamma}(0)\big) \tag{3.129a}$$

$$\mathcal{B} = \alpha(T_{\Gamma}(0) - T_{\mathrm{ON}}) \tag{3.129b}$$

$$\mathcal{C} = \alpha(T_{\Gamma}(l_{\mathrm{ON}}) - T_{\mathrm{ON}}) \tag{3.129c}$$

$$\mathcal{D} = \alpha\big(T_{\mathrm{OFF}} - T_{\Gamma}(l_{\mathrm{ON}})\big). \tag{3.129d}$$

Then

$$M_1 = \frac{1}{\xi_1}\begin{pmatrix} \xi_1 - \mathcal{A} & \mathcal{A} \\ \mathcal{B} & \xi_1 - \mathcal{B} \end{pmatrix} \tag{3.130a}$$

$$M_2 = \frac{e^{-\alpha l_{\text{ON}}}}{\xi_2}\begin{pmatrix} \xi_2 + \mathcal{B} & -\mathcal{B}e^{-\alpha l_{\text{ON}}} \\ \mathcal{B} & \xi_2 - \mathcal{B}e^{-\alpha l_{\text{ON}}} \end{pmatrix} \tag{3.130b}$$

$$M_3 = \frac{1}{\xi_3}\begin{pmatrix} \xi_3 - \mathcal{C} & \mathcal{C} \\ \mathcal{D} & \xi_3 - \mathcal{D} \end{pmatrix} \tag{3.130c}$$

$$M_4 = \frac{e^{-\alpha l_{\text{OFF}}}}{\xi_4}\begin{pmatrix} \xi_4 + \mathcal{D} & -\mathcal{D}e^{-\alpha l_{\text{OFF}}} \\ \mathcal{D} & \xi_4 - \mathcal{D}e^{-\alpha l_{\text{OFF}}}. \end{pmatrix} \tag{3.130d}$$

We already know one of the eigenvalues of the system (λ), and the second eigenvalue is given by $\frac{\det(M)}{\lambda}$. Note that $\det(M) = \det(M_4)\det(M_3)\det(M_2)\det(M_1)$, and

$$\det(M_1) = \xi_1 - (\mathcal{A} + \mathcal{B}) \qquad = -\mathcal{B} - \beta c P_c(1 - \sigma - \rho^*) \tag{3.131a}$$

$$\det(M_2) = (\xi_2 + \mathcal{B}\big(1 - e^{-\alpha l_{\text{ON}}}\big)\big)e^{-\alpha l_{\text{ON}}} \qquad = (\mathcal{B} + \beta c P_c\big(1 - \rho^*\big)\big)e^{-\alpha l_{\text{ON}}} \tag{3.131b}$$

$$\det(M_3) = \xi_3 - (\mathcal{C} + \mathcal{D}) \qquad = -\mathcal{D} + \beta c P_c(\sigma - \rho^*) \tag{3.131c}$$

$$\det(M_4) = \big(\xi_4 + \mathcal{D}(1 - e^{-\alpha l_{\text{OFF}}})\big)e^{-\alpha l_{\text{OFF}}} \qquad = (\mathcal{D} + \beta c P_c \rho^*)e^{-\alpha l_{\text{OFF}}}. \tag{3.131d}$$

We can rewrite λ (see (3.112)) in our new notation as

$$\lambda = \frac{(\mathcal{B} + \beta c P_c(1 - \sigma - \rho^*))(\mathcal{D} - \beta c P_c(\sigma - \rho^*))}{(\mathcal{A} - \beta c P_c(1 - \sigma - \rho^*))(\mathcal{C} + \beta c P_c(\sigma - \rho^*))} e^{-\alpha L} \tag{3.132}$$

which allows us to write

$$\frac{\det(M)}{\lambda} = [\mathcal{A} - \beta c P_c(1 - \sigma - \rho^*)][\mathcal{B} + \beta c P_c(1 - \rho^*)][\mathcal{C} + \beta c P_c(\sigma - \rho^*)][\mathcal{D} + \beta c P_c \rho^*]. \tag{3.133}$$

Denote the second eigenvalue byλ_2, and

$$\lambda_2 = \frac{\det(M)}{\lambda}. \tag{3.134}$$

Since $0 < \mathcal{A}, \mathcal{B}, \mathcal{C}, \mathcal{D} < \alpha(T_{\text{OFF}} - T_{\text{ON}})$, $\sigma \in (0, 1)$ and $\rho^* \in (0, 1)$,

$$|\lambda_2| < [\alpha(T_{\text{OFF}} - T_{\text{ON}}) + \beta c P_c]^4$$

which for our choice of parameter values gives

$$|\lambda_2| < 7.70 \times 10^{-9}.$$

Therefore the absolute value of the second eigenvalue is (significantly) less than 1. The second eigenvalue is within the interval $(-1, +1)$ for any σ and ρ^* for our parameter values[7] and therefore the stability is governed by λ.

By solving for the dividing case $\lambda = 1$ we can create a bifurcation diagram in terms of the parameters σ and ρ^* to show where the single group solution is attracting and repelling. Figure 3.23 sketches the solution, along with the solution for the case when the switching order of the groups is reversed, found by replacing σ with $1 - \sigma$. If in either case (group A switching first or group B switching first) the solution is attracting, then the two groups will merge together into the one group solution. However, if both cases have unstable dynamics then the solutions will never merge. Our simulations showed that in this parameter region the two groups will settle down to a fixed phase distance apart. If the solution is attracting for one switching order and repelling for the other, we find that the typical behaviour is for a small separation in the unstable direction to grow until the phase difference becomes almost a whole cycle, when they merge. Figure 3.24 illustrates how the cycles of the two groups can change over time relative to one another, depending on which of the three regions in the bifurcation diagram their parameters belong to.

What these results show is that when a population is split into two groups, if they are sufficiently similar in size then they will remain apart, effectively trying to counteract one another and balance the frequency fluctuations. Conversely, if one of the groups is significantly larger[8] than the other then it will have too strong an effect on the frequency, and 'pull' on the smaller group's cycle. The closer the proportion switched on in equilibrium is to the proportion switched off (*i.e.* the closer it is to 0.5), the more similar the groups have to be in size to remain distinct.

[7] Parameter values are taken from Table 3.1 with the exception of $\beta = 0.1$. Small β is required to limit the rate of change of the frequency and ensure model validity.

[8] 'significantly' here depends on the size of ρ^*, and may be very small if $\rho^* \approx 0.5$.

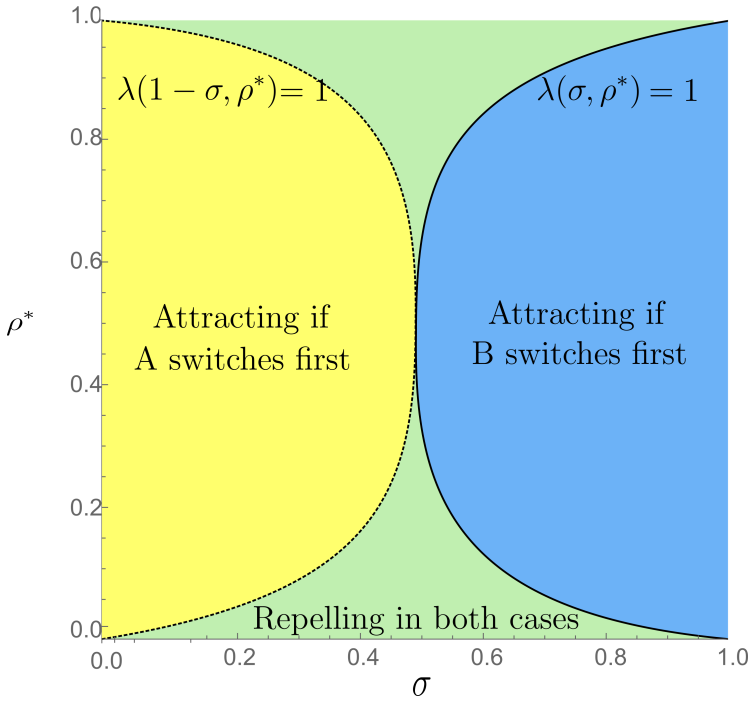

Figure 3.23: Bifurcation diagram for the stability of the single group solution to splitting in two. Stable if the parameters lie in the yellow or blue regions (the groups will ultimately merge), unstable in the green parameter region (the groups will never merge). Boundary lines are solutions to (3.112) as a function of σ (or $1-\sigma$ to capture switching order reversal) and ρ^*.

3.4.7 N synchronised groups

Beyond two synchronised groups of TCLs the number of switching events becomes too large for analytical approaches to be feasible. When we have one group there are two possible states, on and off (1 and 0). There are two possible events: $1 \to 0$ and $0 \to 1$. One event always follows the other and it is possible to find implicit equations for the periodic solution. With two groups we have four possible states: (0,0), (0,1), (1,0) and (1,1). From each state we can transition to any of the other three and so there are $4 \times 3 = 12$ events, as shown in Figure 3.12. Given the temperature and state of each group, the previous state of the system is required to know which switch event comes next. This requirement leads to the 32 possible 'switching event transitions' shown in Figure 3.13.

For three groups we now have $2^3 = 8$ possible states, and therefore $8 \times 7 = 56$ switching events. Our formulae for N groups is thus 2^N states and $2^N(2^N - 1)$ switching events. The results for N equals 1 to 5 are shown in Table 3.2. The

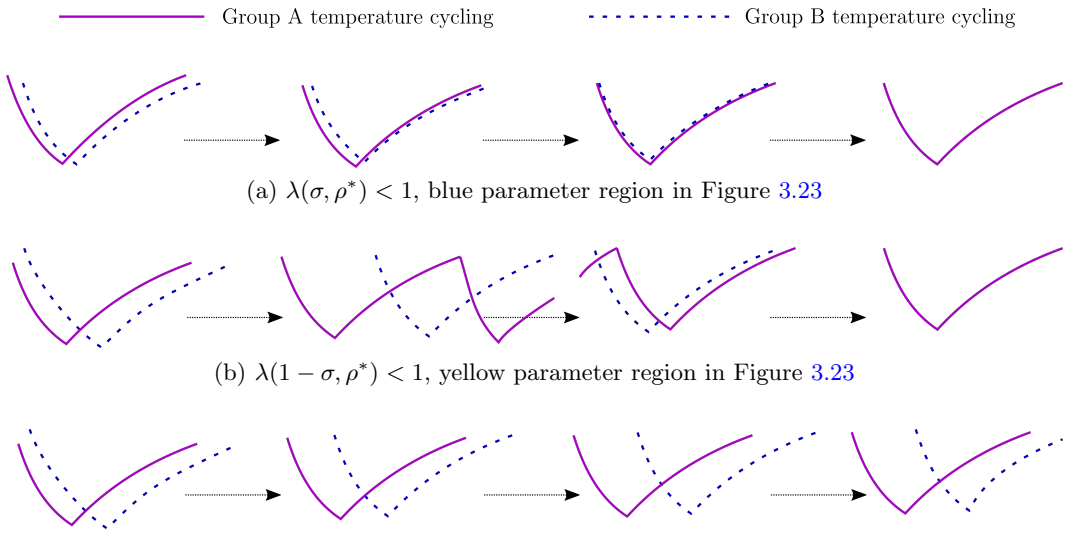

(a) $\lambda(\sigma, \rho^*) < 1$, blue parameter region in Figure 3.23

(b) $\lambda(1-\sigma, \rho^*) < 1$, yellow parameter region in Figure 3.23

(c) $\lambda(\sigma, \rho^*) > 1, \lambda(1-\sigma, \rho^*) > 1$, green parameter region in Figure 3.23

Figure 3.24: Illustration of the three types of cycling behaviour of two-groups relative to one another, based on simulations. Arrows indicate the occurrence of many cycles and the central illustrations are snapshots of the cycling behaviour between the start and the final behaviour. Synchronisation occurs in cases (a) and (b), while in case (c) each group tends fixed phase difference apart.

exponential growth in the number of states leads to a huge number of switching events, even when there are only three groups.

Table 3.2: The number of states and switching events for different numbers of synchronised groups of TCLs

Number of Groups	**1**	**2**	**3**	**4**	**5**
Number of States	2	4	8	16	32
Number of Switching Events	2	12	56	240	992

We found analytically that two groups will remain distinct if their relative sizes are sufficiently similar. Figure 3.23 shows the regions in (σ, ρ^*) parameter space in which the groups will merge or synchronise. When there are three groups there are three possibilities: full synchronisation, partial synchronisation (only two groups synchronise) and no synchronisation. The large number of possible switching events prevents us from studying the three group case analytically, however, we are able to run simulations for three groups. We can visualise the results in two dimensions using a triangular simplex when ρ^* is fixed.

A triangular simplex allows us to represent data with three coordinates in two di-

mensions, by making use of the fact that our system is only two-dimensional. The proportion of TCLs in each group, σ_A, σ_B, and σ_C sum to 1 and therefore lie in a plane, and so we can represent the three proportions on a triangular simplex. Figure 3.25 shows our simplex, an equilateral triangle with height 1. Figure 3.25(a) shows the Cartesian coordinates (x, y) for a point in the triangle, 3.25(b) shows the corresponding values of $(\sigma_A, \sigma_B, \sigma_C)$, the proportion in group A, B and C respectively. At the vertices all TCLs belong to just one of the groups and at the centre the proportions are equal.

The application of basic geometry allows us to find the simplex Cartesian coordinates (x, y) for point $(\sigma_A, \sigma_B, \sigma_C)$ using the relation

$$\begin{pmatrix} x \\ y \end{pmatrix} = \begin{pmatrix} -\frac{2}{\sqrt{3}} & -\frac{1}{\sqrt{3}} \\ 0 & 1 \end{pmatrix} \begin{pmatrix} \sigma_A \\ \sigma_B \end{pmatrix}. \tag{3.135}$$

Conversely, the proportions σ_A, σ_B and σ_C can be found from the Cartesian simplex coordinates according to

$$\begin{pmatrix} \sigma_A \\ \sigma_B \\ \sigma_C \end{pmatrix} = \begin{pmatrix} -\frac{\sqrt{3}}{2} & -\frac{1}{2} \\ 0 & 1 \\ +\frac{\sqrt{3}}{2} & -\frac{1}{2} \end{pmatrix} \begin{pmatrix} x \\ y \end{pmatrix} + \begin{pmatrix} 1 \\ 0 \\ 0 \end{pmatrix}. \tag{3.136}$$

Figures 3.26, 3.27 and 3.28 show the final condition of our system (full, partial or zero synchronisation) after 1000 days of simulation for different values of ρ^*. The proportions in each group are given by the location on the simplex. Due to the perfect symmetry of the three groups, it was only necessary to take points from one sixth of the triangle, and then to reflect the results in the lines of symmetry to see the full picture. Certain regions are more densely packed than others - these were found to be where the boundaries between outcomes existed and so were more densely sampled for simulations.

Figure 3.26 shows the results for our typical value of $\rho^* = 0.3355$. The sides of the triangle represent 2 groups with non-zero proportions, and so the results match the results from the two group case we saw earlier. There is a small region where the two groups remain distinct (pink), and outside of this region the groups fully synchronise (green). In the centre of the triangle exists a region where the three groups will remain distinct, the blue region. The three bands of pink that form a triangular shape approximately follow the lines where half of the TCLs belong to one of the groups. Figures 3.27 and 3.28 show the results when parameter T_{ON} is changed

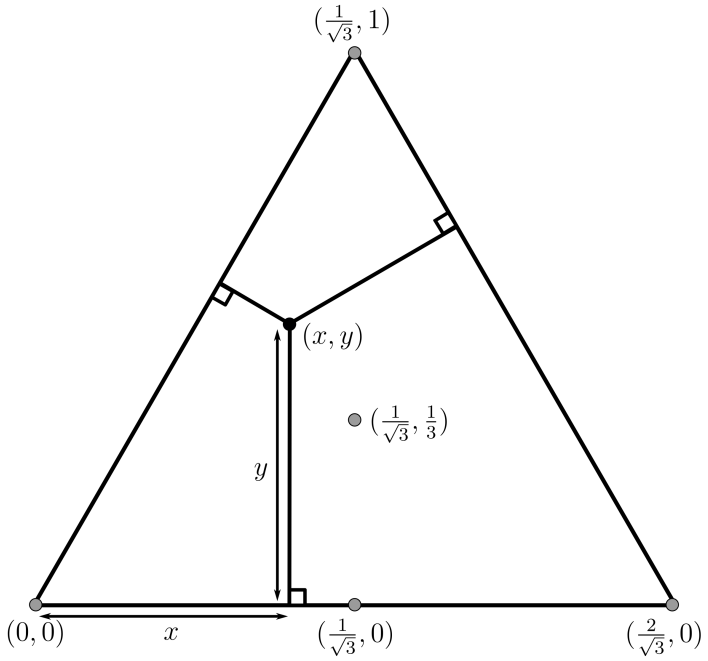

(a) Simplex with Cartesian coordinates

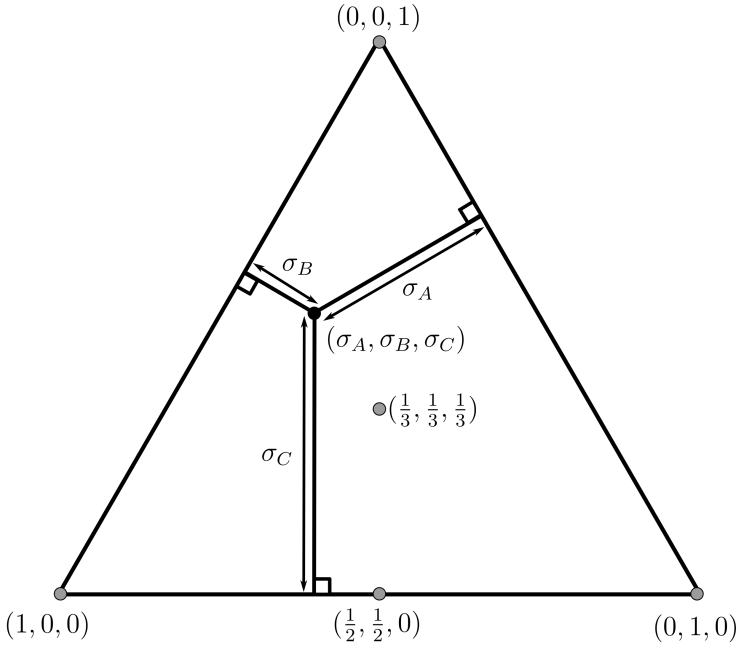

(b) Simplex with σ coordinates

Figure 3.25: Simplex Cartesian coordinates (a) and σ coordinates (b).

to change ρ^* to $\rho^* = 0.2370$ and $\rho^* = 0.4692$ respectively. When ρ^* decreases the partial synchronisation region increases in size and the central zero synchronisation region reduces. When ρ^* increases towards $1/2$ the partial synchronisation reduces to what may be a very thin hollow triangle, but the sampling of the space only found a few points in parameter space where this was the case. The zero synchronisation region has also become much smaller, which is likely to be due to ρ^* being further from $1/3$, just as in the two-group case the largest region for zero synchronisation was when $\rho^* = 1/2$.

These results suggest that when a population is split into N groups of similar size they can remain distinct. If one or more of the groups contains proportion $1/m$ of the population, with $0 < m < n$, then partial synchronisation may occur.

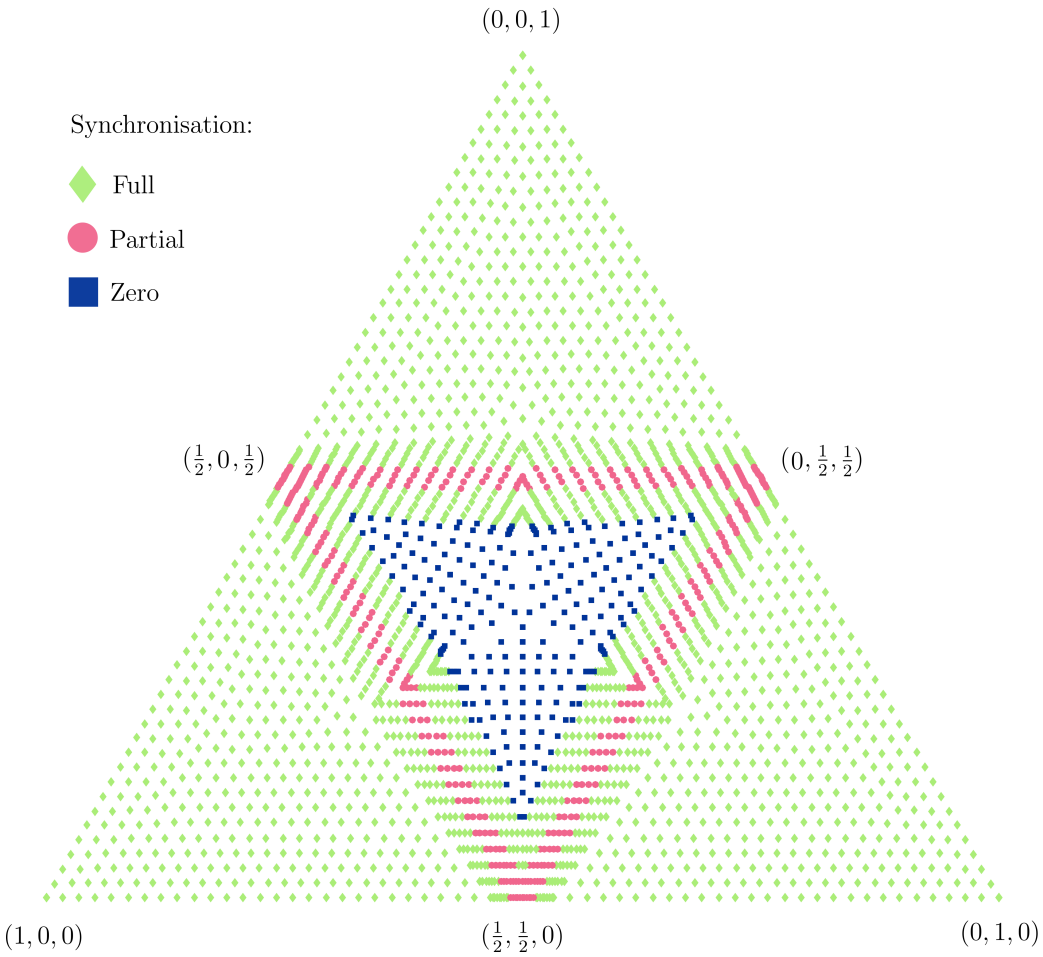

Figure 3.26: Long-term behaviour of three groups when $\rho^* = 0.3355$.

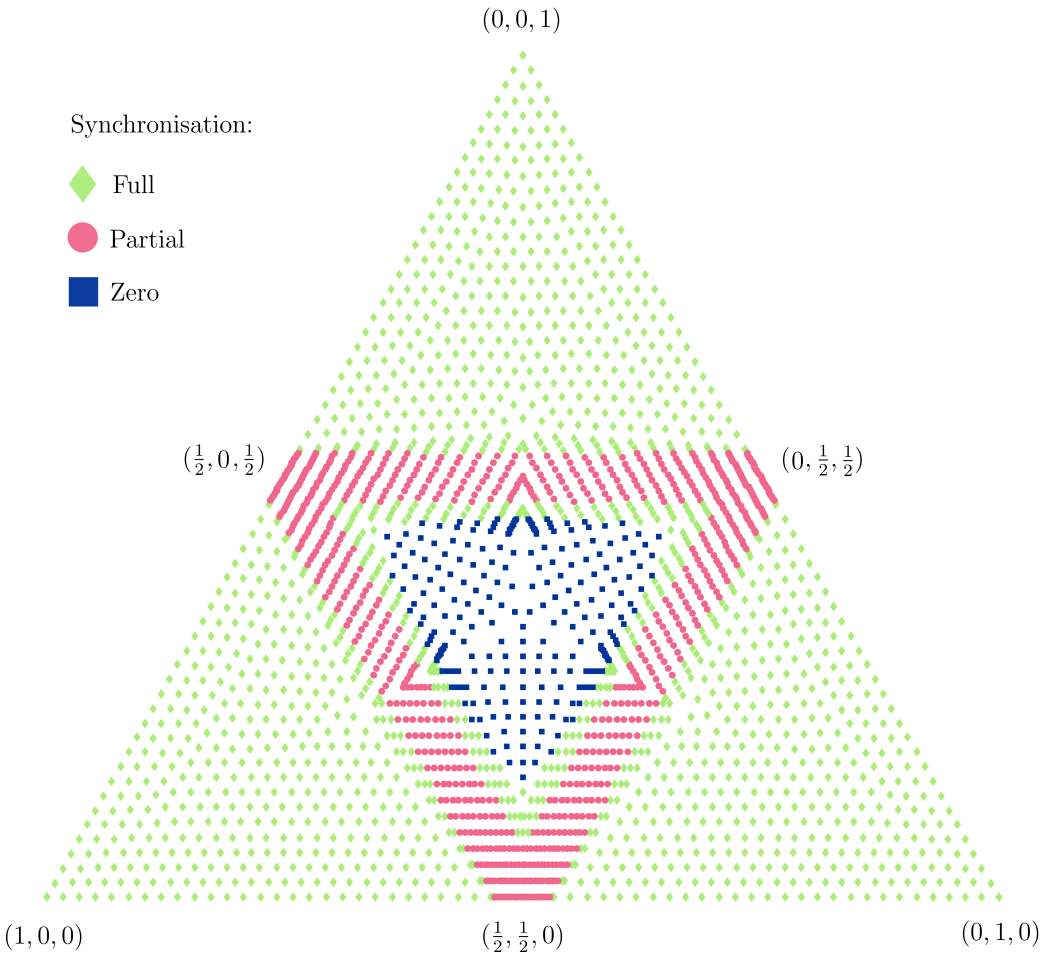

Figure 3.27: Long-term behaviour of three groups when $\rho^* = 0.2370$.

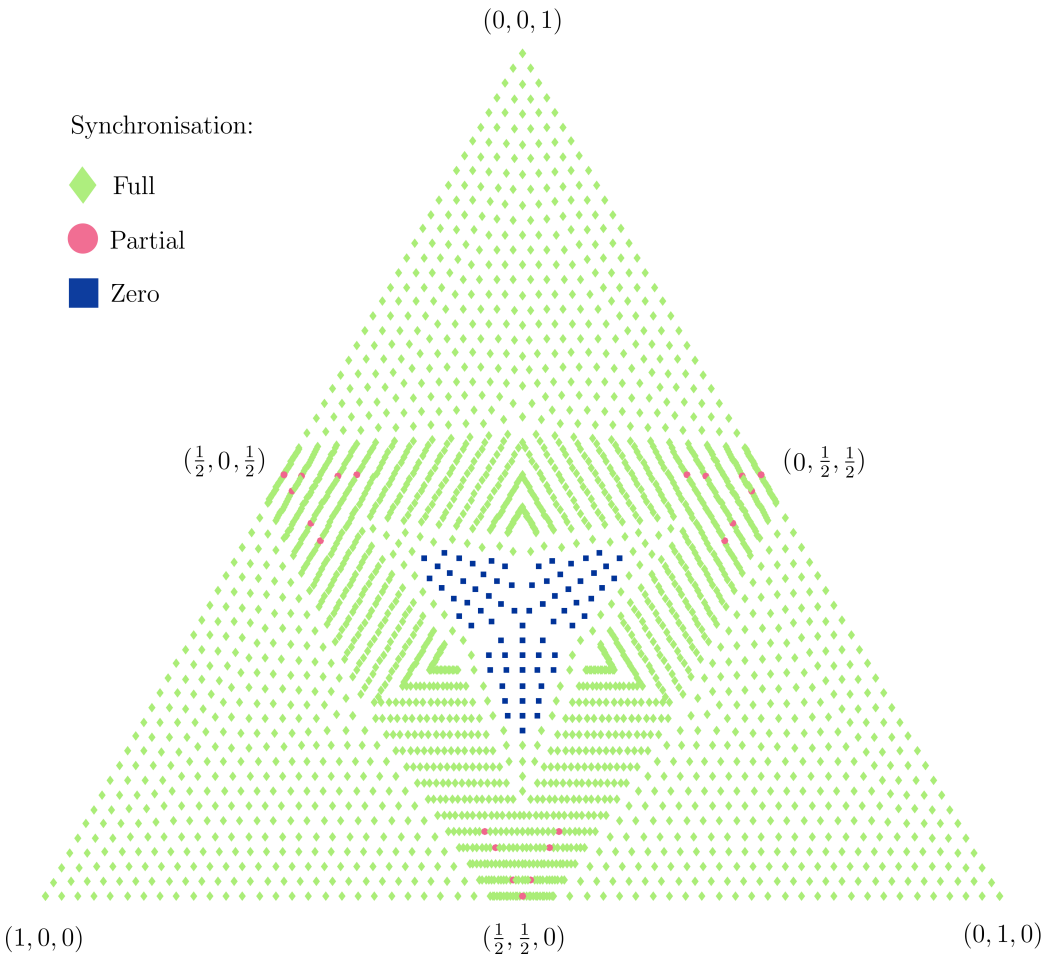

Figure 3.28: Long-term behaviour of three groups when $\rho^* = 0.4692$.

"You see, Freddy believes that if a fridge falls off a minivan, you better swerve out of its way. I believe it's the fridge's job to swerve out of mine."

Frank Underwood,
House of Cards (2013), Season 1, Episode 4

4 Simulations

4.1 Introduction

In Chapter 3 we took a number of analytical approaches to study the stability of a population of identical frequency-sensitive TCLs. We found evidence of stability to small perturbations but that initial conditions with synchronised groups of sufficiently different sizes tend to synchronise more. Nevertheless, synchronised solutions are unstable to splitting into roughly equal sized groups. In this chapter we use simulations to test the analysis done in Chapter 3 and to take more real-world details into account.

Section 4.2 shows the results of simulating an identical population of frequency-sensitive TCLs and the grid frequency, in the absence of any other agent. This corresponds directly to the modelling and analysis from Section 3.3. We simulate the system from a number of different initial states (perturbations of the initial distribution of TCLs away from equilibrium), and find that although the perturbations initially die down (as predicted by the linear analysis), ultimately they lead to larger, growing perturbations.

In Section 4.3 we describe a different model that incorporates real data from the GB

electricity grid, allowing us to include the effects of naturally-occurring supply and demand fluctuations as well as the actions of other frequency response providers. In Section 4.4 we present the results from using this model to simulate a homogeneous population of fridges, finding evidence of synchronisation and detrimental system effects. In Section 4.5 we present the results from introducing heterogeneity to the population, and we investigate the amount of heterogeneity required to prevent synchronisation issues, comparing our result with the equivalent result from the Kuramoto model.

4.2 Perturbations of a uniform distribution of TCLs

In Section 3.3 we analysed the stability of a large population of TCLs uniformly distributed in each part of the on/off cycle. In this section we simulate a large population of fridges with initial conditions close to the equilibrium distribution (the uniform distribution), and compare the results with our analytical work.

The model is the same as presented in Section 3.2, and unless stated otherwise, the parameter values are as in Table 3.1 on page 42. In the previous chapter we modelled our population as a continuum. For our simulations we split the fridge population into 10000 'agents' (groups of fridges) that are each represented by a temperature and state, and who operate according to the switching rules and temperature progression equations in Section 3.2.2. These 10000 agents are representative of the million fridges we assume are participating in our DSR scheme (*i.e.* operating in frequency-sensitive mode), since one million (or more) individuals would require very large amounts of computing time and memory. The power consumption of each agent is taken to be the total possible population consumption P_c divided by the number of agents, 10000. Each time step is taken to be 1s, and at each time step each agent updates its temperature, and based on the frequency at the previous time step, may switch on or off. The exact switch time is approximated using linear interpolation between the current and previous time step, and the new temperature is adjusted accordingly (see Appendix B for details).

To perturb the TCL distribution $u(\theta)$ we can alter the number of TCLs switched on or off from the equilibrium proportions ρ^* and $(1-\rho^*)$ respectively, and we can perturb the uniform distributions within each on/off half of the θ interval. We choose to perturb the distributions by the addition of a sine wave to u^*, and we refer to the normalised wave peak amplitude Δu (normalised by dividing by u^*). This normalisation means that when we plot $\frac{u(\theta,0)}{u^*}$, the zero perturbation case is 1 for all θ both on and off and the results are more clear. Table 4.1 shows eight combinations of choices for these perturbation parameters. All other parameters are as stated in Table 3.1 in Section 3.2.4.

Figure 4.1 shows the effects of these perturbations on the initial conditions in each case, plotting $\frac{u(\theta,0)}{u^*}$ against θ. Figure 4.2 shows the final fridge distributions after ten days. The unperturbed case (a.i) has remained uniform, while the peaks of the perturbation cases have all grown by varying amounts. In cases (a.ii)-(a.iv) (no perturbation to the proportion switched on) the final distributions exhibit increasing levels of synchronisation, but the clustering is far less than in cases (b.i)-(b.iv) which

Table 4.1: Parameter values for plots in Figures 4.1, 4.2 and 4.3.

Plot number	$\rho_{\mathbf{on}}(0)$	Δu
a.i	ρ^*	0
a.ii	ρ^*	0.1
a.iii	ρ^*	0.25
a.iv	ρ^*	0.5
b.i	$1.5\rho^*$	0
b.ii	$1.5\rho^*$	0.1
b.iii	$1.5\rho^*$	0.25
b.iv	$1.5\rho^*$	0.5

see the population synchronised into seven or fewer groups. The effects of this synchronisation on the electricity grid frequency can be seen in Figure 4.3.

Interestingly, in each case with perturbations, the frequency oscillations initially die down to close to 50Hz. This means that to begin with the fridges are controlling the frequency oscillations caused by their initial condition perturbations. This aligns with our analysis from the previous chapter, in which we found that the uniform distribution of a continuum population is stable to small perturbations. What that analysis was unable to capture was the long-term effects of frequency sensitivity. In each case the frequency oscillations grow after less than a day, becoming very large in several cases. Before the large spikes in (b.iii) we see the frequency oscillations shrink down. This shows the inherently volatile nature of the system, and potentially explains why the the oscillations in (b.iv) are ultimately less severe. It could be that these lower oscillations will shortly become much larger. In either case, the size of most of the final oscillations would be too large for the system to cope without frequency response from other providers.

These simulations reveal that while a homogeneous population of TCLs will act to dampen system perturbations, their behaviour to support the electricity grid will, given sufficient time, lead to further oscillations. The larger the perturbations, the sooner these detrimental effects will occur.

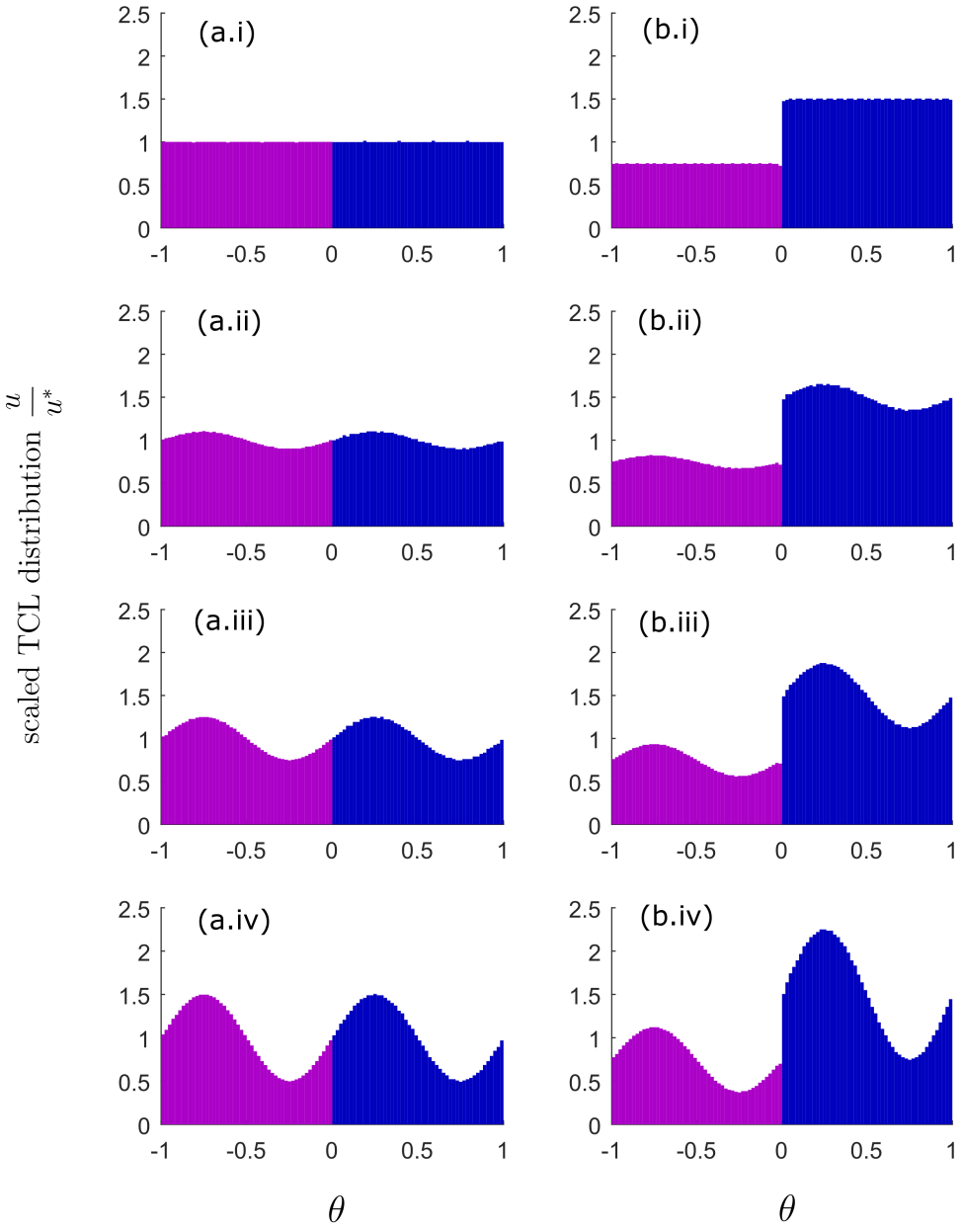

Figure 4.1: Initial fridge distributions in phase, with labels matching those in Table 4.1. Pink indicates switched off fridges, blue indicates switched on. Distributions scaled by $\frac{1}{u^*}$ and histograms formed of 100 bins. Left-hand figures have no perturbation to the proportion of fridges switched on, right-hand figures have increasing perturbation (going downwards) to the number of fridges switched on. All involve sinusoidal distribution perturbations.

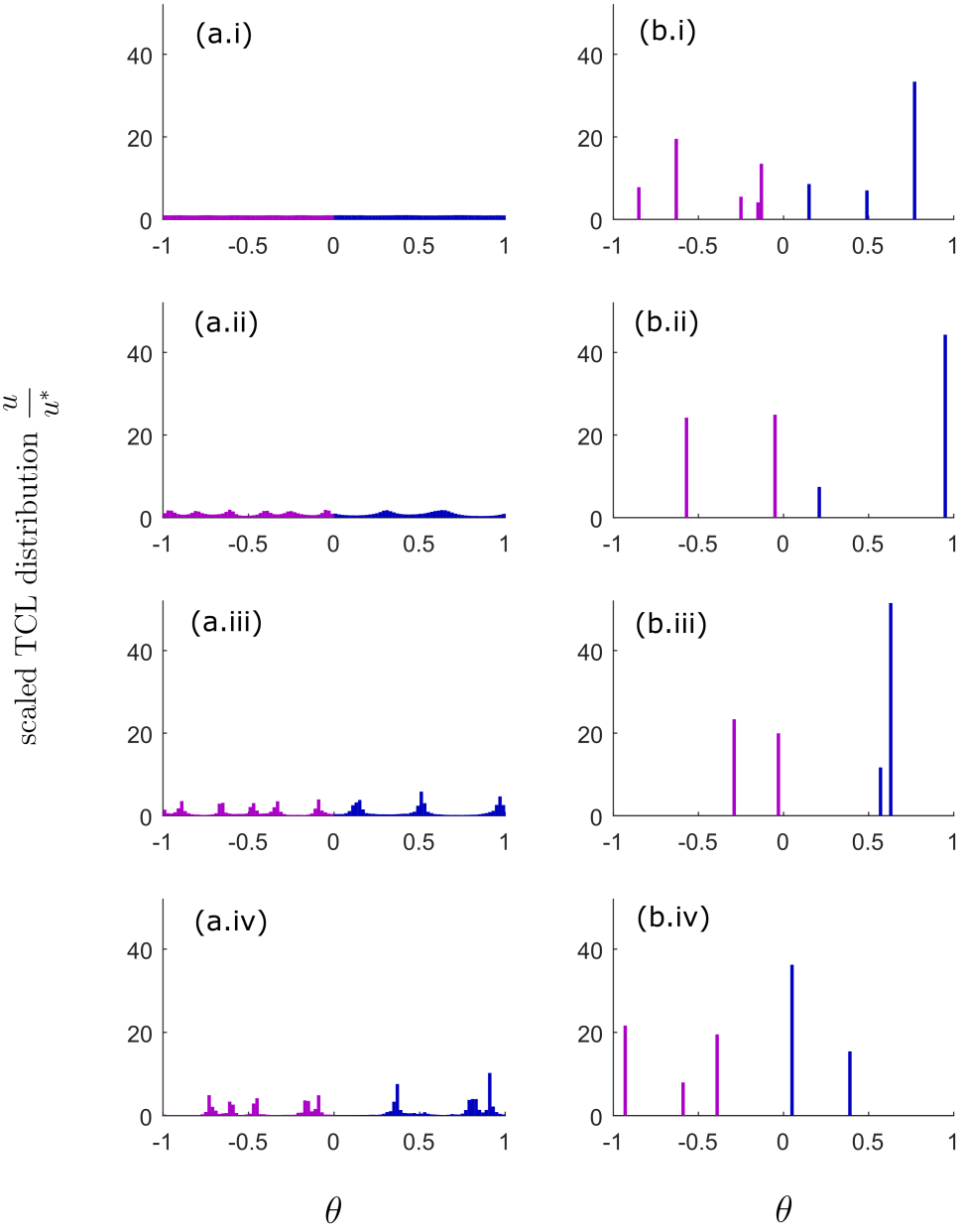

Figure 4.2: Final fridge distributions after 10 days in θ-space, with properties as given in Table 4.1 and initial distributions as shown in Figure 4.1. Perturbations have grown (except for the zero perturbation case (a.i)).

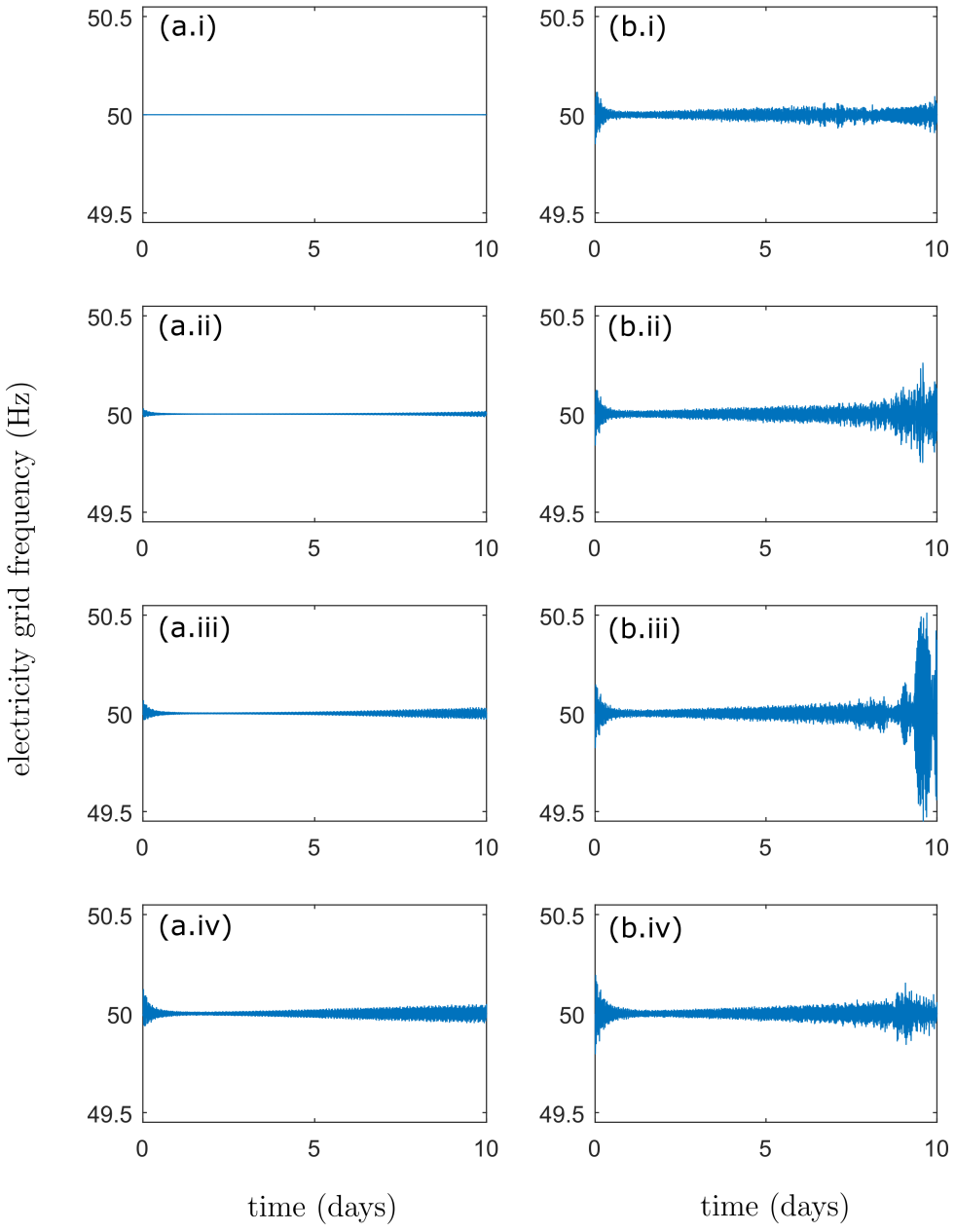

Figure 4.3: Electricity grid frequency over 10 days (values plotted once per 5 minutes), with fridge distributions as described in Table 4.1 and Figures 4.1 and 4.2. The perturbed systems (all but (a.i)) see an initial reduction in oscillation amplitude followed by oscillation growth.

4.3 GB electricity grid simulations: Methodology

Our model and simulations have thus far reduced the complexity of the problem by assuming that apart from the TCL population and the grid frequency, all other network conditions remain constant. This was necessary for our model to be tractable, and to ensure that any results from the simulations were attributable to the frequency-sensitive TCL population. An important next step is to consider the TCL population in the context of a real system. In collaboration with the GB System Operator National Grid, we are able to model the GB system with real data from 36 separate 10-day periods during 2015-2016, and simulate what would have happened if a frequency-sensitive fridge population had been active. We consider how the distribution of TCLs changes over this period, and the reduction in the amount of response that other providers needed to supply because of the contribution from the fridges.

We simulate a population of TCLs (specifically fridges) that respond to the grid frequency according to the rules in Section 3.2.2. To simulate the grid frequency, we use various historic data from National Grid and model what would have happened had the population of fridges been frequency responsive at the time. By considering the population in the context of real data including response provision from other sources such as power generators, we are able to get a better understanding of the potential impact of the fridges compared to, say, modelling them in isolation responding to a one-off frequency event.

Figure 4.4 gives an overview of the simulation process. The rhombus symbol is used for inputs and outputs, rectangles indicate methods used in the simulation. Methods are applied working downwards, except for the dashed arrows which create the iterative loop.

4.3.1 Inputs

As shown in Figure 4.4, there are four types of data input, in addition to the fridge population initial conditions. We use 36 consecutive samples of ten days' worth of continuous data from the period July 2015 - June 2016. Summary statistics and plots of the input data are presented in Appendix C.

Kinetic energy data consists of National Grid's best estimate for the total stored kinetic energy in MVAs (megavolt-ampere seconds) [21]. Values are calculated by

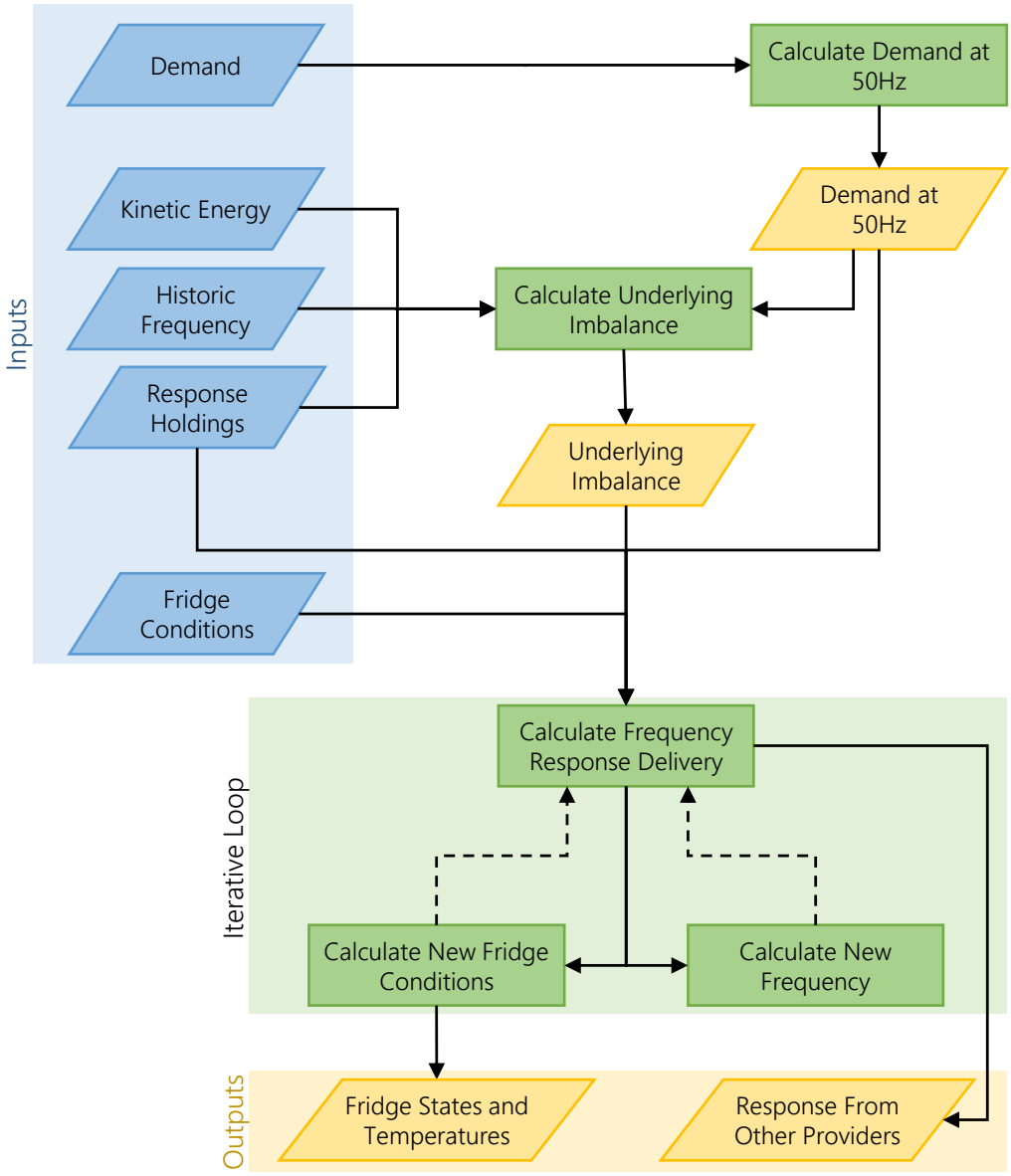

Figure 4.4: Simulation methodology diagram. Rhombi indicate input or calculated data/simulated data, rectangles indicate methods/calculations. Events occur from top to bottom with the exception of the dashed arrows which form the iterative loop.

summing the inertia of all running synchronised generators[1] with an estimate of kinetic energy from demand. The kinetic energy data provided (confidentially from

[1]This is a generator-specific constant provided to the System Operator by each power generator.

National Grid) is per settlement period[2] and repeat each value for the full 30 minutes (rather than interpolating). Typical kinetic energy values are in the range of 20000 - 40000 MVAs.

Demand data consists of per-second metered demand given to us by National Grid. This is a sum of the power leaving the electricity transmission system, including any power exports through the interconnectors. Half-hourly demand data is currently accessible via the 'Data Explorer' page National Grid website[3].

Historic frequency data consists of per-second system frequency data in hertz. Frequency measurements are taken in multiple locations to ensure reliable data availability in the event of any metering faults. The frequency data provided by National Grid has undergone a cleaning process that takes advantage of the multiple readings. It is available via National Grid's 'Enhanced Frequency Response' page[4].

Response holdings refers to the amount of frequency response delivery in MW (as a function of grid frequency) that National Grid expect each second. Response holdings are positive (or negative) for 'low (high) frequency response delivery' (when the frequency is below (above) 50Hz), respectively. For each time step (1 second), 9 different values for response holding are listed. These take the form of primary, secondary and high response.

Primary response values are given for trigger points at 49.9Hz, 49.5Hz and 49.2Hz. This means that at these frequencies the power response provided through various types of primary response service are the historic response holding values given, subject to a 1 second reaction delay. We assume that the response increases linearly from 0 between 49.985Hz and 49.8Hz, and likewise linearly between all other frequency trigger values. Below 49.2Hz the response is assumed to be the constant 49.2Hz response value. The starting frequency trigger value of 49.985Hz is used to take into account the Grid Code deadband of (50 ± 0.015)Hz, within which response is not required. Secondary response values are given for frequency trigger points 49.8Hz and 49.5Hz, and response is modelled in the same was as for primary response, only with an 11s response delay. High response values have trigger points 50.2Hz and 50.5Hz. Just as for primary response, the time lag is 1s and again, response is modelled as linear interpolation through these points, starting at the edge of the deadband at 50.015Hz, and remaining constant beyond 50.5Hz. Figure 4.5

[2] Settlement periods split up the day into 48 half hour units starting on the hour and half hour.

[3] http://www2.nationalgrid.com/UK/Industry-information/Electricity-transmission-operational-data/Data-Explorer/

[4] http://www2.nationalgrid.com/Enhanced-Frequency-Response.aspx

illustrates an example of how response holding data (Table 4.2) are interpreted in the model. Values given are indicative only of possible values.

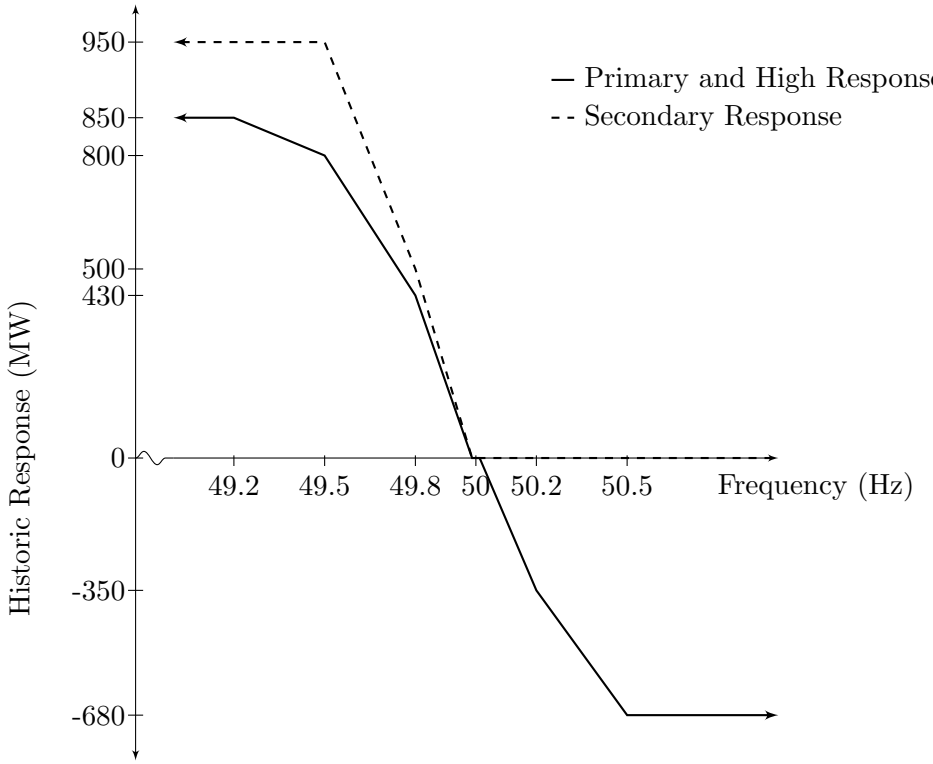

Figure 4.5: Representative historic response data with interpolation method for primary response (solid line below 50Hz), secondary response (dashed line) and high response (solid line above 50Hz). Zero response in the deadband (50 ± 0.015)Hz.

Table 4.2: Illustrative historic response holding data behind Figure 4.5.

	Primary			Secondary		High	
Frequency Trigger (Hz)	49.2	49.5	49.8	49.5	49.8	50.2	50.5
Response (MW)	850	800	430	950	500	-350	-680

Fridge conditions refers to the initial on/off state and initial temperature of each fridge in the population. For the simulations presented here we take the zero perturbation case (a.i) (Table 4.1) from the previous section.

4.3.2 Calculating the demand at 50Hz

Deviations in grid frequency away from 50Hz affect the total system demand. We make the assumption that demand increases linearly by approximately 2.5% of its value at 50Hz for every 1Hz increase in frequency above 50Hz (and decreases by the

same amount as frequency decreases below 50Hz). In order to know the demand at the nominal frequency, 'demand at 50Hz', $\text{Dem}_{\omega 0}(t)$, we need to calculate it from the (measured) demand data input, $D(t)$.

$$D(t) = \text{Dem}_{\omega 0}(t)[1 + 0.025(f(t) - 50)] \tag{4.1}$$

$$\text{Dem}_{\omega 0}(t) = \frac{D(t)}{1 + 0.025(f(t) - 50)}. \tag{4.2}$$

We use this new demand data to calculate the underlying imbalance and the response from demand in the presence of the fridge population.

4.3.3 Calculating the underlying imbalance

In order to calculate the effects of the fridge population on the system frequency, we first need to calculate the underlying supply-demand imbalance (in MW) that caused the original system frequency deviations away from 50Hz. At this point it is necessary to distinguish between two important, similar-sounding terms: *underlying imbalance* and *total imbalance*. By underlying imbalance, $\text{Imb}_{under}(t)$, we mean the generation-demand imbalance that occurs independently of the system frequency. This may be due to, for example, fluctuations in wind or solar power generation, or discrepancies between the total predicted system demand and the actual real-time demand. In contrast, total imbalance, $\text{Imb}_{tot}(f, t)$, includes both the underlying imbalance and, additionally, what we shall refer to as *dynamic imbalance*.

There are two sources of dynamic imbalance; *generator response* (frequency response provided by power generators as the frequency changes), and *demand response* (the automatic change in demand as frequency changes)[5]. Generator response, Gen_{resp}, consists of the actual response delivered by generators, calculated as described above from the response holdings and the historic system frequency. Generator response is assumed to have a small time lag δt, which we take to be 1 second. In contrast, demand response, Dem_{resp}, is assumed to occur instantaneously, and is defined as the measured system demand $D(t)$ minus the demand at 50Hz, $D_{\omega 0}(t)$ (see 'calculating demand at 50Hz'). Therefore by (4.1)

$$\text{Dem}_{resp}\big(f(t), t\big) = 0.025 D_{\omega 0}(t)\big(f(t) - 50\big). \tag{4.3}$$

[5]Note that in this context 'demand response' is completely different to demand-side response services, which, given their current low penetration of the response market, we exclude from our simulations.

Both sources of dynamic imbalance will change when we introduce the population of responsive fridges (because of their impact on the frequency) and therefore will need to be re-calculated.

We use a linear approximation for the rate of change of frequency [1], which in our notation, is given by

$$\frac{\mathrm{d}f}{\mathrm{d}t} = \frac{50\ \mathrm{Imb}_{tot}(t)}{2E_k(t)} \tag{4.4}$$

where 50 is the nominal frequency 50Hz and $E_k(t)$ is stored kinetic energy in MVAs. Since

$$\mathrm{Imb}_{tot}(t) = \mathrm{Imb}_{under}(t) + \mathrm{Gen}_{resp}\big(f(t-\delta t), t\big) - \mathrm{Dem}_{resp}\big(f(t), t\big) \tag{4.5}$$

we are able to find

$$\mathrm{Imb}_{under}(t) = \frac{E_k(t)}{25}\frac{\mathrm{d}f}{\mathrm{d}t} - \mathrm{Gen}_{resp}\big(f(t-\delta t), t\big) + \mathrm{Dem}_{resp}\big(f(t), t\big) \tag{4.6}$$

which for simulation time step size Δt gives

$$\mathrm{Imb}_{under}(t) = \frac{E_k(t)[f(t) - f(t-\Delta t)]}{25\Delta t} - \mathrm{Gen}_{resp}\big(f(t-\delta t), t\big) + \mathrm{Dem}_{resp}\big(f(t), t\big). \tag{4.7}$$

We take $\Delta t = 1$s, so $\Delta t = \delta t$, the generator response time lag. Generator response is calculated using historic response holdings and the frequency $t - \delta t$ seconds ago along with some constraints on the generator ramp rates.

4.3.4 The iterative loop

Once the underlying imbalance has been calculated for all time steps it can be used along with the response holdings and fridge conditions to begin a loop formed of three calculation steps, that iterates over all time steps (see the 'iterative loop' in Figure 4.4). The steps are as follows:

1. **Calculate the frequency response delivery** from the fridge population and from the dynamic response providers based on the previous frequency value[6]. For the fridge population this requires summing the switched on fridges

[6]The first iteration takes the first historic frequency value, after which the 'new frequency' values are used.

multiplied by their individual power consumption, and subtracting the power consumption of the population if the fridges were not frequency-sensitive. Response from the dynamic response providers is described above.

2. **Calculate the new frequency** $f^*(t)$ using the equations from 'calculating the underlying imbalance', and beginning with the approximation

$$\begin{aligned} f^*(t) &= f^*(t-\Delta t) + \Delta t \frac{\mathrm{d}f^*}{\mathrm{d}t}(t) \\ &= f^*(t-\Delta t) + \Delta t \frac{25\ \mathrm{Imb}^*_{tot}(t)}{E_k(t)} \end{aligned}$$

and since

$$\mathrm{Imb}^*_{tot}(t) = \mathrm{Imb}_{under}(t) + \mathrm{Gen}_{resp}(f^*(t-\delta t), t) - 0.025\ \mathrm{Dem}_{\omega 0}(f^*(t) - 50)$$

we get

$$f^*(t) = \frac{f^*(t-\Delta t) + \frac{25\Delta t}{E_k(t)}\left(\mathrm{Imb}_{under}(t) + \mathrm{Gen}_{resp}(f^*(t-\delta t), t) + 1.25\mathrm{Dem}_{\omega 0}\right)}{1 + 0.625\frac{\delta t}{E_k(t)}\mathrm{Dem}_{\omega 0}}.$$

Note that we let $f^*(0) = f(0)$, the original frequency value at time 0.

3. **Calculate the new fridge conditions** by updating their temperature set points with the new frequency f^* calculated in step 2, according to equations (3.4a) and (3.4b). Each fridge temperature is evolved one time step according to (3.5a) or (3.5b). If a switch on or off should have occurred during the time step then the exact time of switch is estimated and the temperature is recalculated from the switch time to the end of the time step using linear interpolation (see Appendix B for details).

4.3.5 Outputs

There are two key outputs for our analysis. Firstly, the temperatures and states of each fridge over time, and secondly, the frequency response supplied by all other providers on the grid. Since response can be positive or negative depending on the frequency, but both incur payment, we take the absolute value of the response at each time step. We take the cumulative sum of the difference between this response in the presence of TCLs and the original system response, and call it 'cumulative response savings', which we measure in MWh. This allows us to find out how much

benefit (or detriment) the fridges provided the system, and how that changes over time as they respond to frequency perturbations. We explain the specifics below.

Cumulative response savings

The other frequency response providers change their output depending on the value of the frequency, under certain ramping constraints. We can compare the amount of response they provide in the original case[7] (without fridges in frequency-sensitive mode, but with all of the fluctuations inherent in the data), with the amount of response they provide with the new frequency, that evolves over time according to the actions of these providers and the fridge population. We define the following terms to make this comparison precise. Let

- $origResp(t)$ be the original response from other providers (*i.e.* before we introduce frequency-sensitive fridges to the population) at time t
- $nonTclResp(t)$ be the response from the other providers at time t
- $newTotResp(t)$ be the total response of the system (fridges plus others) at time t
- $tclDem(t)$ be the total demand of the TCL (in our case fridge) population at time t
- $respSavings(t)$ be the difference between the original response and the new response from the other providers at time t
- $cumulativeSavings(\hat{t})$ be the cumulative response savings from the first time step to time step $\hat{t}$

The expected demand from the fridge population is given by $\rho_0 P_c$ where $\rho_0 := \frac{\tau^0_{\text{ON}}}{\tau^0_{\text{ON}}+\tau^0_{\text{OFF}}}$, and so we calculate

$$nonTclResp(t) = newTotResp(t) - \big(\rho_0 P_c - tclDem(t)\big) \tag{4.8a}$$

$$respSavings(t) = |origResp(t)| - |nonTclResp(t)| \tag{4.8b}$$

$$cumulativeSavings(\hat{t}) = \sum_{t=1}^{\hat{t}} respSavings(t) \tag{4.8c}$$

[7] For further details about the response from other providers, see the 'Response holdings' topic in Section 4.3.1.

We use the absolute value of response as it can be positive or negative, depending on whether the frequency is above or below 50Hz. If the fridges are acting beneficially to the system the cumulative response will grow over time, and if they cause more harm than good then the cumulative response will become negative.

The remainder of this chapter is devoted to the results from our simulations of a homogeneous, and then a heterogeneous population of fridges using this methodology.

4.4 GB electricity grid simulations: Homogeneous population results

In this section we analyse the results from simulations of a population of identical fridges in the presence of other frequency response providers and underlying system imbalances, as described above. We group the fridges into 10000 groups (or agents) in order to represent between one and ten million fridges without requiring very large amounts of computational time. We simulate the system every second over a 10-day period and record the impact on both the other response providers and the individual fridges. We repeat the simulations for 36 consecutive 10-day periods over 12 months starting from 1st July 2015. We repeat these 36 simulations for different values of our main control variables.

In Section 4.4.1 we consider the impact of varying the total fridge load, P_c, in the range 70 - 700MW. In our simulations we find that increasing the participation level 10 fold only increases the potential benefits by a factor of 7, but increases the potential harm by a factor of 15. We present the cumulative response savings (defined in Section 4.3.5) in both absolute terms (MWh) and as a proportion of the original response provided. We also show the maximum savings reached over the 10-day periods, and when this maximum occurred. As the results implicate synchronisation, we present a way to visually assess the amount of synchronisation in the population using a histogram approach. Finally we consider the impact on fridge temperatures of their frequency-sensitive behaviour, finding minimal impact.

Section 4.4.2 has a similar structure to Section 4.4.1 except that we vary the sensitivity of the fridges to the frequency, β, between 1.2 - 6.0°C/Hz. All other values are as in Table 3.1 or from the GB system data[8]. We find that with greater sen-

[8]This means that when we vary the total MW load of the fridges, $\beta = 2.4$°C/Hz, and when we vary β the total fridge load = 70MW.

sitivity to the frequency, both the potential for harm and good increase, and the results become more variable. Again we show the cumulative response savings at the end and at their highest during the period, and when the maximum occurred. We also repeat our study of synchronisation with our histogram approach, finding very high levels of synchronisation again. For greater sensitivity we see a higher impact on fridge temperature, as would be expected. We summarise our findings in Section 4.4.3.

4.4.1 Varying total fridge load

Varying the total fridge load, P_c is equivalent to increasing the number of fridges participating in our demand-side response scheme (*i.e.* the number of fridges that are in frequency-sensitive mode). We consider four different participation levels: P_c equals 70MW, 280MW, 490MW and 700MW, which corresponds to 1m, 4m, 7m and 10m fridges in our model. Note that we continue to simulate the population using 10000 groups of fridges in all cases. We begin by analysing the impact of the frequency-sensitive population on the system, in particular, the savings (or additional requirements) of response supplied by other frequency response providers.

Cumulative response savings over time

We begin with two examples ($P_c = 70$MW (a) and $P_c = 700$MW (b)) of the cumulative response savings for each of the 36 data sample simulations. Figure 4.6 shows $cumulativeSavings(\hat{t})$ for each parameter choice (a) and (b). Each plotted line shows the results for one of the 36 10-day simulations. After an initial increase in the savings, for many of the simulations (at least one third in both cases) the savings decrease to reach negative final savings (*i.e.* additional requirements). Increasing participation ten-fold (from a to b) increases the maximum savings by a factor of 7, but amplify the worst case by a factor of 15. When there are fewer participants ($P_c = 70$MW), the results are more erratic over time, which we attribute to there being less response on the system, and so a less smooth frequency trace to respond to. To see the effects of varying the parameters, in the plots that follow we present only the final value of cumulative savings at the end of the ten-day period.

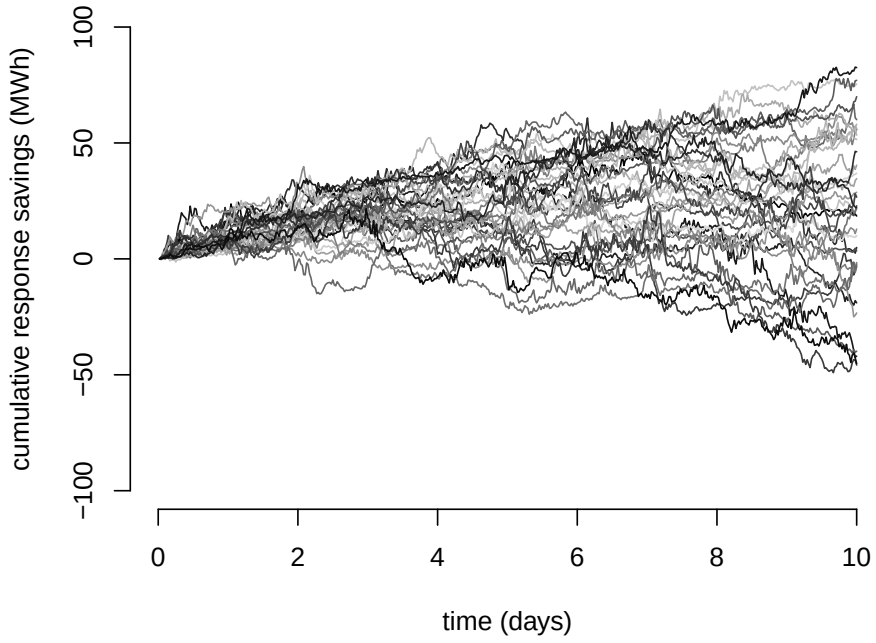

(a) $P_c = 70\text{MW}$

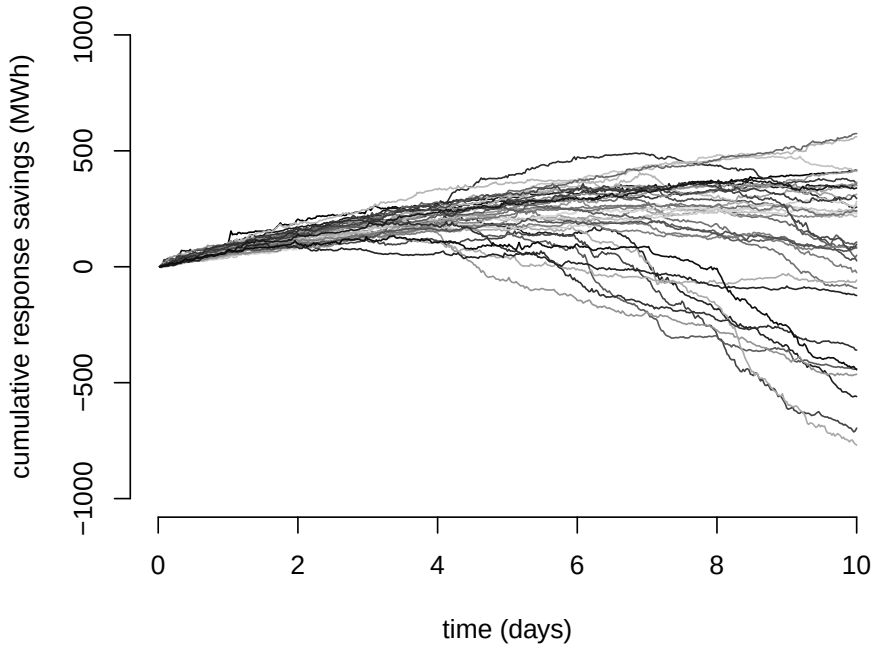

(b) $P_c = 700\text{MW}$

Figure 4.6: Cumulative response savings (MWh), the difference between other providers' response with and without the frequency-sensitive fridge population (cumulatively) for the 36 data samples over one year for two different participation levels. Negative results indicate the other providers had to compensate for detrimental fridge behaviour.

Final and maximum cumulative response savings

Figure 4.7(a) shows the cumulative response savings at the end of each 10-day period, for each of the 36 data samples over the 12 month period (blue) and the mean for each choice of total fridge load, P_c, in red. We see that as P_c increases the results become far more variable. In the best case there is an approximately linear increase in the cumulative response savings, from around 100MWh to around 550MWh. However, with the increased potential for beneficial savings comes a highly increased risk for increased response requirements. That is to say, at the end of the 10-day period of study the other providers on the system were required to provide more response overall when the fridges were frequency-sensitive, for some of the periods studied. This is possible in all cases, but particularly severe when the total fridge load is 700MW, with the worst-case simulation requiring almost 800MWh of additional response when the fridges were trying to help.

A natural next question is to compare the response with and without the frequency-sensitive fridges as a proportion of the original response from the providers. Some periods will require more response than others, and so dividing by the amount of response originally required allows us to compare all periods fairly, and to give us an idea of the scale of the impact of the fridges on the system. Figure 4.7(b) shows these results. The best impact is to make savings of around 5%, while the worst is to require around 8% more response from other providers. In all parameter cases the mean (in red) is limited to between 0% and 2% of original response. We see that after 10 days the impact of the fridges can be detrimental for any of the four choices of P_c, and as the participation level increases the effects can be highly unpredictable, depending on the conditions of the system during the period studied. But perhaps the detrimental populations did not cause problems throughout the period, but became synchronised and reduced the cumulative savings part-way through?

Figure 4.8 shows a much more positive outlook. It shows the peak of the cumulative savings over the 10-day period, whenever it occurred. Increasing the level of participation increases the mean of the maximum savings as well as the maximum, which reaches around 550MWh (almost 7% of original response). It is worth noting the decreasing returns on participation, in that the 10-fold increase from 70MW to 700MW of total fridge load increases the mean of the maximum cumulative response savings by an approximately 6-fold increase in savings. In the worst case for 490MW and 700MW the response savings are about the same (around 125MWh, 1% of original savings).

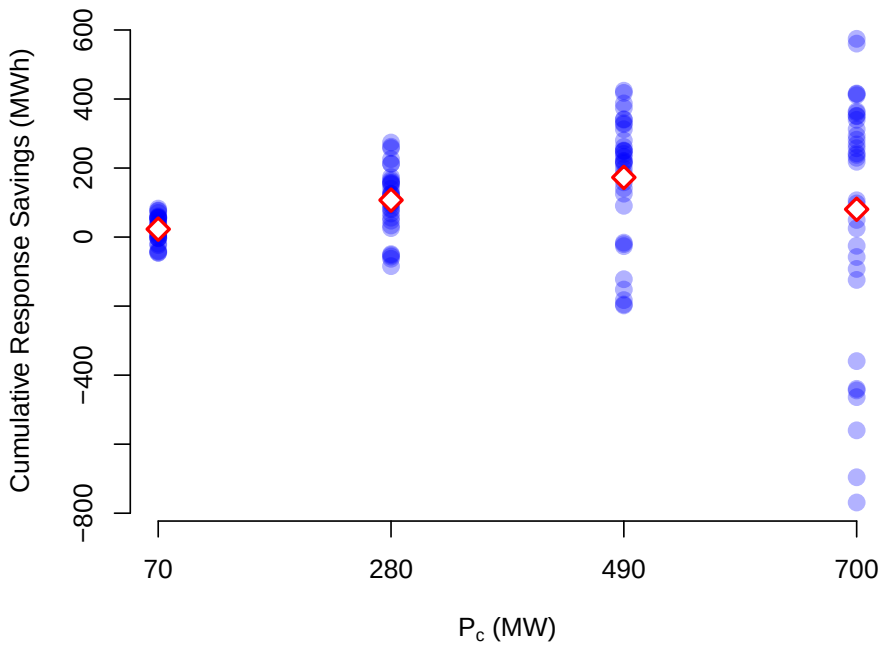

(a) Total savings (MWh)

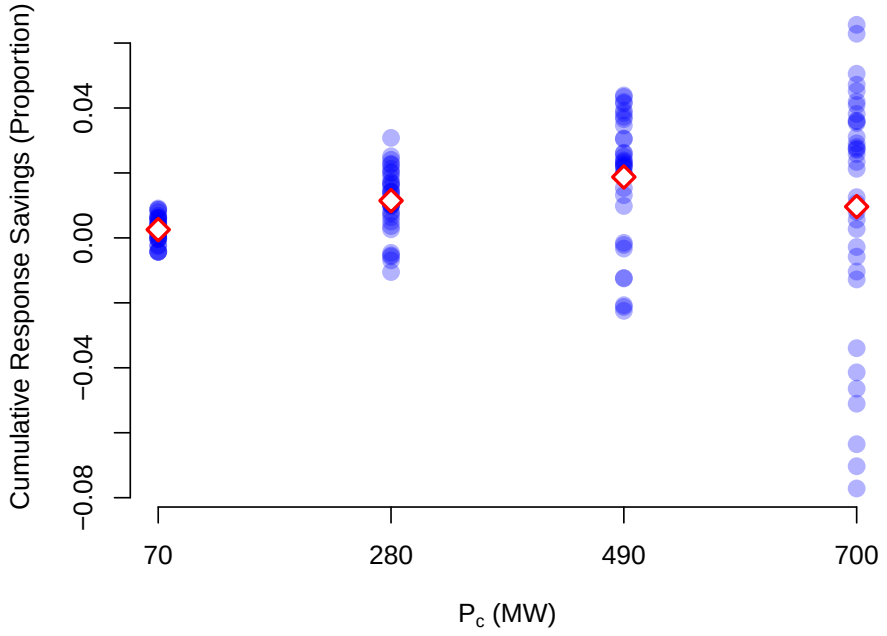

(b) Savings as a proportion of original response

Figure 4.7: Final cumulative response savings for each of the 36 10-day data samples over the 12 month period (blue) and the mean for each choice of total fridge load (red).

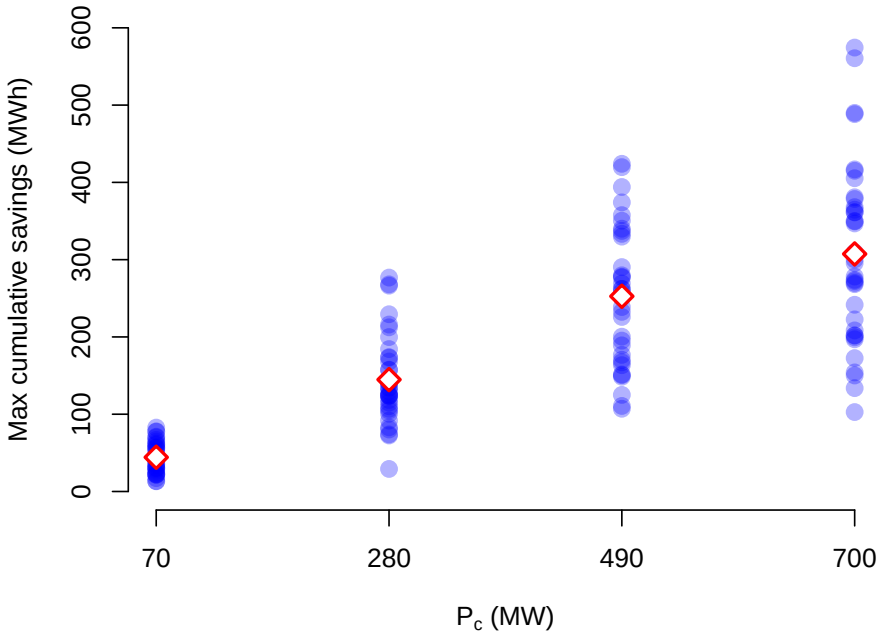

(a) Maximum (MWh)

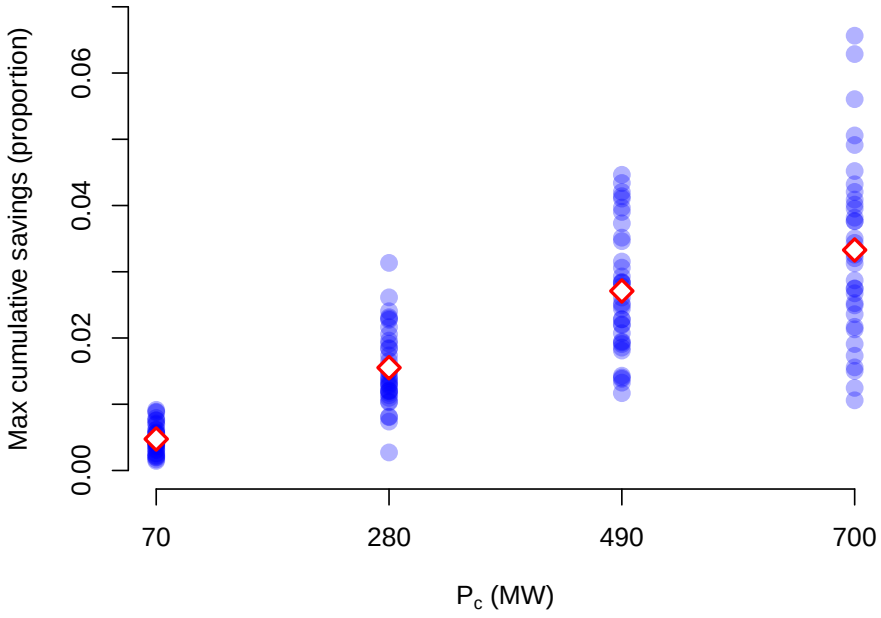

(b) Maximum (as a proportion of original response)

Figure 4.8: Maximum cumulative response savings for each of the 36 10-day data samples over the 12 month period (blue) and the mean for each choice of total fridge load (red).

Given that these results are generally much better than at the end of the 10-day period, when do these maxima occur? That is to say, at what point (if possible) should a population of fridges receive a signal to return to their original desynchronised state? Figure 4.9 shows the time at which the cumulative savings peak for each simulation. Immediately we see a wide range of results for all parameter values, between 1 and 10 days. The mean is around 7 days after the start of the simulation for all participation levels. Unpredictability is highly undesirable when balancing the electricity grid. To ensure no detrimental effects on the system, assuming these results are representative of system conditions going forward, we would need to desynchronise the population after at most 1 day. Later in this chapter we will introduce diversity to our fridge population to see whether this will reduce the potential for the early onset of detrimental effects on the system.

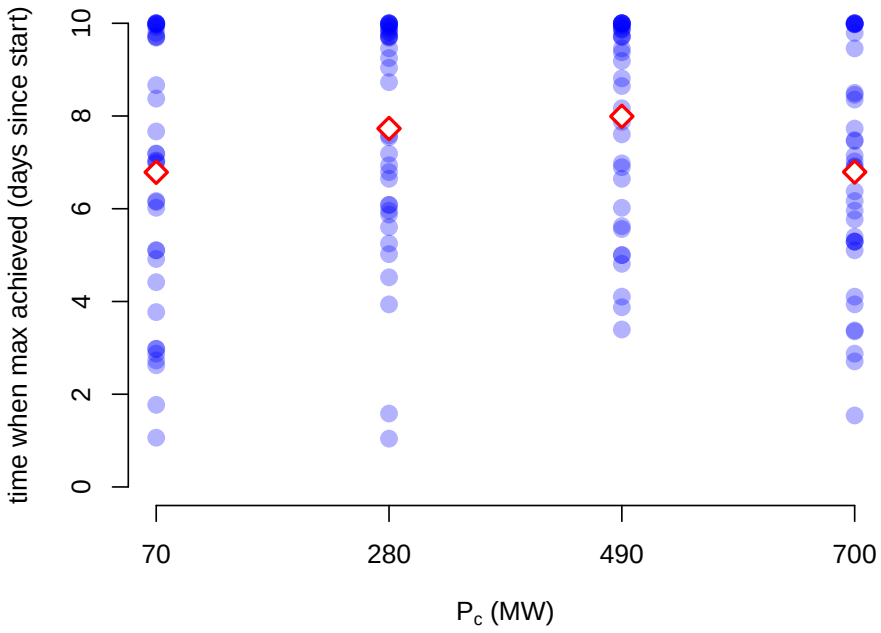

Figure 4.9: Time (in days since start) of maximum cumulative response savings for each of the 36 10-day data samples over the 12 month period (blue) and the mean for each choice of total fridge load (red).

Evidence of synchronisation

It is likely that the detrimental effects that can occur are caused by the synchronisation of the population into groups which makes them a less effective response provider, with the potential to do harm. We can investigate the synchronisation of the populations by mapping the temperature and state of each fridge to θ-space (defined in Section 3.3), and creating a histogram of the results.

Figure 4.10 shows how our histogram would look when the population is in its equilibrium distribution (the initial condition). Proportion ρ_0 is switched on ($\theta \in [0, 1)$) and proportion $1 - \rho_0$ switched off $\theta \in [-1, 0)$). This difference in densities requires different bin widths on each of the two halves. This is our base case with zero synchronisation, against which we shall compare distributions after 10 days of simulation.

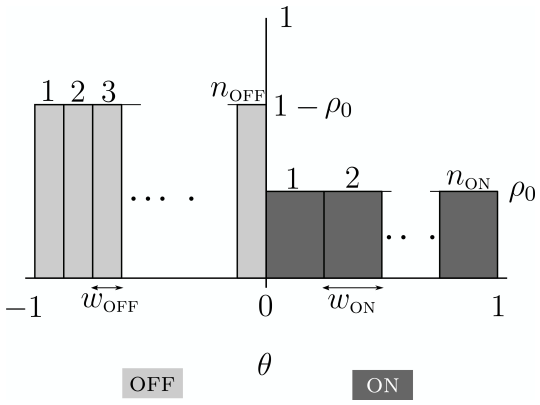

Figure 4.10: How we split the TCL population into bins for a histogram, accounting for the different 'normal' densities in each half of the interval. This example shows the population when it is completely non-synchronised.

We create the bin widths for the on and off halves, w_{ON} and w_{OFF} respectively, so that in this distribution the number of fridges in each bin will be identical across θ. We divide the interval into 1000 bins, which means in equilibrium 10 fridges (0.1% of the population) will be in each bin. Then we require

$$w_{\text{ON}}\rho_0 = w_{\text{OFF}}(1 - \rho_0) \tag{4.9a}$$

$$w_{\text{ON}}n_{\text{ON}} = 1 \tag{4.9b}$$

$$w_{\text{OFF}}n_{\text{OFF}} = 1 \tag{4.9c}$$

$$n_{\text{ON}} + n_{\text{OFF}} = 1000 \tag{4.9d}$$

and so we can write

$$1 + \frac{n_{\text{OFF}}}{n_{\text{ON}}} = \frac{1000}{n_{\text{ON}}} \tag{4.10a}$$

$$1 + \frac{1-\rho_0}{\rho_0} = \frac{1000}{n_{\text{ON}}} \tag{4.10b}$$

$$\therefore n_{\text{ON}} = [1000\rho_0] \tag{4.10c}$$

$$w_{\text{ON}} = \frac{1}{[1000\rho_0]} \tag{4.10d}$$

$$w_{\text{OFF}} = \frac{1}{[1000(1-\rho_0)]} \tag{4.10e}$$

where the notation $[x]$ denotes x rounded to the nearest integer. We round because for a histogram we require an integer number of bins.

Rather than present the histograms for each of the 36 simulations for each of the 4 parameters, we order the bins from smallest to largest (the size refers to how many fridges are in the bin) and present the number of fridges in the nth largest bin for each simulation at the end of the 10-day period. It turns out that in each case the fridges have become highly synchronised, and so the results, shown in Figure 4.11, are for the 20 largest bins only. That is to say, for all four choices of the total fridge load, fridges have become clustered in 1-2% of the θ-interval. Perhaps surprisingly, the greatest levels of synchronisation occur for the smallest participation level (70MW). We hypothesize that when more fridges are providing frequency response the frequency (at least to begin with) is kept closer to 50Hz, and so the population experiences lower fluctuations to respond to. The fridges are not only displacing the need for other providers to supply response, but are increasing the total level of response and keeping the frequency closer to 50Hz. When we introduce diversity to the population we will be able to use this measure of synchronisation to see whether/how increasing population diversity reduces these high levels of synchronisation.

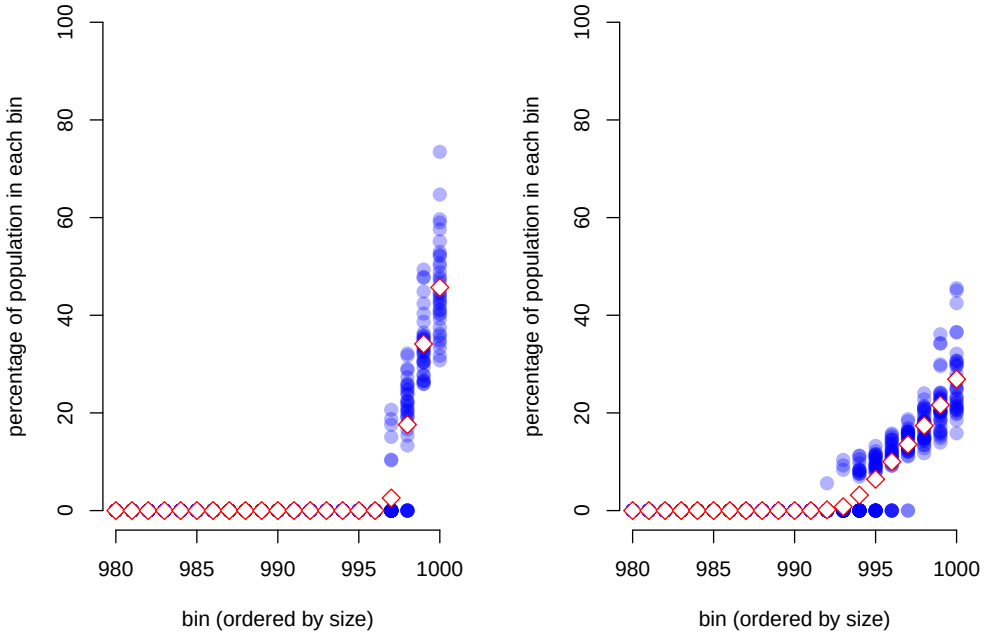

(a) $P_c = 70\text{MW}$

(b) $P_c = 280\text{MW}$

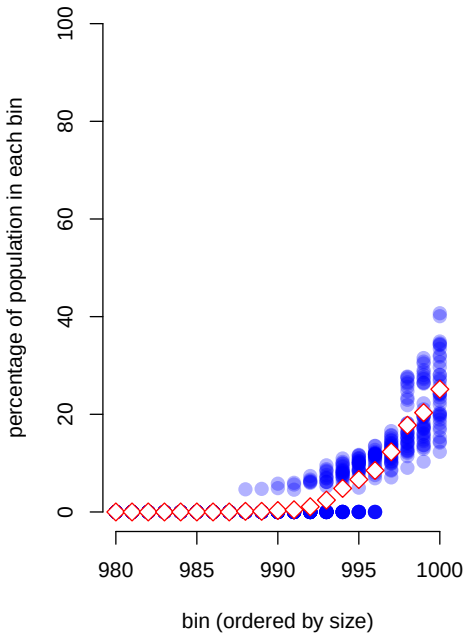

(c) $P_c = 490\text{MW}$

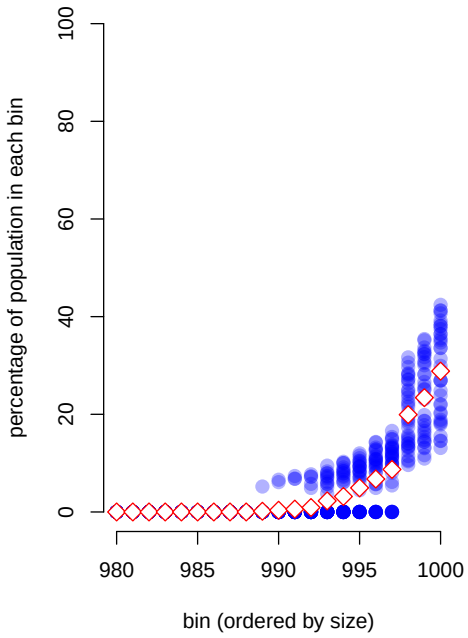

(d) $P_c = 700\text{MW}$

Figure 4.11: The percentage of fridges in the 20 fullest bins for different total fridge loads. Individual simulation results shown in blue, mean in red.

Impact on fridge temperatures

In addition to the benefits or costs to the system, introducing frequency sensitivity to a population will also impact the fridges themselves. An effective control design will ensure that the impact to any individual is minimal. Figure 4.12 shows the lowest, highest, and mean of the temperature extrema of the simulations from the 36 time periods for each parameter. There is little difference between the results for any time period or value of P_c. This shows that our choice of $\beta = 2.4$ is a good choice for the impact on the fridges. We will explore the effects of varying this parameter in the next section.

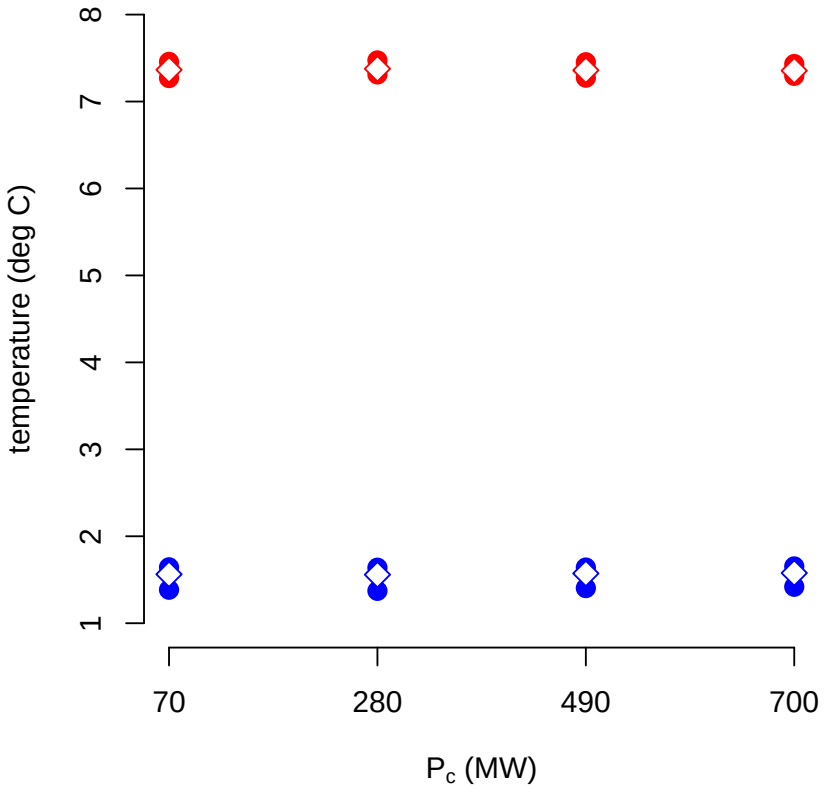

Figure 4.12: Circles show the minimum and maximum of the lowest (blue) and highest (red) temperatures for each parameter. Diamonds show the mean of the lowest (blue) and highest (red) temperatures reached over all simulations for the same parameter.

4.4.2 Varying fridge sensitivity to the frequency

Another key control parameter is the sensitivity of each fridge to the electricity grid frequency, parameter β (setting $\beta_+ = \beta_-$). Our chosen value of β has so far been $\beta = 2.4$°C/Hz, to ensure that a fridge with lower temperature set point 2°C will not reduce below freezing point so long as the frequency stays within statutory limits. In this section we explore the effects of taking β to be 1.2° C/Hz, 2.4°C/Hz, 3.6°C/Hz, 4.8°C/Hz and 6.0°C/Hz. Note that the case $\beta = 2.4$ has exactly the same parameter values as the $P_c = 70$ case above.

Final and maximum cumulative response savings

As we increase the sensitivity of the fridges to the frequency the cumulative response savings have greater variance, and the potential increased response requirements also increase, as shown in Figure 4.13. In the most extreme cases the other response providers have to provide over 300MW of extra response over the course of the 10-day period, around 3-4% of the original amount.

Figure 4.14 shows the maximum cumulative response savings for each value of β. The mean and highest value increases with β, with the highest savings reaching over 300MWh (over 3%) of savings. However, the minimum value possible in each case changes little with β.

Figure 4.15 shows the time when these maxima occurred. As β increases the mean of the times occur earlier in the period (apart from the highest β value), from just under 9 days to 6-7 days. As in the case for varying participation levels, there is a wide range of peak times for all choices of β.

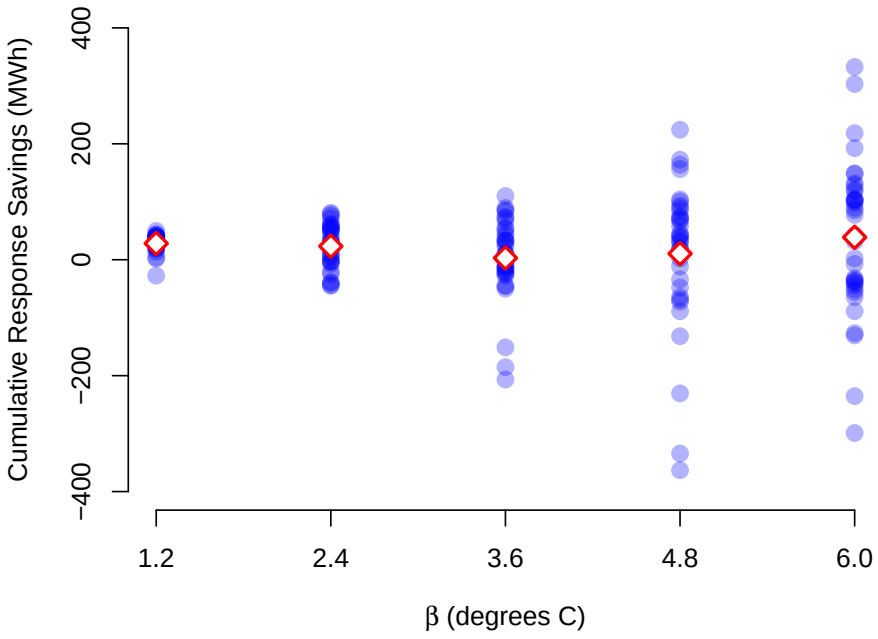

(a) Total savings (MWh)

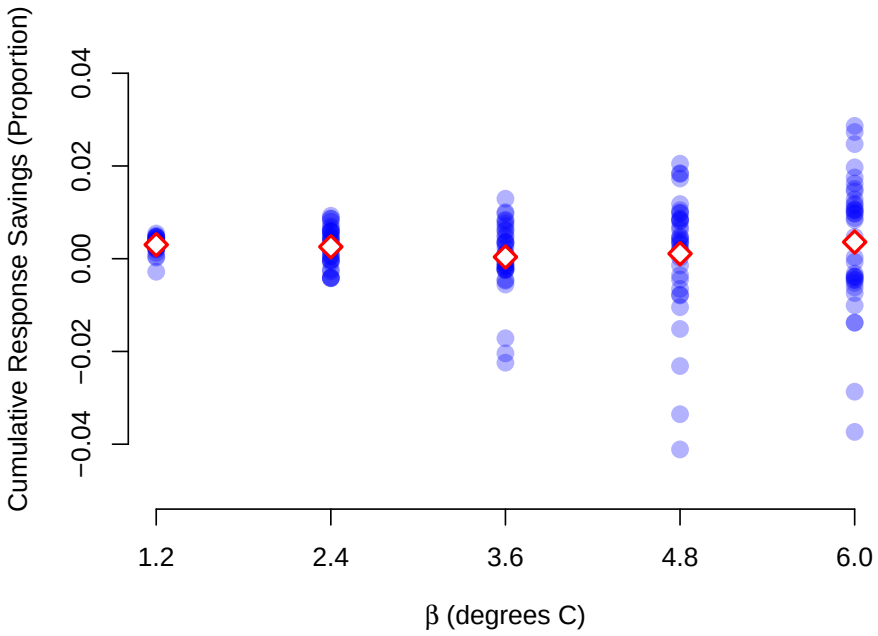

(b) Savings as a proportion of original response

Figure 4.13: Final cumulative response savings for each of the 36 10-day data samples over the 12 month period (blue) and the mean for each choice of β.

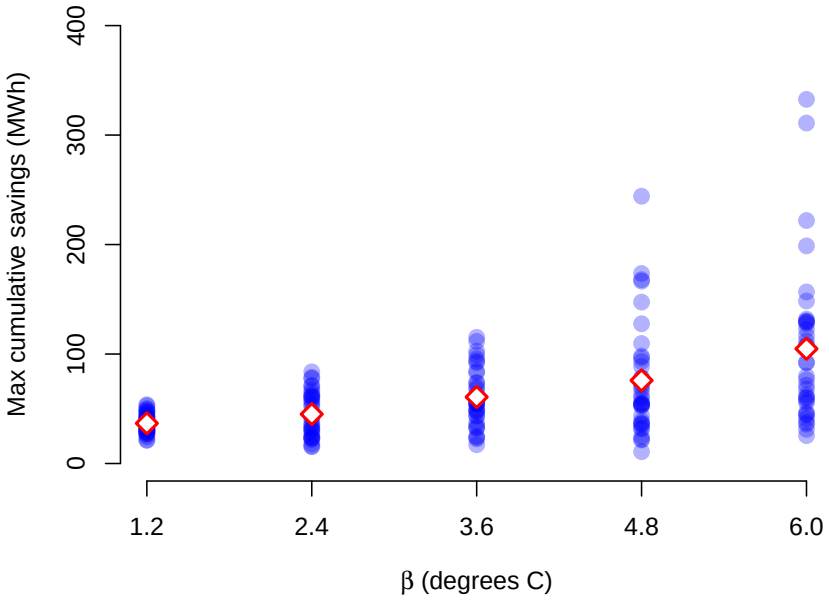

(a) Maximum (MWh)

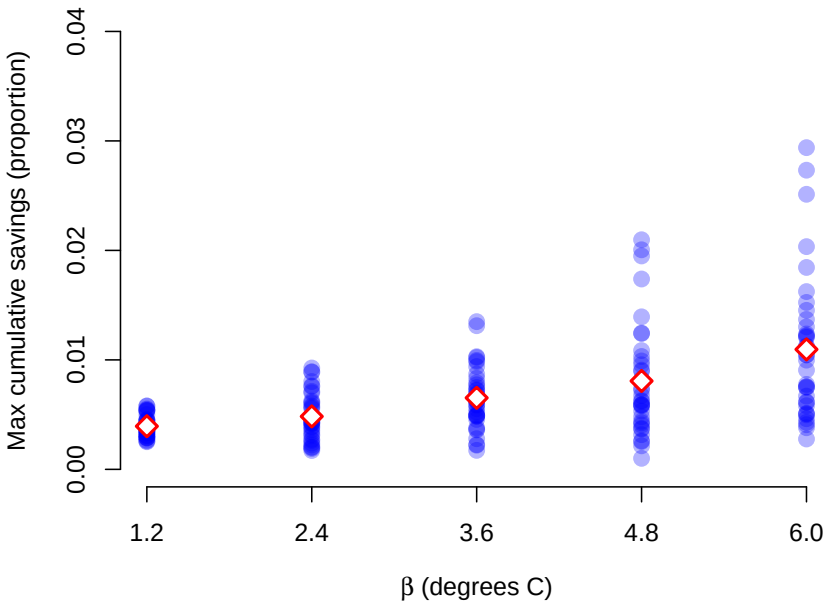

(b) Maximum (as a proportion of original response)

Figure 4.14: Maximum cumulative response savings for each of the 36 10-day data samples over the 12 month period (blue circles) and the mean for each choice of β (red diamonds).

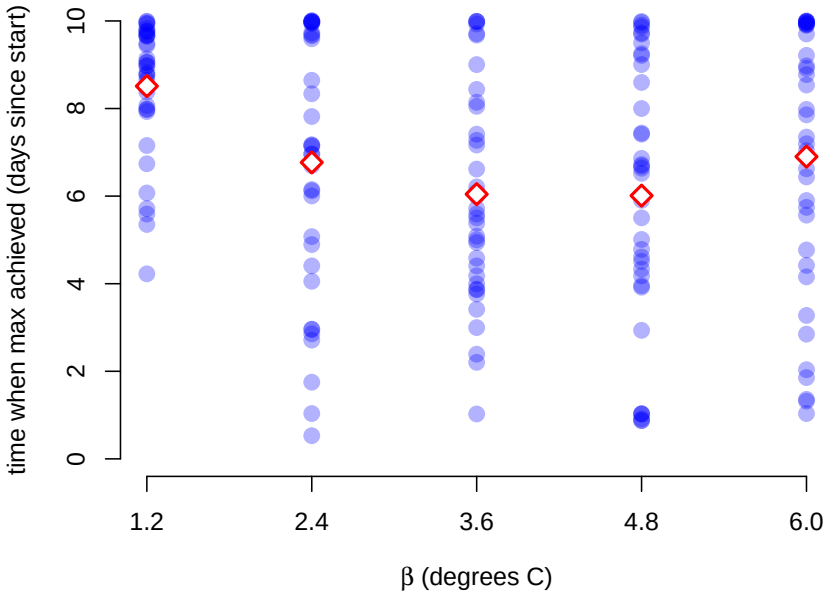

Figure 4.15: Time (in days since start) of maximum cumulative response savings for each of the 36 10-day data samples over the 12 month period (blue circles) and the mean for each choice of β (red diamonds).

Evidence of synchronisation

Figures 4.16 and 4.17 show the percentage of fridges in the largest (most full) 2% of histogram bins, as described above. As β increases the level of synchronisation of the populations increases, from highly synchronised to almost completely synchronised (note that $\beta = 6.0$ results in all fridges existing in just two of the 1000 histogram bins). These results make sense because the more sensitive the fridges are to the frequency, the greater the impact will be on their cycling.

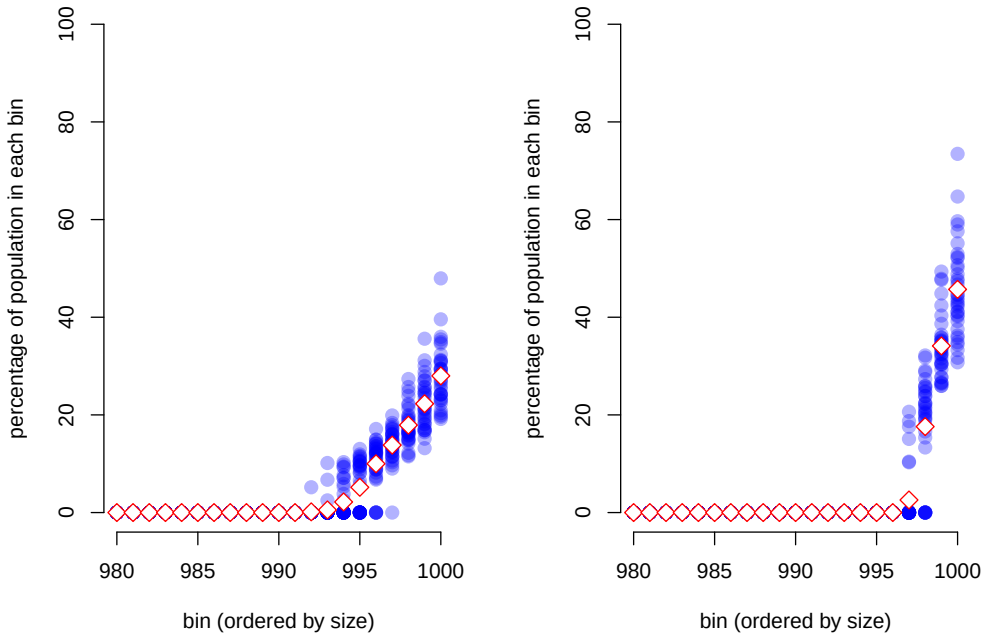

(a) $\beta = 1.2$ (b) $\beta = 2.4$

Figure 4.16: The percentage of fridges in the 20 fullest bins for $\beta = 1.2, 2.4$. Individual simulation results shown in blue, mean in red.

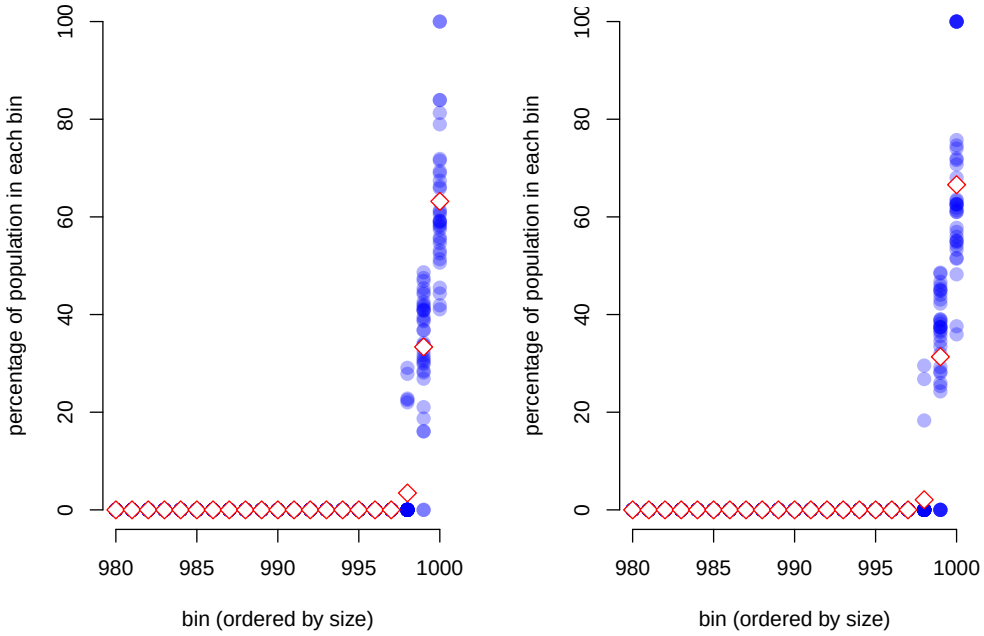

(a) $\beta = 3.6$

(b) $\beta = 4.8$

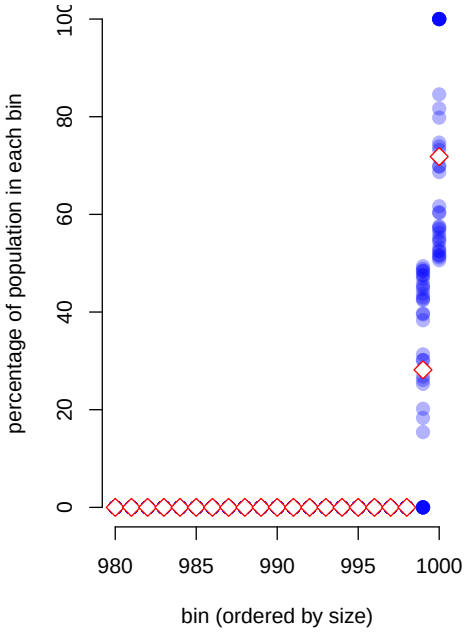

(c) $\beta = 6.0$

Figure 4.17: The percentage of fridges in the 20 fullest bins for $\beta = 3.6, 4.8, 6.0$. Individual simulation results shown in blue, mean in red.

Impact on fridge temperatures

Finally we consider the impact of varying fridge sensitivity to the frequency on their temperatures. Figure 4.18 shows the range of lowest and highest temperatures of the fridges over the 10-day period over all 36 time periods. Naturally, as the sensitivity increases we see greater shifts in temperature away from the nominal temperature set points, 2°C and 7°C. The range of minimum and maximum temperatures also increases. It is worth noting that even in the extreme cases, the temperatures never drop to less than 0°C or increase to more than 8°C.

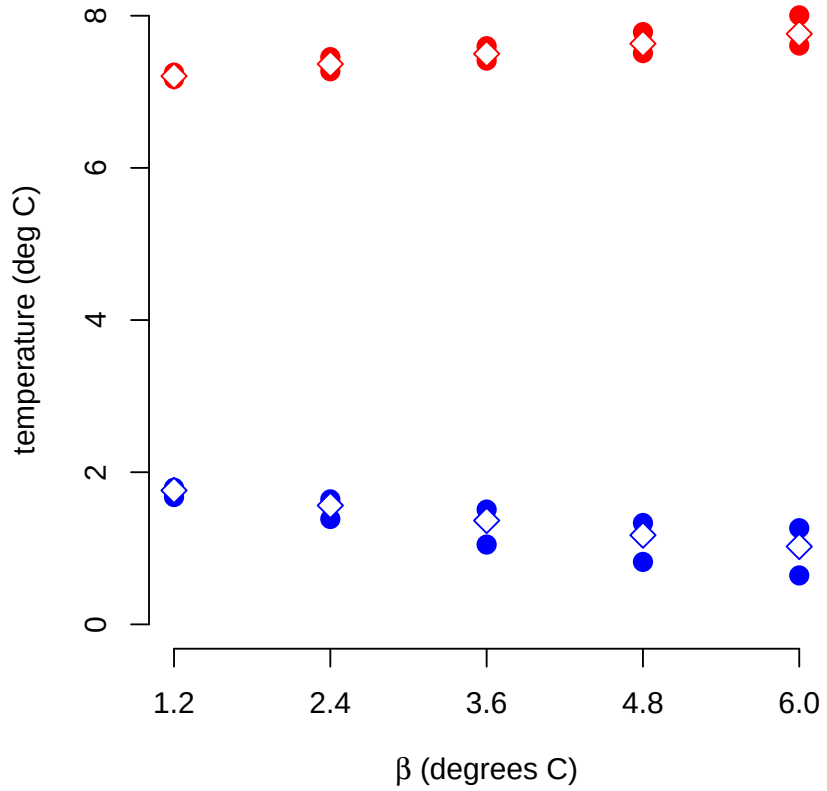

Figure 4.18: Circles show the minimum and maximum of the lowest (blue) and highest (red) temperatures for each parameter. Diamonds show the mean of the lowest (blue) and highest (red) temperatures reached over all simulations.

4.4.3 Summary

We find that by increasing the level of participation from 70MW of total fridge load to 700MW we have the potential to save 100-600MWh (1-7% of original response). However, the population becomes highly synchronised in all cases, and the time when these savings occur is unpredictable, ranging between 1 and 10 days of frequency-sensitive behaviour. This leads to detrimental effects on the network by the end of the 10-day period in a large number of cases. Increasing fridge sensitivity to the frequency also exacerbates these problems. Increasing sensitivity beyond 2.4°C/Hz shows potential benefits to the maximum cumulative savings that could be achieved in this period, but the time at which the maximum is reached showed a trend towards the beginning of the period, and for all but the lowest fridge sensitivity, the maximum is reached in under 2 days in multiple cases. Reducing the sensitivity reduces the negative effects but also reduces the potential benefits. All simulations (varying P_c and β) show no adverse temperature impact on the fridges during the 10 days of study.

4.5 GB electricity grid simulations: Heterogeneous population results

Thus far all of our simulations have involved populations of identical fridges, that is to say, all parameter values pertaining to fridge operation have been identical. In this section we diversify some of the parameters and study the effects. In Section 4.5.1 we explain our method for parameter diversification, and introduce our 'diversity factor' δ. In the following two sections we present the same graphs as in Sections 4.4.1 and 4.4.2 (homogeneous population varying load or sensitivity), only now the parameter we vary is the diversity factor. The difference between these sections is that Section 4.5.2 takes our lower bound on participation, $P_c = 70$MW, and Section 4.5.3 takes the upper bound, $P_c = 700$MW. In both cases we find negligible synchronisation for even our lowest diversity factor, and so in Section 4.5.4 we explore the minimum diversity requirements for synchronisation and compare the numerical results with a an approximately equivalent result using the Kuramoto model. We summarise the findings of our heterogeneous simulations in Section 4.5.5.

4.5.1 Diversifying the TCL population

In the literature the studies with parameter diversity typically take a few or all parameters from a uniform distribution, with upper and lower bounds within 20% of the mean. Table 4.3 contains a survey of ten different papers, summarising their approach to parameter heterogeneity. The uniform distribution is a popular choice, although normal and log-normal distributions are also used. Unfortunately there is a large absence of justification for these choices.

In the absence of data on realistic distributions for the parameters, we consider the normal distribution to be the most natural choice. We choose a uni-modal distribution because we have no evidence to suggest that it should be multi-modal, and we expect the occurrence of parameter values to become less likely as they get further from the mean (as opposed to the uniform distribution which considers all values to have probability p or probability 0). The zero diversity case for each parameter taking value x corresponds to a normal distribution with mean x and standard deviation 0. We therefore increase the standard deviation to increase the level of heterogeneity. As such, we take the means as the values from the homogeneous population simulations. For each parameter, we increase the diversity by choosing a value for the standard deviation, and multiplying all standard deviations

Table 4.3: Parameter heterogeneity literature survey.

Reference	**TCL type**	**Parameter(s)**	**Diversification Method**
Borsche *et al.* [56]	refrigerator	all	$\sim \mathcal{U}[0.85\hat{x}_i, 1.15\hat{x}_i]$ where $\hat{x}_i$ denotes mean of parameter i
Callaway [57]	building temperature regulation	thermal capacitance C (kWh/°C)	$C \sim$ Lognormal(10,2)
		thermal resistance R (°C/kW)	$R \sim$Lognormal(2,0.4)
		energy transfer rate P (kW)	$P \sim$Lognormal(14,2.8)
Dehghanpour & Afsharnia [110]	refrigerator	all	within ±20%
Hao *et al.* [111]	air conditioner	thermal capacitance C (kWh/°C)	$C \sim \mathcal{U}[1.5, 2.5]$
		thermal resistance R (°C/kW)	$R \sim \mathcal{U}[1.5, 2.5]$
		rated electrical power P (kW)	$P \sim \mathcal{U}[4, 7.2]$
		temperature setpoint θ_r (°C)	$\theta_r \sim \mathcal{U}[18, 27]$
		temperature deadband δ (°C)	$\delta \sim \mathcal{U}[0.25, 1.0]$
Kremers *et al.* [60]	refrigerator	door opening	opening$\sim$Exp(15), duration$\sim \mathcal{N}(20, 50)$
		all	"varied by 5%"
Short et al. [69]	fridge-freezer	all	within ±20%
Soudjani & Abate [90]	air conditioner	thermal capacitance C (kWh/°C)	$C \sim \mathcal{U}[8, 12]$ and $C \sim \mathcal{U}[2, 18]$
Soudjani *et al.* [89]	air conditioner	thermal resistance R (°C/kW)	switches between two values according to a (homogeneous) Poisson process
		ambient temperature T_{OFF} (°C)	$T_{\text{OFF}} \sim \mathcal{U}[30, 34]$
Trovato *et al.* [112]	8 types of refrigeration	all	varied independently by ±15%
Wai *et al.* [74]	refrigerators	ambient temperature T_{OFF} (°C)	$T_{\text{OFF}} \sim \mathcal{N}(20, 2)$
		thermal conductance C (W/°C)	$C \sim \mathcal{N}(9.426, 0.9426)$

by a common factor. We call this factor the 'diversity factor', δ, and we multiply the standard deviation for each parameter by δ simultaneously. We simulate five different levels of diversity by taking diversity factors 0, 0.25, 0.5, 0.75 and 1.

For example, room temperature (T_{OFF}) in GB is unlikely to vary across the country by more than a few degrees Celsius, and a range of 8°C would be a reasonable maximum range. Hence with the mean of 20°C, we'd like our simulation with the greatest diversity to have almost all[9] room temperatures within the range 16 − 24°C[10]. To achieve this we set the standard deviation σ, by taking $3\sigma = 4$ and then the standard deviation for diversity factor δ, $\sigma(\delta) = \frac{4}{3}\delta$. Table 4.4 shows our choice of standard deviation for each parameter, for each diversity factor. Note that the aforementioned example corresponds to the final column of T_{OFF}, with value 4/3. For T_{ON} we let $3\sigma = 6$ which is just over 20% of the mean value, -26°C, similar to the three references above. Rather than treat the temperature set points T^0_- and T^0_+ independently, which could result in fridges with impossibly short or overly long cycle times, we instead diversify their difference. For each fridge, after T^0_- and $(T^0_+ - T^0_-)$ have been selected (independently) from their normal distributions, T^0_+ is calculated from their sum. Fridge cooling rates will vary depending on the age and model of the appliance. We allow the cooling/heating rate α to vary such that $3\sigma = \frac{\alpha}{2}$ in the largest diversity case. Table 4.5 shows the expected parameter range for different percentages of the population for each diversity factor and parameter. For example, with 0.25% diversity we expect 68.3% of the population to have room temperature T_{OFF} within the range (19.67,20.33)°C.

[9] By 'almost all' we mean the expectation of 99.7% of the population, which is equivalent to roughly three times the standard deviation.

[10] Note that this is the mean ±20%, as used by [69, 74, 110]. We mention percentages for comparison with other references, but of course in the context of temperature in degrees Celsius, percentage differences have no sensible meaning.

Table 4.4: Mean and standard deviation for each parameter and diversity factor. First 5 parameters are set, final 4 parameters are estimated from the data. Temperatures in degrees Celsius, times (τ_{ON}, τ_{OFF}) in minutes.

		Diversity Factor				
		0	0.25	0.5	0.75	1
Parameter	**Mean**	**Standard Deviation**				
T_{ON}	-26	0	0.50	1.00	1.50	2.00
T_{OFF}	20	0	0.33	0.67	1.00	1.33
T_{-}^{0}	2	0	0.13	0.25	0.38	0.50
$(T_{+}^{0} - T_{-}^{0})$	5	0	0.08	0.17	0.25	0.33
$\alpha \times 10^5$	18.08	0	0.75	1.51	2.26	3.01
T_{+}^{0}	7.00	0	0.15	0.30	0.45	0.60
τ_{ON}	15.15	0	0.73	1.49	2.31	3.27
τ_{OFF}	30.00	0	1.55	3.16	4.91	6.91
duty cycle	33.55%	0	0.70	1.34	2.02	2.69

Table 4.5: Expected parameter range for different percentages of the population for the five diversity factors.

Diversity	**Population**	$\mathbf{T}_{\text{ON}}$	$\mathbf{T}_{\text{OFF}}$	$\mathbf{T}_{-}$	$\mathbf{T}_{+}^{\mathbf{0}} - \mathbf{T}_{-}^{\mathbf{0}}$
0	100%	-26	20	2	5
0.25	68.3%	(-26.5,-25.5)	(19.67,20.33)	(1.875,2.125)	(4.92,5.08)
	95.5%	(-27.0,-25.0)	(19.33,20.67)	(1.750,2.250)	(4.83,5.17)
	99.7%	(-27.5,-24.5)	(19.00,21.00)	(1.625, 2.375)	(4.75,5.25)
0.5	68.3%	(-27.0,-25.0)	(19.33,20.67)	(1.750,2.250)	(4.83,5.17)
	95.5%	(-28.0,-24.0)	(18.67,21.33)	(1.500,2.500)	(4.67,5.33)
	99.7%	(-29.0,-23.0)	(18.00,22.00)	(1.250, 2.750)	(4.50,5.50)
0.75	68.3%	(-27.5,-24.5)	(19.00,23.00)	(1.625,2.375)	(4.75,5.25)
	95.5%	(-29.0,-23.0)	(18.00,22.00)	(1.250,2.750)	(4.50,5.50)
	99.7%	(-30.5,-21.5)	(17.00,23.00)	(0.875, 3.125)	(4.25,5.75)
1	68.3%	(-28.0,-24.0)	(18.67,21.33)	(1.500,2.500)	(4.67,5.33)
	95.5%	(-30.0,-22.0)	(17.33,22.67)	(1.000,3.000)	(4.33,5.67)
	99.7%	(-32.0,-20.0)	(16.00,24.00)	(0.500, 3.500)	(4.00,6.00)

Diversity	**Population**	$\alpha \times \mathbf{10^5}$
0	100%	18.08
0.25	68.3%	(17.33, 18.83)
	95.5%	(16.57, 19.59)
	99.7%	(15.82,20.34)
0.5	68.3%	(16.57, 19.59)
	95.5%	(15.07, 21.09)
	99.7%	(13.56,22.60)
0.75	68.3%	(15.82, 20.34)
	95.5%	(13.56, 22.60)
	99.7%	(11.30,24.86)
1	68.3%	(15.07, 21.09)
	95.5%	(12.05, 24.11)
	99.7%	(9.04,27.12)

4.5.2 Simulation results for $P_c = 70$MW

We simulate the heterogeneous populations for each of the five diversity factors, with all parameters as given in Table 3.1. Note that $\delta = 0$ is identical to the $\beta = 2.4$, $P_c = 70$ case above.

Final and maximum cumulative response savings

Figure 4.19 shows the the final savings in MWh as a proportion of the original response from other providers. We see that even with the smallest introduction of diversity studied, $\delta = 0.25$, there are no longer any cases in which the population causes more harm than good by the end of the ten-day period (savings <0). The mean increases with diversity, and the variance is lower in all cases compared to the homogeneous case.

Figure 4.20 shows the maximum of the cumulative savings over the ten-day period. The plots are very similar to those in Figure 4.19, which indicates that the cumulative savings rarely peak and start to reduce within the period. This is confirmed by Figure 4.21, which shows that the maximum cumulative savings are indeed achieved at the end of the 10 days studied in almost all cases. The difference between the results for $\delta = 0$ and $\delta = 0.25$ is dramatic. Even the introduction of this small amount of diversity has removed the early peaking of the cumulative savings and the harmful effects of the population.

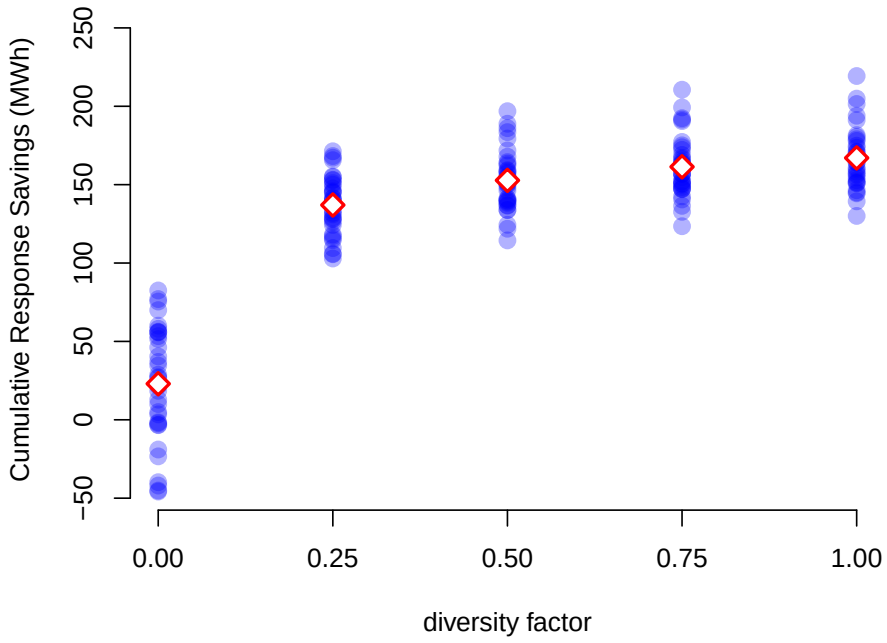

(a) Total savings (MWh)

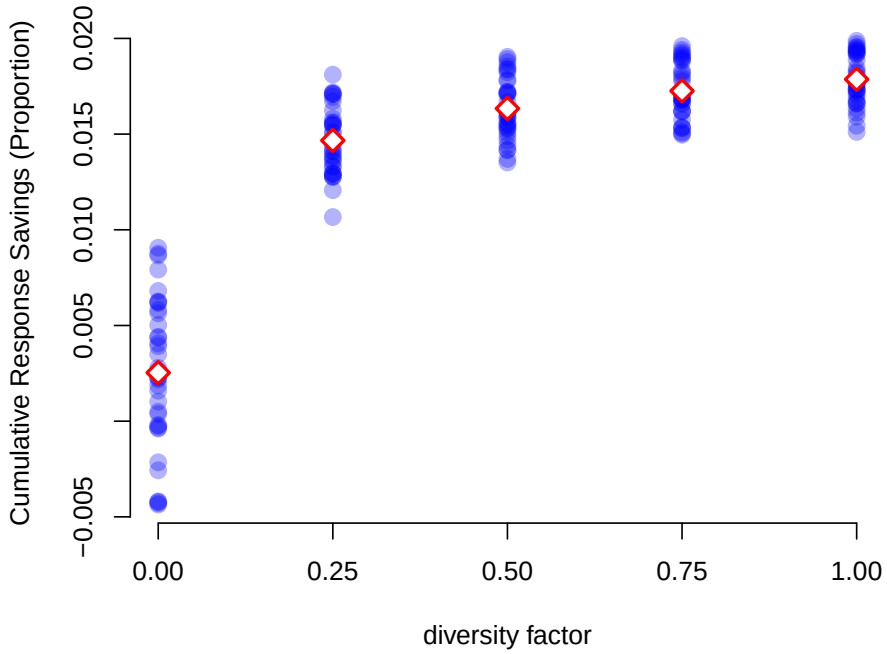

(b) Savings as a proportion of original response

Figure 4.19: Final cumulative response savings for each of the 36 10-day data samples over the 12 month period (blue) and the mean for each diversity factor (red).

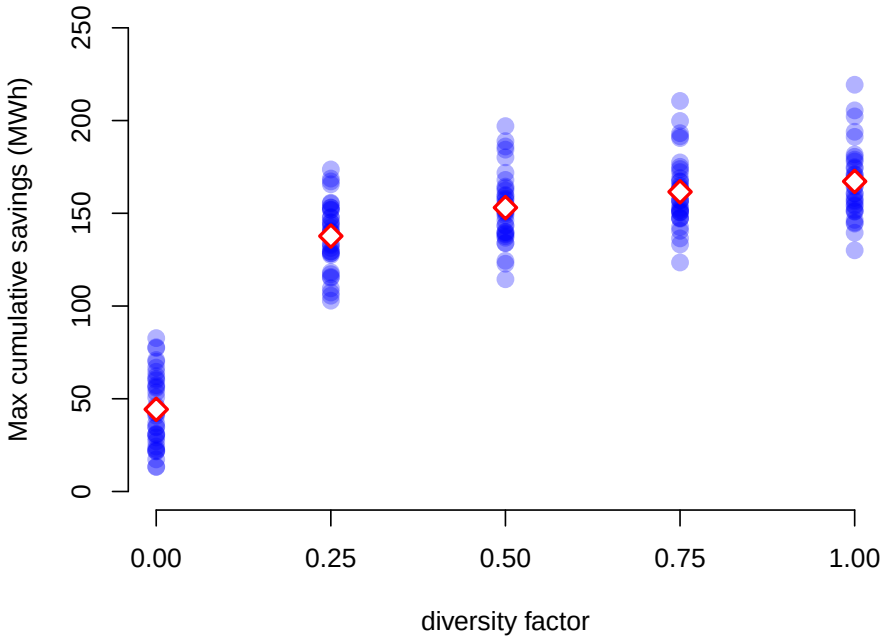

(a) Maximum (MWh)

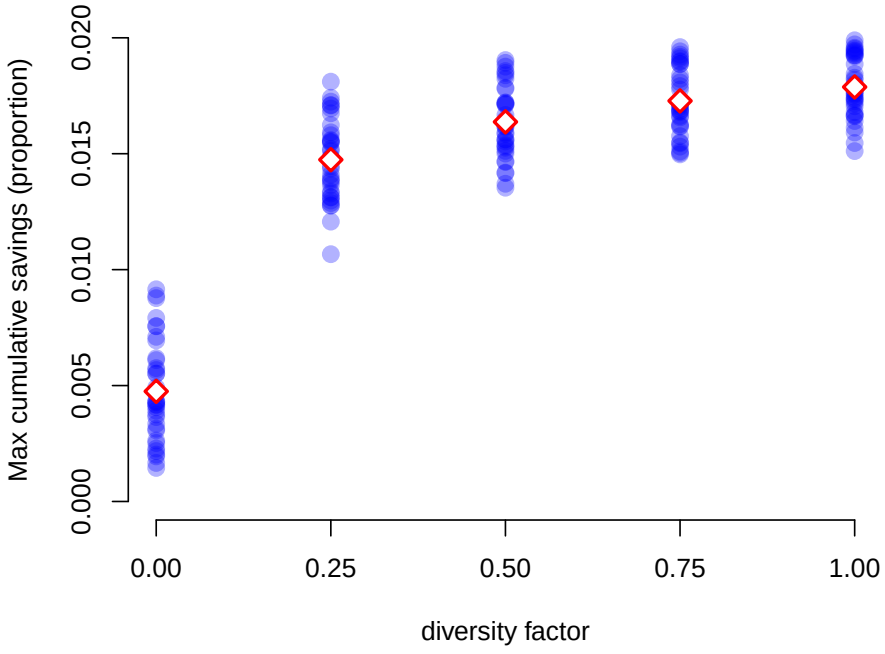

(b) Maximum (as a proportion of original response)

Figure 4.20: Maximum cumulative response savings for each of the 36 10-day data samples over the 12 month period (blue) and the mean for each diversity factor (red).

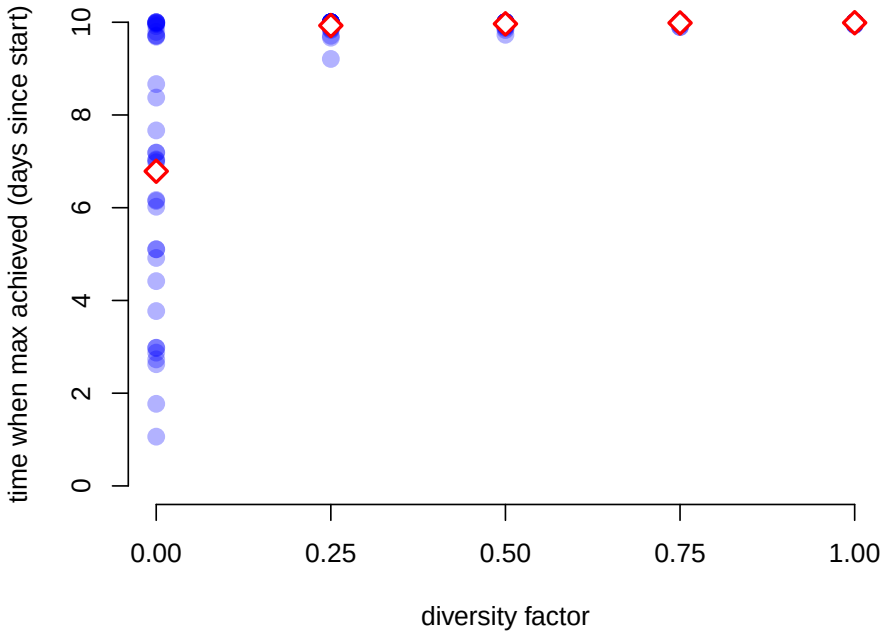

Figure 4.21: Time (in days since start) of maximum cumulative response savings for each of the 36 10-day data samples over the 12 month period (blue) and the mean for each diversity factor (red).

Evidence of synchronisation

The results thus far all indicate that synchronisation in our populations with $\delta > 0$ will be far lower than in the cases with $\delta = 0$. As before, we plot the percentage of fridges in each of the fullest 2% of bins. As expected, Figures 4.22 and 4.23 show negligible amounts of synchronisation for all populations with $\delta > 0$.

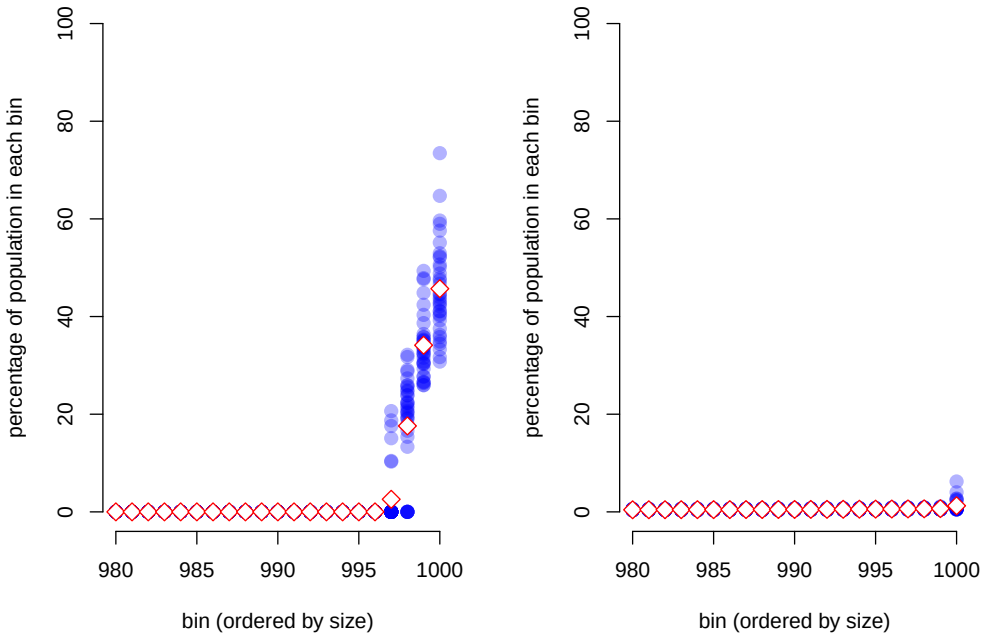

(a) diversity factor = 0

(b) diversity factor = 0.25

Figure 4.22: The percentage of fridges in the 20 fullest bins for each diversity factors 0 and 0.25. Individual simulation results shown in blue, mean in red.

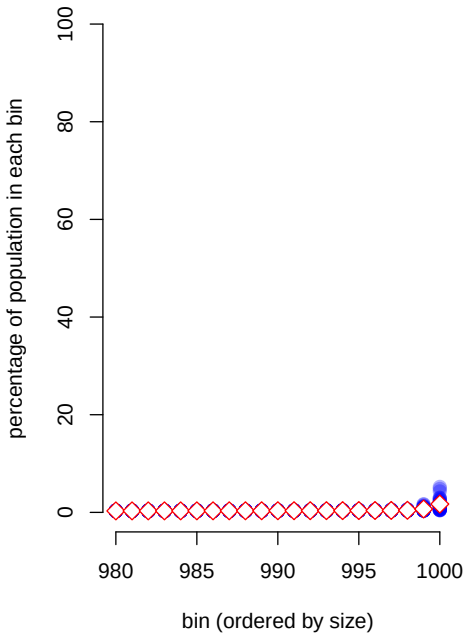

(a) diversity factor = 0.5

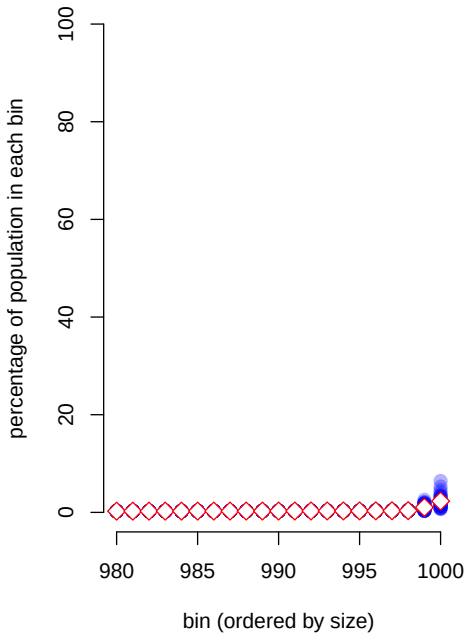

(b) diversity factor = 0.75

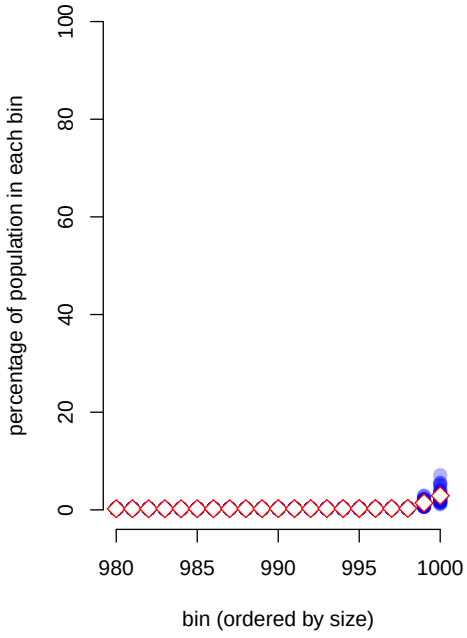

(c) diversity factor = 1

Figure 4.23: The percentage of fridges in the 20 fullest bins for diversity factors 0.5, 0.75 and 1. Individual simulation results shown in blue, mean in red.

4.5.3 Simulation results for $P_c = 700$MW

When we increased the level of fridge participation in our DSR scheme from 70MW up to 700MW, the homogeneous population showed an increase in the mean final and maximum response savings, but also a much higher propensity for detrimental effects. To what extent does the introduction of heterogeneity improve these results? We repeat our simulations with an increase in total participating fridge load from 70MW to 700MW.

Figure 4.24 shows that even for our lowest level of diversity, $\delta = 0.25$, none of the 36 10-day simulations result in negative final response savings. Even the best case with zero diversity is worse than the worst case with a little diversity. With $\delta > 0$ the response savings are on the order of 10%, or 1GWh of response. The results for the maximum savings (Figure 4.25) are almost identical for $\delta > 0$ because, as Figure 4.26 shows, the maximum is reached at the end of the period.

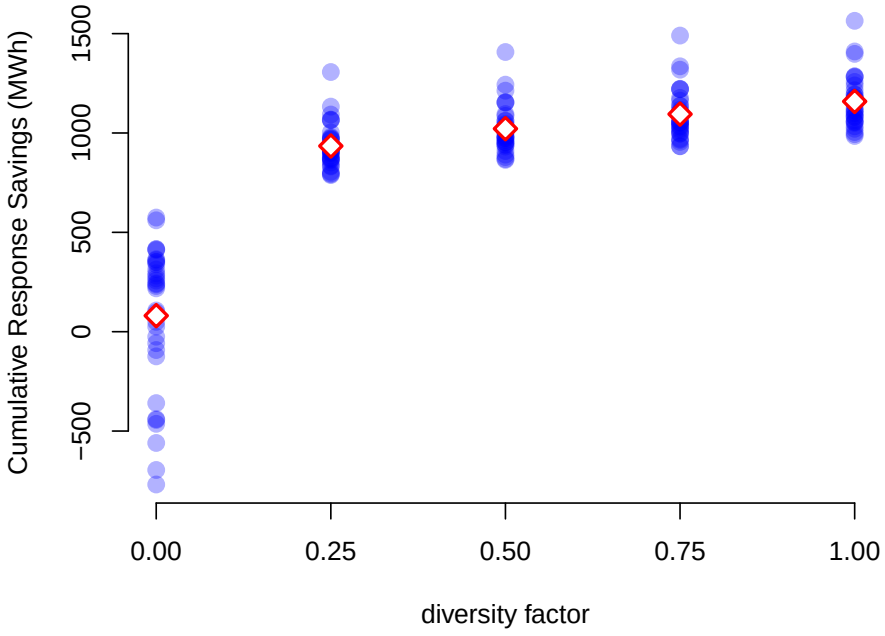

(a) Total savings (MWh)

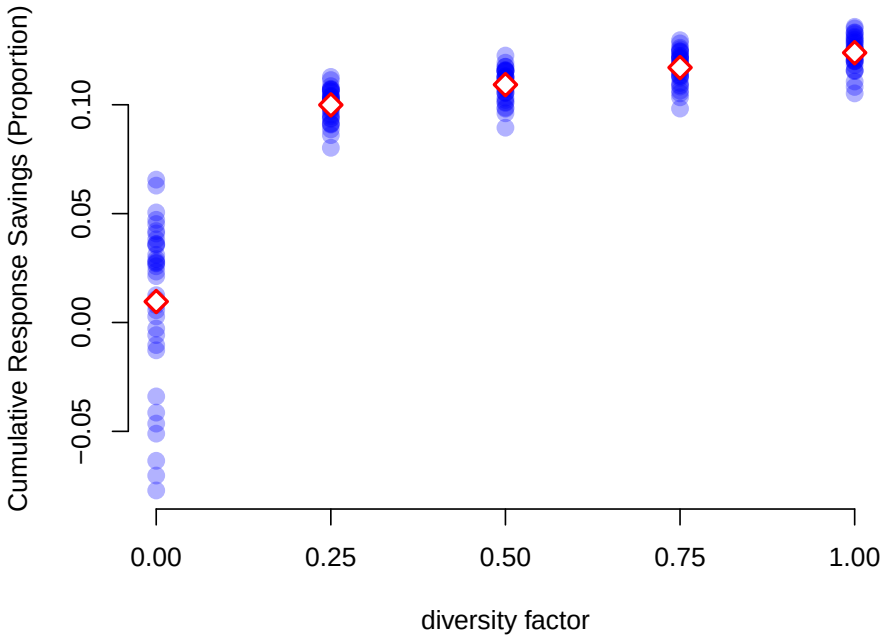

(b) Savings as a proportion of original response

Figure 4.24: Final cumulative response savings with $P_c = 700$MW for each of the 36 10-day data samples over the 12 month period (blue) and the mean for each diversity factor (red).

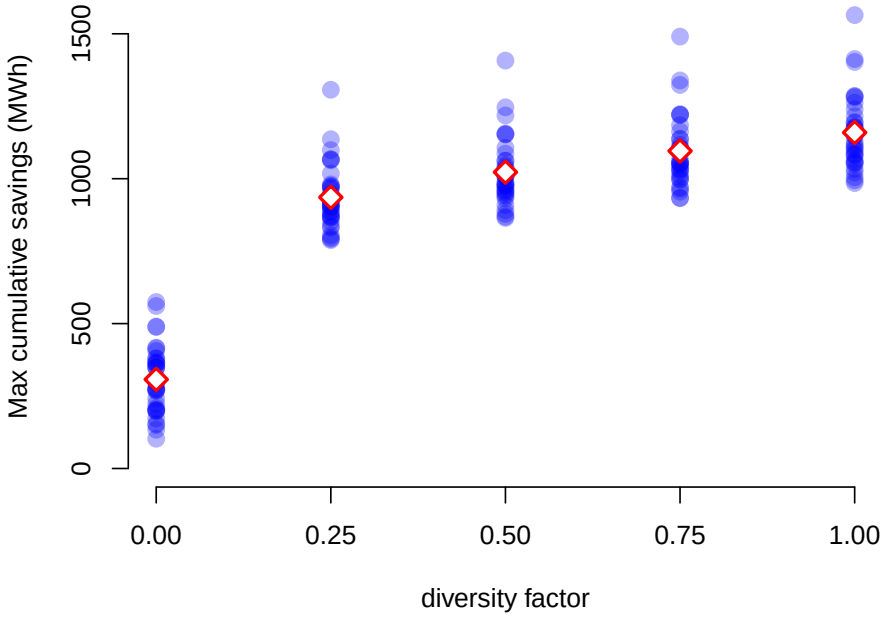

(a) Maximum (MWh)

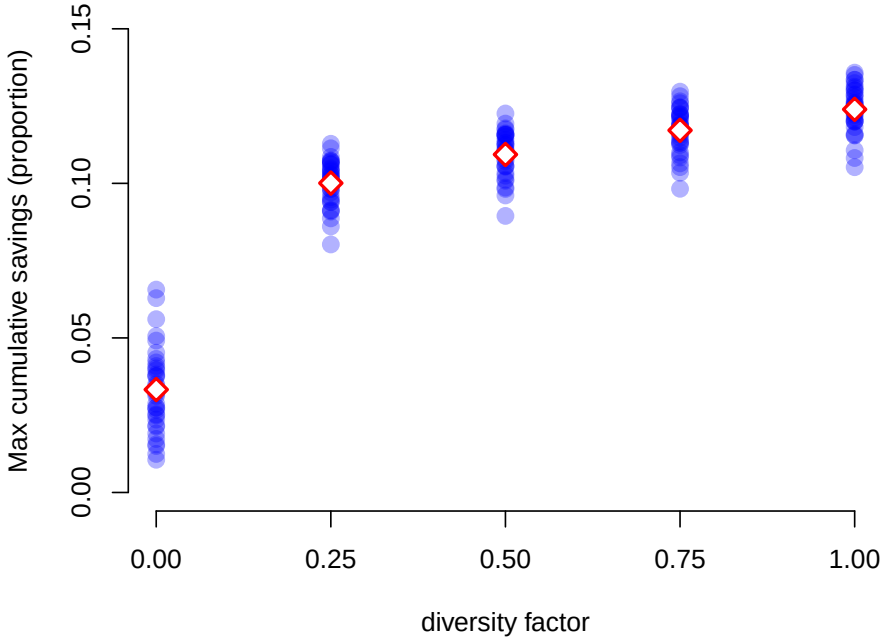

(b) Maximum (as a proportion of original response)

Figure 4.25: Maximum cumulative response savings for each of the 36 10-day data samples over the 12 month period (blue) and the mean for each diversity factor (red).

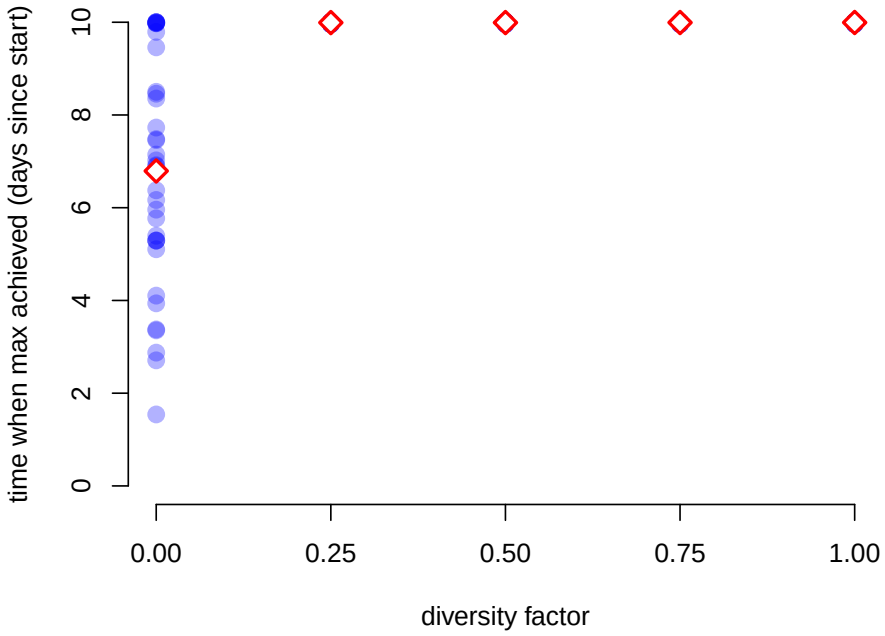

Figure 4.26: Time (in days since start) of maximum cumulative response savings with $P_c = 700$MW for each of the 36 10-day data samples over the 12 month period (blue) and the mean for each diversity factor (red).

As in the 70MW case, there is negligible evidence of synchronisation for diversity factor $\delta > 0$, as seen in Figures 4.27 and 4.28.

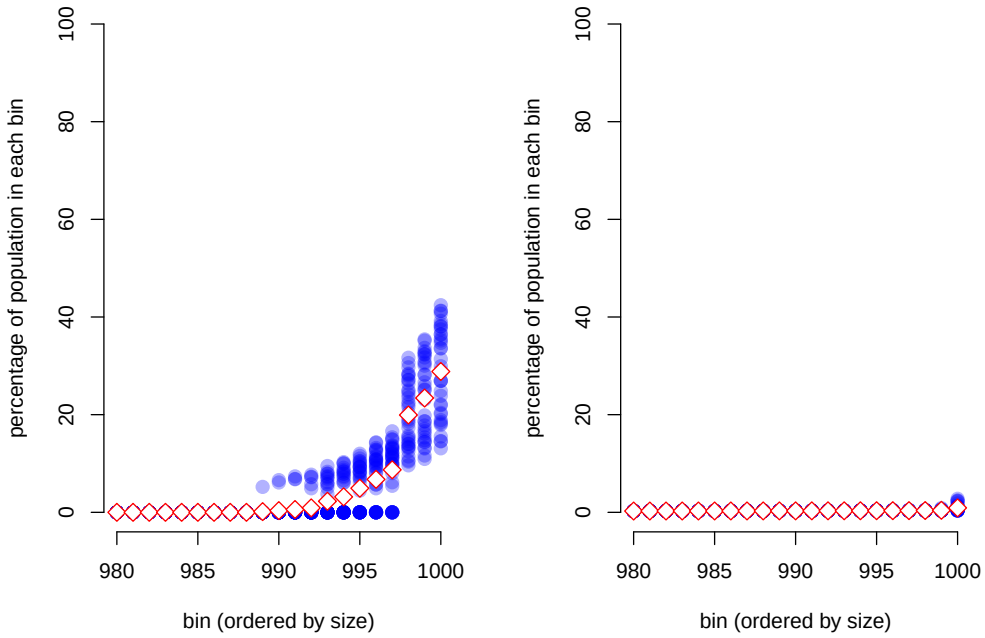

(a) diversity factor = 0

(b) diversity factor = 0.25

Figure 4.27: The percentage of fridges in the 20 fullest bins for diversity factors 0 and 0.25, with $P_c = 700$MW. Individual simulation results shown in blue, mean in red.

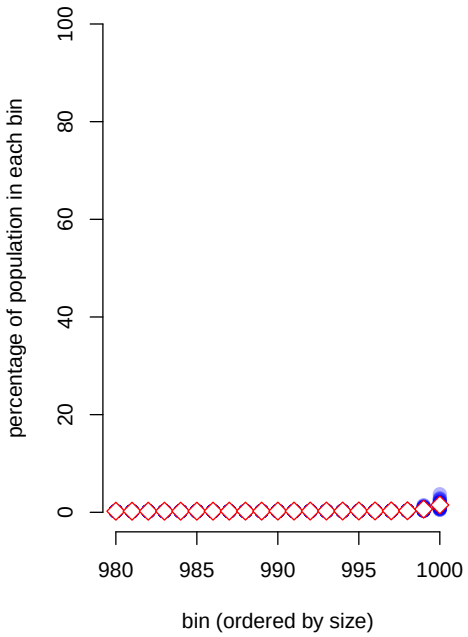

(a) diversity factor = 0.5

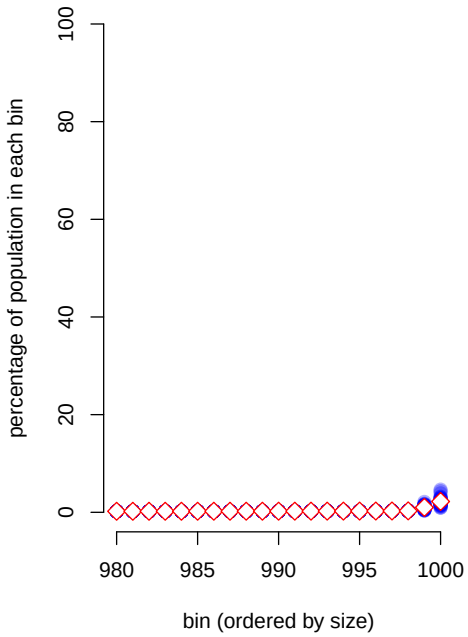

(b) diversity factor = 0.75

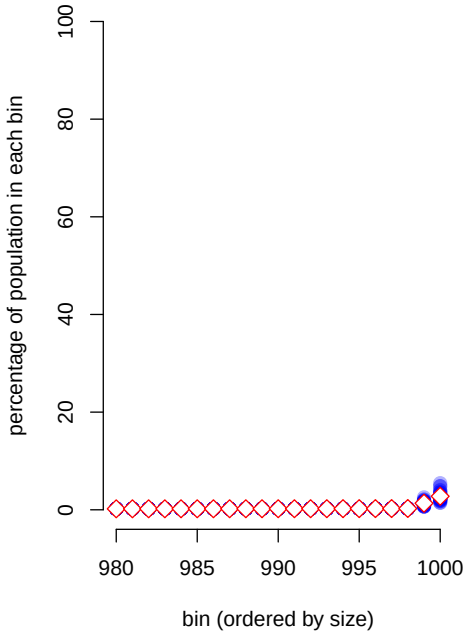

(c) diversity factor = 1

Figure 4.28: The percentage of fridges in the 20 fullest bins for diversity factors 0.5, 0.75 and 1, with P_c = 700MW. Individual simulation results shown in blue, mean in red.

4.5.4 Minimum diversity requirements

Simulations

Having found negligible evidence of synchronisation of a fridge population with even our lowest diversity factor, the natural question is to ask where the diversity threshold lies between synchronisation and (effectively) none. We can repeat our simulations for 70MW with decreasing levels of diversity δ, to see at what level the synchronisation observed for $\delta = 0$ sets in. The most effective approach turns out to be reducing δ by powers of ten, as simply reducing δ from 0.25 by small increments is insufficient to detect synchronisation. For this reason our plots have a logarithmic horizontal axis with a discontinuity to allow us to plot the results from $\delta = 0$.

Figure 4.29(a) shows the cumulative response savings at the end of the 10-day simulation as a proportion of original system response. Figure 4.29(b) shows the maximum cumulative savings during the 10-day period, again as a proportion of original response. The trend is almost identical in each figure. Again, the results seem to be split into two regions; above $\delta \approx 10^{-3}$ there is an upwards trend that starts close to horizontal. We interpret this as the diversity being initially sufficient to prevent synchronisation, but with little more to offer, but as the diversity factor increases it is able to provide additional benefits. For the smallest values, $\delta < 10^{-3}$, the mean savings drop rapidly, with many instances of negative savings. For $\delta \leq 10^{-5}$ the results look very similar to the case with zero diversity.

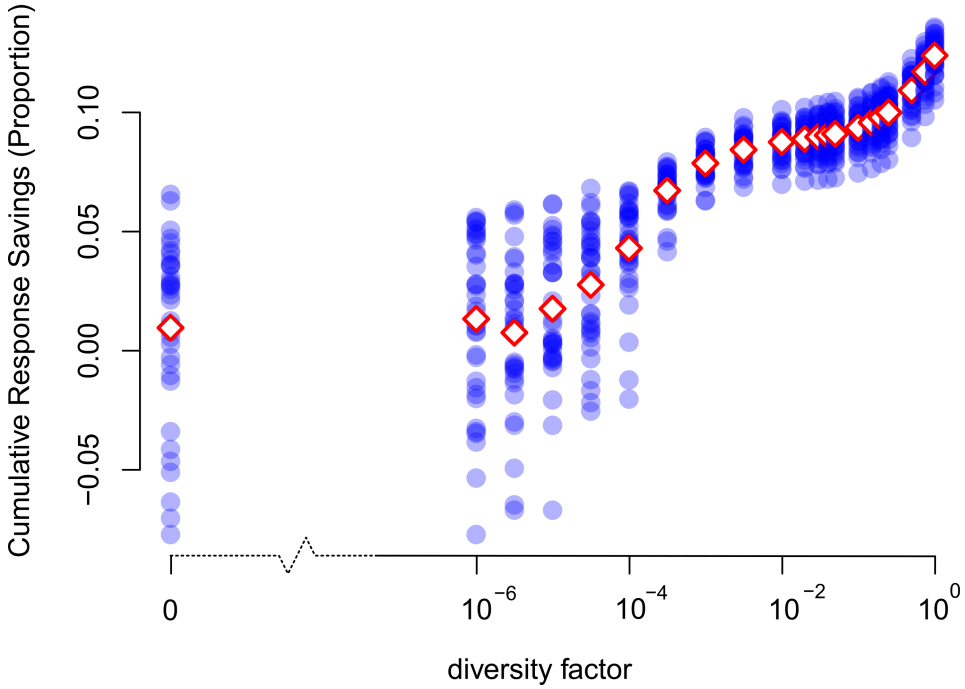

(a) Final savings

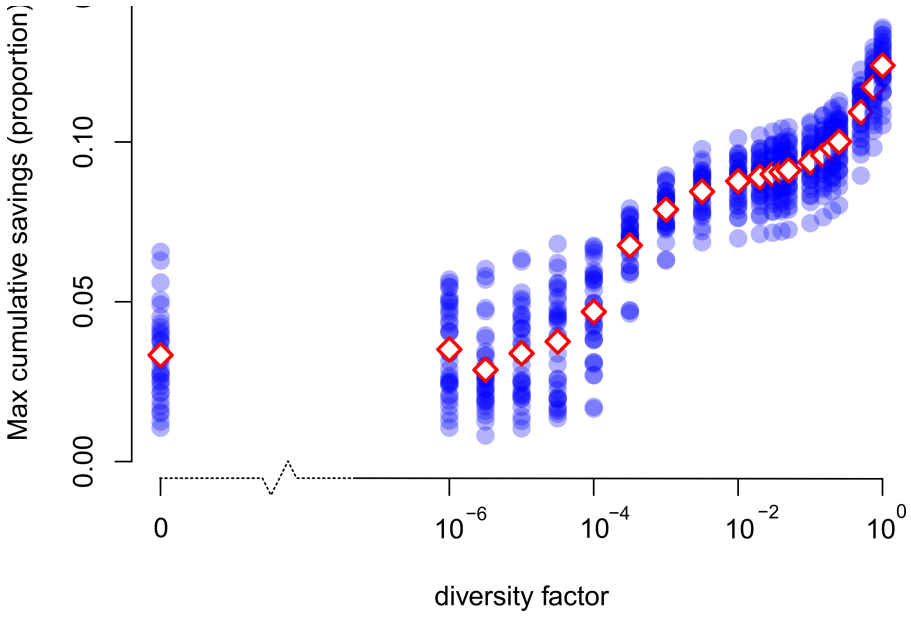

(b) Maximum savings

Figure 4.29: Final (a) and maximum (b) response savings for each of the 36 10-day data samples over the 12 month period (blue) and the mean for each diversity factor (red). Logarithmic horizontal axis to permit careful exploration of very small diversity factors.

Figure 4.30 shows the time during each 10-day simulation when the maximum response savings was reached. Recall that values noticeably less than 10 days indicate synchronisation, and the closer to 0, the stronger the effect. For (relatively) large δ, *i.e.* $\delta \in (10^{-3}, 1]$ there is no evidence of synchronisation. At $\delta = 10^{-3}$ we see a potential turning point. Below this at least one simulation reaches its maximum savings before nine days. The mean descends swiftly and the variance increases rapidly as we decrease δ.

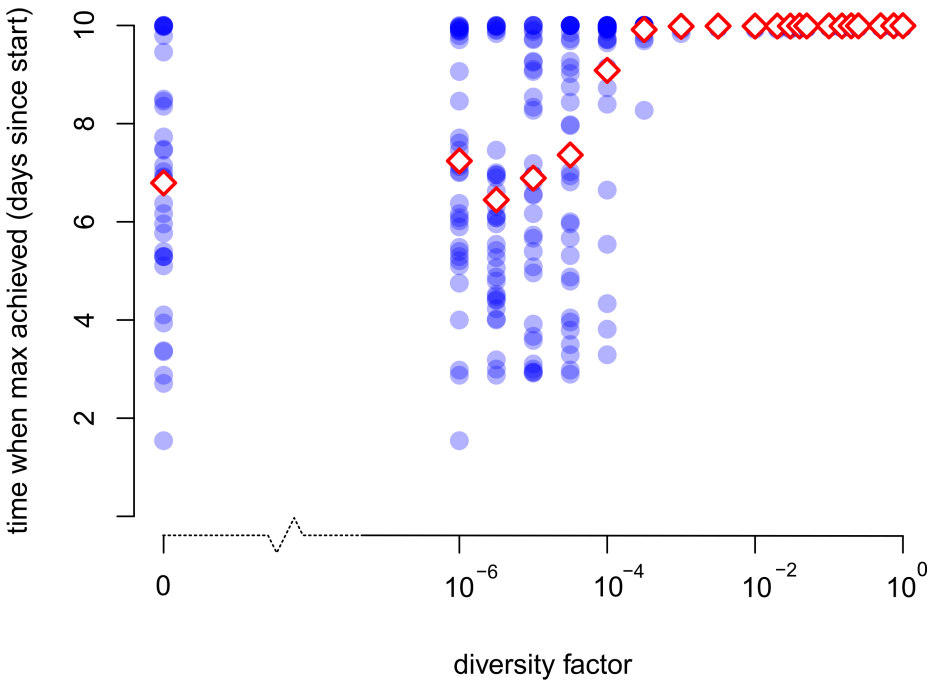

Figure 4.30: Time (in days since start) of maximum cumulative response savings for each of the 36 10-day data samples over the 12 month period (blue) and the mean for every diversity factor simulated (red). Logarithmic horizontal axis to permit careful exploration of very small diversity factors.

These results are very encouraging, since requiring a diversity factor of only 10^{-3} means we need only a very small amount heterogeneity in our population to avoid synchronisation problems. We can see what $\delta = 10^{-3}$ means for the interval within which we expect 99.7% of our population to belong for each parameter in Table 4.6.

Table 4.6: Implications of $\delta = 10^{-3}$ for each parameter. The third column gives the expected interval for 99.7% of the population to belong to.

parameter	**standard deviation**	**99.7% interval**	**units**
T_{ON}	0.020	-26 ± 0.060	°C
T_{OFF}	0.133	20 ± 0.040	°C
T_{-}^{0}	0.005	2 ± 0.015	°C
$(T_{+}^{0} - T_{-}^{0})$	0.003	5 ± 0.010	°C
$\alpha \times 10^{5}$	0.030	18.08 ± 0.090	s^{-1}
T_{+}^{0}	0.006	7 ± 0.018	°C
τ_{ON}	0.033	15min 9s ± 5.89s	min, s
τ_{OFF}	0.069	30min ± 12.44s	min, s
duty cycle	0.027	33.55 ± 0.081	%

Comparison with the Kuramoto model

We can compare these results with the analytical results for the Kuramoto model. In the Kuramoto model, when the coupling strength K reaches a critical value K_c the order parameter solution bifurcates. That is to say, for $K < K_c$ the order parameter is 0 (no synchronisation), and for $K > K_c$ the order parameter increases towards 1 (partial synchronisation). The synchronisation threshold is $K_c = \frac{2}{g(\bar{\omega})}$, where g is the distribution of natural frequencies ω and $\bar{\omega}$ is the mean of g [113]. If we define $\Delta\omega$ to be the full width at half maximum of distribution g, then if g is normal then $g(\omega) \approx \frac{1}{\Delta\omega}$. Since we have taken our parameters to be constant (notably our form of coupling strength, which we define later) and vary the width of the distribution, we would like to find the critical $\Delta\omega$, which we call $\Delta\omega_c$. Rearranging the formula found by Kuramoto (above), $\Delta\omega_c = \frac{\pi}{2}K$. We should see partial sync for $\Delta\omega < \Delta\omega_c$ (going to full sync as $\Delta\omega \to 0$), and no sync for $\Delta\omega > \Delta\omega_c$.

For our system the coupling strength is determined by the sensitivity of the TCLs to the frequency, and the sensitivity of the frequency to the TCLs. We have seen these parameters together before, namely they combine to form $\beta c P_c$ (we assume $\beta_- = \beta_+ = \beta$). The natural period for each TCL is given by $\tau^0_{\text{ON}} + \tau^0_{\text{OFF}}$ and so their natural frequencies are given by $\frac{2\pi}{\tau^0_{\text{ON}} + \tau^0_{\text{OFF}}}$. In order to compare our system with the Kuramoto model we need to non-dimensionalise the key equations in our system. We do this for our original model, which is an approximation of the system equations, since the inertia, underlying demand and response from other providers changes over time on the real system. As such, our results will be an approximation for the simulation results. We make the following non-dimensionalisation, using 'hat' notation to denote non-dimensional variables, and 'bar' notation to denote the mean of a parameter.

$$\dot{\hat{T}} = \begin{cases} -\frac{\alpha}{\bar{\alpha}}\left(\hat{T} - \frac{T_{\text{ON}}}{T_{\text{OFF}} - T_{\text{ON}}}\right) & \text{if on} \\ -\frac{\alpha}{\bar{\alpha}}\left(\hat{T} - \frac{T_{\text{OFF}}}{T_{\text{OFF}} - T_{\text{ON}}}\right) & \text{if off} \end{cases} \tag{4.11a}$$

$$\hat{T}_\pm = \hat{T}^0_\pm - \hat{\beta}_\pm \hat{f} \tag{4.11b}$$

$$\dot{\hat{f}} = \hat{C}(\rho^* - \rho) - \hat{\gamma}\hat{f} \tag{4.11c}$$

where

$$\begin{aligned} \hat{T} &= \frac{T}{T_{\text{OFF}} - T_{\text{ON}}} & \hat{T}^0_{\pm} &= \frac{T^0_{\pm}}{T_{\text{OFF}} - T_{\text{ON}}} \\ \hat{t} &= \bar{\alpha} t & \hat{\beta}_{\pm} &= \frac{\beta_{\pm}}{T_{\text{OFF}} - T_{\text{ON}}} \\ \hat{f} &= \frac{f}{f_0} & f_0 &= 50\text{Hz} \\ \hat{C} &= \frac{cP_c}{\bar{\alpha} f_0} & \hat{\gamma} &= \frac{\gamma}{\bar{\gamma}} \end{aligned} \tag{4.12}$$

and so our coupling strength

$$K = \hat{\beta}\hat{C} = \frac{\beta c P_c}{\bar{\alpha} f_0 (\bar{T_{\text{OFF}}} - \bar{T_{\text{ON}}})} \approx 0.0404 \tag{4.13}$$

and the 'natural frequency' of each TCL is given by

$$\omega = \frac{2\pi}{\log\left(\frac{(T^0_+ - T_{\text{ON}})(T_{\text{OFF}} - T^0_-)}{(T^0_- - T_{\text{ON}})(T_{\text{OFF}} - T^0_+)}\right)}. \tag{4.14}$$

Hence for our parameter choices $\Delta\omega_c = \frac{\pi}{2}K \approx 0.634$. By taking data samples we find that ω is approximately normally distributed. This allows us to use the result that the full width at half maximum $\Delta\omega_c \approx 2\sqrt{2\log(2)}\sigma$. By taking large data samples for each of our parameters we are able to estimate the standard deviation σ_ω for different diversity factors. We find that $\delta = 10^{-1.915}$ gives $\Delta\omega \approx \frac{\pi}{2}K$. This is a little higher than our estimated threshold ($\delta = 10^{-3}$), but our model does have some key differences from the Kuramoto model, and this value is still very reasonable. It is also still very small, and so little variation is required to prevent partial synchronisation.

4.5.5 Summary

Our simulations have shown that even with a very small amount of parameter diversification, our populations that when identical became highly synchronised with often very detrimental effects, no longer exhibit such behaviour. Figure 4.31 shows just one example of the cumulative response savings over time, when $\delta = 0.01$, $\beta = 2.4°C/Hz$ and $P_c = 700MW$. Comparing this with Figure 4.6 on page 119 shows the benefits of a small amount of diversity very clearly.

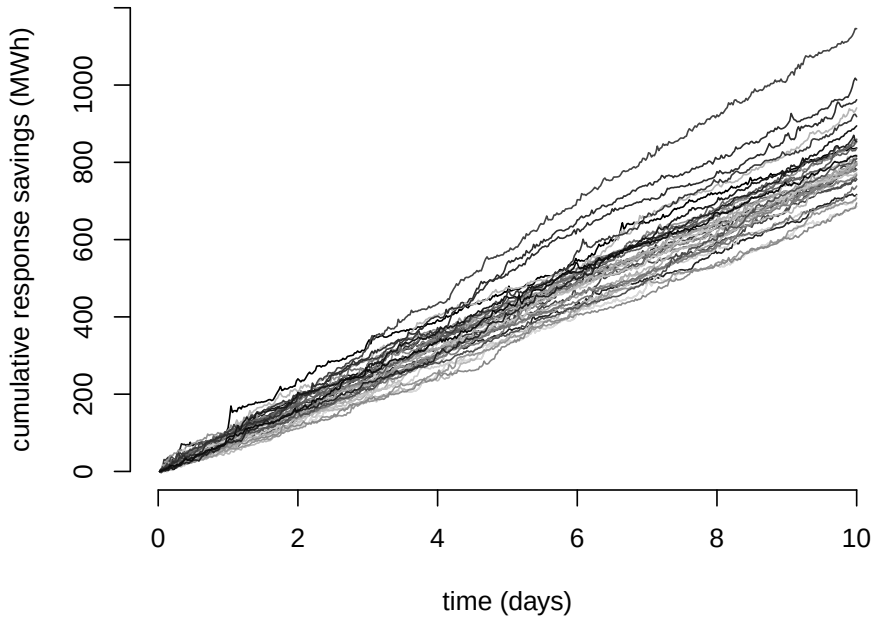

Figure 4.31: Cumulative response savings (MWh) for a heterogeneous fridge population with $\delta = 0.01$, $\beta = 2.4°C/Hz$ and $P_c = 700MW$. The introduction of a very small amount of diversity has eradicated the detrimental behaviour in all cases and the fridges provide a clear benefit to the system.

Increasing our diversity factor δ from 0 to 0.25 showed the greatest improvement, with additional (although less strong) benefits from further increases. In the 70MW case the response savings were within 100-200MWh, approximately 1-3% savings. Increasing the participation level ten fold to 700MW increased these savings to the 750-1500MW range (depending on the diversity factor), around 7.5-15% savings. With the introduction of diversity the maximum savings was no longer reached before the 10th day of the simulation, compared to a wide range of peak times without diversity (between day 2 and 10). We can conclude that the introduction

of diversity to our model removes the harmful effects of synchronisation seen in the homogeneous population case, even when a substantial number of fridges are participating on the system (700MW). While we cannot say how much diversity is realistic on the system, our studies have shown that even for small levels of diversity, the issues have disappeared.

"We can only see a short distance ahead, but we can see plenty there that needs to be done."

Alan Turing, *Computing Machinery and Intelligence* [114]

5 Conclusions

In the words of the World Energy Council, "disruptive trends are emerging that will create a fundamentally new world for the energy industry" [115]. To balance the 'energy trilemma' - ensuring a power supply that is simultaneously secure, affordable, and environmentally sustainable - will be a tough challenge that no single solution can address. Innovation needs to be sought across the entire system, in technologies, energy markets and government policies. Greater contribution to system security from the demand side will be needed, motivating further research and development in this area. Thermostatically-controlled loads are just one of many options for demand-side response that have been proposed, but have yet to be rolled out at scale. A few small-scale trials [41–45] have been carried out, and in recent years the topic has gained popularity in the research community. We agree with Oldewurtel *et al.* that "while some [demand-side response] schemes are already in place, it can be expected that TCLs will play a much more important role in providing a fast and accurate source of flexibility in the future electricity grid" [35].

In order for a large number of frequency-sensitive TCLs to play such a role, their capabilities and associated risks need to be fully understood. Our goal in this thesis has been to further this understanding. For our mathematical analysis we chose a simple, deterministic model for TCL control, as proposed by Short *et al.* [69]. This

allowed us to analyse the stability of the system from two different perspectives. For the first, we developed a continuum model which enabled us to analyse the stability of the uniformly distributed (in phase) population at nominal frequency. We found that the equilibrium is stable, even in the absence of a stabilising external force (γ in the model). This result was surprising, but indicated that our analysis could not capture the full picture.

Thinking that the system might be unstable to larger perturbations, we next sought to model one and then two synchronised groups of TCLs. We solved for the periodic solution of one group, and then explored the many different types of switching behaviour available to two groups. We mapped out the possible switching events of two groups and simulated the event progressions for different initial conditions to reveal insights into the long-term periodic behaviour, finding evidence that two groups will each tend towards a periodic solution (which may be the same solution). To study the system analytically, we modelled two groups of TCLs cycling close to the single group periodic solution, and solved for the stability of the system. We found the parameter region in which the two groups will synchronise, and the region in which they will remain forever distinct. We were able to hypothesise that if N groups are very similar in size, or distributed so that a few groups could merge so that the resulting groups were all approximately the same size, then the groups may spread out and avoid total synchronisation. This matched with our previous work, since modelling a continuum of TCLs is effectively modelling N synchronised groups in the limit $N \to \infty$.

In Chapter 4 we presented the methods and results behind our simulations. In the Section 4.2 we simulated a population using the model from Chapter 3, to compare the continuum model with 10000 groups of fridges with different amounts of perturbation away from equilibrium. We found that although in the short term the TCLs acted to reduce the resulting frequency perturbations, synchronisation accumulated and eventually led to larger frequency oscillations.

In Sections 4.3-4.5 we modelled homogeneous and heterogeneous populations of fridges as if they had been frequency-sensitive on the GB grid during 2015-2016. By accounting for how frequency response is provided by other generators, we were able to determine the impact of the fridge population on the actions of these other providers. In the homogeneous case the results had huge variation depending on the 10-day period from which the system data was taken. Synchronisation was a big problem in many cases, causing the other providers to work harder than they did without the frequency-sensitive fridges. Part of our initial motivation for

using a deterministic model was our hypothesis that the parameter diversity which exists naturally in a population could be sufficient to prevent the accumulation of synchronisation and the associated issues. Our simulations of non-identical TCLs revealed that even with very small levels of parameter diversification these issues were indeed prevented. In fact, our initial heterogeneous simulations revealed no evidence of such problems, and so diversity had to be reduced by factors of ten until we were able to observe the threshold at which the population showed the same issues as the homogeneous case.

It is important to consider the real-world implications of our results in the context of the modelling assumptions that underpin them. We have assumed that grid frequency is the same everywhere on the network, when in reality fluctuations will originate in specific locations and spread across the network. This means that TCLs could potentially prevent local issues from becoming grid-scale. Imbalances at the distribution network level are becoming increasingly important to manage, and so our results are strengthened by the removal of this assumption. We have also assumed that all parameters remain constant over time. This ignores any fridge door opening and food addition or removal, as well as change in room temperature or long-term changes such as appliance efficiency reduction. In general, fridge usage (door opening and contents changing) are random events, with some correlation around meal times, and will typically diversify the population states and parameter values. The minimum diversity requirements we found were necessary to prevent synchronisation mean that even if many people went to open their fridge at a similar time, the difference in room temperatures and durations for which the doors remain open would be highly unlikely to counteract the natural population diversity and cause synchronisation. Our assumptions that require further investigation are the absence of measurement delay or error, which could be tested with a small number of appliances and sensors, and the energy consumption of each TCL, which in reality would exhibit a small spike when an appliance switches on.

There are several key requirements for moving this work beyond the theoretical and into practical application. Simulations of different types of TCL, such as fridge-freezers, air conditioners and hot-water tanks would be useful to understand exactly how the results apply beyond a population of fridges. We have explored changing the value of control parameter β, but an optimal value of both β_- and β_+ would be beneficial to protect the TCLs and give the optimal frequency response to the system. Anyone proposing to use TCLs for frequency response would need to give the System Operator an estimate of how much response will be provided from a

population of TCLs under different frequency conditions, and be able to provide confidence in such an estimate. This would likely require additional simulations. A small-scale trial would be useful to test the assumptions we have made, as discussed above. This could also be used to select the most effective and affordable control equipment to fit (or retro-fit) into TCLs. A theoretical analysis of the stability of a heterogeneous population was a subject we did not have time to explore in any depth, although our continuum model was developed to be sufficiently general that it could be used to model a heterogeneous population.

Economic analysis of the benefits of using TCLs, and the decreasing returns on investment as more TCLs participate would be valuable for developing potential business models. These would need to consider how the value of system flexibility will change as system inertia reduces and the generation mix evolves. The response capabilities and costs of TCLs could be compared with those of other response providers, such as different types of electricity storage. Finally, there is a requirement for greater policy research into the best strategies for a large-scale roll-out of frequency-sensitive TCLs. Participation incentives (either market or government-led) or mandates would be needed to motivate the development of this service.

Our work has advanced our collective understanding of the nature of frequency-sensitive TCLs and shown that they can make a positive contribution to the operation of the electricity grid. Therefore, despite the additional work required to further their development, we hope that frequency-sensitive TCLs for power system frequency control will continue to be an active area of research, which could lead to real benefits for the secure, affordable and low-carbon operation of the power system.

Appendices

A Derivation of model validity condition (3.10)

The sufficient condition for a fridge to change its power consumption as required by the system frequency (3.10) is derived as follows. We would like to know how the typical power consumption over one cycle changes as system frequency changes. Typical power consumption per cycle $\bar{p}$ is given by

$$\bar{p} = p_{\text{ON}} \frac{\tau^0_{\text{ON}}}{(\tau^0_{\text{ON}} + \tau^0_{\text{OFF}})} \tag{5.1}$$

where p_{ON} is the power a TCL consumes when switched on.

$$\frac{\partial \tau^0_{\text{ON}}}{\partial f} = \frac{\beta_-(T^0_+ - T_{\text{ON}}) - \beta_+(T^0_- - T_{\text{ON}})}{\alpha(T^0_- - T_{\text{ON}})^2} \tag{5.2a}$$

$$\frac{\partial \tau^0_{\text{OFF}}}{\partial f} = \frac{\beta_-(T_{\text{OFF}} - T^0_+) + \beta_+(T_{\text{OFF}} - T^0_-)}{\alpha(T_{\text{OFF}} - T^0_+)^2}. \tag{5.2b}$$

Therefore

$$\begin{aligned}\frac{\partial \bar{p}}{\partial f} \quad = \quad & \frac{p_{\text{ON}}}{\alpha^2(\tau^0_{\text{ON}} + \tau^0_{\text{OFF}})^2} \left[\frac{-\beta_+(T^0_- - T_{\text{ON}}) + \beta_-(T^0_+ - T_{\text{ON}})}{(T^0_- - T_{\text{ON}})^2} (\alpha\tau^0_{\text{ON}} + \alpha\tau^0_{\text{OFF}}) \right. \\ & \left. - \left(\frac{\beta_-(T^0_+ - T_{\text{ON}}) - \beta_+(T^0_- - T_{\text{ON}})}{(T^0_- - T_{\text{ON}})^2} + \frac{\beta_-(T_{\text{OFF}} - T^0_+) + \beta_+(T_{\text{OFF}} - T^0_-)}{(T_{\text{OFF}} - T^0_+)^2} \right) \alpha\tau^0_{\text{ON}} \right].\end{aligned} \tag{5.3}$$

Since $p_{\text{ON}} > 0$, $\frac{\partial \bar{p}}{\partial f}$ is strictly positive if and only if

$$\begin{aligned} & \beta_+ \left(\frac{\tau^0_{\text{ON}}(T_{\text{OFF}} - T^0_-)(T^0_- - T_{\text{ON}}) - \tau^0_{\text{OFF}}(T_{\text{OFF}} - T^0_+)^2}{(T^0_- - T_{\text{ON}})(T_{\text{OFF}} - T^0_+)^2} \right) \\ + \quad & \beta_- \left(\frac{\tau^0_{\text{OFF}}(T_{\text{OFF}} - T^0_+)(T^0_+ - T_{\text{ON}}) - \tau^0_{\text{ON}}(T^0_- - T_{\text{ON}})^2}{(T_{\text{OFF}} - T^0_+)(T^0_- - T_{\text{ON}})^2} \right) \quad > \quad 0 \end{aligned} \tag{5.4}$$

which is the case if and only if

$$\begin{aligned} & \beta_+ \left(\tau^0_{\text{ON}}(T_{\text{OFF}} - T^0_-)(T^0_- - T_{\text{ON}}) - \tau^0_{\text{OFF}}(T_{\text{OFF}} - T^0_+)^2 \right)(T^0_- - T_{\text{ON}}) \\ + \quad & \beta_- \left(\tau^0_{\text{OFF}}(T_{\text{OFF}} - T^0_+)(T^0_+ - T_{\text{ON}}) - \tau^0_{\text{ON}}(T^0_- - T_{\text{ON}})^2 \right)(T_{\text{OFF}} - T^0_+) \quad > \quad 0 \end{aligned} \tag{5.5}$$

which is equivalent to

$$\begin{aligned} & \tau^0_{\text{ON}}(T^0_- - T_{\text{ON}})^2 \Big(\beta_+(T_{\text{OFF}} - T^0_-) - \beta_-(T_{\text{OFF}} - T^0_+) \Big) \\ + \quad & \tau^0_{\text{OFF}}(T_{\text{OFF}} - T^0_+)^2 \Big(\beta_-(T^0_+ - T_{\text{ON}}) - \beta_+(T^0_- - T_{\text{ON}}) \Big) \quad > \quad 0. \end{aligned} \tag{5.6}$$

Therefore a sufficient condition for the derivative of $\bar{p}$ wrt Δf to be positive, is that both terms in the preceding equation be strictly positive. Since τ^0_{ON}, τ^0_{OFF} and the squared terms are always strictly positive this leaves us with two sufficient criteria:

$$\begin{aligned} \frac{\beta_+}{\beta_-} \quad &< \quad \frac{T^0_+ - T_{\text{ON}}}{T^0_- - T_{\text{ON}}} \qquad && > 1 \\ \frac{\beta_+}{\beta_-} \quad &> \quad \frac{T_{\text{OFF}} - T^0_+}{T_{\text{OFF}} - T^0_-} \qquad && < 1 \end{aligned} \tag{5.7}$$

(recall that $T_{\text{ON}} < T^0_- < T^0_+ < T_{\text{OFF}}$).

B Simulations

In all of our simulations, at each time step we update the temperature set points based on the grid frequency at the previous time step, and evolve the temperature of each TCL using (3.5a) or (3.5b). We test to see whether the TCL should have switched on/off since the previous time step, and if so, we estimate the time at which the TCL switched, and recalculate the temperature at the new time step. We use the following equations, illustrated in Figure B1.

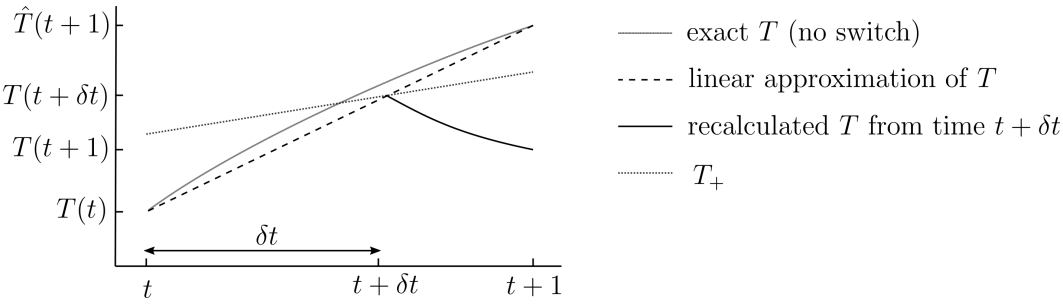

Figure B1: Method for updating TCL temperature after a switch (on).

We approximate the time δt after the previous time step t when the TCL temperature was equal to the upper (or lower) temperature switch point as follows. We shall use the notation $T_\bullet$ to denote T_{ON} if the TCL was on at time t, or T_{OFF} if the TCL was off. A linear approximation for T between the time steps is given by the equation $\hat{T}(t+\tilde{t}) \approx T(t)+(\hat{T}(t+1)-T(t))\tilde{t}$ (we use the hat notation to indicate that the temperature will be updated, initially $\hat{T}(t+1) = T(t+1)$). The equation for the temperature set points is given by $T_\pm(t+\tilde{t}) = T_\pm(t+1) + (T_\pm(t+1) - T_\pm(t))\tilde{t}$. Equating these to find the time δt when they intercept gives

$$\delta t = \frac{T_\pm(t) - T(t)}{\hat{T}(t+1) - T(t) - \big((T_\pm(t+1) - T_\pm(t)\big)} \tag{5.8}$$

and so we find an approximation for the temperature at the switch time

$$T(t+\delta t) = T(t) + (\hat{T}(t+1) - T(t))\delta t \tag{5.9}$$

therefore the TCL temperature post-switch is given by

$$T(t+1) = \big(T(t) - T_\bullet\big)e^{-\alpha(1-\delta t)} + T_\bullet. \tag{5.10}$$

In Figure B1 we exaggerate the curvature of the temperature curves to show that there will be a small error created by the initial linearisation. However, the temperature is very close to linear on the scale of one second, and so we deem the approximation worthwhile for the computational time saved solving for the intercept, which would still be an approximation. What the figure also shows is the benefit of estimating the switch time, since the recalculated temperature at time $t+1$ can be significantly different to the original temperature. This is particularly true when a TCL would have switched near the beginning of a time step.

Once the TCL temperatures at time $t+1$ have been calculated the frequency for time $t+1$ is calculated.

C Data

In this appendix we present more details about the system data provided by National Grid and described in Section 4.3.1 on page 109 . Some of the data was given confidentially, and so we present summary statistics to indicate approximate means and ranges of the data for each of the 36 10-day simulation periods. We number the periods chronologically from 1 to 36, taken from the period July 2015 - June 2016.

C.1 Stored kinetic energy

Fig C1 shows a box plot of the stored kinetic energy (MVAs) for each 10-day period. Each box shows the interquartile range and median, and the whiskers show the minimum and maximum of the data range. The data shows a seasonal trend with higher stored kinetic energy tending to occur in the winter months, with a couple of exceptions.

C.2 Demand

Stored kinetic energy is highly influenced by total system demand (MW), and we see this in Figure C2. Again, demand is significantly higher in the winter months, with two exceptions. This is likely to be due to reduced demand over the holiday season.

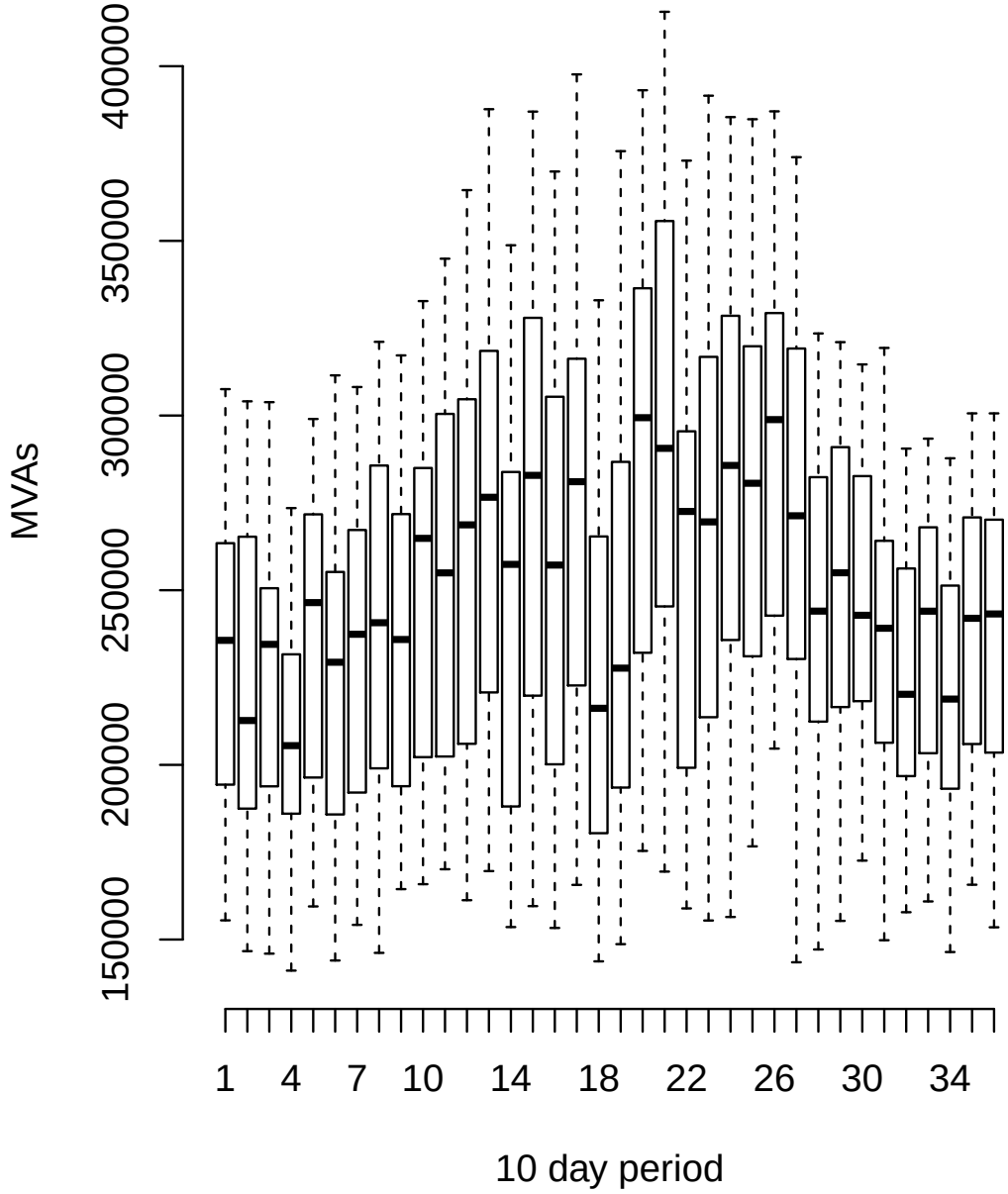

Figure C1: Summary of stored kinetic energy data.

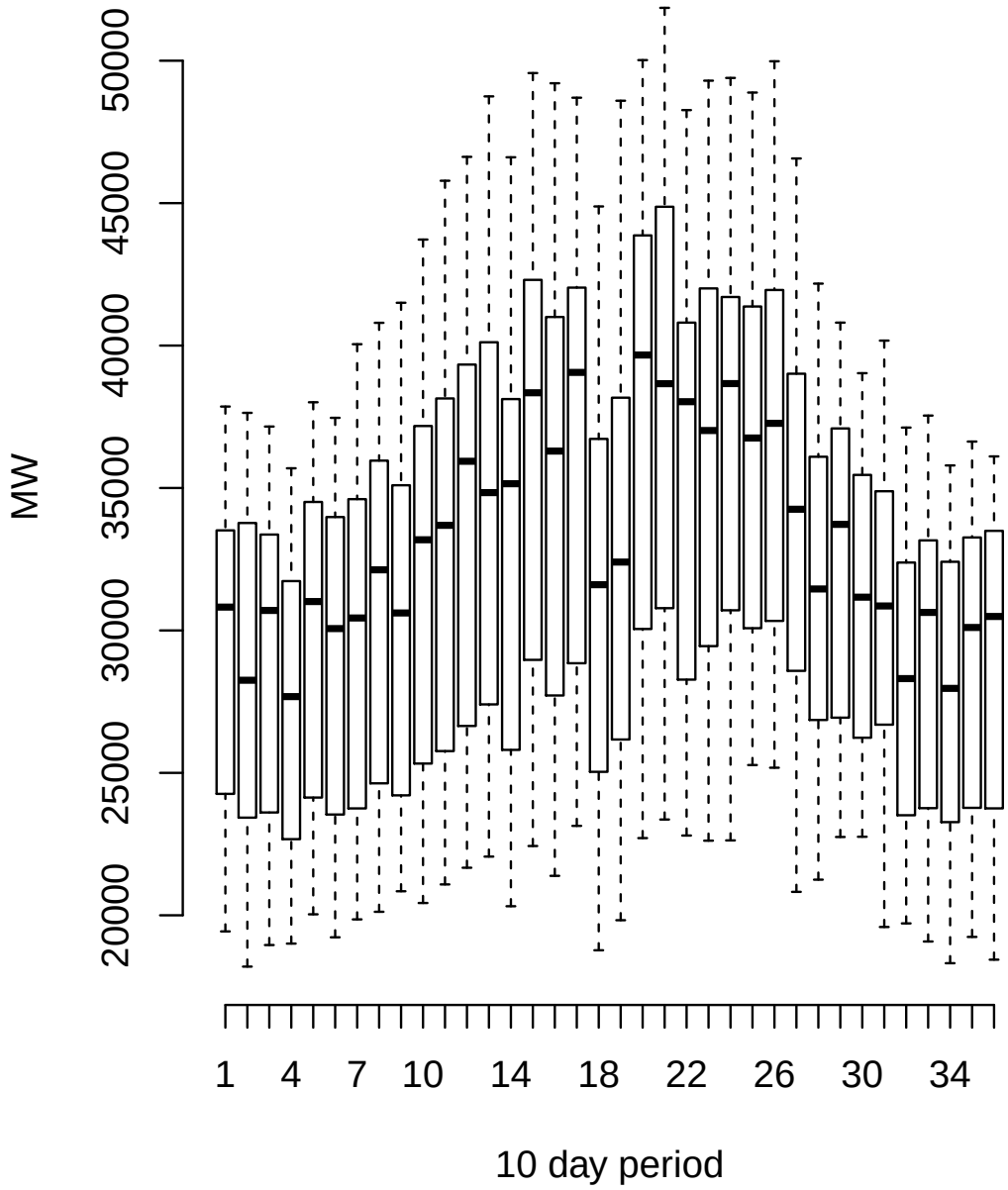

Figure C2: Summary of system demand data.

C.3 Historic frequency

At almost all times the electricity grid frequency is very close to 50Hz. We are most interested in the tails of the data distribution, and so we give them special attention in our summary. In Figure C3 the crosses show the mean frequency for each 10-day period, and the triangles above (and below) show the mean plus (or minus) one standard deviation. We define 'high frequency' to be data points greater than or equal to 50.2Hz, and 'low frequency' to be data points less than or equal to 49.8Hz. The figure includes a box plot of both the high and low frequency data. The box width is proportional to the number of high (or low) data points. No box implies there were no times during the 10-day period when frequency was high/low. Periods 8 and 18 have two erroneous high outlier values which extend beyond the plot. They are each greater than 52Hz, and only occur for one second each. These are impossibly high, therefore we conclude that they are measurement errors, which will not effect the simulations in any meaningful way due to their negligibly short duration. The large variation in high and low frequency values helps us to understand the wide range of results from our simulations, and motivates our use of many time periods.

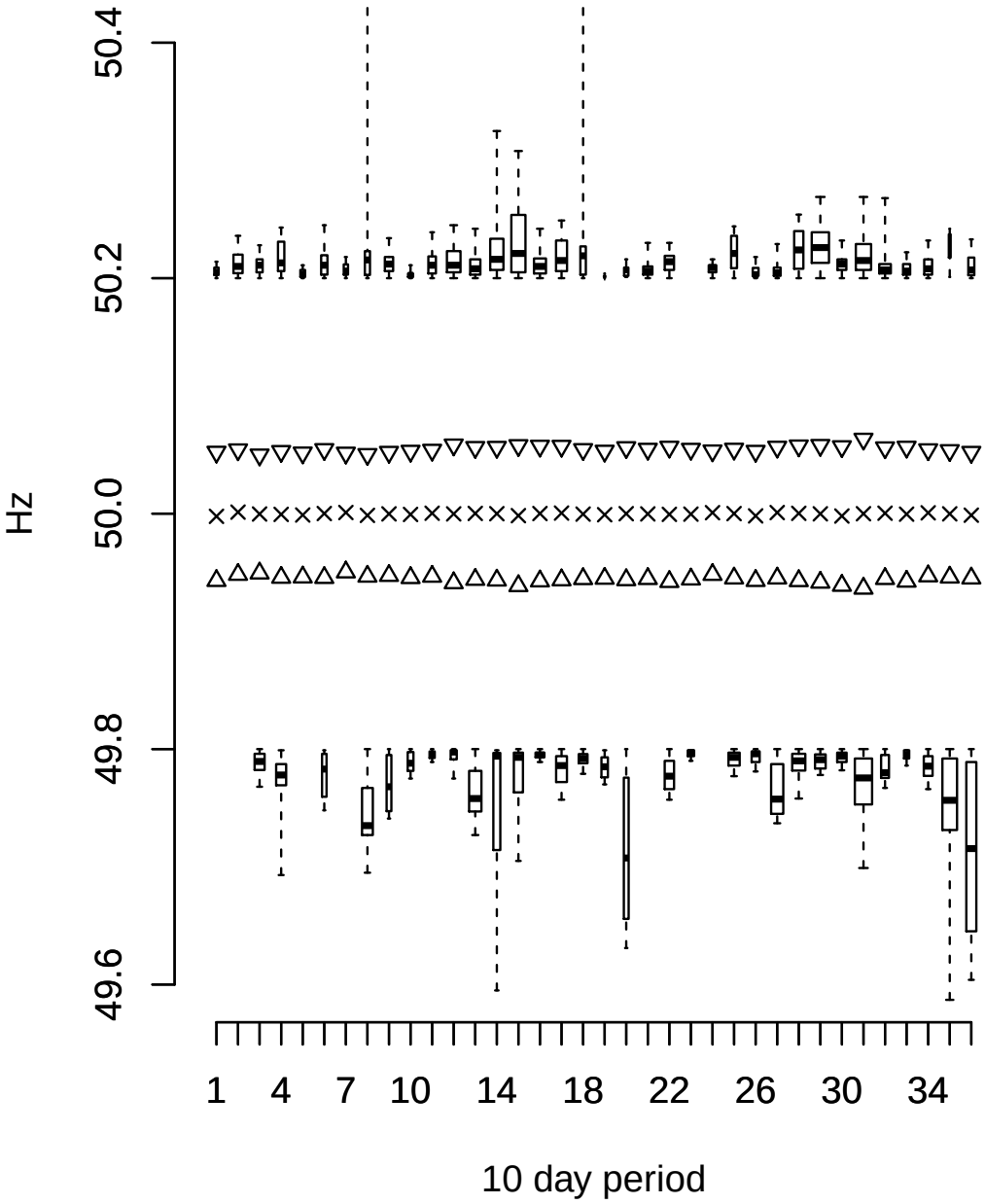

Figure C3: Summary of historic frequency data.

C.4 Response holdings

There are three types of response holding data; primary, secondary and high. For each of the seven 'trigger points' (see Table 4.2 and Figure 4.5 on page 112) there is a corresponding MW level of response that is held. For each of primary, secondary and high response we combine the amount of response held at each of the two or three trigger levels, and present the total response held (for confidentiality reasons). Figure C4 shows the amount of high response held in each period using box plots in the same manner as the previous plots. Figure C5 shows the equivalent data statistics for primary and secondary response holdings. Note that in many cases the same provider will be supplying response at all two (or three) trigger points, and so the sum of response is not a sum of maximum available response, due to double (or triple) counting.

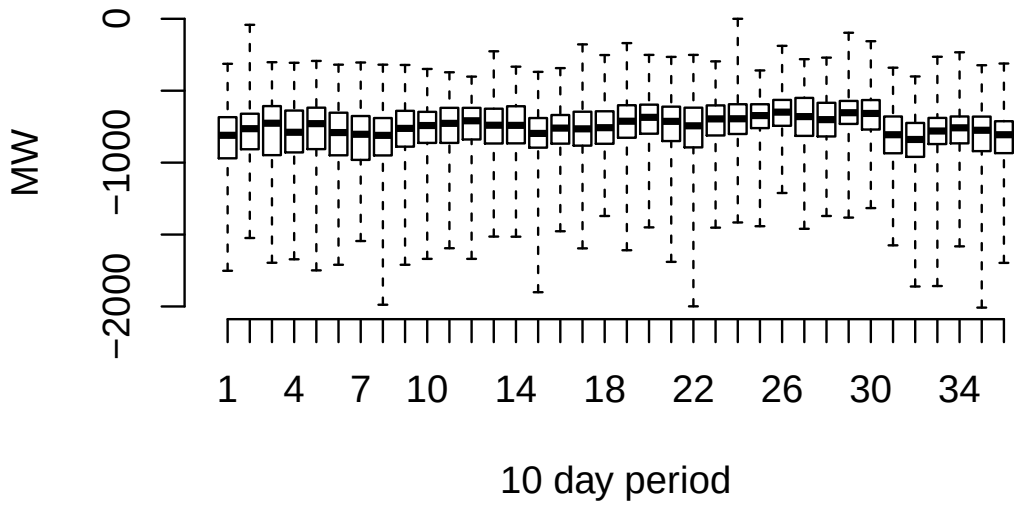

Figure C4: Summary of high response holdings.

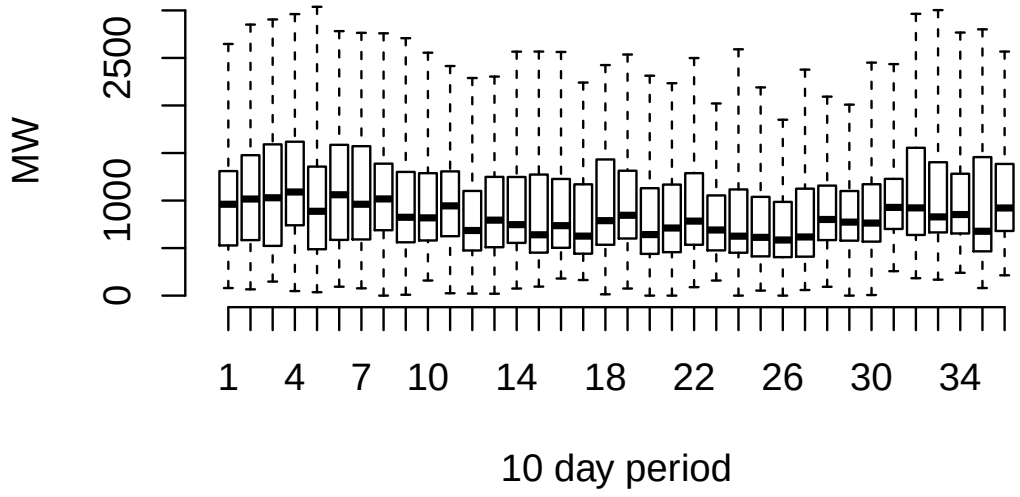

(a) Primary

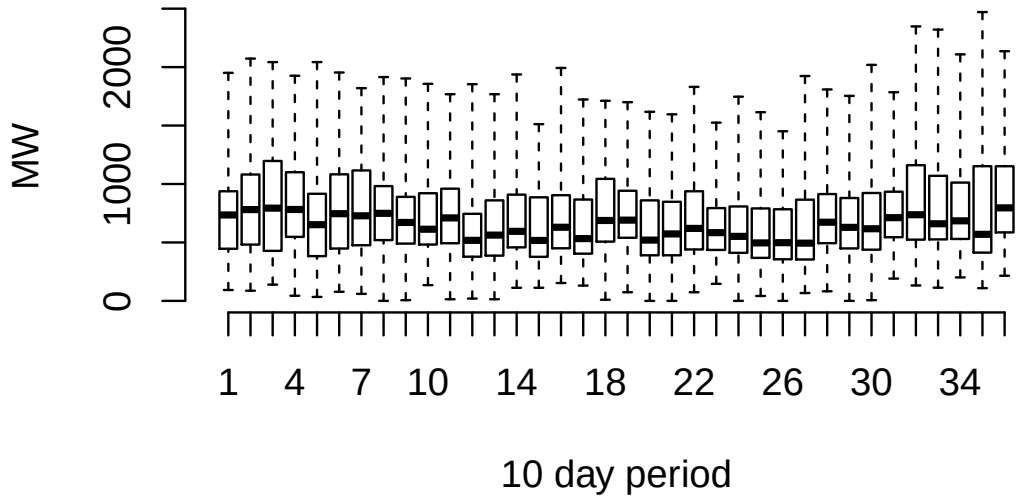

(b) Secondary

Figure C5: Summary of low response holdings.

Bibliography

[1] National Grid. System operability framework, 2016. URL http://www2.nationalgrid.com/UK/Industry-information/Future-of-Energy/System-Operability-Framework/.

[2] Liam Stoker. GB energy supply enjoys coal-free day for 'first time since the industrial revolution'. *Clean Energy News*, April 2017. URL https://www.cleanenergynews.co.uk/news/solar/gb-energy-supply-enjoys-coal-free-day-for-first-time-since-the-industrial-r.

[3] Adam Vaughan. This summer was greenest ever for energy, says National Grid. *The Guardian*, September 2017. URL https://www.theguardian.com/business/2017/sep/26/summer-green-energy-national-grid-carbon-emissions-solar-uk#img-2.

[4] Reuters Staff. Britain opens first subsidy-free solar power farm. *Reuters*, September 2017. URL https://uk.reuters.com/article/us-britain-solar-subsidies/britain-opens-first-subsidy-free-solar-power-farm-idUKKCN1C10L5.

[5] Ben Mouncer. Jaguar land rover to build electric and hybrid new vehicles only from 2020. *Business Review Europe*, September 2017. URL http://www.businessrevieweurope.eu/technology/1430/Jaguar-Land-Rover-to-build-electric-and-hybrid-new-vehicles-only-from-2020.

[6] Department for Business, Energy and Industrial Strategy. Historical electricity data: 1920 to 2016, July 2017. URL https://www.gov.uk/government/statistical-data-sets/historical-electricity-data-1920-to-2011. Accessed 2017-09-28.

[7] UK Wind Energy Database (UKWED). Wind energy statistics. URL http://www.renewableuk.com/page/UKWEDhome. Accessed 2017-09-28.

[8] David JC MacKay. *Sustainable Energy - without the hot air*. UIT, 2011.

[9] National Grid. System operability framework, 2015. URL http://www2.nationalgrid.com/UK/Industry-information/Future-of-Energy/System-Operability-Framework/.

[10] Energy Department for Business and Industrial Strategy. Solar photovoltaics deployment, September 2017. URL https://www.gov.uk/government/statistics/solar-photovoltaics-deployment. Accessed 2017-09-28.

[11] Philip Heptonstall, Robert Gross, and Florian Steiner. The costs and impacts of intermittency - 2016 update, February 2017. URL http://www.ukerc.ac.uk/programmes/technology-and-policy-assessment/the-intermittency-report.html. Accessed 2017-09-28.

[12] Steven Strogatz. *Sync: The emerging science of spontaneous order*. Penguin UK, 2004.

[13] Prabha Kundur, Neal J Balu, and Mark G Lauby. *Power System Stability and Control*. McGraw-Hill, Inc., New York, 1994.

[14] Stuart Borlase, editor. *Smart grids: infrastructure, technology, and solutions*. CRC Press, 2016.

[15] World Energy Council. World energy perspectives: Executive summary. https://www.worldenergy.org/wp-content/uploads/2016/09/Variable-Renewable-Energy-Sources-Integration-in-Electricity-Systems-2016-How-to-get-it-right-Executive-Summary.pdf, 2016.

[16] Steve Blume. Global energy storage market overview & regional summary report. *Energy Storage Council*, 2015.

[17] Jerry C Whitaker. *AC power systems handbook*. CRC Press, 2006.

[18] Mircea Eremia and Mohammad Shahidehpour, editors. *Handbook of electrical power system dynamics: modeling, stability, and control*, volume 92. John Wiley & Sons, 2013.

[19] *The Electricity Trading Arrangements: A Beginner's Guide*. Elexon, November 2015. Version 5.0.

[20] P. Kundur, J. Paserba, V. Ajjarapu, G. Andersson, A. Bose, C. Canizares, N. Hatziargyriou, D. Hill, A. Stankovic, C. Taylor, T. Van Cutsem, and V. Vittal. Definition and classification of power system stability ieee/cigre joint task

force on stability terms and definitions. *IEEE transactions on Power Systems*, 19(3):1387–1401, 2004.

[21] John R Cogdell. *Foundations of electrical engineering*. Prentice-Hall, Inc., 1995.

[22] John J Grainger and William D Stevenson. *Power system analysis*, volume 621. New York: McGraw-Hill, 1994.

[23] *EPRI Power System Dynamics Tutorial*. EPRI, Palo Alto, CA, 2002.

[24] Ofgem. Electricity interconnectors. URL https://www.ofgem.gov.uk/electricity/transmission-networks/electricity-interconnectors. Accessed: 2017-02-27.

[25] National Grid. Keeping the electricity transmission system in balance. URL http://www2.nationalgrid.com/uk/services/balancing-services/. Accessed: 2016-08-04.

[26] Committee on Climate Change. Reducing carbon emissions. URL https://www.theccc.org.uk/tackling-climate-change/reducing-carbon-emissions/. Accessed 2017-09-20.

[27] National Grid. Future energy scenarios charts workbook version 2.2, July 2017. URL http://fes.nationalgrid.com/fes-document/. Accessed 2017-09-20.

[28] JA Pecas Lopes, N Hatziargyriou, J Mutale, P Djapic, and N Jenkins. Integrating distributed generation into electric power systems: A review of drivers, challenges and opportunities. *Electric power systems research*, 77(9):1189–1203, 2007.

[29] Henrik Lund. Renewable energy strategies for sustainable development. *Energy*, 32(6):912–919, 2007.

[30] GM Shafiullah, Amanullah MT Oo, Dennis Jarvis, ABM Shawkat Ali, and Peter Wolfs. Potential challenges: Integrating renewable energy with the smart grid. In *Universities Power Engineering Conference (AUPEC), 2010 20th Australasian*, pages 1–6. IEEE, 2010.

[31] Mohammad Dreidy, H Mokhlis, and Saad Mekhilef. Inertia response and frequency control techniques for renewable energy sources: A review. *Renewable and Sustainable Energy Reviews*, 69:144–155, 2017.

[32] National Grid. Future energy scenarios, July 2017. URL http://fes.nationalgrid.com/fes-document/. Accessed 2017-09-20.

[33] Electric Power Research Institute (EPRI), National Institute of Standards, and Technology. Report to NIST on the smart grid interoperability standards roadmap. Technical report, August 2009.

[34] Kaveh Dehghanpour and Saeed Afsharnia. Electrical demand side contribution to frequency control in power systems: A review on technical aspects. *Renewable and Sustainable Energy Reviews*, 41:1267–1276, 2015. ISSN 13640321. doi: 10.1016/j.rser.2014.09.015.

[35] Frauke Oldewurtel, Theodor Borsche, Matthias Bucher, Philipp Fortenbacher, Marina Gonzalez Vaya Haring, Tobias Haring, Johanna L Mathieu, Olivier Mégel, Evangelos Vrettos, and Göran Andersson. A framework for and assessment of demand response and energy storage in power systems. In *Bulk Power System Dynamics and Control-IX Optimization, Security and Control of the Emerging Power Grid (IREP), 2013 IREP Symposium*, pages 1–24. IEEE, 2013.

[36] Duncan S Callaway. Can smaller loads be profitably engaged in power system services? In *Power and Energy Society General Meeting, 2011 IEEE*, pages 1–3. IEEE, 2011.

[37] Arteconi, Alessia and Hewitt, Neil J and Polonara, Fabio. State of the art of thermal storage for demand-side management. *Applied Energy*, 93:371–389, 2012.

[38] Alec Brooks, Ed Lu, Dan Reicher, Charles Spirakis, and Bill Weihl. Demand dispatch. *IEEE Power and Energy Magazine*, 8(3):20–29, 2010.

[39] Fred C Schweppe. Frequency adaptive, power-energy re-scheduler, 1982. US Patent 4,317,049.

[40] David R Hirst. Grid stabilising system, November 9 2010. US Patent 7,830,037.

[41] Philip J Douglass, Rodrigo Garcia-Valle, Preben Nyeng, Jacob Østergaard, and Mikael Togeby. Smart demand for frequency regulation: Experimental results. *IEEE Transactions on Smart Grid*, 4(3):1713–1720, 2013.

[42] Peter Cappers, Charles Goldman, and David Kathan. Demand response in US electricity markets: empirical evidence. *Energy*, 35(4):1526–1535, 2010.

[43] Jay W Zarnikau. Demand participation in the restructured electric reliability council of Texas market. *Energy*, 35(4):1536–1543, 2010.

[44] DJ Hammerstrom, J Brous, TA Carlon, DP Chassin, C Eustis, GR Horst, OM Jarvegren, R Kajfasz, W Marek, P Michie, T Oliver, W Munson, and RG Pratt. Pacific Northwest GridWise^{TM} testbed demonstration projects; Part II. Grid Friendly^{TM} appliance project. Technical report, Pacific Northwest National Laboratory (PNNL), Richland, WA (US), 2007.

[45] Brendan J Kirby. *Spinning reserve from responsive loads*. United States Department of Energy, 2003.

[46] Duncan S Callaway and Ian A Hiskens. Achieving controllability of electric loads. *Proceedings of the IEEE*, 99(1):184–199, 2011.

[47] Zhao Xu, Jacob Østergaard, and Mikael Togeby. Demand as frequency controlled reserve. *IEEE Transactions on power systems*, 26(3):1062–1071, 2011.

[48] CY Chong and AS Debs. Statistical synthesis of power system functional load models. In *Decision and Control including the Symposium on Adaptive Processes, 1979 18th IEEE Conference on*, volume 18, pages 264–269. IEEE, 1979.

[49] Chee-Yee Chong and Roland P Malhamé. Statistical synthesis of physically based load models with applications to cold load pickup. *IEEE transactions on power apparatus and systems*, 7:1621–1628, 1984.

[50] Roland Malhamé and Chee-Yee Chong. Electric load model synthesis by diffusion approximation of a high-order hybrid-state stochastic system. *IEEE Transactions on Automatic Control*, 30(9):854–860, 1985.

[51] Roland Malhamé and Chee-Yee Chong. On the statistical properties of a cyclic diffusion process arising in the modeling of thermostat-controlled electric power system loads. *SIAM Journal on Applied Mathematics*, 48(2):465–480, 1988.

[52] Richard E Mortensen and Kevin P Haggerty. A stochastic computer model for heating and cooling loads. *IEEE Transactions on Power Systems*, 3(3): 1213–1219, 1988.

[53] David Angeli and Panagiotis-Aristidis Kountouriotis. A stochastic approach to "dynamic-demand" refrigerator control. *IEEE Transactions on Control Systems Technology*, 20(3):581–592, 2012.

[54] Marko Aunedi, P.-Artistidis. Kountouriotis, J. E. Ortega Calderon, David Angeli, and Goran Strbac. Economic and environmental benefits of dynamic demand in providing frequency regulation. *IEEE Transactions on Smart Grid*, 4(4):2036–2048, 2013.

[55] Fabio Bagagiolo and Dario Bauso. Mean-field games and dynamic demand management in power grids. *Dynamic Games and Applications*, 4(2):155–176, 2013. ISSN 2153-0785. doi: 10.1007/s13235-013-0097-4.

[56] Theodor Borsche, Uros Markovic, and Göran Andersson. A new algorithm for primary frequency control with cooling appliances. *Computer Science - Research and Development*, 1, 2014. ISSN 1865-2034. doi: 10.1007/s00450-014-0289-1.

[57] Duncan S. Callaway. Tapping the energy storage potential in electric loads to deliver load following and regulation, with application to wind energy. *Energy Conversion and Management*, 50(5):1389–1400, May 2009. ISSN 01968904. doi: 10.1016/j.enconman.2008.12.012.

[58] Kostadin Fikiin, Borislav Stankov, Judith Evans, Graeme Maidment, Alan Foster, Tim Brown, Jonathan Radcliffe, Mohammed Youbi-Idrissi, Adrian Alford, Liz Varga, Graciela Alvarez, Ivan Evg. Ivanov, Carole Bond, Ina Colombo, Gabriel Garcia-Naveda, Ivaylo Ivanov, Kazuhiro Hattori, Daisuke Umeki, Tsvetan Bojkov, and Nikola Kaloyanov. Refrigerated warehouses as intelligent hubs to integrate renewable energy in industrial food refrigeration and to enhance power grid sustainability. *Trends in Food Science & Technology*, 60:96–103, 2017.

[59] Stephan Koch, Johanna L Mathieu, and Duncan S Callaway. Modeling and control of aggregated heterogeneous thermostatically controlled loads for ancillary services. In *Proc. PSCC*, pages 1–7, 2011.

[60] Enrique Kremers, José María González de Durana, Oscar Barambones, and André Lachaud. *Synchronisation Phenomena in Electrical Systems: Emergent Oscillation in a Refrigerator Population.* Springer Berlin Heidelberg, 2013.

[61] Enrique Kremers, José María González de Durana, and Oscar Barambones. Emergent synchronisation properties of a refrigerator demand side management system. *Applied Energy*, 101:709–717, 2013. ISSN 03062619. doi: 10.1016/j.apenergy.2012.07.021.

[62] Yashen Lin, Prabir Barooah, and Sean P Meyn. Low-frequency power-grid ancillary services from commercial building hvac systems. In *Smart Grid Communications (SmartGridComm), 2013 IEEE International Conference on*, pages 169–174. IEEE, 2013.

[63] Ning Lu and David P Chassin. A state-queueing model of thermostatically controlled appliances. *IEEE Transactions on Power Systems*, 19(3):1666–1673, 2004.

[64] Ning Lu, David P Chassin, and Steve E Widergren. Modeling uncertainties in aggregated thermostatically controlled loads using a state queueing model. *IEEE Transactions on Power Systems*, 20(2):725–733, 2005.

[65] Mohammad R Vedady Moghadam, Richard TB Ma, and Rui Zhang. Distributed frequency control via demand response in smart grids. In *2013 IEEE International Conference on Acoustics, Speech and Signal Processing*, pages 5233–5237. IEEE, 2013.

[66] Angel Molina-García, François Bouffard, and Daniel S Kirschen. Decentralized demand-side contribution to primary frequency control. *IEEE Transactions on Power Systems*, 26(1):411–419, 2011.

[67] Shashi Kant Pandey, Soumya R. Mohanty, and Nand Kishor. A literature survey on load-frequency control for conventional and distribution generation power systems. *Renewable and Sustainable Energy Reviews*, 25:318–334, 2013. ISSN 13640321. doi: 10.1016/j.rser.2013.04.029.

[68] Cristian Perfumo, Ernesto Kofman, Julio H Braslavsky, and John K Ward. Load management: Model-based control of aggregate power for populations of thermostatically controlled loads. *Energy Conversion and Management*, 55: 36–48, 2012.

[69] Joe A Short, David G Infield, and Leon L Freris. Stabilization of grid frequency through dynamic demand control. *IEEE Transactions on Power Systems*, 22 (3):1284–1293, 2007.

[70] Nikolai A Sinitsyn, Soumya Kundu, and Scott Backhaus. Safe protocols for generating power pulses with heterogeneous populations of thermostatically controlled loads. *Energy Conversion and Management*, 67:297–308, 2013.

[71] Michael Stadler, Wolfram Krause, Michael Sonnenschein, and Ute Vogel. Modelling and evaluation of control schemes for enhancing load shift of electricity

demand for cooling devices. *Environmental Modelling & Software*, 24(2):285–295, 2009.

[72] Vincenzo Trovato, Simon H Tindemans, and Goran Strbac. Controlling the synchronization and payback associated with the provision of frequency services by dynamic demand. In *22nd International Conference and Exhibition on Electricity Distribution*, pages 1–4. IET, 2013.

[73] Simon H Tindemans, Vincenzo Trovato, and Goran Strbac. Decentralized control of thermostatic loads for flexible demand response. *IEEE Transactions on Control Systems Technology*, pages 1–16, 2015.

[74] Chon Hou Wai, Marc Beaudin, Hamidreza Zareipour, Antony Schellenberg, and Ning Lu. Cooling devices in demand response: A comparison of control methods. *IEEE Transactions on Smart Grid*, 6(1):249–260, 2015.

[75] Wei Zhang, Jianming Lian, Chin-Yao Chang, and Karanjit Kalsi. Aggregated modeling and control of air conditioning loads for demand response. *IEEE Transactions on Power Systems*, 28(4):4655–4664, 2013. ISSN 0885-8950. doi: 10.1109/TPWRS.2013.2266121.

[76] Soumya Kundu, Nikolai Sinitsyn, Scott Backhaus, and Ian Hiskens. Modeling and control of thermostatically controlled loads. *arXiv:1101.2157v1*, 836, 2011. URL http://arxiv.org/abs/1101.2157.

[77] He Hao, Borhan M Sanandaji, Kameshwar Poolla, and Tyrone L Vincent. Aggregate flexibility of thermostatically controlled loads. *IEEE Transactions on Power Systems*, 30(1):189–198, 2015.

[78] He Hao, Borhan M Sanandaji, Kameshwar Poolla, and Tyrone L Vincent. A generalized battery model of a collection of thermostatically controlled loads for providing ancillary service. In *51st Annual Allerton Conference on Communication, Control, and Computing*, pages 551–558. IEEE, 2013.

[79] Melanie Mitchell. *Complexity: A guided tour*. Oxford University Press, 2009.

[80] M Klein, GJ Rogers, and P Kundur. A fundamental study of inter-area oscillations in power systems. *IEEE Transactions on Power Systems*, 6(3):914–921, 1991.

[81] Arturo Roman Messina. *Inter-area oscillations in power systems: a nonlinear and nonstationary perspective*. Springer Science & Business Media, 2009.

[82] Giovanni Filatrella, Arne Hejde Nielsen, and Niels Falsig Pedersen. Analysis of a power grid using a Kuramoto-like model. *The European Physical Journal B*, 61(4):485–491, 2008.

[83] Martin Rohden, Andreas Sorge, Marc Timme, and Dirk Witthaut. Self-organized synchronization in decentralized power grids. *Physical review letters*, 109(6):064101, 2012.

[84] Martin Rohden, Andreas Sorge, Dirk Witthaut, and Marc Timme. Impact of network topology on synchrony of oscillatory power grids. *Chaos: An Interdisciplinary Journal of Nonlinear Science*, 24(1):013123, 2014.

[85] Adilson E Motter, Seth A Myers, Marian Anghel, and Takashi Nishikawa. Spontaneous synchrony in power-grid networks. *Nature Physics*, 9(3):191–197, 2013.

[86] Florian Dörfler, Michael Chertkov, and Francesco Bullo. Synchronization in complex oscillator networks and smart grids. *Proceedings of the National Academy of Sciences*, 110(6):2005–2010, 2013.

[87] Peter J Menck, Jobst Heitzig, Jürgen Kurths, and Hans Joachim Schellnhuber. How dead ends undermine power grid stability. *Nature communications*, 5, 2014.

[88] Shuai Lu, Nader Samaan, Ruisheng Diao, Marcelo Elizondo, Chunlian Jin, Ebony Mayhorn, Yu Zhang, and Harold Kirkham. Centralized and decentralized control for demand response. In *Innovative Smart Grid Technologies (ISGT), 2011 IEEE PES*, pages 1–8. IEEE, 2011.

[89] Sadegh Esmaeil Zadeh Soudjani, Sebastian Gerwinn, Christian Ellen, Martin Fränzle, and Alessandro Abate. Formal synthesis and validation of inhomogeneous thermostatically controlled loads. In *International Conference on Quantitative Evaluation of Systems*, pages 57–73. Springer, 2014.

[90] Sadegh Esmaeil Zadeh Soudjani and Alessandro Abate. Aggregation and control of populations of thermostatically controlled loads by formal abstractions. *IEEE Transactions on Control Systems Technology*, 23(3):975–990, 2015.

[91] Chuen-Chien Lee. Fuzzy logic in control systems: fuzzy logic controller. I. *IEEE Transactions on systems, man, and cybernetics*, 20(2):404–418, 1990.

[92] MK El-Sherbiny, G El-Saady, and Ali M Yousef. Efficient fuzzy logic load–frequency controller. *Energy conversion and management*, 43(14):1853–1863, 2002.

[93] Kumarjit Bhattacharyya and ML Crow. A fuzzy logic based approach to direct load control. *IEEE Transactions on Power Systems*, 11(2):708–714, 1996.

[94] L Goel, Qiuwei Wu, and Peng Wang. Fuzzy logic-based direct load control of air conditioning loads considering nodal reliability characteristics in restructured power systems. *Electric Power Systems Research*, 80(1):98–107, 2010.

[95] Ertuğrul Çam and Ilhan Kocaarslan. Load frequency control in two area power systems using fuzzy logic controller. *Energy Conversion and Management*, 46 (2):233–243, 2005.

[96] Krishnan Pandiaraj, Philip Taylor, Nicholas Jenkins, and Charlie Robb. Distributed load control of autonomous renewable energy systems. *IEEE Transactions on energy Conversion*, 16(1):14–19, 2001.

[97] Severin Borenstein, Michael Jaske, and Arthur Rosenfeld. Dynamic pricing, advanced metering, and demand response in electricity markets. *Center for the Study of Energy Markets*, 2002.

[98] Daniel S Kirschen. Demand-side view of electricity markets. *IEEE Transactions on Power Systems*, 18(2):520–527, 2003.

[99] Fred C Schweppe, Michael C Caramanis, Richard D Tabors, and Roger E Bohn. *Spot pricing of electricity*. Springer Science & Business Media, 2013.

[100] Benjamin Schäfer, Moritz Matthiae, Marc Timme, and Dirk Witthaut. Decentral smart grid control. *New Journal of Physics*, 17, Jan 2015. ISSN 1367-2630. doi: 10.1088/1367-2630/17/1/015002.

[101] Daniel Trudnowski, Matt Donnelly, and Eric Lightner. Power-system frequency and stability control using decentralized intelligent loads. In *2005/2006 IEEE/PES Transmission and Distribution Conference and Exhibition*, pages 1453–1459. IEEE, 2006.

[102] Y Kuramoto. *Chemical Oscillations, Waves, and Turbulence*. Springer, Berlin, 1984.

[103] Steven H. Strogatz. From Kuramoto to Crawford: exploring the onset of synchronization in populations of coupled oscillators. *Physica D: Nonlinear Phenomena*, 143(1-4):1–20, 2000. ISSN 01672789. doi: 10.1016/S0167-2789(00)00094-4.

[104] Steven H. Strogatz, Daniel M. Abrams, Allan McRobie, Bruno Eckhardt, and Edward Ott. Theoretical mechanics: Crowd synchrony on the Millennium Bridge. *Nature*, 438(7064):43–44, 2005. ISSN 0028-0836. doi: 10.1038/43843a.

[105] Steven H. Strogatz and Renato E. Mirollo. Stability of incoherence in a population of coupled oscillators. *Journal of Statistical Physics*, 63(3-4):613–635, 1991. ISSN 00224715. doi: 10.1007/BF01029202.

[106] Energy & Industrial Strategy Department for Business. Energy consumption in the UK, 2016.

[107] Office for National Statistics. Overview of the UK population: November 2015, 2015.

[108] G Batchelor. An introduction to fluid mechanics. *Cambridge Press, Cambridge UK*, 1967.

[109] Inc. Wolfram Research. Mathematica version 11.0, 2017.

[110] Kaveh Dehghanpour and Saeed Afsharnia. Designing a novel demand side regulation algorithm to participate in frequency control using iterated mappings. *IET Generation, Transmission & Distribution*, 8(10):1687–1699, 2014.

[111] He Hao, Borhan M. Sanandaji, Kameshwar Poolla, and Tyrone L. Vincent. A generalized battery model of a collection of thermostatically controlled loads for providing ancillary service. *2013 51st Annual Allerton Conference on Communication, Control, and Computing, Allerton 2013*, pages 551–558, 2013. doi: 10.1109/Allerton.2013.6736573.

[112] Vincenzo Trovato, Simon H Tindemans, and Goran Strbac. Leaky storage model for optimal multi-service allocation of thermostatic loads. *IET Generation, Transmission & Distribution*, 10(3):585–593, 2016.

[113] Juan A Acebrón, Luis L Bonilla, Conrad J Pérez Vicente, Félix Ritort, and Renato Spigler. The Kuramoto model: A simple paradigm for synchronization phenomena. *Reviews of modern physics*, 77(1):137, 2005.

[114] A. M. Turing. Computing machinery and intelligence. *Mind*, 59(236):433, 1950.

[115] World Energy Council in collaboration with Accenture Strategy and Paul Scherrer Institute. World energy scenarios 2016 - the grand transition, 2016. URL https://www.worldenergy.org/publications/2016/world-energy-scenarios-2016-the-grand-transition/.